A Tribological Study Of A Detonation Gun Coating Of Tungsten Carbide For Use In A Subsea Gate Valve

By

Mark L. Binfield

Department Of Materials Technology

Brunel University

March 1995

Submitted For The Degree Of Doctor Of Philosophy

Abstract

Detonation gun coatings of tungsten carbide have been widely recognised as one of the most effective anti-wear coatings for oilfield applications. However, very little fundamental tribological information exists for the material, which hinders coating development and the evolution of correct specifications. This study redresses this problem by conducting adhesive, abrasive and erosive tests upon the coating and relating the findings to the coated microstructure.

The intention has been to simulate the in-service behaviour of parallel gate valves, which are used primarily to control flow in remote locations where reliability and freedom from maintenance are essential. Although problems with such valves are rare, costs associated with replacement are exceptionally high and therefore a high research priority has been placed on valves of this type. Currently, new designs of valve are tested using a pipe loop rig at BP Research Centre. However, such tests are both expensive and time consuming and with the increasing desire to bring products to market more quickly an alternative is sought. Probably, the area offering most scope for improvement is in material specification of the sealing surfaces and this work sets out to produce a first stage selection procedure for candidate materials. Uniquely, the study has taken one component, systematically categorised its failure mechanisms using non-destructive replication techniques and then reproduced them in the laboratory.

The failure analysis has pointed to three-body abrasion, erosion and adhesion being the dominant failure modes and therefore, a suite of tribo-test methods have been developed to replicate them. These are namely reciprocating diamond-on-flat, slurry erosion and reciprocating pin-on-plate tests. The material studied was a proprietary detonation gun coating of tungsten carbide, LW45, which is currently the most popular seal facing material specified for gate valves. A conformal contact geometry was chosen for the reciprocating pin-on-plate tests and problems with alignment were overcome by using a pre-test running-in procedure with 1 μm metallographic paste.

Wear of LW45 occurring during the pin-on-plate test was not affected by test speed over the range selected, but was highly dependent upon load. Four different categories ranging from minimal wear to catastrophic wear have been identified. Extensive post test analysis using optical and scanning electron microscopy has further classified the failure that occurs into two groups, termed *mild* and

severe. In the *mild* regime wear occurs by preferential removal of the binder phase, which is minimised on further sliding by protruding carbide particles. Eventually sufficient binder is removed for carbide fall-out to occur, upon which the cycle is repeated. A greater wear volume is produced by the *severe* wear mechanism which is caused by the interlinking of cracks present within the microstructure of the coating. To ensure operation in the *mild* regime, continuous sliding under operating pressures of above 7.84 MPa should be avoided.

Abrasive wear simulated by the diamond-on-flat test increased with load. However, the failure mechanisms produced were independent of load and consist of a combination of plastic deformation and brittle fracture with plastic deformation representing the rate controlling step in the wear process.

Slurry erosion tests have shown that LW45 wears by a brittle erosive mechanism and is therefore best able to resist erosion at low impingement angles. The volume loss per particle impact for LW45 is proportional to the kinetic energy of the impinging particles. The failure mechanism involved the growth of cracks in the microstructure by a fatigue action eventually leading to crack interlinking and material fall out. For all wear conditions, it is suggested that the removal of microcracking from the coating microstructure will lead to significant improvements in wear performance.

A simplified design guide has been produced that gives a weighted importance to the various failure modes attributable to the respective tests. A significant improvement in performance was recorded by LW45 in comparison to typical substrate materials such as AISI 410 and Ferralium F255 stainless steels.

Acknowledgement

Thanks to all the many people who have helped me during the period of this work.

In particular, I would like to thank Dr Terry Eyre for his expert guidance and assistance throughout. In addition, I have received invaluable assistance from many of the academic and technical staff in the Department of Materials Technology, in particular Ken Dutta and Prakash Dodia.

Thanks to SERC for granting me a CASE studentship and to Brunel University for providing the facilities.

I would like to convey my gratitude to BP Research Centre, Sunbury for providing the project and granting me a bursary for the duration of the study. I was fortunate indeed to be able to call on advice from such a wide band of technical experts at the Research Centre, in particular Dr Francis Davis, who acted as a "second personal tutor" and gave me many ideas for the presentation of tribological data. Also thanks to Dr Robert Wood for his guidance on erosion studies and to Dr David Harrison and Derek Butler for their insight into valve testing and operation.

Thanks are also due to Praxair Surface Technologies, who kindly supplied all of the Detonation Gun samples. Special thanks to Chris Guest for conveying his expertise on the D-Gun process and to Peter Stephenson for organising the coating of the samples.

A special mention for my colleagues at Lucas Advanced Engineering Centre who have helped immeasurably during the writing-up process, in particular, Terry Hirst, Dr Kevin Watts and Asha Arora.

Many thanks to Mom, Dad and especially Maria for their patience and understanding.

Finally, a mention to all the many friends I have made during my time at Brunel who have contributed to me having such a happy time there.

I hope that you enjoy reading this thesis and that it is of some benefit to you.

Mark Binfield,
Solihull,
March 1995

Contents

1.0 Introduction

Wear, corrosion and fatigue, are the most common problems that limit the life of engineering components. Increasingly, however, users of such components are demanding extended service life and reductions in frequency of maintenance.

To achieve this goal requires a systematic appraisal of the component under operating conditions to determine the failure modes that limit service life. By taking a systems approach to the operating system, it is often possible to suggest design changes that overcome such problems. More frequently, however, the only route to improvement is by specifying a different material combination to that in current use.

The parallel gate valve is an excellent case in point. It is predominantly used to control flow in subsea pipelines, for instance in the North Sea, where the cost of failure is exceptionally high, as replacement would require subsea plugging, waterflood and welding operations. If downtime involving lost production is taken into account the costs run into £ millions. Furthermore, future energy needs will dictate that the search for oil will progress to more remote locations where retrieval costs are at present uneconomic. Often these locations will correspond to hostile environments where requirements on valves are far greater in terms of reliability and freedom from maintenance. Therefore, it is essential to fully understand the tribological characteristics of such components and a high research priority has been given to this type of valve.

In recent years, widespread problems associated with all classes of valve, including poor valve reliability and high costs resulting from valve failure, have become an industry-wide cause for concern. Within BP alone, a survey has shown that 10% of the valves give problems, mainly associated with leakage and jamming, with an estimated cost due to valve failure in the order of £30 million per annum [1].

Nearly a quarter of a million valves were included in BP's survey comprising wedge gate valves, ball valves, globe check and safety valves, and the less common butterfly, plug, diaphragm and choke valves. Gate valves only accounted for 5% of the valves used in this survey, however, they are amongst the most expensive, costing in the region of £150,000 per valve.

The failure mechanisms of gate valves will be dealt with in much greater depth later on. For the moment suffice it to say that the main problems are associated with the presence of hard sand particles within the crude resulting in erosion and three-body abrasion. Furthermore, the contribution of adhesive wear cannot be discounted and, therefore, several wear resistant materials have been developed for the sealing surfaces, normally in the form of hard, thick coatings.

Although the understanding of wear mechanisms has certainly improved, wear is such a complex phenomenon that there is no reliable general law for its solution[2]. The complex nature of the subject is attributable to the large number of variables that may influence it; including the type and mode of loading, interaction rate and time, component geometry, materials properties, and environmental factors. As such, friction and wear are not only determined by the properties of the wearing materials but by the characteristics of the engineering system as a whole. Although the selection of materials for use in situations involving wear is of great importance, it must be remembered that the selection of a more "wear resistant" material is only one of the ways that the wear performance of a system may be improved.

Wear resistant materials for engineering components may be obtained by the use of the appropriate bulk material. However, most wear resistant materials are hard and have low values of toughness, making fabrication difficult and expensive. Since friction and wear are essentially surface phenomena, the presence of a suitable surface layer of material may have a significant effect and therefore, the application of surface coatings or treatments is the most attractive method, yielding the desired combination of material properties. It allows the substrate to be

chosen for its structural properties and ease of manufacture and can also result in substantial cost savings.

A great variety of surface engineering technologies have been developed for improving wear properties, and new techniques are being developed faster than our rate of understanding of their precise wear characteristics [3]. There is, therefore, a problem in how to apply surface engineering correctly for tribological purposes and to overcome this a fundamental study of the wear behaviour of surface treatments and coatings is necessary.

1.1 BP's involvement

At BP's Sunbury Research Centre, a pipe loop rig has been developed to model conditions that a gate valve may be required to experience. BP works closely with valve manufacturers who send new valve test designs to Sunbury for evaluation. After testing, the valves are returned to the manufacturers for stripdown and examination. As a result of the tests each valve is awarded a rating of between 1* (poor) and 5* (excellent). The primary method of wear prevention to the sealing interface has tended to concentrate on the use of hard surface coatings and generally it has been found that harder materials such as stellite, tungsten carbide and ceramic have provided the greatest resistance. As a result, work at BP within the Tribology Resource has tended to concentrate on the evaluation of candidate materials in terms of wear performance and the production of service guidelines. This Thesis is an extension of that work.

1.2 Involvement of other industrial organisations

It has already been stated that BP liaises closely with suppliers of both valves and surface technologies. However, it should be remembered that BP does not actually manufacture or produce either of the above. From BP's viewpoint therefore, the objective of all such work is to leave it in a position of an "informed buyer" of such technology as, after all, it is BP that must bear the consequences of any related costs resulting from valve failure. Consequently, the work

involved in this Thesis has also been conducted in collaboration with these other organisations, in particular Praxair Surface Technologies.

1.3 Overall Objectives

The use of a pipe loop rig is one way to assess valve performance, as it most closely simulates the service conditions of the component. To gain confidence in prospective valves will always require that such testing is carried out. However, the test is expensive and perhaps more importantly with the increasing desire to bring products to market more quickly, takes a considerable period of time. Furthermore, the results obtained only reflect a comparison in performance between valves; hence the fundamental understanding of the tribological characteristics of seal facing materials is not being advanced. The aim of this work, therefore, is to fundamentally assess the failure mechanisms taking place within the gate valve and to simulate them in the laboratory. Simplified laboratory tests are developed that imitate the real-life condition but in a way that does not introduce too many variables that make overall understanding more difficult.

To develop a suitable test methodology, test samples of the most frequently encountered seal face material detonation gun coated, tungsten carbide LW45, were prepared. The test programme includes reciprocating pin-on-plate, diamond-on-plate and erosion tests, which allows the fundamental process of failure for the coating to be assessed under a controlled laboratory environment.

Once confidence has been gained in the test procedure, it is possible to determine the performance of LW45 over a wide range of conditions. Therefore, two major advances will be made from this work: the development of a suitable test methodology for simulating gate valves and the fundamental appreciation of the tribological characteristics of LW45.

The outline of the Thesis is shown schematically in Figure 1.

2.0 Literature Review

The economic importance of parallel gate valves has been shown and, in particular, it is clear that a greater understanding of the tribological characteristics of the valve is required to ensure optimum materials selection. This Chapter highlights in more detail the operational features of the valves and methods by which materials selection is based. It follows by discussing the most commonly encountered wear mechanisms and where they are related to gate valves. A further section is dedicated to surface engineering with particular emphasis on the theory of detonation gun coatings used in this work.

2.10 Gate Valves

Gate valves receive a high research priority because they are primarily designed for subsea use. It would be useful before proceeding further to review the service conditions that are frequently encountered.

2.11 Service Conditions

- Downhole temperatures of generally 110 - 150°C.
- The presence of hard sand particles, typically 50 ppm.
- Variable sand size but typically 70 μm.
- Variable velocity but for long distance oil pipelines is approximately 5 ms^{-1}.
- The velocity through the valve will change through an opening/closing cycle.
- The presence of corrosive agents such as sulphur and water in the crude.
- The service conditions will vary from field to field and application to application.
- Infrequent valve operation

A schematic diagram of a typical manually operated gate valve is shown in Figure 2.1, with the principle of operation shown more clearly in Figure 2.2. Sealing is primarily achieved by the pressure of the processing liquid forcing the gate onto the downstream seat. Additionally, spring loaded upstream seats are frequently employed to further increase the effectiveness of the seal. Figure 2.3 shows a typical gate with seats and Figure 2.4 shows the seats in position in an actual valve after the gate has been removed.

As the valve is closed the area through which flow can occur is reduced until complete closure is reached. Because flow rate is fixed and we have the relationship:

$$Q = A.v \qquad \textbf{2.1}$$

where:

Q = Flow rate (m^3/s)

A = area (m^2)

v = velocity (m/s)

As the area is reduced velocity will increase up to a limiting value at around 5% open, where cavitational effects will start to take over and prevent any further increase in velocity [4].

The tribological aspects of these valves are of particular importance. The subsea valves have to transport crude oil which contains corrosive agents and abrasive sand particles. Valve problems have been mainly due to smaller particles, typically of 10 μm size, since larger particles tend to drop out of suspension. With soft seated designs, failure is usually caused by the particulate debris in the fluid stream entering the seating area and either damaging the sealing surfaces or increasing the coefficient of friction between the seal and the closing member. This leads to valve sticking or jamming. This problem, alongside the fact that polymer seats are more temperature sensitive, has led manufacturers away from their use.

With hard-faced valves, sand particles are still the primary cause for concern, although corrosion can still be a factor. In this case, however, abrasion or erosion of sealing surfaces and the clogging of clearances are the principle effects, again leading to high operating torques, sticking, jamming and through-leakage during operation. Hence it is necessary to exclude as many fluid-borne particles as possible from the seat/gate interface and this is best achieved by an effective wiping action during operation. This means that a sharp edge rather than a rounded one is required, and this is a problem if a coating is used as it contradicts normally accepted coating design.

As well as mechanical design features to reduce wear, careful application of materials selection principles has also been used. This has generally been in the form of hard surface coatings. Generally, harder materials such as stellite, tungsten carbide and ceramic provide the greatest resistance. Tungsten carbide LW45 is a coating designed specifically for this application, and is currently the most popular. It is deposited by detonation gun (D-Gun) giving thicknesses of around 100 μm. Where the process fluid contains corrosive agents such as sulphur or chlorides, it is necessary to use a corrosion resistant substrate, such as AISI 410 stainless steel. In extreme cases it may be necessary to use a duplex stainless steel substrate.

2.20 Wear

Wear can be described as the progressive loss of material from the operating surface of a body occurring as a result of relative motion at the surface. Alongside fatigue and corrosion, it is one of the three most commonly encountered industrial problems leading to the replacement of components and assemblies in engineering.

As befits its economic importance, wear generates a volumous scientific and technological literature. In the eleven years following the coining of the term *tribology* by the Jost Committee (1966), Czichos [5] reported that 55,000 papers were published on the subject and that the total was increasing by 8,000 per annum.

The subject of wear is complicated by a confusion of nomenclature and the lack of good definition of the different types of wear found in engineering situations. In the first volume of the international journal *Wear*, Burwell[6] proposes four principle types of mechanical wear, namely adhesive, abrasive, corrosive and surface fatigue and a fifth group entitled minor wear types. However, it is now widely agreed that just about every failure mechanism plays some part in wear behaviour. Eyre[7] has divided wear that occurs in industry into the following groups:

Abrasive	50%
Adhesive	15%
Erosion	8%
Fretting	8%
Chemical	5%

In the example of the gate valve, most of the above types constitute possible wear mechanisms. Pressures of up to 14 bar are used in the test rig and this enhances the possibility of adhesion between the gate and seat. The presence of sand particles means that three-body abrasion and erosion are likely, and because of corrosive agents in the processing fluids, corrosion cannot be ignored.

2.21 Abrasive Wear

Abrasive wear occurs when hard particles penetrate a surface and displace material in the form of elongated chips or slivers. It may take the form of either two-body abrasion (grinding) or three-body abrasion (lapping). Wear rates due to three-body abrasion are generally lower than those due to two-body abrasion. Furthermore, the terms *high-stress* and *low-stress* abrasion are often used. In high-stress abrasion, the crushing strength of the abrasive particles is exceeded, so that they are broken up during the wear process, whilst in low-stress abrasion the particles remain unbroken. The result of abrasion is that an otherwise smooth surface becomes roughened with fairly regular grooves. Macmillan[8] has shown that the nomenclature by which this damage is described is a matter of contention. Typical terms used are scratching, scoring or gouging depending on the degree of severity of the damage. However, the distinction between these types is far from clear and this is a typical problem evident throughout tribology where a

qualitative approach based on experience rather than a more precise quantitative one has been used.

Two body abrasive wear is perhaps the simplest and best understood of all the wear processes since it involves bulk properties rather than surface properties[9]. The primary requirement for its occurrence is that there is a great dissimilarity in hardness between the two rubbing surfaces and in addition that the harder of the two possesses a certain definite amount of roughness. Hence, the importance of surface finish becomes evident, especially in situations where there is a great difference in hardness. Two-body abrasive wear is also predominant in the transport of loose minerals, i.e. a low stress condition with little breakdown in particle size of the abrasive.

The removal of metal by abrasion by a small hard particle of grit or dust caught between the two rubbing surfaces (i.e. three-body abrasion) is an extremely important factor in the total occurring wear and is probably responsible for the largest amount of wear in industrial machinery. This is due mainly to the environmental conditions which exist in industrial plants, the major part of the wear producing abrasives coming from the surrounding atmosphere or from contaminants prevalent when processing liquids. However, it must be noted that the external environment is not the only source of such hard particles. For instance, corrosive wear products often in the form of metallic oxides, which are generally harder than the parent metal, can cause three-body abrasion if they are not removed from the operating system. Hence, the oxide particles produced initially by corrosive wear, if they remain between the surfaces, will then cause abrasive wear. This is a good example of the interaction between two wear types; another is where work-hardened debris from adhesive wear may be hard enough to abrade one or the other of the parent surfaces. This shows the difficulty that a tribologist may encounter in determining the controlling wear mechanism. For instance in the case of either of the two previous examples, the worn surface when examined will show all the hallmarks of abrasion, whereas to minimise wear it is necessary to prevent either corrosion or adhesion. These examples show that a systems approach to tribology is required, i.e. it is not possible to prescribe a "cure" by just looking at the "symptoms", it is first necessary to know the underlying

cause. For instance, the use of better air filtering systems for engines operating in, let us say, desert conditions where there is a prevalence of hard abrasive sand particles, will provide a better tribological solution than will merely selecting harder operating surfaces.

The properties of the abrasive particles themselves have significant effects on surface wear. For a material to be scratched or worn, the abrasive must normally be harder than that material where the degree of penetration is given by

$$\frac{load\ on\ the\ particle}{hardness\ of\ the\ surface} = \frac{W}{H_v} \qquad \textbf{2.2}$$

$$Giving\ a\ volume\ wear = \frac{W}{H_v}.A.L \qquad \textbf{2.3}$$

Where A is the area of a cross-section of the groove and L is the length of the groove.

Therefore, it can be seen that the damage caused by abrasion can be controlled to some extent by the relative hardness of the abrasive and the surface being abraded. It is found that particles with lower hardnesses than that of the surface cause much less wear than harder particles. For particles significantly harder than the surface, the exact value of their hardness matters much less. Moore[10] found that the wear rate becomes much more sensitive to the ratio of abrasive hardness, H_a to the surface hardness H_s, when H_a/H_s is less than approximately 1. To cause plastic deformation of a surface the ratio H_d/H_s must be greater than 1.25 and this relationship has been observed experimentally[11]. The morphology of the particles is also of significance with angular particles causing greater wear than rounded ones.

Oberle[12] pointed out that if, in the presence of abrasive particles, a surface can elastically deform sufficiently to allow the particle to pass, then permanent damage to the surface would be avoided. This would indicate that the important parameter is the limit of elastic strain, that is, the yield stress divided by the Young's Modulus. It should be stated, however, that Spurr and Newcombe[13] interpreted their results to indicate that wear resistance increases with increasing elastic modulus in direct disagreement with the work of Oberle.

As well as their hardness other properties of abrasive particles are important. Due to size considerations, only a small fraction of the particles cause wear. Smaller particles will play a secondary role as the separation of the surfaces is governed by the size of larger particles and hence particles much smaller than this separation are effectively excluded from participation. Conversely, in the case of slurry erosion larger particles will tend to drop out of suspension and the majority of wear is caused by smaller particles. Particle hardness relative to the two surfaces will also determine whether the debris remains free or whether it becomes embedded in the softer surface to act as a lap. It is also found that particle shape exerts some influence in that angular particles produce greater wear than rounded ones. The attack angle is also significant, with those particles that roll or slide contributing little to wear. High wear rates are caused by attack angles between 80° and 100°.

2.22 Adhesive Wear

Adhesive wear is also often called *galling* or *scuffing*, but the latter are ill-defined again showing the problem of nomenclature within tribology. It may be distinguished as the most fundamental of the wear types, in the sense that it is a basic phenomenon that takes place whenever two solid surfaces are in rubbing contact. Other types of wear can be completely eliminated in the laboratory by careful control of the environment (exclusion of dust particles and corrosive media for instance) but it is not possible to eliminate completely the small amounts of wear due to adhesion.

Engineering surfaces though macroscopically smooth are rough on an atomic scale[14], with geometric texture of the surface controlled by the characteristics of the finishing process by which it is produced. The roughness is formed by fluctuations in the surface of short wavelengths (microroughness), characterised by hills (asperities) and valleys of varying amplitudes. Hence when two engineering surfaces come into contact the real area of contact is vastly lower than the nominal contact area (it is seldom greater than 1/100 of the apparent area and is often as small as 1/10,000[15]). There are great practical difficulties in determining surface topography and suffice it to say that very little is known about either the Newtonian mechanics or the Euclidean geometry of the contacts in most examples of sliding wear. The development of Scanning Tunnelling and Atomic Force Microscopy may be the answer to these problems, allowing for the determination of the number of asperities per unit area and their distribution of size and shape.

As a normal load is applied the local pressure at the asperities becomes extremely high, so much so that the yield stress is exceeded and the asperities deform plastically, until the real contact area has increased sufficiently to support the applied load. If a surface film or a contaminant is present such as an oxide, it will prevent the two surfaces adhering. Hence cleanliness of the surface will greatly enhance adhesion. For instance, in a vacuum where there is an absence of any adsorbed oxide films the two surfaces will stick together under the slightest of pressure and can only be parted with difficulty.

Under purely normal loading the interposing films will prevent adhesion, but if relative tangential motion at the interface is now introduced, it will act to disperse the contaminant films at the points of contact, and cold welding of the junctions can then take place. Continued sliding will lead to shearing and if shear takes place at the position of the interface, then wear is zero. However, if shear takes place away from the interface, then material will have been transferred from one surface to the other. This may lead to an enormous increase in both wear and surface damage for only a small increase in friction. Further rubbing may cause this material to be detached altogether forming loose wear particles.

From the simple picture that has been created it can be seen that although all the junctions contribute to friction not all of them contribute to wear. Archard[16] has described the wear process in terms of a factor K which represents the fraction of the wear junctions producing wear but only has any real meaning provided that the wear mechanism does not change, i.e. there is no change from mild to severe wear. If $K = 1$ it means that every junction involved in the friction process produces a wear fragment. If $K = 0.1$ then one tenth of the friction junctions produce wear fragments. Archard has produced a formula which shows the dependence of wear rate on a number of important factors.

$$wear\ volume = \frac{KSP}{P_m (\text{alternatively}\ \ H_v)} \qquad \textbf{2.4}$$

where K is the wear constant, S is the sliding distance, P is the applied load, and P_m is the flow stress of the wearing surface. For example, clean gold surfaces K is between 0.1 and 1. For clean copper surfaces K is between 0.1 and 0.001. Evidently clean gold surfaces wear about ten times more rapidly than clean copper surfaces. From Equation 2.4 it can be seen that the actual wear rate depends not only on K but also on the hardness of the solids. Hardness is important because at a given load the area of friction junctions for harder materials will be significantly less. However, in general the smaller the value of K the smaller the wear rate.

The amount of adhesive transfer and wear can be profoundly affected by the nature of the surfaces and the ambient conditions. In general, high temperature increases and accelerates adhesive wear. This is to be expected since the formation of the weld is on an atomic scale and is, therefore a surface chemical reaction and, as is well known, the rates of most chemical reactions increase greatly with temperature.

Rabinowicz[17] has expressed the dependence of adhesion of pure metals on their ability to form solid solutions. For instance, lead has extremely low solubility with chromium, cobalt, nickel and iron and would, therefore, be a good choice for a counterface material. Of course, other

factors such as the low strength of lead play a part which infers that it is not always suitable or must be used in the alloy form. Essentially the same or similar materials show greater transfer than very dissimilar ones. Hence the ultimate may be to select a polymer or ceramic material to slide against metals. Therefore many surface diffusion treatments rely upon their ability to improve wear performance by chemical contamination to produce non-adhesive or anti-welding characteristics.

Unlike abrasive wear, sliding under metal-to-metal conditions is subject to sharp transitions in behaviour. Variations in load and speed may bring about marked thermal changes which precede, and cause, wear changes. Welsh[18] was one of the first to systematically examine the concept of mild wear (oxidative) and severe wear (metallic) and the sharp transitions between these which he refers to as the T_1 and T_2 transitions.

Mild wear results when the wearing conditions are not severe enough to remove the oxide film faster than it can be reformed. An oxide film of low adhesion is maintained and fine oxide debris and a smooth surface result. This type of wear occurs in most moderately loaded sliding applications and is often termed *oxidational* wear. Mild wear also results when sliding materials have low adhesion, irrespective of whether oxide films are formed, e.g. with hardened surfaces or non-metallic materials. Surface hardness is the principle factor affecting mild wear but microstructural factors are also important. For instance adhesive wear is reduced if the structure is discontinuous such as lamellar pearlite.

Severe wear results at higher speeds and/or loads, or under other conditions in which a stable oxide film is not maintained at the surfaces. It is characterised by non-oxidised torn surfaces and coarse metallic debris. Because of their nature, materials which show good oxidation resistance tend to have poor adhesive wear characteristics. However, excessive oxidation is undesirable because a large amount of free oxide will lead to abrasive wear.

Below T_1 wear occurs by the removal of oxide debris from an oxidised surface. T_1 is a transition to severe wear initiated by the breakdown of the protective surface oxide produced at lower loads. Plastic deformation of the substrate occurs, caused by a higher bulk temperature, and the wear rate increases considerably with the production of a metallic debris. Between T_1 and T_2 severe wear persists. At the T_2 transition the surface temperature is high enough for phase hardening to produce a hard "white layer" structure which prevents deformation and helps to establish an oxidised surface once more. The wear rate is reduced considerably but is not as low as the wear rate below the T_1 transition, Figure 2.5.

2.23 Erosion

Burwell[6] refers to erosion as one of the minor types of wear. However, Eyre[7] states that erosion is the third most common wear mechanism and, therefore, we can see the greater significance that it now holds. This is because of the continuing development of mechanisms operating at high speed, together with the need for materials with high strength to density ratios.

The term erosion is usually taken to cover that form of damage experienced by a solid body, when a fluid or gas, which contains many solid particles, impinges onto the surface of the body. Whilst relatively little detailed analysis has been made of erosion in slurry flow streams, much more is known about the corresponding dry problem for gas-borne streams of particles.

Finnie[19], Sheldon[20] and Bitter[21] have shown that the effect of impact angle on wear differs for hard materials susceptible to fracture and ductile materials susceptible to cutting. Wear for hard materials is most severe under normal impact conditions and decreases as impact angle falls to zero. In contrast, wear for ductile materials is notionally zero at normal incidence but rises to a maximum in the 15° to 30° range. Intermediate forms of behaviour are also known to occur[20]. The wear rates for ductile and brittle solids follow different curves as shown in Figure 2.6 which suggests two different mechanisms of erosion, dependent on whether the eroded solid is ductile or brittle.

For a ductile solid the peak wear rate occurs at around 20°. In this case, material is removed by a micro-cutting action and the surface is scratched in the direction of fluid flow in the localised areas of impingement. Therefore, high surface hardness is used to resist this form of erosion and brittle materials may be used since fracture is unlikely at low impact angles unless the particle velocity is high.

Brittle materials show maximum wear at approximately 90°. At these angles for a ductile material a fatigue mechanism is probably predominant. For brittle materials surface cracks are formed which link to give the wear particles. A deformed or roughened surface is evident with some surface pitting which may be on a large scale if the impact velocity is high. The ability of a material to resist high impact angle erosive wear depends on the amount of energy it can absorb before fracture, as indicated by the area under its stress-strain curve. Thus, tough ductile materials are superior to hard brittle materials when the impact angle is high. In both forms of wear, ductile and brittle, the wear rate is proportional to the kinetic energy of the impinging particles, that is to say, the square of the velocity of the particles.

Although the above introduction to erosion would seem to render it quite a straightforward wear process, actually defining it is a more difficult matter. For instance, there are different sub groups of erosion, fluid erosion (caused by small drops of liquid travelling at speeds of about 1000 ms^{-1}), cavitation erosion (when bubbles formed in a fluid implode against the surface of a solid) and spark erosion (when an electric spark occurs between two surfaces resulting in permanent damage in the form of metal removal and deposition). Macmillan[8] has suggested that the common feature in all of the forms is *removal of material from a target via a series of independent but qualitatively similar impact events.* The important word in the preceding definition is *independent*. To achieve this the duration of each particle-target interaction must be short compared with the time between particle-particle collisions.

2.24 Corrosive Wear

Corrosive wear is one of the examples of two wear mechanisms operating simultaneously. When rubbing takes place in a corrosive environment, either gaseous or liquid, then surface reactions take place and reaction products are found on one or both surfaces. These reaction products are commonly poorly adherent to the surfaces, and further rubbing causes their removal, rendering fresh material that is susceptible to further corrosion. Alternatively, many metals are resistant to progressive reaction with mildly reactive media by virtue of oxide films or passive reactive layers. In a wearing situation, these films or layers may be removed by mechanical interaction so that bare metal is continuously exposed to the medium. Thus corrosive wear is a synergistic process involving both corrosion and rubbing. That is to say, media not normally corrosive to the protected metal become so and this may accelerate the loss of material to a value greater than that which would be lost by either the corrosion or the wear process alone. For example, the rate of growth of an oxide film on steel will decrease exponentially with time, and therefore unless the oxide film is removed by rubbing, the metal-to-oxide reaction will become negligibly small.

The presence of a lubricant usually protects the surfaces from the corrosive environment. However, it is not uncommon for corrosive elements to be dissolved in lubricants, for example water in oil, and also lubricants can be degraded in time and become progressively more corrosive.

Where corrosion is a major cause of wear, there is usually a complex interaction between various mechanisms. The original wear of surface films can be due to either adhesion or abrasion. Since many commonly occurring films, notably iron oxides, are abrasive, the corrosion and abrasion will combine. High contact stresses can cause enhanced corrosion locally, leading to pitting. It is well known that internal stresses in metals, caused during forming operations, cause stress-corrosion cracking when in a corrosive atmosphere. This, combined with surface rubbing, can result in catastrophic wear.

Corrosion and corrosive wear increase with increasing temperatures. At high temperatures (say, above 500°C) the process is mainly one of gross oxidation, and frequently high chromium alloys are used because of their ability to form protective chromium oxide layers. In any wear situation involving fluid flow (e.g. impact by fluids and cavitation erosion) corrosion may also be a problem. It is impossible to generalise on the appearance of corrosively worn surfaces because such a large number of situations are possible that identification is a matter of judgement.

Selection of surfaces to resist corrosive wear is usually made on the basis of preventing the corrosive effect.

2.25 Fretting

Fretting is a wear phenomenon occurring between two surfaces loaded together having oscillatory relative motion of small amplitude. This is a common occurrence, since most machinery is subjected to vibration, both in transit and in operation. Basically fretting is a form of adhesive wear, the normal load causing adhesion between asperities and the vibrations causing rupture as described earlier. The characteristic feature of the mechanism is the appearance of a reddish brown surface and a debris which is often referred to as "cocoa". Because of the oscillatory small amplitude motion (130 μm) the surfaces are never brought out of contact and, therefore, there is little opportunity for the products of the action to escape. The oxide particles are abrasive and, because of the close fit of the surface, cannot readily escape. Further oscillatory motion causes abrasive wear and oxidation and so on, showing that fretting is another combined wear type.

Fretting appears to consist of three basic processes:

(i) oxide films on the surface are disrupted by mechanical action exposing clean and possibly strained metal, which would be reactive and in the presence of the atmosphere would oxidise rapidly during the half cycle after the disruption, to be redistributed on the return half cycle.

(ii) the removal of metal particles from the surface in a finely divided form by a mechanical grinding action or by the formation of welds at points of contact which are subsequently broken at a surface other than the original interface, either by direct shearing or by a local fatiguing action.

(iii) oxide debris resulting from (i) or (ii) act as an abrasive powder which continues to damage the surfaces.

As fretting generally occurs because of vibration, the problem may be eliminated by removing the source of vibration. Other measures may also help such as surrounding the contact area with lubricant reducing adhesion. At the same time oxygen may be eliminated which prevents the formation of iron oxide. Hence adequate sealing can prevent fretting. Also particular fretting problems have been overcome by employing suitable surface coatings which help to prevent adhesion.

2.26 Fatigue Wear

Surfaces can wear by several processes which are initiated and controlled by a fatigue mechanism. This form of damage occurs on surfaces which come into repeated contact at stresses higher than the fatigue limit. Surfaces can wear by loss of fragments separated from the surface by fatigue cracks. The cracks form at or beneath the surface and propagate in a direction dependent on the sub-surface stress distribution and stress-raising discontinuities.

With concentrated loads, the cracks often originate at the surface and propagate into the material along a curved path leading back to the surface. The resulting damage is termed pitting as smooth bottomed cavities or pits are formed. The number of stress cycles required to initiate pitting decreases with increasing stress level and data is frequently presented as a stress vs. cycles (S/N) curve. Pitting, once initiated, is progressive unless arrested by increased material strength due to work hardening or by reduced localised stresses after bedding-in.

The evidence of fatigue is usually fairly obvious and takes the form of the characteristic striations radiating from the point of fatigue initiation. The fatigue striations may not be so obvious where the surfaces continue to rub against each other after fracture initiation or if they are obscured by corrosion products.

Two approaches are adopted in trying to achieve greater fatigue resistance, the first of which should be an attempt to reduce the surface contact stress level while the second involves improved materials. Often it is the surface properties of a material that play a crucial role in preventing fatigue. For this reason, hardened layers (e.g. carburized, nitrided) are widely used.

Besides having increased fatigue strength the case usually has beneficial residual compressive stresses. Care is needed in selecting the appropriate case depth in relation to the applied stress levels and the strength of the underlying material as sub-surface shear stresses reach a maximum at some depth beneath the surface. Sub-surface fatigue may be initiated if the shear stresses are sufficiently high. Also, if the material below the case deforms excessively under load, fatigue cracks may be initiated at the interface between the substrate and the hardened case. Cracks will propagate readily along a case/subsurface boundary if the hardness gradient is severe or if the bond, as with overlay coatings, is poor. Where large areas of case are removed the damage is termed spalling or case-exfoliation.

Surface fatigue may also be initiated by alternating stresses produced by the expansions and contractions of a material subjected to temperature gradient fluctuations. This is termed thermal fatigue and, in the context of wear is mainly associated with non-ductile materials having poor thermal conductivity, although if temperature gradients are severe other materials can suffer from this type of damage.

2.30 Surface Engineering

It was in the early 1980's that the multidisciplinary subject of *surface engineering* was developed. It was brought about by the recognition that the vast majority of engineering components can degrade or fail catastrophically in service through such surface related phenomena as wear, corrosion and fatigue. Bell [22] has given us what is generally accepted as the current definition of surface engineering:

> "Surface Engineering involves the application of traditional and innovative surface technologies to surface engineering components and materials in order to produce a composite material with properties unattainable in either the base or surface material. Frequently, the various surface technologies are applied to existing designs of engineering components but, ideally, surface engineering involves the design of the component with a knowledge of the surface treatment to be employed."

Another factor which has stimulated the development of surface engineering is the growing commercial maturity of surface technologies, such as electron beam processing, plasma thermochemical techniques, innovative engineering coatings (e.g. electroless nickel), ion implantation and, more recently, duplex surface modification methods.

From the discussion of wear in the previous section, it is clear that wear is overridingly a surface phenomena. Therefore, alongside better component design, the use of surface engineering is the most common solution to tribological problems. The section on wear also gave an idea of the material properties required to resist the differing forms of wear. These properties can either be obtained in the bulk form or in layers produced on the surface of different substrate materials. Most wear resistant materials are hard and have low values of toughness and are, therefore, more difficult to process than traditional forming materials and consequently, can only be made in simple shapes. However, the use of surface layers enable a tougher substrate of a more complex shape to be processed at a far lower cost.

There are essentially two broad categories of surface modification, those in which the hardened surface is produced by a heat treatment, usually accompanied by or preceded by the diffusion of elements, e.g. carbon or nitrogen, into the surface and those in which a layer of hard material is formed or deposited on the surface. Coatings may generally be classified as either *thick* or *thin*. Initially this was determined solely by the coating thickness but now a new definition has been advanced[23]. It states that if a coating is used for its surface properties (electronic conductivity, catalytic activity etc.) it is a *thin* film, whereas, if it is used for its bulk properties (corrosion resistance, thermal barrier etc.) it is a *thick* coating.

Figure 2.7 shows the principal processes which appear within these two categories. Most of these contain sub-variants making a vast array of surface coatings and treatments. Therefore, it would be impossible to give a detailed description of all of the surface treatments that exist in this review, instead the reader is referred to some of the many textbooks that are written upon the subject[24,25,26].

Unfortunately, selection of coatings or treatments is complicated by the use of trade names and the fact that similar surfaces can be obtained by different procedures. Davis et al[27] have highlighted the lack of tribological input into typical selection procedures as shown in Figure 2.8. In recommending a surface engineering solution to a wear problem several fundamental points need to be considered (Figure 2.9).

2.31 Gate Valve Requirements

In the case of the gate valve, the surface must be hard enough to resist sand particle abrasion and erosion. A tough material would also be desirable with a strong coating/substrate bond strength. Corrosion resistance must also be considered, although this can largely be overcome by use of a corrosion resistant substrate. Cost is not a factor in subsea applications. Of the surface coatings listed in Figure 2.7, the ones that have found use in the application are cast or weld surfaced stellite, thermally sprayed tungsten carbide, hard chromium plating or electroless nickel plating

(ENP). The last two have tended to be avoided in recent years due to a widespread history of difficulties in achieving satisfactory quality control during manufacture.

Hard seated valves do not allow the same amount of compliance as that permitted by soft seated valves. Consequently, far higher engineering tolerances are required and this may be the reason why diffusion treatments that produce distortion are not favoured. However, a ferritic treatment such as nitriding which offers low distortion of the workpiece may be worth investigation and, in fact, some valve manufacturers are considering using this idea.

2.32 Diffusion Treatments

Diffusion coatings are produced by bringing suitable elements into contact with the surface of a metal at high temperatures so that those elements diffuse into the surface, change its composition and improve its properties. Diffusion treatments are widely used to improve wear resistance as well as corrosion and heat resistance. By incorporating various elements into the base metal it is possible to combine a hard and wear-resistant surface with a low cost, strong and tough base. It also has the advantage over surface coatings in that there is no distinct coating-substrate interface, which can prove to be a weakness in coatings.

2.33 Carburizing

The most commonly used diffusion treatment, which is also the oldest historically and the cheapest is carburizing with approximately 20% of all heat treatment furnaces used for this treatment, at least on an intermittent basis[28]. Essentially, the carbon content of the surface is increased by introducing it to a carbonaceous environment, either solid, liquid or gas at a temperature of 850-950°C to obtain reasonable diffusion rates. The surface is subsequently hardened and tempered. The process is applied to steels with a low initial carbon content (<0.45%), which readily absorb more carbon.

Depending upon the composition and processing variables, the carburized surface can have a hardness of up 800 H_v and a case depth from less than 0.5 mm to more than 1.5 mm. Some distortion occurs during processing and subsequent grinding is frequently necessary which can prove a limitation in tight tolerance components.

2.34 Nitriding

The principle of nitriding involves nitrogen being introduced to the steel surface by heating to 490-530°C in an atmosphere of ammonia (gas nitriding) or exposing it to a low pressure nitrogen-hydrogen atmosphere in an electric glow discharge (plasma nitriding). Plain carbon steels will not harden substantially so alloy steels must be used with nitride-forming elements, Al, Cr, Mo, V etc. required to confer maximum hardness[29]. As the process is carried out at a low temperature and no subsequent heat treatment is required, there is little distortion of the component. Moreover, the hardness developed is temper resistant up to at least 500°C. However, because of the low temperature of the treatment, process times are much longer than in carburizing for a given depth of surface layer and, therefore, layer depths are usually not greater than 0.7 mm.

2.35 Weld Surfacing

The technique is similar to welding where a consumable electrode is deposited on the surface. Any of the normal welding processes can be used: oxyacetylene, manual metal arc (MMA), tungsten inert gas (TIG), plasma arc, metal inert gas (MIG) etc., allowing a great flexibility of choice.

The cobalt based alloys developed under the trade name of Stellite are the most commonly used in gate valves. They are based on the ternary system cobalt-chromium-tungsten. The presence of chromium forms a closely adherent oxide film which provides oxidation and corrosion resistance and this element, together with tungsten brings about appreciable secondary hardening by the precipitation of carbides.

Welded deposits can be deposited in thicknesses greater than most other techniques, typically in the range 3-10 mm. The adhesion to the substrate is high as a metallurgical bond is formed which will withstand mechanical and thermal shock without detachment.

2.36 Thermal Spraying

Thermal spraying has the advantage that it possible to produce coatings of materials that are unable to be reproduced by other means, in particular ceramic coatings. Thermal spraying can be sub-divided into flame, arc and plasma spraying as well as high velocity processes such as detonation gun. All are line-of-sight processes and, therefore, only limited shapes may be coated.

Thermal spraying is a particulate deposition process where solid powder particles are injected into a high temperature gas where they are heated, softened and melted and then sprayed at relatively high velocity onto a substrate where they impact and form a coating consisting of many layers of thin overlapping lenticular particles, or splats.

It differs from other surface coatings and treatments by the following typical features:

(i) It is a cold process. The energy source is separated from the substrate so that it is possible to realise refractory coatings on low melting point materials.
(ii) The particles of the injected powder undergo physical changes such as melting followed by freezing and even sometimes chemical modifications during the spraying process.
(iii) The coatings are built up particle by particle and have a lamellar structure.
(iv) When impacting and crushing onto the substrate surface, the particles are quenched rapidly (up to 10^6 Ks^{-1}). The resulting coatings may consist of metastable or even amorphous phases.

The properties of the coating will depend upon the starting materials, on the microstructures obtained, on the residual stresses induced whilst spraying and on the porosity of the coating (open or closed). However, the coating/substrate interface is also a critical factor.

2.37 Flame Spraying

The simplest form of thermal spraying is by heating coating particles or wire to their melting point, by the continuous chemical combustion of gases, usually oxygen with acetylene or oxygen with hydrogen. Flame spraying can be split into two sub-groups: *powder spraying* and *wire spraying*.

In powder spraying, the velocity of the flame accelerates the molten particles to over 100 ms^{-1} and impacts them on the substrate surface.

In wire spraying, the coating material in wire form is fed through the flame. Compressed air is directed at the near molten tip reducing it to a spray stream of small particles (up to 0.15 mm in size). This has a heat source temperature of nearly 3000°C and gives particle velocities of 200 ms^{-1}.

2.38 Electric Arc Spraying

In this method of thermal spraying two metallized wires are melted in an electric arc and the molten particles are projected by compressed air on to the prepared workpiece. The wires are fed through electric contact tubes which electrically energise the wires and guide them to an intersecting point in front of the compressed air nozzle. The speed of the two wires is adjusted so that a continuous electric arc can be maintained between the ends of the two wires.

In general, however, the relatively low spraying velocities used in these processes result in lower density coatings with higher values of porosity and, therefore, they have not proved suitable for gate valve applications.

2.39 Plasma Spraying

Plasma arc spraying uses the very high temperatures (greater than 10,000°C) that exist in a gas constricted electric arc in a water cooled nozzle. The heated expanded gas is used to melt and propel powder particles onto a substrate to form a dense, well bonded coating. It is a continuous coating process and not only can high melting point materials be applied, but the starting powder composition can be retained in the coating because an inert gas is used.

Although plasma spraying has been used to some effect on oilfield components it has now been found that best results are obtained with the thermal spraying process that boasts the maximum particle exit velocity (and therefore the densest coating); the Detonation-Gun.

2.40 New Developments

2.41 The High Velocity Oxy Fuel (HVOF) Gun

The first HVOF developments were made only about 10 years ago so it can still be considered an emerging process. In the process a fuel gas such as propane, propylene or hydrogen is burned with oxygen at a high pressure to generate a high velocity exhaust jet. The powder is axially injected into the jet using a carrier gas. A schematic of the HVOF gun is shown in Figure 2.10[30,31]. The HVOF processes are particularly suitable for the deposition of carbide containing coatings with a metallic matrix. The limited temperature of the particle in the stream avoids a significant amount of the transformation of tungsten carbide. Barbezat et al[30,31] have shown that the very high kinetic energy of the particles is very important in relating to the density and the properties of the coatings produced. These coatings have similar densities, properties and wear resistance to D-gun coatings.

2.50 The Detonation Gun

For severe operating conditions, the economical way of increasing service life is to deposit ceramic or cermet hard coatings onto cheaper substrate materials. The two most important methods of producing thick coatings are plasma spraying and detonation gun. Although much work has been carried out upon the wear and friction performance of plasma sprayed coatings, little has been reported on the behaviour of detonation gun coatings. This is mainly because the detonation gun is a proprietary process of Praxair which has limited the availability of test samples.

2.51 Tungsten carbide deposits

At present, the deposition of tungsten carbide in a cobalt matrix by detonation gun is by far the most widely used treatment for gate valves and seats. Although expensive (over twice that of plasma sprayed coatings), the coating possesses the best available coating substrate bond strength (up to 170 N/mm^2), a porosity of 0.5% and a hardness of approximately 1300 H_v.

2.52 The Detonation Gun Process

The Detonation Gun (or D-Gun) is a member of the family of thermal spray processes. It has been used in industry for over thirty years and was developed and patented by Union Carbide Corporation[32].

The Corporation is the sole operator of the process and has one or more plants in most Western countries. In the U.K. the coatings are only available through Union Carbide's coating arm, Praxair. The higher prices charged for coating components by D-gun are accounted for by the comparatively high cost of installation and the low spray rate. The process is mainly used to coat components which are to operate under conditions of severe abrasive or percussive wear where the abrasion resistance or the bond strength of plasma sprayed coatings is inadequate.

The main D-gun coatings are either oxides or carbide-metal cermets, such as alumina or tungsten carbide, the properties of tungsten carbide coatings are given in Table 2.1. The coating structure, like that of other sprayed coatings, consists of a series of laminations parallel to the substrate surface. The porosity is usually low (½ to 1%) and the reported coating substrate bond strength for tungsten carbide-cobalt coatings is above 170 N/mm^2. This value is more than twice that reported for the corresponding plasma sprayed coatings.

2.52.1 Principle

The Detonation Gun consists of a water-cooled barrel approximately 1.4 m long with an inside diameter of 25 mm closed at one end, Figure 2.11. At the closed end is a sparking plug and a system of valves through which are metered the appropriate quantities of acetylene, oxygen and the powder to be sprayed. The gas mixture is ignited either 4.3 or 8.6 times per second (generally the latter), depending on the type of coating being applied. A short period of burning or combustion ensues, the flame front accelerates, compressing and heating the gas zone immediately ahead of it. Depending upon the gas mixture being compressed, a critical temperature is reached and self-ignition of the gas occurs, producing a detonation or shockwave. The shockwave compresses and raises the gas temperature inducing chemical reaction of the gas mixture, producing gas temperatures greater than 3,000°C. The detonation wave in the case of oxygen and acetylene mixtures of 50/50 volume percent travels at 2930 ms^{-1}.[33] If the powder particles are suspended in the gas mixture prior to detonation the rapid expansion of the reacted gases forces the particles from the nozzle at approximately 800m/s, with the higher particle velocity than a plasma device being achieved because of the greater distance the powder is carried through the gun[34]. The actual particle velocity reached will depend upon a number of factors: chemical gas mixture, barrel length, size of powder particle and position of the suspended powder prior to detonation. The maximum free burning temperature of oxygen acetylene mixtures occurs with 45% acetylene and is about 3140°C, but under detonation conditions probably exceeds 4200°C, so most, but not all materials can be melted[35]. After the powder has exited the barrel, it is purged by a pulse of nitrogen.

The repeated detonation cycle produces a coating structure which is built up of a series of detonations or *pops* on the prepared substrate which is placed 50-100 mm in front of the barrel. Each pulse of powder results in the deposition of a circle of coating about 50 μm in diameter and a few microns thick. This circle is, of course, composed of many overlapping thin lenticular particles or splats corresponding to the individual powder particles. The total coating is, in turn, produced by many overlapping circles or coatings. Large areas can be coated by movement of the workpiece to overlay successive pops.

The molten coating powder particles which leave the end of the detonation gun barrel impact on the substrate and form a fine grained, dense, laminar coating composed of many layers. On impact, the molten particles are flattened by the release of their high kinetic energy into thin overlapping platelets such that their diameter is many times greater than their thickness (approximately 50 μm and 6 μm thick). The high kinetic energy of the particles is approximately twenty-five times that of the energy in particles produced by combustion spraying processes. This energy is converted to additional heat on impact and, with some coatings, produces a metallurgical and mechanical bond between the coating and the substrate and also between coating particles. However, as the particles are generally extremely fine, the overall heat input into the substrate is very low. Deformation and/or modification of the substrate microstructure can be avoided by cooling the substrate with a jet of CO_2 which maintains the temperature below 150°C. The cooling gas stream may be from an annular ring around the flame nozzle, or separately directed jets. The high kinetic energy generated enables the particles to completely deform on impact and so result in high density, extremely low porosity coatings. Coating thicknesses are usually in the order of 0.1 to 0.3 mm.

A characteristic of all detonation gun coatings is their high substrate to coating bond strength. For some applications, however, it has been considered advisable to increase further this bond strength and this is accomplished by heat treatment at an elevated temperature (e.g. at 1080°C for 4h in vacuum) to create a diffusion bond between the coating and the substrate[36].

The combustion gas can be neutral, oxidising or reducing and its temperature can be controlled by addition of nitrogen (to cool) and hydrogen (to heat). The rate of deposition for a 250 μm coating is either 48 or 96 mm^2/s, depending on whether the gun is operated at 4.3 or 8.6 detonations per second.

Due to the extreme noise level of the process (150 dB), the equipment is housed in sound-proof double walled concrete cubicles. Spraying is carried out remotely from a console located outside the cubicle, with components being mechanically rotated and/or traversed in front of the gun.

2.53 Loss of Tungsten Carbide During Deposition

The most important work that has been conducted concerning the theory of how detonation-gun coatings are formed was produced by Simma and Ratnichkin[37], who investigated the loss of tungsten carbide from a detonation-deposited coating of mechanically mixed tungsten carbide and nickel. Chemical analysis of the coating revealed that the nickel content of the coating had risen to 30-35 wt% and the tungsten carbide had reduced by 15-20%.

2.53.1 Particle Deposition

Simma and Ratnichkin's work continued by spraying both tungsten carbide and nickel particles into water and onto glass respectively.

Spraying nickel into water was found to produce some spheroidal particles of less than 6 μm. Particles above this size had not undergone any change. Particles deposited on glass were examined and because of the difference in sizes between the particles and hence the variation in kinetic energy they possessed, some particles were found to melt and spread on the glass surface, whilst some drops on hitting the surface had disintegrated. It is known that nickel experiences practically no melting in the barrel of the gun so it could be concluded that the particles melted on hitting the base plate.

Conversely, the deposition of tungsten carbide particles on glass, produced chipping of the glass which was caused by particles which did not melt during impact, and did not take part in coating formation.

2.53.2 Particle temperatures and velocity on impact

On the basis of the above experiments, the temperature and velocity at the instant of impact for the particles could be calculated, with the assumption that at the instant of impact the whole kinetic energy of a particle was converted into heat.

From the equality of the kinetic energy of a nickel particle and the amount of heat required for melting it, it is possible to find the velocity attained by particles as a result of the action of detonation products in the barrel of the gun:

$$v = \sqrt{2[c(t_m - t_{im}) + \lambda]} \qquad \textbf{2.5}$$

where c = specific heat of nickel ($Jkg^{-1}K^{-1}$)

t_m = melting point of nickel (K)

t_{im} = temperature of a nickel particle at the instant of impact against the base surface being coated (K)

λ = latent heat of melting of nickel (J/kg)

The temperature at the instant of impact against the surface being coated must be determined first, before the velocity of the particle can be calculated in Equation 2.5. A calculation for the thermal state of particles was made with the assumption that all the particles, irrespective of their size, remained in the detonation products for the same length of time.

The experiments on the deposition of nickel into water had revealed the maximum diameter of spheroidized particles to be 6 μm. The amount of heat required for melting these particles (where m is the mass of the particle) can be found by:

$$Q = m[c(t_m - t_o) + \lambda] \qquad 2.6$$

If the initial temperature, t_0, of the powder being deposited was not more than 20°C (temperature of the room in which deposition was performed), then the amount of heat necessary for melting a 6 μm diameter nickel particle was 9.5×10^{-10}J. In Equation 2.5, both the velocity of the particles being deposited and the temperature of the gas are variable, so the use of an equation for convective heat exchange between a gas stream and solid particles to determine their temperature is difficult. However, it is possible to determine approximately the amount of heat received by particles of various sizes during their residence in the gas stream, Q, from the specific amount of heat, Q_0, because the amount of heat received by particles during convective heat exchange depends on their surface area.

$$Q = mc(t_{im} - t_0) \qquad 2.7$$

The temperature of a particle at the instant of its impact against the base plate can be obtained by transforming Equation 2.7 and introducing the specific amount of heat Q_0.

$$t_{im} = \frac{6\,Q_0}{(\gamma\, c d_i)} - t_0 \qquad 2.8$$

where d_i = the size of an i^{th} particle (m)

— γ = density of nickel (kgm^{-3})

Q_0 = Q/F specific amount of heat (Jm^{-2})

Q = amount of heat necessary for melting a 6μm diameter particle (J)

F = surface area of 6μm particle (m^2).

2.53.4 Nickel particle velocity

Figure 2.12 shows the particle dependence of the temperature attained by nickel particles prior to the instant of the impact against the surface being coated. With nickel particles in the range of 20-40 μm, calculations established that at the instant of impact against the base plate, nickel particles had heated up to between 300°C and 600°C. When this temperature is known, it is possible from Equation 2.5, to calculate the velocity required for the particle to completely melt. For complete melting of a 40 μm diameter nickel particle a velocity of 1280 ms^{-1} was required, i.e. the maximum kinetic energy of the nickel particle in the detonation-deposition process attained 8.2 x 10^{-6} J. The maximum velocity of the particles and their kinetic energy were slightly less than the values obtained as a result of certain assumptions made in the calculations.

2.53.5 Tungsten carbide particle velocity

The velocity of tungsten carbide particles was also close to the values given by the calculations. However, it was discovered by experiment that the velocity of the particles was insufficient to melt the particles due to the much higher melting point of tungsten carbide. During the deposition of tungsten carbide particles without a binder, the particles, being hard, experienced no deformation on hitting a hard plate. The high temperature reached by the particles, however, resulted in their oxidation and for these reasons it is not possible, at present, to produce a tungsten carbide coating without a binder.

2.53.6 Mechanism of the formation of a tungsten carbide-nickel coating

On impact with the surface being coated particles penetrate into it. The nickel particles deform and melt completely, whilst the tungsten carbide particles implant themselves in the melt. The molten nickel particles solidify almost instantaneously, firmly gripping the tungsten carbide

particles. The process is repeated in each cycle. As noted previously, the coating experiences a considerable loss of tungsten carbide on being formed.

The loss of tungsten carbide during deposition, may be reduced by coating the carbide particles with a nickel shell prior to deposition, to prevent the disintegration of the tungsten carbide particles. On colliding with the surface being coated, the nickel shell melts and molten metal flows off the tungsten carbide particles. Under these conditions the tungsten carbide particles are surrounded by molten nickel which reduces the loss of the carbide to not more than 2-5 wt%.

2.53.7 Coating adhesion

The adhesion of the nickel coated tungsten carbide particles coating is lower than the coating of mechanically mixed tungsten carbide and nickel coatings. This is accounted for by the fact that adhesion of a coating depends on the number of its metallic bonds with the substrate, so that the higher nickel content of the mechanically mixed particles gives a stronger adhesion to the substrate.

2.54 Bond Generation

The conditions under which bonds are established during deposition between the particle and substrate are of considerable importance from the point of view of reliable operation of the coating. The mechanical action of the particles being deposited on the surface layer of the substrate play the key role, i.e. the velocity of its particles determine the adhesion of a coating to its substrate. Under detonation spray-deposition conditions the substrate surface can also become activated by the local heating of contact sites during the melting of particles. Contact between a particle at high temperature and the substrate will be longer the greater the mass of the particle and the less intense the heat transfer to the substrate surface.

2.55 Bond strengthening

The activation of the surface, by the mechanical action of the deposited particles on the substrate surface and mutual local heating of the particles and their sites of contact on the substrate, is not always sufficient for the formation of strong bonds. By employing deformation of the surface layer of the substrate as an additional means of activating the surface, the bonds between the substrate and the coating particles can be strengthened. The surface is also rougher which increases the strength of adhesion of the coating.

2.56 Substrate Material

Most metallic materials can be coated by Detonation-Gun, the only restriction being that surface hardness should not exceed 58-60 Rockwell C. Generally, non-metallic substrates cannot be coated. Because of the exceptionally high particle velocity of the D-Gun it is not always necessary to grit blast softer substrates, as the particles themselves will cause substantial surface roughening.

2.56.1 Substrate Preparation

Substrate surfaces are first degreased and then grit blasted, usually with alumina. Other types of grit are also used, mainly chilled iron, however, alumina is preferred as it has been found to offer the least contamination of the substrate material. Grit blasting will create enough surface roughness to ensure a strong mechanical bond between the coating and substrate and leave a chemically active surface which, providing the spraying process is carried out shortly after grit blasting will also provide a strong metallurgical bond. However, the treatment also leaves a certain amount of grit residue, normally referred to as contamination, trapped in the surface. These residues are known to weaken the adherence of the coating, especially for those coatings operating at high temperatures and exposed to mechanical loading. Wigren[38] has carried out a survey of the influence of grit blasting parameters on surface roughness and contamination for plasma spraying (the grit blasting procedure is similar to D-Gun) and found that the effect of grit blasting passes through an optimum with respect to blasting time. A 45° attack angle led to

less residue than 90° and higher pressures coupled with shorter blast times are preferred over lower pressures and longer times in order to obtain a certain R_a. It is also advisable to warm the substrate slightly, usually with a pass of the torch without powder flowing, to remove any adsorbed gases from the surface before applying the coating[35].

Regardless of the method used, the surface roughness should normally exceed 6 μm R_a. In addition the surface topography should be sharply peaked not smoothly undulating. Excessive grit blasting, on the other hand, can be detrimental due to work hardening, blunting of the peaks and increased grit entrapment.

Grit blasting increases the surface area significantly, so whether bonding discussed elsewhere, is due to mechanical interlocking, interdiffusion, surface reaction or a combination of these, it is advantageous in increasing bond strength. In whatever circumstance the coating should be applied as soon after grit blasting as possible to ensure an active, clean surface.

2.57 Masking

The masking of component areas, which are not to be coated, is more difficult for detonation-gun than for other thermal spray processes. The coating particles have a very high energy and will quickly erode masking tapes and stop-off paints. It is, therefore, necessary to use metal masks placed adjacent to the coating area. The shape and position of the mask is important so as not to deflect coating particles off the mask into the coating area.

2.58 Mechanised coating equipment

The detonation-gun is similar to other thermal spray processes in that it is essential to apply the coatings in a systematic, consistent manner in order to achieve high quality, reliable coatings. It is now common practice to mechanise the movement of the coating equipment and substrate component. Hand held torches lead to varying stand-off, poor thermal control and non-uniform thickness - all of which result in varying coating properties across the part. The main parameters

that must be controlled include the gun to workpiece or *stand-off* distance, the relative speed of the torch to workpiece and correct overlap pattern of each coating pass. The coating effluent angle of impingement must also be controlled so that it is in the range 90° to 45° to the workpiece surface for optimum coating properties. The most commonly used method of part and torch motion control utilises a modified lathe concept, with the torch mounted on what would be the tool post and the parts to be coated either rotated as a cylinder or mounted on an annulus plate. One method of controlling relative motion, particularly suitable for D-Gun where lower surface speeds can be used, is that of traversing and indexing in a raster pattern. Using this technique, very large flat surfaces can be coated. More extensive automation has been developed including part transfer handling and computer control of the torch, which tremendously increases the productivity of the equipment[33].

2.59 Limitations

The D-Gun cannot fit into a cylinder or other cavity. It can be used, however, to coat an inside diameter to a depth about equal to the diameter; i.e. to an angle of deposition of about 45°. Whilst there is some change in microstructure as the angle decreases, the inherently high density and bond strength still allows superior coatings to be deposited at lower angles.

2.60 Powder

Most powder used for D-Gun deposition falls between 5 μm and 60 μm in size. To achieve uniform heating and acceleration of a single component powder, it is advisable to have as narrow a size range as is possible. The additional cost of sizing is, at least partially, recovered in higher deposition efficiency and better coating quality. The specific powder size range to be used is a function of the gun design and heating characteristics of the powder discussed earlier. Generally speaking, fine powders are accelerated and heated more rapidly in the gas stream, but they also tend to lose momentum more rapidly when spraying at the longer distances. They generally result in denser, but more highly stressed coatings. Finer powders also tend to create more torch operating problems and have higher oxide contamination levels.

Good quality control of powder is essential, not only during manufacture, but during storage and handling. Powder specifications and quality control should include, as a minimum, chemical analysis (including interstitials for metallic powders), shape characterisation, size distribution and flowability. The powder should be kept clean and dry otherwise dispensing problems, torch clogging and lumps in the coating will occur.

It is essential to have efficient dust extraction and adequate ventilation equipment for comfortable, safe working for the operator.

The typical tungsten carbide powders used in the cemented carbide industry cannot be employed for spraying. Powders produced by conventional milling are too fine and do not flow freely. Several processes have been developed for the production of powders suitable for plasma spraying, and similar technologies are used for detonation gun coatings. These include melting and crushing of powders, coating tungsten carbide particles with cobalt or nickel and agglomerating cobalt and WC powders[39]. For LW45 coatings, the powder is a mixture of W-C-Cr-Co.

2.61 Quality Control

Few non-destructive tests are applicable for detonation-gun coatings so control of coating parameters and materials is essential. The common method of quality control is to coat samples for metallurgical evaluation before spraying the components. The coating structure is subsequently examined for freedom from cracks, delamination, grit inclusion, oxide content and porosity. Microhardness may also be measured.

2.62 Finishing

Although detonation-gun coatings can be used "as-coated" (in fact in at least one application, a D-Gun tungsten carbide coating is grit blasted to further roughen the surface for gripping action[35]), it is usual to finish the article in some way so as to give particular topography finishes

and/or dimensional tolerance. As such, the as-coated thickness will be in the order of 0.25 mm before it is finished to its required thickness. The as-coated roughness is in the order of 3.0 μm CLA and is usually reduced by first grinding with silicon carbide or diamond and then lapping the specimen. This can give finishes in the order of 0.5 μm CLA.[40]

Great care should be exercised in finishing operations to avoid damaging the coating through heat checking, pull-out or edge chipping. A typical procedure is used by Praxair[41]. The standard is confidential but a simplified version is given by Tucker[35].

2.70 Wear Testing of Detonation-Gun Coatings

A recent study by Wang[42] has indicated that D-Gun sprayed hard coatings have higher hardnesses, densities and wear resistances than corresponding plasma sprayed coatings. Wang used a pin-on-disc configuration with specimen pins rubbed against a plasma-sprayed WC-12%Co disc. It was found that D-Gun sprayed Cr_2O_3 coating exhibited the highest wear resistance, higher even than that of sintered WC-6%Co hard metal. From examination of worn surfaces, Wang suggests the failure mechanism to be stress fatigue. Although the WC particles possess very high strength, the Co binder around the particles is relatively weak. Hence, the failure originally takes place at the Co binder under the repeated cycle friction force and eventually, the WC particles would be spalled.

2.80 Characterisation of Tungsten Carbide Coatings

Although much work has been carried out on the effects of the characteristics of raw materials on the characteristics of plasma sprayed WC-Co coatings and their wear performance, no published data is available for corresponding D-Gun coatings. Ramnath and Jayaraman[43] found that the coating characteristics were affected by the particle size, chemistry, phase composition and porosity of the powder, factors which are dependent on the method of manufacture of the powder. In turn it was found that the coating characteristics such as phase composition, porosity

and carbide size affected the abrasion wear performance. In general, it was found that better abrasion wear resistance is provided by denser coatings, which have a very fine distribution of hard phases (such as η-carbides) and an absence of softer phases.

2.81 Microstructure

The major microstructural difference from other sprayed coatings is that the D-Gun coatings generally have a higher density. The microstructure consists of many layers of thin lenticular particles, the result of the impact of molten or semi-molten powder particles[44]. The impacting particles may be split with some small droplets branching out or separating from the central particle. Thus the average splat volume may be smaller than the average starting powder size and the total surface area much larger in the coating. The interface between the coating and substrate shows low grit inclusion and excellent bonding of the coatings. The proportions of coating phases in the resultant coatings will differ from that of the starting powder due to melting of fine particles, reaction with the detonation gas mixture and with the ambient air as the powder leaves the barrel. The powder can react, within the D-Gun, with the gases and result in a carbon gain or loss depending on the flow parameters chosen. The high hardness of many D-Gun coatings illustrate their high density and internal strength.

Even with high powder feed rates, the particles are deposited on already solidified layers[45]. Heat transfer calculations indicate that freezing of the particles occurs in a few microseconds and that the complete cooling cycle amounts to perhaps only 100 μsec. The zone of the underlying materials is therefore quite small, so that the temperature gradients reach 10^5 Kcm^{-1}. The wetting and flow properties of the liquid droplets are of primary importance, since they will influence the porosity within the coating and the substrate interface.

The cooling rate of the impacting particles has been estimated to be 10^4 to 10^6 Ks^{-1} for oxides and 10^6 to 10^8 Ks^{-1} for metals[46]. It is evident, however, that cooling rates may vary significantly with the substrate material and thickness of the coating. As a result of the rapid cooling, some coatings have been found to have no crystallographic structure by x-ray or neutron diffraction[35],

whereas others may have a thin amorphous layer next to the substrate followed by crystalline layers[46]. Many coatings form columnar grains within the splat in one or two layers perpendicular to the surface of the substrate.

In almost all cases where crystalline structure can be determined by x-ray diffraction, the peaks are quite broad, indicative of high local residual stresses due to rapid quenching. Phase changes have also been shown to occur[47] in plasma sprayed alumina.

In addition to phase shifts due to rapid quenching, some changes in composition may occur due to selective evaporation of one component in an alloy, to decomposition to a gas, or to reaction with the atmosphere. If the loss of a component with a high vapour pressure can be predicted, it can be compensated for in the powder manufacture. It must be remembered, however, that such a loss will be more rapid from a fine powder than it will be from a coarse powder, and it becomes more imperative to use a very narrow powder particle size distribution to ensure an homogenous coating composition.

The loss of carbon from tungsten carbide plasma coatings through oxidation of WC to form CO, W_2C and free tungsten has been reported [39,48]. Similar effects have been obtained with D-Gun coatings, both by reaction with the detonating gas mixture and with air after the powder leaves the barrel[35].

If the influence of surface tension is neglected, and assuming that the particles flatten before solidification occurs, the degree of flattening (ratio of the diameter of flattened disc, *D*, to the diameter of the initial particle, *d*.)

$$D/d = 1.29 \left(\frac{\rho . v . d}{\mu}\right)^{0.2} \qquad \textbf{2.9}$$

where:

ρ= liquid density

μ= liquid velocity

v = droplet impact velocity

The ratio will be higher either if the particle is above its melting point with reasonable velocity or if it is below its melting point, but already in the plastic deformation temperature area with very high velocity (~1000 ms^{-1}). It can be seen that the structure of a coating depends upon the velocity, temperature and size of the particles at the moment of impact.

2.90 Bond Strength

Bond strength is one of the most important properties of a coating; however difficulties are encountered in measuring it. The most frequently used test is a tensile test (ASTM-633) in which the coating is applied to the face of a one inch diameter round bar and a mating bar is epoxied to it. The limit of the test is the strength of the epoxy, about 69 MPa to 83 MPa. Most D-Gun coatings have bond strengths that exceed this so the test can only be used as a proof test. However, tests have been carried out where the mating bar was brazed to a D-Gun coating and the tensile strengths exceeded 172 MPa. Some reduction of residual stress with enhancement of bond strength could have occurred, however, during brazing.

A variety of other tensile bond strength and shear strength tests have been used, but most introduce undue stress risers. An epoxied lap shear is still used for some quality control purposes. It would be advantageous if more satisfactory shear tests were developed, as more often the coatings are loaded in shear rather than tension.

The role of grit blasting contributing to mechanical bond strength and interaction has already been discussed. There is also some microstructural evidence that when the refractory metals are sprayed onto steel, nickel or chromium, there is some interdiffusion; i.e. a metallurgical bond is formed[49]. Because of the unusually high velocity of D-Gun particles, they are actually driven into the surface of most metallic substrates. As previously mentioned, some substrates require

no grit blasting to achieve adequate bonding, since the coating itself roughens the interface. This embedding/roughening process creates atomically clean interfaces between the coating and substrate over most of the coating area which facilitates chemical bonding and can be likened to the explosive bonding of sheets of metals. This undoubtedly plays a large role in forming the unusually high bond strengths of D-Gun coatings.

Subrahmanyam et al [39], plasma sprayed tungsten carbide on to a mild steel followed by treatment at 1373 K for 1 hour in vacuum. They found that WC and tungsten react with cobalt forming Co_3W_3C and also that interdiffusion of cobalt and iron occurred at the interface. It was found that the heat treatment improves the adhesion of the coating to the substrate and also its scratch resistance.

2.91 Residual Stress

Residual stress occurs as a result of cooling individual powder particles or splats from above their melting point to the temperature of the part. The magnitude of the residual stress is a function of torch parameters, deposition rate, torch to part speed, the thermal properties of both the coating and the substrate and the amount of cooling used. It has also been found that the use of finer powders leads to higher residual stresses, but this can generally be controlled by adjusting the coating parameters[35]. Residual stress increases linearly with coating thickness above some minimal initial thickness[50]. The rate of increase, however, is a function of the parameters of deposition already listed and of the coating material.

Residual stress has a significant effect on bond strength and must be considered when the coating is placed in service, since it detracts from the inherent mechanical strength of the coating. For example, coatings are normally in tension as a result of the residual stresses, and this stress must be subtracted from the allowable fracture stress, calculated from mechanical property tests, of free standing specimens. Residual stress is, however, reproducible and can be accounted for by adequate control of the coating parameters.

The residual stresses which develop in coatings may be subdivided into microstresses within the individual particles and macrostresses within the coating as a whole. Microstresses arise because of the restraints due to thermal contraction of individual particles as they cool in the solid state and are bonded to the underlying material, which remains at a relatively constant temperature. These stresses will, therefore, depend upon the thermal expansion coefficients of the coating material and the elastic constants of the coating and the substrate, as well as their temperature dependencies. They would also be expected to be influenced at the interface by the yield strength of the substrate, the plastic deformation of which could allow for stress relaxation, and also the effectiveness of the particle to substrate bonds.

Macroscopic residual stresses will arise during cooling of the coated structure to ambient temperature because of the differences in thermal expansion between the coating and the substrate and the presence of temperature gradients during coating formation. High interfacial stresses may lead to the peeling of the coating, whilst high tensile stress within the coating may lead to it cracking. A residual compressive stress could, however, be desirable as a method of increasing their strength. To minimise residual stresses it is necessary to reduce thermal gradients as much as possible and to keep the complete assembly at a low temperature by cooling the surface while spraying.

The maximum thickness of coating that may be deposited is often limited by internal stresses. This maximum can be extended substantially by continuous cooling of the surface during spraying but the resultant high cooling rates may correlate to a microstructure that contains amorphous or metastable phases. Coating thickness will normally be in the order of 0.1-0.2 mm for LW45 coatings.

2.92 Density

The density of detonation gun coatings is greater than 95% of theoretical, usually greater than 98 or 99%. This density is due, as with other properties, to the unusually high kinetic energy of the particles on impact.

2.93 Mechanical Properties

The mechanical properties of D-Gun coatings are anisotropic because of their splat structure and directional solidification. This anisotropy is more pronounced for cermets than for other coatings because of a greater abundance of oxidised splat boundaries.

The most frequently quoted material property is hardness. Detonation gun coatings are generally harder than corresponding plasma sprayed ones of the same composition, primarily due to their higher density and greater cohesive strength. Hardness is often used as a guideline for wear resistance and also to give an indication of coating strength. In both cases, it can be misleading and thought should also be given to impact strength and toughness when considering coating selection.

The modulus of rupture, elastic modulus and strain-to-fracture in bending both D-Gun and plasma coatings is measured more often than conventional uniaxial tensile and compressive properties because the former measurements can be made on easily fabricated, free-standing rings of coatings. However, it is often difficult to produce thick enough coatings for conventional specimens, because of thickness limitations imposed by residual stresses and the inherent brittleness of the coatings. Even most metallic coatings have a strain to failure of less than 1%. Increasing the cobalt binder content increases the strain to fracture.

LW45 coatings have a strain to fracture of around 0.2-0.3% and, therefore, the properties of the substrate material cannot be ignored when considering a coating application. One of the first considerations is that the substrate must be able to support the coating without yielding beyond the coating's strain-to-failure ratio. In some applications it is also a concern that the coating may decrease the fatigue life of a substrate. D-Gun coatings in particular are so well bonded that a crack generated in the coating may propagate into the substrate under sufficient cyclic stress. However, provided that the strain to failure ratio of the coating is not exceeded, the coating should have no measurable effect on the fatigue strength of the substrate.

2.94 Porosity

Although high porosity is desirable for some thermally protective coatings, porosity greatly reduces the strength of the coatings. Interconnected porosity is undesirable in coatings for oxidation or corrosion resistance and porosity at the interface can greatly affect the coating adhesion. The nature of coating formation by impact and solidification of separate particles, either solid or melted, necessarily results in some porosity and depends both on the spraying parameters and the material being sprayed. The porosity will then depend upon the trajectories of the particles into the hot gas used for spraying, of their heat treatment and of their final velocities; very high velocities being necessary when the particles are not melted and lower velocities when they are well melted, for they will have to flatten and not explode when they are liquid.

The porosity, although low may be interconnected and hence may have a strong influence on the corrosion rates of components in different environments. In some low temperature applications an epoxy resin is applied to seal the coating.

2.95 Corrosion Properties

The use of a coating in a corrosive environment requires that the coating itself is able to resist the corrodent, but it should be kept in mind that the corrosion resistance of a wrought, cast or sintered composition may change when coated.

All plasma and D-Gun coatings have varying degrees of interconnected porosity that allow attack of the substrate in corrosive environments. For most applications at temperatures up to about 175°C this problem can be overcome by the proper selection and application of sealant.

2.100 Summary

The operation of the gate valve and problems associated with it can now be understood. The tribological system involved is complex and can involve the majority of the different types of wear described in 2.20. Currently, the most common response has been to specify detonation gun deposits of tungsten carbide. However, in the western world, the process has remained proprietary and therefore there is a clear void in the literature concerning the tribological performance of such coatings. The following chapters aim to overcome this problem, both by assessing the fundamental wear characteristics of D-gun tungsten carbide coatings and by showing how this may be specifically related to the gate valve.

3.0 Experimental

3.10 Methodology

To achieve maximum benefit a piece of research work should have a clear methodology. In the case of this work the following procedure was used:

i) Examination of worn components to evaluate failure mechanisms.

ii) Selecting laboratory tests that mirror most closely the operating environment.

iii) Selecting the most suitable materials to test.

iv) Designing new equipment and preparation of samples.

v) Conducting the tests.

vi) Examination of test specimens to determine whether test failures are similar to real-life failures.

vii) Presentation of wear data.

viii) Discussion, conclusions and recommendations for improvement.

3.20 Examination of Worn Components

For logistical reasons it is very difficult to obtain failed real-life components and therefore, examination must be made on gates and seats that have been obtained from the valve test loop facility at BP Research Centre, Sunbury. However, valves that have been tested are always returned to the manufacturers, who are mainly located in Scotland, for stripdown and evaluation. Therefore, it is not easy to arrange the examination of worn surfaces in laboratory conditions. This problem is further complicated in that the samples are both large and heavy, making direct examination very difficult.

For the purposes of this project it was arranged for two failed valves to be sent from the manufacturers to Brunel. Because of the difficulties previously explained, examination was not only carried out directly but also extensive work was carried out using a range of replication

techniques in order to judge their effectiveness in identification of failure mechanisms. The work was also useful in that it enabled the relative effectiveness of different classes of replica to be determined.

The replication techniques to be described have been found ideal for examining the operating surfaces of gate valves in both service and test conditions, as the components are both too heavy and too large for direct examination and too valuable (and very difficult) to section. However, it should be noted that the replication techniques to be described would be just as suitable for many other components.

There is nothing fundamentally new in the replication techniques, which have been used before[51,52,53], but they have not received the attention they deserve in identification of wear mechanisms on service components. Essentially, there are three different classes of replica; namely acetate sheet, polymethylmethacrylate (PMMA) and silicone rubber. All three techniques are similar in that they polymerise on the surface to be examined resulting in an inverted impression of the surface. When removed, the replicas allow the surface topography features to be examined indirectly. The technique is non-destructive and easy to carry out. Although it is best to take a replica on a horizontal surface, they may with care and the use of suitable moulds where necessary, be obtained from both vertical and overhead surfaces.

When taken, the replicas can be examined using both optical techniques and scanning electron microscopy (SEM). Alongside this visual examination, it is possible to get quantitative three-dimension information by use of surface profilometry and by the taking of stereological pairs under the SEM. From the information obtained it is possible to identify the wear mechanisms taking place within the gate valve.

3.21 Replication Methods

A gate from a valve that had been used in BP's valve evaluation programme was obtained and upon it were marked three areas (Figure 3.1). Areas 1 and 2 have been identified as areas where

surface damage can be seen to have taken place, whereas Area 3 resembles the original surface finish. All three replication techniques were used on each of these three areas.

3.22 Acetate Replicas

A piece of acetate film (0.125 mm thick) is cut to a convenient size. The surface to be replicated is thoroughly degreased and then flooded with acetone. The acetate sheet is then placed in position in the flooded area and firmly pressed upon the surface. The acetone first softens the film allowing it to consolidate itself upon the surface before evaporating away and after approximately 20 minutes, it is possible to gently peel the acetate film off the surface. Great care is required at this stage or slight damage to the replica may occur. After peeling, the replica is inverted, placed on a glass slide and secured to the slide either by using double-sided adhesive tape or single-sided tape around the edges.

3.23 PMMA Replicas

The surface to be replicated is thoroughly degreased before a thin layer of release agent, usually silicone oil, is smeared onto the surface. It is important that the release agent layer is not too thick as air bubbles may become entrapped in it, resulting in a poor replica. The area to be replicated is enclosed either by plasticine or a pre-formed mould. The replicating powder and liquid are then thoroughly mixed together, normally in the ratio of 2:1. The resulting mixture is then poured slowly into the mould and left to stand for approximately 30 minutes, by which time polymerisation is complete and the replica is fully hard. The replica is removed from the surface by gently tapping it from a sideways direction. After inversion, the replica is ready for examination.

3.24 Silicone Rubber Replicas

The area to be replicated is thoroughly degreased and enclosed by a mould. A release agent is only necessary on very rough surfaces. The two precursors are mixed together thoroughly in a ratio of approximately 10 parts powder to 1 part liquid and poured slowly into the mould. The

time required for full polymerisation is dependent upon the particular compound used, but typically the replica will be ready for removal in 2 hours. The replica is removed by gently peeling it off the surface from one side.

3.25 Examination

All of the replicas produced were first examined under the optical microscope, before each had a layer of gold/palladium evaporated onto the surface. This was both to improve contrast under the optical microscope and to allow the replicas to be examined under the SEM.

Whilst in the SEM, stereological pairs were taken on areas of interest; this technique involves photographing the same area twice at different rotations (usually 12° apart). When viewed under a stereo imager, a three-dimensional image is obtained from which quantitative information about depths of pits etc. can be obtained by a technique shown schematically in Figure 3.2. Talysurf measurements were taken on all of the replicas to evaluate surface finish and wear scar depths and volumes.

To enable the accuracy of the replication technique to be evaluated, optical micrographs of the actual surface were taken using a specialist surface examination microscope as well as Talysurf measurements of the same area.

3.30 Wear Testing

Wear testing differs from other methods of determining a material's characteristics such as hardness testing, tensile testing etc., in that wear resistance is not an intrinsic material property, but a property of the whole operating system under examination. It is relatively straightforward to conduct the first mentioned category of test, such as hardness, and the values found can be matched to specifications. However, rarely do such tests attempt to correlate material properties directly with service behaviour, although in a few cases design codes of practice are available for this purpose. It can, therefore, be seen that the adaptation of a wear test so that the results can

be interpreted in the manner required for an effective outcome is considerably more difficult than it would be for a normal material property test and, therefore, a great deal of thought must be given into the design of the test programme.

Gee at the National Physical Laboratory in his role as co-ordinator of the UK Forum on Friction and Wear Testing has issued a set a guidelines for unlubricated sliding wear tests[54]. Many of the ideas proposed by Gee were adopted in this thesis and the author believes a review of the more important points, with notes on the relevance to this work, would not be wasted.

3.31 Reasons For Testing

In an ideal world, work conducted in the laboratory would be the first part of a comprehensive three stage study; also involving simulative testing (e.g. the BP pipe loop test) and finally evaluation in service.

Although there are hundreds of different test methods and these are still increasing in number, there are relatively few reasons for testing [55] ; these being:

1. To obtain fundamental information on mechanisms; it is usually necessary to simplify the test procedure, by running at low loads and speeds, in a controlled atmosphere using pure materials.

2. To characterise materials and to determine the effect of variations in composition, microstructure and mechanical properties on tribological behaviour.

3. To simulate service behaviour, where it is generally felt necessary to reproduce all of the variables experienced in service in the simulating test, otherwise misleading information is obtained and incorrect decisions may be made.

The third type is the most difficult because of the complexity of the situation, the tendency being either to miss out or be unaware of some important variables, or if all factors are taken into account the simulation machine ends up as a copy of the service system.

As one approaches field trials from simple laboratory bench tests, it becomes increasingly difficult to define and control the complex set of intermeshing factors that combine to determine the performance of the test system [56]. Therefore, there are many advantages in running laboratory type tests, not least an obvious cost benefit by running simple geometries on simple specimens, which are cheap and easy to manufacture. It is normally much easier to achieve good control of test conditions in the laboratory and furthermore, laboratory tests also offer more flexibility because of the ease with which the test conditions can be controlled over wide ranges, in a way not feasible for field trials.

It is important to ensure that the results from laboratory tests compare well with observed performance in practice. The final test for any product is its performance in real-life applications, but confidence in laboratory tests can be gained if the laboratory conditions simulate the real life conditions as closely as possible, although because of the difficulty of defining the conditions in applications, and because of the limitations in the test system, the match is unlikely to be perfect. It is also important to check that the mechanisms that are observed in the laboratory tests are the same as those observed in practice.

This thesis would fall into Category 1 of the above. The failure mechanisms seen in service have been examined in the laboratory and the objective of this work is to repeat such failures in the laboratory under a controlled environment and then to fundamentally review the failure mechanisms. However, Category 2 testing will also be pursued, in order to categorise the performance of the material under different loads and speeds. Because the material to be evaluated is already the one chosen for service, there is little benefit in conducting further simulative or service tests using these coatings. However, the knowledge gained should be useful in finding ways in which the coating can be improved, if any. Furthermore, the wear test

parameters specified could be used as a comparison for future work on other candidate surfaces and the data generated would serve as a useful baseline.

Generally it is not possible to completely simulate the conditions found in the application because of the difficulty of defining the conditions in that application. Of course, the test system itself will have limitations that will mean the match is unlikely to be perfect.

3.32 Wear Test Selection

The full findings of the failure examination will be discussed later, but the main mechanisms of failure were concerned with sand particles that either impinged on the surface causing erosion or became entrapped between the two sealing surfaces causing three-body abrasion. It is also known from past experience that galling during assembly has been observed and is still viewed as a potential problem [57].

As a result of these findings, two tests were identified as being of particular relevance to this application. These are:

1. **Reciprocating tests.** This most closely resembles the sliding action of the gate upon the seat. Two differing pin geometries were used; a conformal contact to simulate galling problems and a Rockwell diamond pin to simulate abrasion.
2. **Slurry erosion** tests (to be conducted at BP).

The latter two types of test are more straightforward in that wear is only being measured on the one surface. This allows for the generation of more repeatable results and furthermore, the results can be readily compared with those for different materials. The slurry erosion tests will obviously give information about the erosive characteristics of the material. The diamond-on-flat test will be able to simulate high stress abrasion very similar to a hard particle trapped between the two surfaces.

The reciprocating pin-on-plate (sometimes called pin-on-flat) was identified as being the most representative test for the sliding action present during operation of the gate valve. It is different in that it involves an interaction between the two surfaces that must both be measured. In many ways it is the most important of the tests because all of the sealing pressures introduced will involve the contact of the respective coating surfaces. It is also the most difficult test to perform and interpret. Furthermore, it is the most useful test in determining the sliding wear performance of the D-gun coatings and consequently, decisions must be made into the influence of test parameters.

The test has an advantage over the pin-on-disc in that the testing conditions will be identical for each test. The pin-on-disc has the disadvantage that the operating radius will differ from test to test and, as a result, in order to keep the sliding speed the same the rotational speed must vary. Although the sliding distance for the test will remain constant, the duration between contacts for different points on the disc will vary and this may affect parameters such as heat dissipation which can lead to differences in wear rates.

3.40 Test Parameters

The factors that are controlled during a test can be grouped into those concerned with the mechanical test conditions such as contact load or pressure, speed and test environment, and sample parameters such as materials composition, structure and surface finish. A full programme of testing under all combinations of these factors would be very expensive and may well not be required. Often a single factor can be identified as key to the material response. In this case, a good approach is to fix all other factors at constant values and vary the chosen factor in a controlled way in a series of tests. This approach is termed parametric study.

The importance of the various testing parameters will to some degree depend on the application considered, but the most important parameter in any test must be the material structure and composition. Other parameters which have a major affect (listed in descending order of likely importance) are contact geometry, load, speed, test environment and surface finish. A further

parameter that must be considered is the dynamics of the test machine which has been shown to have a significant effect on results [58].

3.41 Test Materials

As a reference point, tungsten carbide LW45 detonation-gun coating was identified as the best starting material. It is a coating specifically designed for subsea use and has been very effective in reducing problems associated with gate valves and, as such, it has become the most popular coating used in service for such valves. Furthermore, it corresponded to the coating that was used on the two gate valves that were subjected to failure analysis techniques.

For comparative purposes, tests were also conducted on the substrate material AISI 410 ferritic stainless steel.

3.42 Test Environment

Although the working environment of a gate valve involves the processing of petrochemicals, the tests conducted were run dry. This has the benefit of not introducing another test parameter that would make analysis more difficult. No attempt was made to control the temperature and humidity of the environment. Therefore, standard laboratory conditions were used which corresponded to 20 ± 3 °C and a relative humidity of 55-70%.

3.43 Surface Finish

Surface finish of the test samples was measured by profilometer and corresponded to 0.05 μm R_a.

3.50 Test Conditions Pin-on-Plate

3.50.1 Contact Geometry

A conformal contact geometry between the pin and the plate was chosen. This has the advantage that it most closely resembles the real-life application and also it corresponds with

what is generally considered to be good coating practice for D-gun coatings, i.e. to coat on a flat surface.

3.50.2 Load

For fundamental analysis, the load was determined that caused failure in a reasonable period of time, and still corresponded with limits imposed by the test apparatus. For the pin-on-flat tests, loads of 98.1, 196.2, 294.3 and 392.4 N were employed.

3.50.3 Speed

The speed of the test is also a critical parameter that needs to be considered carefully. The gate valve is not normally a component that would be associated with continuous sliding and certainly not at high frequencies. Therefore, the lowest sliding velocity currently available on the test machine (i.e. 41 rpm) was selected for the tests. This has the added benefit that the heat generated during the test will be minimised.

3.50.4 Duration

The duration of the tests is determined by the time required to generate a measurable quantity of wear. This time will be the useful minimum and the effect of sliding distance can be determined for greater distances. For this study test durations of between 6 and 420 minutes were used corresponding to sliding distances of between 9.84 and 688.8 m. The wear track length was 20 mm.

3.50.5 Test Machine

Initial tests were carried out on a pin-on-plate tribometer that utilised a gantry style loading configuration as shown in Figure 3.3. This system is particularly useful in aiding alignment; the wear pin is in a holder that is precision made to slide accurately down through a set of rollers and, therefore, is presented squarely to the surface. The placement is consistent and does not rely on the amount that the pin protrudes from the holder. The machine was specifically

developed to aid alignment of piston ring segments on cylinder liner segments. Load is applied by a traditional lever arm, which normally has the disadvantage that it will distort the alignment of the pin in the direction of the loading. However, with this rig the weight is transferred down the rollers and, therefore eliminates this effect. However, the rig was designed for lubricated sliding and, as it soon became apparent that very high loads were necessary to generate any significant wear with these types of coating, significant misalignment was still seen to occur.

At first this was thought to be the result of poor roller alignment and inaccurate machining of the pin holder. Consequently, two more pin holders were machined but these offered little improvement. The gantry was adjusted on a flat bed engineers table but again this proved to be of no benefit. Now that both of these problems had been rectified it could be seen that the whole gantry moved during sliding leading to a rocking motion on the pin. Thus, only opposite edges of the pin were in contact with the plate during the testing cycle, leading to a completely artificial testing environment. In an attempt to secure the housing more rigidly, it was found that there was still deformation in the gantry. It was, therefore, concluded that the machine was not sufficiently rigid for this type of testing.

Several designs of a self aligning pin holder were considered mainly centred on the idea of applying the load through a spherically shaped joint to the pin. This would allow the pin to align with the surface that it is rubbing against, However there are fundamental flaws in the theory. Firstly the holder would be difficult to machine to those tolerances necessary i.e. allowing full movement whilst maintaining no machine lash when the pin changes direction. Secondly the gantry would still be a weak link in the machine. Thirdly, the set up assumes that the two surfaces can be completely mated together whilst experience would suggest that the latter is not the case. On several occasions, the test was set up so as to be perfectly aligned using engineers blue and run under low load. No rocking of the pin could be seen but when the surfaces were examined after testing, misalignment was still seen to have taken place.

As a result of these problems, it was decided to transfer the pin-on-flat tests to a different machine. The machine was still of the reciprocating type but was of a simpler design using a

cantilever load arm loading arrangement (Figure 3.4). The machine is more rigid than its predecessor, however it is more difficult to align the specimen as the machine is not as readily adjustable. As before, alignment was obtained by using engineers blue so that when run under low load total contact of the surfaces could be observed. However, as mentioned previously when the test itself was actually run significant misalignment was still seen to occur.

As a result of these findings and also the results of tests run under this alignment procedure, where vast differences in wear rate were seen to exist during repeatability studies, it was decided that a new approach to alignment was necessary. For many conformal tests, problems of alignment exist during the first stages of wear testing. However, the materials will soon either wear or become plastically deformed to achieve conformity and the wear test will then proceed in the expected manner. This type of wear is often referred to as "running-in" wear and needs to be separated from the results of the latter part of the test. However, due to the failure mechanisms of these coatings (to be discussed later), this running in period did not occur.

As a result, a technique was developed to artificially run-in the specimens to obtain conformity. The technique involves two stages; firstly the samples are aligned as closely as possible by eye and then by using a small quantity of engineers blue. When this operation is completed to satisfaction, a small quantity of 1 μm diamond paste (as used for metallographic polishing) is applied to the contact area. The specimens are then run under a low load until total alignment was seen. This period can be anything from a few minutes to several hours depending on how good the initial alignment was. The resulting surface will have directionality but will still be relatively smooth. The resulting tests showed near perfect alignment.

As a result of this running in process, it is not possible to use conventional techniques for measuring wear such as weight loss because the specimens cannot be removed from the holder. It has been found that the best method of measuring wear is by taking a profile of the scar after testing and calculating the volume (this would be an average of at least three traces transverse to the wear direction). The wear volume attributable to the test could then be determined by subtracting the small volume of the scar produced by the running-in procedure.

3.51 Specimen Cleaning

Prior to testing, it is essential that the contacting surfaces of the specimens are carefully cleaned to remove as much dirt, grease and other unwanted material from the surface as possible. Care must also be taken to prevent the entrapment of cleaning solvent in any porosity that might be present in the samples.

The as-received samples were degreased with teepol, ultrasonically cleaned in distilled water, rinsed with methanol and blow dried in warm air. After the alignment process, it is not possible to remove the samples from their holders and, therefore, *in situ* cleaning was necessary. This involved degreasing with acetone, rinsing with methanol and hot air drying using a portable dryer.

3.52 Sample Holders

The sample holders used for the pin-on-flat tests are shown in Figure 3.5. Relatively high loads are used and consequently high tangential forces are generated during the test and therefore, the wear plate must be very securely held in position. Because of this it is not possible to use an adhesive such as double-sided tape and therefore a mechanical clamp was designed. The sample is firmly clamped in position by a pinching effect which forces the sample against a fixed support.

The main concern with the pin holder is that it is sufficiently stiff to prevent any horizontal deflection during sliding. Therefore, the holder was manufactured out of BS970 817M40 steel which was subsequently heat treated. The tolerance into which the pin fitted was kept as tight as possible to prevent any movement in the pin holder. The shoulder of the pin is a stress concentrator and therefore the pin was recessed into the holder to relieve the stress at this point.

3.53 Testing

To start a test the chart recorder was switched on, the motor started and the pin was gently lowered on to the surface. Due to the nature of the tests, the apparatus was closely monitored throughout its duration to ensure that everything was running as planned. After the desired test duration, the pin was raised from the surface and the drive switched off.

A linear variable differential transducer (LVDT) were used to monitor the friction and the wear characteristics continuously throughout the tests. For the wear transducer, the appropriate range was selected and calibration was conducted on the chart recorder with feeler gauges. In the case of the friction transducer, calibration was carried out using a spring balance applied at the pin position.

3.54 Ramp Tests

To cut down the number of tests required, a series of ramping tests was conducted initially on a range of loads and speeds. The speed was kept constant for each test but the load was incrementally increased (from 98.1 to 392.4 N) until failure occurred. Three differing speeds were used for these tests; 0.027, 0.054 and 0.108 ms^{-1} (41, 82 and 164 r.p.m.).

3.55 Pin-on-Flat Testing of Substrate Material

The AISI 410 material used as a substrate material on the gate valve was also tested in the pin-on-flat configuration. Although there is no possibility of the material being used for the application itself, the data generated is useful in providing baseline information against which the LW45 coatings can be compared. The composition of the material is as follows:

0.15C, 1.00Si, 1.00Mn, 0.04 P&S, 11.5/13.5Cr, 1.00Ni.

It is tested in a non heat treated condition and has a hardness of 280-300 H_v10.

The material was provided from off-cuts of samples that were sent to Praxair for coating. The samples were lapped at BP to a finish of 0.05 μm R_a. The pins were turned down to 6 mm diameter and 20 mm long.

However, due to problems aligning the pins, testing was conducted using ½" diameter AISI 304 stainless steel balls. A track length of 20 mm was employed at a speed of 0.027 ms^{-1} (41 rpm) for a periods of 2½, 5 and 10 minutes. Loads employed were 19.62, 39.24 and 58.86 N.

Wear was determined by measurement of ball scar diameter which was subsequently converted to wear volume (W_v) by use of the following equations:

$$h = R - (R^2 - \frac{d^2}{4})^{0.5} \qquad \textbf{3.1}$$

where h = the linear wear of the ball
R = the radius of the contact
d = the mean diameter of the wear scar

hence

$$W_v = \frac{\pi}{3}.h^2(3R - h) \qquad \textbf{3.2}$$

3.60 Reciprocating Diamond-on-Flat Testing

The test is used to simulate high stress abrasion. The reciprocating arrangement is similar to that used in pin-on-flat tests with an average speed of 0.027 ms^{-1} (41 rpm). The track length is 20 mm and durations of 5, 10 and 20 minutes (8.2, 16.4 and 32.8 m respectively). Loads of 19.62, 39.24 and 58.86 N were used. Wear was measured by profilometer traces across the wear scar and converted into wear volume. Because the contact is non-conformal, there is no problem with alignment with this type of test.

Identical tests were performed on the AISI 410 stainless steel substrate material.

3.70 Erosion Testing

The erosion apparatus used in this study was located at BP Research Centre Sunbury. It consists of a 10 litre tank in a small pipe loop around which slurry is circulated. The tank acts as a reservoir for the slurry and also locates the wear specimen in position in front of the returning slurry jet (Figure 3.6). Circulation is effected by a variable speed, mono pump controlled by a frequency inverter, while flow rate is logged by an electromagnetic flowmeter attached to a chart recorder. Pressure in the delivery line is monitored by a pressure gauge.

Jet velocities (v) are determined by the flow rate of the slurry (q) and the diameter (d) of the nozzle:

$$v = \frac{4q}{\pi d^2} \qquad \textbf{3.3}$$

Velocities thus determined indicate that the potential energy of a slurry in the delivery line is almost completely converted into kinetic energy. Flow rates in the range 0.3 to 1.0 kgs^{-1}, combined with nozzle diameters of 6, 8 and 10 mm, yield jet velocities of between 4 and 22 m/s.

3.71 Test Method

Fresh slurry samples were prepared for each test by mixing 9 litres of either Sunbury well water or distilled water with 0.78% by volume of particulate material. Such relatively low solids concentrations represent a *worst case* condition in which every particle impinges upon the target surface unhindered by a protective boundary layer.

Test samples were mounted 40 mm below the nozzle outlet and at 90° to the impinging jet (either of these values can be varied to observe, in particular, the influence of impingement angle on erosion). Slurry was circulated for a set period and the wear specimen then removed and washed. Wear was determined by mass loss with samples weighed to an accuracy of ±0.02 mg using a Metler balance, both before and after testing. The samples were allowed to dry for a period of 24 hours after testing to eliminate any possibility of water absorption.

3.72 Materials

This thesis was part of a larger, more comprehensive, study which aimed to review the performance of candidate materials for several oilfield applications, including subsea gate valves. Materials tested included tungsten carbide (Boart grade V7), cast Stellite 6, a detonation-gun coating of tungsten carbide (Praxair grade LW45), Ferralium and mild steel. The findings of the wider study are to be published separately [59] and in the interests of clarity are not included with this work. This work concentrates in depth on the slurry erosion properties of tungsten carbide LW45 coatings in respect of their failure mechanism and also the influence of test duration on wear. For comparison, similar tests are conducted on Ferralium F255 (ideally this would have been AISI 410 stainless steel as in the other types of wear test, however no suitable samples were available). Nevertheless, F255 is a widely used oilfield material and so, in many ways, the work is perhaps more appropriate. It has a composition of Fe, 6%Ni, 25%Cr, 3%Mo, 2.2%Cu, 0.05%C, 0.18%N; with a hardness of 250 H_v30.

Test specimens were prepared either as 50 mm x 50 mm or 50 mm diameter plates. The thickness was dependant upon the supplier but was typically 10 mm. All materials were lapped to a surface finish of 0.05 μm R_a and were ultrasonically cleaned in petroleum ether prior to testing.

Sand was the erosive media used with two different size distributions correlating to Redhill 50 (235 μm) and Redhill 110 (135 μm). As a comparison, sand from a Forties oil field separator was sieved to a mean diameter of 120 μm.

3.73 Test constraints

Test conditions were chosen to avoid a number of difficulties that can arise in erosion experiments. Drawing from previous experience, the flow rates were high enough to give measurable wear and avoid particle drop-out, but not so high as to cause significant particle degradation or temperature rises of more than a few degrees Celsius. Sensitivity of wear detection is the main limitation experienced with such tests.

3.80 Preparation of test samples

Once the structure of the testing programme had been decided, it was necessary to produce the test specimens. The material selected for this study was a detonation gun coating of tungsten carbide LW45, which is currently the most popular coating employed in subsea gate valve applications. The coating was designed for this and other high pressure applications and has been in production for about 8 years. The process is exclusive to Praxair Surface Technologies (formerly Union Carbide Coatings Service) and the company kindly supplied test samples.

The detailed description of the coating procedure is confidential but the design of the test specimens and mounting plates required careful consideration and provide an interesting case study.

3.81 Properties of LW45 [60]

Nominal Composition	W-Co-Cr-C*
Hardness (H_v)	900
Tensile bond strength ($kpcm^{-2}$)	10,000 min
Metallographic apparent porosity (vol%)	2% max
Density (gcm^{-3})	12
Modulus of rupture (MPa)	3.3
Modulus of elasticity (GPa)	1.75
Maximum Operating Temperature (°C)	425

3.82 Coating Considerations

With any thermal spray process, one of the major considerations is providing an adequate clamping force for samples during spraying. This is especially true for detonation gun coatings. The velocity of the impinging particles is in the order of 800 ms^{-1} and, therefore, any small workpiece such as these wear samples could be easily lost if they are not firmly secured. Furthermore, distortion of the workpiece readily occurs and, as a result, the substrate must be of a sufficient thickness to be able to withstand the rigours of the process. For this study the substrate material chosen was to be AISI 410 ferritic stainless steel as this is the most frequently encountered substrate material in gate valve applications. The substrate material is <u>not</u> heat treated prior to spraying.

3.83 Erosion Samples

The erosion samples are shown in Figure 3.7. and are essentially 50 mm x 50 mm x 10 mm and are the standard size samples for the test rig. The samples are drilled and tapped on the surface

* Exact composition confidential

not to be coated to enable easier location in the erosion testing chamber (note the screw fittings were not actually used during the experiment). Holding of the samples during spraying is relatively easy for these test pieces and does not require any specialist tooling.

3.84 Pin-on-Flat Samples

The pin-on-flat samples are shown schematically in Figure 3.8. The main consideration is a size that is easy to locate on the pin-on-flat tribometer and to allow as many tests as possible on each sample. Therefore, a size of 50 x 40 x 12 mm was decided with the top edges chamfered to facilitate an easier lapping operation. Again no specialist clamping arrangement is necessary.

3.85 Wear Pins

The wear pins differ significantly from the other two types of sample, in that their weight is considerably less and there are significantly more pins to produce.

The design of the uncoated specimen is given in Figure 3.9. The pin diameter in the coated region (also the diameter of contact during the test) was set at 5 mm. The pin was produced with a head 4 mm deep after which the diameter was reduced to 4 mm. This was to give the pins a shoulder for positioning in the grinding and lapping block and, at a later stage, during the wear testing itself. Because of the large quantity of pins, it would be uneconomic to spray each one individually and furthermore, to align an individual pin would be difficult. Therefore, a block capable of holding 100 pins was machined to the dimensions shown in Figure 3.10. Pins were secured in place by M2.5 screws that locate through the plate into the reverse side of the pins.

If a block similar to the one used for grinding and lapping were to be used for the spraying process itself, then problems would occur with some of the coating material sticking the pins to the baseplate, preventing their removal. Consequently, a separate spraying block shown in Figure 3.11 was designed so that up to 100 pins can be sprayed simultaneously with each pin being held in position with the M2.5 screw. However, on this occasion the screw fits through a

4 mm outside diameter protection tube, which is used to prevent the pin from becoming bonded to the plate and also to prevent any of the coating becoming deposited on the sides of the pin.

3.86 Spraying Procedure

All samples were machined to the specifications given in the drawings marked with a distinctive code prior to being sent to Praxair. This information was then stored in a database system.

3.86.1 Pre Spraying

The initial step prior to coating was a random inspection of the sample dimensions followed by a preparation grinding (deburr) stage with the pin samples located in the grinding plate. The samples were then transferred to the spraying block and any unused holes masked. Other samples were also transferred to their coating fixture at this stage.

The samples were degreased in their fixture and then grit blasted at a 90° impact angle using a 60 mesh alumina grit (as per normal procedure for production of gate valves). The samples were then coated in successive layers to a thickness of 0.25 mm (250 μm) using a cross hatched traverse procedure.

3.86.2 Finishing

A large part of the effectiveness of the coating is dependent on the finishing techniques employed. The finishing operation involves grinding to a finish of 0.40 μm R_a, which reduces thickness to approximately 125 μm followed by lapping to a target surface roughness of 0.15 μm R_a.

The use of improper grinding techniques can cause heat checking, particle pullout, chipping and consequent failure of otherwise flawlessly coated parts. Heat checking is caused by insufficient cooling during grinding. D-gun coatings are thin and possess low thermal conductivity, making it absolutely necessary to remove the generated heat by flooding with coolant.

After grinding the parts are rinsed in clean water and dried to prevent corrosion. A neutral pH rust inhibitor, UCAR 100, is then applied to the parts in order to protect the base material as well as the finished coating.

D-gun coatings can be lapped to fine finishes using any one of many standard lapping techniques. The finest lapped finish obtainable on the coatings differs from that on ductile metals in one respect, i.e. slight amounts of surface porosity. This porosity is a result of small particles having been torn from the coating's surface during the lapping operation. Under a microscope at 20X to 40X, a number of well distributed tiny pits or pores can be seen, even though the surface appears highly polished to the naked eye. The extent of this surface porosity is largely determined by the lapping technique employed. If necessary, lap flatness can be checked by measuring directly with an optical flat and a monochromatic light source. The samples should be flat to 2-3 light bands.

Final Quality Assurance checks would include flatness, R_a and dimensional tolerance. Sample micrographs are also taken with QA personnel certifying any faults.

3.90 Post Wear Test Examination

A better understanding of the success or otherwise of a wear simulation is achieved if a wide range of diagnostic techniques is used to interpret the damage at and below the wear surface and also the characteristics of the wear debris.

3.91 Visual Examination

All samples were examined after each type of wear test to identify changes in colour, surface topography, material transfer and shape change.

3.92 Optical Microscopy

Optical microscopy was used to investigate the subsurface of both the pins and flats after wear testing. This allows any metallurgical changes in the microstructure to be observed. Normal sections of the surface were taken transverse to the sliding direction but it was found that the layers were more easily observed through the use of a taper section.

The taper technique uses trigonometry in a very simple way that is best shown by reference to Figure 3.12. The specimen is mounted on a dummy plate and polished at an angle. By knowing the angle of the dummy plate it is possible to work out the magnification. In this study an angle of 12° was used, giving a magnification of X5. Samples were prepared as described in Section 3.93 and initially observed unpolished, before being etched in $KMnO_4$-8KOH.

3.93 Metallographic Preparation

Samples were prepared by taking the appropriate cross section of the sample and mounting in bakellite. The samples were prepared in the normal metallographic manner by progressively grinding on finer papers and then polishing with diamond paste to a finish of 1 μm. Samples prepared at BP were obtained by using the Buehler Dialog Principle [61].

Several factors must be considered when preparing samples for metallography. Firstly, the sample must be representative of the area to be examined. Secondly, the sample should if possible be prevented from damage during preparation. The most serious damage usually occurs during cutting, which is normally with an abrasive cut-off wheel which stresses the material in excess of its elastic limit, causes plastic deformation and cracking of the material being cut. This is a problem for hard brittle coatings such as tungsten carbide, in that parts of the coating may break away completely from the surface. To overcome this problem, the area to be cut was firstly coated with *Araldite* and allowed to set completely before being cut. This procedure will minimise coating "fall-out". Furthermore, care was taken to ensure the correct cutting conditions, including wheel type, cutting speed and lubricant, were used. Initial stages of

grinding were sufficiently long to ensure that all surface damage caused by the cutting action was removed.

There are particular difficulties involved when preparing coated cermets. A common problem is that the initial grinding operation may cause sub-surface damage. This damage can lead to the plucking of grains during subsequent polishing steps, so that it is difficult to distinguish between genuine porosity and tear out. Another difficulty is that the cermet covers a wide range of hardness values between phases, so that the conditions for each grinding and polishing step need to be optimised for each type of material.

Microhardness tests were conducted on the taper sections to determine if any work hardening had taken place underneath the wear track.

3.94 Scanning Electron Microscopy (SEM)

One limitation of optical microscopy is the limited depth of field and the limited resolution. Both of these can be overcome by using the SEM. Furthermore, samples may either be viewed in the topographical mode (secondary electron image) or compositional mode (back scattered electrons). Because of the preferential etching of cobalt binder during preparation, a certain amount of relief is created and this allows better quality micrographs to be obtained in the SEM. The SEM was used to examine sections, surface topography and also in the case of taper sections, the surface and the microstructure together.

No preparation of the wear surfaces was made. However, for samples mounted in bakellite, it was found that the image was improved by sputtering with carbon, which whilst improving conductivity and overcoming charging problems, still allows compositional contrast to be used.

Debris obtained from the tests was sprinkled onto double sided adhesive tape, carbon coated and analysed in the SEM.

Three separate SEM's were used in this study:

A Jeol 100, which was used to study erosion tests.

A Cambridge S250, which was used for general SEM work and large samples.

A Jeol 840SX, which was used for all compositional analysis.

The latter machine allows **Electron Probe Micro Analysis (EPMA)** to be conducted. The technique utilises the characteristic wavelength of x-rays generated by the interaction of the electron beam with a sample and can be useful in ascertaining the presence of elements present on the sample surface. The technique was used to find the difference in compositional analysis between debris from different tests.

3.95 X-ray Diffraction

The EPMA technique described above allows the determination of elements present but does not supply information concerning their phase composition. If this data is required, the most useful technique to employ is x-ray diffraction analysis.

The x-ray analysis was carried out using Cu Kα radiation (wavelength $\lambda = 1.5406$ nm) on a Philips PW1050 vertical diffractometer in conjunction with a wide range goniometer and stabilised x-ray generator. The samples were scanned over an angular range 2θ of 10° to 120° with a step size of 0.02° and a scan speed of 0.01°/min. Generator voltage and current were 30 kV and 20 mA respectively. Phase identification was determined using JCPDS (Joint Committee on Powder Diffraction Standards).

4.0 Results

4.10 In Service Failure Mechanisms

The first stage of this study was to determine the failure mechanism(s) prevalent within gate valves. Because of the difficulty of obtaining real-life samples and also the fact that the samples are both large and heavy to examine directly and also very difficult and expensive to section, this work was carried out predominantly by replication techniques.

This work shows a replication study carried out on a typical gate valve that has been subjected to the standard BP test loop. It has a D-Gun tungsten carbide coated surface sprayed on AISI 410 stainless steel.

4.11 Results of Replication Studies

Three classes of replica were used for this study: acetate, polymethylmethacrylate (PMMA) and silicone rubber. The results from each are discussed and used when they are most appropriate to the method of examination. Finally, a comparison of the usefulness of the differing types of replica is made.

The silicone rubber replicas gave good results when viewed optically but proved difficult to photograph due to a lack of rigidity. Also it was not possible to evaporate a metallic film onto their surface, probably due to outgassing under vacuum. Finally, because the surface of the rubber is not as rigid, the talysurf measurements were not as accurate. Therefore, because in this case no extra information could be obtained from the silicone rubber replicas, they do not feature in the results.

Figure 4.111a shows a PMMA replica of the typical as-supplied surface finish of the gate taken from Area 3 (of Figure 3.1). The gate consists of a ferritic stainless steel onto which a detonation-gun deposit of tungsten carbide has been coated. The characteristic cross-hatched

lapping marks can clearly be seen, as can a certain degree of porosity. Figure 4.111b shows two talysurf traces of the surface, one taken from the actual surface and one taken from the PMMA replica. It is found that the PMMA replicas are superior for profile measurements due to the extra rigidity, although fair results may also be obtained from acetate. Both traces are similar, with the real surface giving an R_a of 0.10 μm and the replica giving an R_a of 0.15 μm. Note that the trace of the replica has been inverted so that it resembles the actual surface.

Figure 4.112 shows a selection of micrographs from Area 1, where a longitudinal gouge can be seen macroscopically in the direction of sliding. The area that is shown in the micrograph is the point of initiation of the gouge. The coating has been deformed under high angle stress resulting in chevron cracks in the sliding direction. Figure 4.112a shows the actual surface as seen under the surface examination microscope and Figures 4.112b and 4.112c show uncoated and coated acetate replicas of the same area. This shows that the information obtained from the replica is representative of the true surface. Also, note the greater detail that can be seen on the coated replica. Figure 4.113 shows a three-dimensional talysurf trace of the wear scar taken from the PMMA replica, noting that the image is inverted and the peaks that can be seen are in fact valleys on the real surface. This is supplemented by top and bottom also becoming inverted (Figure 4.114) after replication and, therefore, care must be taken or the results obtained can cause great confusion and may be misleading. When the direction of features on a surface is not readily apparent, it is often beneficial to mark directions on the replica immediately after removal. Initially, interpretation of replicas may prove quite difficult but with experience should become more straightforward. From Figure 4.113 it is possible to calculate the wear volume of the scar as $9.52 \times 10^{-2}\,mm^3$ and the depth to be approximately 12 μm.

Figure 4.115a shows an optical micrograph of a coated acetate replica from the damaged Area 2. None of the original lapping marks are now visible suggesting that the surface in the area has been uniformly worn away in a manner typical of erosion. This is confirmed by looking at the talysurf trace of the area (Figure 4.115b); the much rougher profile is reflected in the R_a value rising from 0.10 μm to 0.77 μm and a peak depth of approximately 3 μm. The surface is better seen under the SEM where a greater depth of field can be obtained. Figure 4.115c shows an

individual erosion scar. Again it must be remembered that the image is inverted and although the micrograph is showing a "hill", a "valley" will be present on the surface. The micrograph also shows that a resolution in the order of 1 μm is possible with this replication technique. It is possible to identify surface features such as this and take stereological pairs to yield three-dimensional information. By using this technique, it is possible to calculate the pit depth as 5 μm which corresponds well with the talysurf measurement.

4.12 Analysis

The results show that a great deal of useful information can be obtained by the use of the various replication techniques. However, due to the resultant inversion of the replication process, care must be taken in interpretation of direction. Also replicas will be unable to identify certain surface features, particularly undercuts. Acetate is the most convenient and cheapest and probably gives the best results for microscopy, particularly when coated. PMMA replicas are more rigid and therefore give more accurate results from profilometry. Table 4.1 summarises the relative merits of the three different classes of replica.

4.13 Gate Valve Failure Mechanisms

Three areas of the gate have been examined. The first area has shown the typical as-supplied lapped finish. Area 1 encompasses a gouge of approximately 12 μm deep that runs in the direction of sliding. The crude oil that is processed through the valve contains corrosive agents and abrasive sand particles, typically of 10 μm size. Figure 4.112 shows the point of initiation of the scratch which corresponds to a sand particle becoming entrapped between the sealing surfaces. The substrate has deformed plastically under the pressure, which may be up to 40 MPa and the coating, being unable to withstand the resultant strain, has fractured. This is endorsed by the fact that the original lapped finish is still evident within the crack. The sand particle is then forced further along the interface causing cracks to follow the chevron pattern as seen in the micrograph.

Figure 4.115 shows the eroded surface evident in Area 2. The erosion is again caused by the sand particles resident within the crude. Of interest is the position of the erosion on the gate, just below the bore (Figure 3.1). This corresponds to the pinch-point, where oil flow velocity is greatest when the valve is in the nearly closed position.

To summarise, it can be seen that failure in this particular case is caused predominantly by hard sand particles, that either become entrapped between the sealing surfaces resulting in three-body abrasion, or impinge around the pinch point resulting in solid particle erosion.

4.20 Microstructural Classification of LW45

Optical micrographs of sections of LW45 are shown in Figure 4.201. A comparison is seen between an as-supplied quality tested sample from Praxair and a typical cross-section of a coated wear pin prior to testing. The samples are shown unetched and it is difficult to get sufficient contrast in this condition. As a result, differential interference contrast (DIC) is used. The main difference between the two samples is the coating substrate interface. The grit blasted surface of the wear pins is rougher than that on the test sample and can be seen to contain considerably greater quantities of grit residue. Figure 4.202 shows the typical wavy microstructure of thermal spray coatings and is due to what is known as *shadowing*, shown schematically in Figure 4.203. When the molten particles impinge on the substrate at 90° some of them will fly off and be lost from the coating, others will be deflected at varying degrees and become adhered to the surface. If they encounter some embedded grit or other build up then the coating will tend to build up around it. This will lead to possible porosity and the characteristic wavy appearance of detonation gun (and indeed other thermally sprayed) coatings. The higher magnification micrograph, Figure 4.204 shows clearly the microcracks that are evident throughout the coating structure. Porosity is also present.

If the samples are etched with $KMnO_4$-8KOH, the binder phase is removed leaving the structure shown in Figure 4.205. The coating thickness can be seen to be approximately 100 μm. The wavy lamellar structure is visible along with entrapped grit in the substrate. Figure 4.206 shows

the same coating in greater detail and individual grains of tungsten carbide (white particles) can be seen.

4.21 SEM Investigation

The microstructure is best seen, however, in the SEM. Figure 4.211 shows the microstructure of the unetched pin, with the coating having a lamellar structure consisting of thin, lenticular particles, which is tightly bonded to the substrate. Porosity and particle pull-out are evident, as is the full extent of the microcracking prevalent throughout the coating. The effect that etching has upon the coating can be seen by reference to Figure 4.212. Binder material has been removed from around the tungsten carbide grains and, in several cases, this has led to the particles becoming completely undermined resulting in fall-out. The etching procedure is ideal, however, in showing the layered way in which the coating is formed. Furthermore, the large quantity of microcracking is evidence of the high internal stresses to which the coating is subjected.

The interface between the coating and the substrate is seen more clearly in Figure 4.213. It can be seen that the coating has penetrated overhangs and undercuts generated by the surface roughening process. This partly explains the high bond strength of D-gun coatings. However, the coating/substrate bond strength is reduced by the presence of entrapped grit particles clearly seen in these micrographs. An x-ray dot map conducted on a similar area clearly shows these particles to be alumina (Figure 4.214).

4.22 Microhardness profile

A microhardness profile for a typical as-supplied D-Gun coating is given in Figure 4.221. The data is obtained from a traverse across a taper section so as to allow the gathering of the maximum amount of data points. The operating load on the microhardness tester was 300 g. Several interesting points can be seen from the plot. Firstly, the trace is typical of that found in a coating where there is a discrete layer applied to the surface compared to a diffusion treatment, where the hardness would fall steadily towards the underlying substrate hardness. From the

evidence of the trace it can be seen that the thickness of the coating in this case is 110 μm. However, there is no complete step from the coating hardness of around 1200 H_v to the substrate hardness of approximately 270 H_v as would be expected in say an electrolytic coating. The hardness value of 606 H_v corresponds to a point just below the interface where hardening of the substrate occurs as a result of the grit blasting process prior to spraying. It is also interesting to note the great variation in hardness throughout the coating itself (approximately 1000 to 1400 H_v). This is a result of the nature of the coating which is a mixture of hard tungsten carbide particles and a softer cobalt based matrix. The exact value at any given point will be the result of what sort of particle or substrate the indenting diamond comes into contact with.

4.23 X-Ray Diffraction

A x-ray diffraction trace of a typical coated sample is shown in Figure 4.231. The trace shows that essentially the coating comprises of 3 distinct phases, namely both the subcarbide (W_2C) and the monocarbide (WC) with the binder material Co in the close packed hexagonal (cph) structure.

The intensity levels of the two carbides suggests that there is a higher proportion of W_2C in comparison with WC.

4.30 LW45 Wear Test Results-Reciprocating Pin-on-Plate

A study of the effect of load and sliding speed was carried out on detonation gun sprayed deposits of tungsten carbide LW45 wearing against itself on the pin-on-plate reciprocating wear test machine. The effect of sliding speed was evaluated using a load ramping test at different speeds.

4.31 Ramping Tests

The speed ramping tests are designed to evaluate the effect of speed over a range of different loads in a way that will allow the maximum information to be obtained using a single test. The

test is usually reserved for lubricated studies where it would predominantly be used to discriminate between different lubricants. However, this approach allows the test programme to be focused on the range of conditions that are most relevant for the application and eliminates the need for "data gathering" tests at loads and speeds that are giving no additional information about the materials being tested.

The ramp testing technique is designed to give comparative data and as such absolute values of wear are not given. However, it is useful to review how wear proceeds and wear, like frictional force is monitored continuously throughout the experiment.

The friction and wear measurements produced during this test are given in Table 4.310, however they are best visualised by considering the three dimensional bar graphs shown in Figures 4.311 and 4.312.

The wear depth as measured by transducer is shown in Figure 4.311 as a function of load and speed. The wear depth increases with load for each of the given speeds. Note that there is a significant increase in wear rate when the load is increased from 196.2 N to 294.3 N. It is interesting to note that the wear performance is essentially similar for all three speeds and, as a result, it can be stated that over this particular range of conditions wear is independent of speed (note that it was not possible to test with 392.4 N at 164 rpm due to excessive machine vibration).

The friction coefficients for the ramp tests are shown in Figure 4.312. The coefficient of friction (μ) is a good way to monitor whether or not there is an underlying change in wear mechanism as there is often a corresponding increase in friction. In this case, μ is fairly constant throughout all of the tests ranging from 0.39 to 0.45, again indicating that speed (over this range) does not significantly affect the wear rates. Subsequent testing was conducted at 41 rpm both for the reason that it most closely resembled the real-life application and also that it entailed the least vibration on the test machine and consequently gave the most repeatable condition available.

4.40 Wear Test Results at 41 rpm

It was not possible to measure wear as a function of mass loss for the plate sample because the weight of material removed is negligible in comparison to the overall weight of the plate, making the resolution of the balance lower than the small masses being removed. Furthermore, the polishing technique employed to gain optimum alignment resulted in a wide scatter of weight values for the test pin. It was, therefore, decided that the only appropriate method of measuring wear was by measuring the volume of the wear scar on the plate after testing. The value is further rationalised by subtracting the wear recorded on an as-polished sample prior to testing. This would ideally be done by using a 3D profilometer, however, none were available during this period of wear testing and therefore, measurements were made by a unidirectional Talysurf 4 machine. Three measurements were taken across each scar. The volume was then determined by carefully cutting out the profile and weighing them. By comparison to a known standard it was possible to determine the area of the scar by knowing the magnification used on the profilometer. The length of the scar was measured using a travelling microscope. This data was then inputted into a spreadsheet and from it the wear volumes and the specific wear rate (SWR) was worked out. The SWR is a way of expressing wear rate in terms of the volume of material removed, V, in a unit distance of sliding, L. It assumes that the wear rate within the design range is proportional to the load, W. Thus:

$$\frac{V}{L} = k.W \tag{4.1}$$

where k is a dimensional coefficient termed the specific wear rate (SWR). SWR is normally expressed in units of m^3/Nm, i.e. the worn volume per unit distance per unit force. It is possible, in some cases, for the SWR to be negative due to transfer of material from one specimen to another. The SWR is particularly useful in monitoring whether there is any change in the

underlying wear mechanism at different loads. Consequently, the load should always be quoted when the dimensional wear coefficient is used.

4.41 Testing at 98.1 N

It was not possible to accurately determine wear volumes at loads lower than 98.1 N and, therefore, this load represents the minimum that is reported in these results.

The wear data as recorded on the spreadsheet program is given in Table 4.41. At a load of 98.1 N, the wear volume is low and varies without any apparent relationship to sliding distance (Figure 4.411). Repeat tests were run in several instances but it should be remembered that each test was painstaking to set up and eventually samples were in short supply. Ideally, at least three repeats for each set of test conditions are required to confirm repeatability, however due to the reasons outlined above this was not always possible during this study. Nevertheless, the tests that were rerun only proved to highlight the vagaries of these particular wear tests.

Figure 4.412 shows the variation of specific wear rate (SWR) with respect to sliding distance for a 98.1 N load. It can be seen that the SWR decreases with time implying that there is a higher wear rate, running-in period before the wear rates settles at a lower value for the further duration of the test. Because wear scars were so small with this load, the accuracy was less than at higher loads.

From the chart recorder trace it was evident that there was no change in wear rate throughout the tests. Friction coefficients were measured between 0.32 to 0.41

4.42 Testing at 196.2 N

Figure 4.421 shows the influence of sliding distance on wear at 196.2 N. At this load wear volume is proportional to sliding distance, although there is considerable deviation from a straight line relationship with the various results.

Figure 4.422 shows the variation in SWR with sliding distance at 196.2 N. In a similar way to the 98.1 N load, the SWR depreciates with sliding distance suggesting a period of running-in wear.

No change in wear rate was evident from chart recorder traces. Friction coefficients were measured between 0.21 to 0.42.

4.43 Testing at 294.3 N

Figure 4.431 shows the influence of sliding distance on wear at 294.3 N. Wear volume increases with sliding distance and, in this case, there is an increase in wear rate by a factor of 3 when compared to the lower loads.

Figure 4.432 shows that SWR decreases with sliding distance. However, in this case the reduction in SWR with respect to sliding distance is not as pronounced, suggesting that the initial wear rates are maintained for the duration of the test. Note that it is more difficult to test at this load because of excessive machine vibration and the fatiguing of test pin holders.

Friction coefficients were measured between 0.20 to 0.43.

4.44 Testing at 392.4 N

Three tests were conducted at this load and they exhibited an order of magnitude increase in wear rate as shown in Figures 4.441 and 4.442. No further testing was conducted above this load.

Friction coefficients were measured between 0.31 to 0.37.

4.45 Post wear examination

The results for the series of reciprocating pin-on-flat tests are drawn together in Figure 4.451. A logarithmic axis for wear volume is used to allow all values to be viewed on the same graph. It can be seen that wear is minimal at the 98.1 N load, increasing slightly at 196.2 N. There is, however, a significant increase in wear rate when the load is further increased to 294.3 N before rapid failure, occurring at 392.4 N.

Figure 4.452 presents the specific wear rates for each load on the one logarithmic chart. It can clearly be seen that there is no difference between the SWRs for 98.1 and 196.2 N. An increase by a factor of 3 can be seen when the load is increased to 294.3 N before an order of magnitude increase is observed with a load of 392.4 N.

Therefore, the wear that is occurring can be broken down into two types, termed *mild* and *severe*, with *mild* wear occurring at or below 196.2 N and *severe* wear occurring at and above 294.3 N. Further discrimination between these *mild* and *severe* wear regimes can be found by examination of the worn specimens.

Figure 4.453 shows SEM micrographs on a flat specimen that has been subjected to a load of 196.2 N over a sliding distance of 727 m. For comparison Figure 4.453a shows the surface of the as-prepared specimen (i.e. after running-in with 1 μm abrasive paste). A similar magnification micrograph of the worn surface, Figure 4.453b, shows that the surface has been further polished during the wear test with a network of fine cracks and interlinked voids now visible across the surface. Furthermore, it can be seen that preferential removal of the binder has taken place, with carbide grains now visible above the wear surface. This can be seen more clearly in the higher magnification micrograph, Figure 4.453c which also shows holes where carbide particle pull-out has occurred. Furthermore, black oxide particles can be seen to have filled the abrasive marks and surface porosity. The cracked nature of this oxide shows that it would be readily removed from the surface under further sliding.

Figure 4.454 shows the much more severe wear that is associated with a wear track that has been subjected to 294.3 N over a sliding distance of 574 m. On this occasion the wear surface has a torn appearance, indicative of plastic deformation. Figure 4.454d shows a large wear particle (approximately 8 μm in diameter) about to be removed from the wear interface. It would appear that such a particle would then be crushed upon further sliding to form the much smaller wear particles that are present alongside it. Note that there is none of the original surface topography remaining on the wear track. Also the wear is so severe that individual carbide particles are not visible.

Frictional values recorded during these experiments showed a large degree of experimental scatter, however it would appear that the friction coefficient is independent of load and wear rate and consequently also of the wear mechanism.

4.46 Wear Debris

Figure 4.461 shows a selection of SEM micrographs from a test of 196.2 N over a sliding distance of 727 m. Figures 4.461a and 4.461b show an agglomeration of loosely bonded, fine oxide particles. Figures 4.461c and d show elongated cutting type debris that is produced during the test.

Figure 4.462 shows corresponding debris from a test at 294.3 N over a sliding distance of 574 m. The debris is of a more metallic appearance indicative of an adhesive wear mechanism and has a similar torn appearance to that of the surface from which it was removed. The debris is of a finer size distribution than that of the milder wear type.

Figure 4.463 shows a x-ray diffraction trace of the debris shown in Figure 4.462. The trace comprises W_2C, WC and Co (hcp) and is identical to that of the as-received coated sample (Figure 4.464). Insufficient mild debris was produced to be able to obtain a meaningful trace.

4.47 Pin Wear

Figure 4.471 shows taper microsections of the two respective pins for the wear scars examined previously. On the *mild* wear scar, there is virtually no evidence of wear, that which has occurred appears to be the result of a mild abrasive action. A far greater degree of wear can be seen on the *severely* worn pin. On this occasion, wear has taken place by a crack interlinking mechanism that is clearly seen in the underlying material microstructure.

4.48 Substrate Material

Reciprocating pin-on-plate tests were also conducted on the substrate material, namely AISI 410 stainless steel. Test conditions were similar to those experienced by LW45, with the exception that ½ inch diameter stainless steel balls were used as wear pins.

The wear volume of the ball is plotted with respect to sliding distance in Figure 4.481. It can be seen that the wear volume increases linearly with sliding distance for each load. Also there is an increase in wear volume with an increase in load.

The specific wear rate (SWR) is plotted against sliding distance in Figure 4.482. Wear rate decreases with time for all loads and this may be due to one or both of two separate effects:

(i) The geometry of the contact will mean that initially a point contact will exist. However, as wear proceeds the contact area will increase, leading to a decrease in contact pressure. This may lead to a corresponding decrease in wear rate.

(ii) Work hardening may occur during sliding that results in an increase in surface hardness and a decrease in wear rate.

It should be noted that after a distance of 24 m there is very little difference in wear rate between the different loads.

The specific wear rates produced are approximately a factor of 10 greater than those produced in the case of LW45. However, it is usual to compare SWR's only when they are at the same applied load and at the loads tested for the substrate material, there was no recordable wear for LW45. For this series of tests therefore, it is not possible to directly compare the two materials, but it is clear that AISI 410 substrate material suffers significantly higher wear rates over all the loads studied.

The study of the wear mechanisms of AISI 410 was not an integral part of the Thesis in that such an alloy would not be used in the type of application reserved for hard coatings such as LW45. However, Figure 4.483 shows two SEM micrographs of the worn surface. Figure 4.483a shows material that has been plastically extruded from the scar which will subsequently be easily removed. Abrasive marks may also be seen on the surface. Figure 4.483b shows another image of the surface, this time it has a torn appearance indicative of adhesive wear, a mechanism that would be anticipated if two like surfaces are rubbed against each other.

4.50 Reciprocating Diamond-on-Flat Tests

The data generated during this series of tests is given in Table 4.501.

Figure 4.501 shows the volume of material removed during reciprocating diamond-on-flat tests conducted on LW45 coatings under three loads (19.62 N, 39.24 N and 58.86 N). It can be seen that wear volume increases as a result of sliding distance and load. For the two highest loads there is a period of higher running-in wear before the wear rate stabilises. A clear trend is seen by reference to Figure 4.502 where, at any given load, the wear rate is directly proportional to sliding distance

Figure 4.503 shows specific wear rate as a function of sliding distance for three loads. It can be seen that the SWR decreases with sliding distance for the highest two loads and remains constant for the lowest load. However, the SWR is approximately equal for each load and,

therefore, it can be stated that, in this case, SWR is independent of load. This implies that the same failure mechanism is prevalent in all of the tests.

This is further reinforced in Figure 4.504 where SWR is viewed as a function of load. In this instance, at a given load the SWR tends to decrease with sliding distance except for the 19.62 N load where it remains approximately constant. There is a large difference in SWR during the initial stages of wear but this stabilises after approximately 10 m to a constant level of approximately 2×10^{-13} m^3/Nm.

4.51 Examination of worn specimens

Figures 4.511 to 4.513 show taper microsections of LW45 after it has been subjected to the diamond-on-flat test and they show how wear proceeds throughout the duration of the test. The taper section has the advantage that the cross section is magnified as discussed in Section 3.92, in this case by a factor of five. Furthermore, if the polished specimen is then broken out of the bakellite, it is possible to view the surface and the microstructure simultaneously in the SEM because of the greater depth of field available.

Figure 4.511 shows the LW45 surface after it has worn under a load of 19.62 N for sliding distances of 1.69 and 3.39 m respectively. A diamond shaped indent that has been made in the coatings can be seen alongside abrasive marks in the direction of sliding. The size of the indentation is clearly getting larger as the sliding distance is increased. The wear tracks also show evidence of large fragments of material breaking off around the edges of the track in particular. There is little information to be obtained by examination of the microstructure underneath the wear tracks. For one of the tracks, microhardness readings were taken immediately below the wear track, however the values were similar to those obtained on a conventional section and, therefore, no work hardening could have taken place.

Figure 4.512 shows a test sample run under 39.24 N for sliding distances of 1.69 and 3.39 m respectively. In this instance, it can be seen that the wear scar is considerably larger in size than

that previously seen and that abrasive marks are apparent on the sides of the track with none present at the bottom of the track. No evidence of the original as-received finish is visible.

Figure 4.513 shows a test sample subjected to loads of 58.86 N for sliding distances of 1.69, 3.39 and 33.67 (the biggest recorded scar) metres respectively. The scars are again larger than those run under a lower load, but on this occasion further information upon the underlying failure mechanism may be obtained by closer examination.

Figure 4.514 gives a higher magnification of the edge of the wear track and it can be seen that the sample at the edge of the track has been extruded out of the track resulting in cracking below this area. Wear by plastic deformation, which results in strains above the strain-to-failure ratio, thereby cracking the material, leads to extremely large material removal rates, and consequently high wear rates. It is also noticeable when all of the diamond-on-flat samples are examined that material removal tends to occur predominantly at the wear track edges. This is because the material is not restrained at the edges and this facilitates easier material removal.

Figure 4.515 shows a higher magnification of the same scar this time at the base of the wear track. Fine abrasive marks can be seen on the sides of the track possibly due to debris entrapment. At the base itself, delamination type cracks are visible transverse to the direction of sliding. Crack interlinking may be seen midway up the wear scar in Figure 4.516.

4.52 Diamond-on-Flat Testing of Substrate Material

The substrate material was tested under three different loads for three different sliding distances, with wear determined from profilometry of the wear scars. It can be seen from Figure 4.521 that wear volume increases with load. However, at any set load there is no increase in wear volume with sliding distance, leading to the horizontal lines shown on the graph. This effect may be due to one of, or a combination of, the following reasons:

(1) Work hardening of the plate material

(2) Reduction in the contact stress at the tip by containment of the diamond tip by the diamond holder that is introduced after a certain depth.

(3) Contact at the top of the scar by the non-diamond part of the pin.

To study the effect of nucleation time, testing was carried out at the 58.86 N test load for shorter sliding distances. The results can be seen in Figure 4.523, where there is a very sharp increase in wear volume up to 1 m sliding distance, after which the wear volume remains constant. It is also interesting to view the specific wear rate (SWR) for this series of results (Figure 4.524). It can be seen that the 1 pass experiment leads to very high SWR's in the region of 1.3×10^{-9} m^3/Nm and as the sliding distance increases the SWR drops markedly to a value of approximately 1×10^{-10} m^3/Nm. This further highlights that SWR's must be quoted as a function of load.

The SWR's for diamond-on-flat tests for the substrate material are a factor of approximately 100 greater than those for LW45 for a typical equivalent set of test conditions. It can therefore, be stated that LW45 is significantly superior at resisting the high stress abrasion that is reproduced in the diamond-on-flat test.

4.60 Erosion results

The results for the series of erosion tests are given in Table 4.600. Some deconvolution of the test results is necessary to fully understand the wear process with the values given equated from the following.

4.61 Erosion formulae

Nozzle velocity (v) $m.s^{-1}$

$$v = \frac{q}{60.a.\rho_w} \qquad (4.2)$$

where a= cross sectional area, q = flow rate

The factor of 60 converts these values into seconds

ρ_w = density of slurry taken to be that of water (1000 $kg.m^{-3}$)

Therefore,

$$v = \frac{q}{60.\pi.r^2.1000} \qquad (4.3)$$

where

r = nozzle radius

Volume loss (V_L)

$$V_L = \frac{mass\ loss}{density\ of\ sample} = \frac{M}{\rho} \qquad (4.4)$$

Total Erodent Volume

$$T.E.V. = \frac{0.021.q.t}{\rho_{sand}} \qquad \textbf{(4.5)}$$

Where

$\rho_{sand} = 2660\ kg.m^{-3}$

t = time (mins)

0.021 = percentage by mass of sand in slurry (hence 189.5 g of sand is always used)

$$Specific Volume(V_s) = \frac{Volume\ Loss}{Total\ Erodant\ Volume} \qquad \textbf{(4.6)}$$

Volume loss due to one sand particle (V_u)

$$V_u = \frac{V_s.\pi.d^3}{6} \qquad \textbf{(4.7)}$$

where d is the mean sand diameter from Table 4.61

The kinetic energy of the eroding particles E_k is

$$E_k = \frac{1}{2} m.v^2 = \frac{\pi.\rho.d^3.v^2}{12} \quad (4.8)$$

Because:

$$m = \rho.V_p = \frac{\rho.\pi.d^3}{6} \quad (4.9)$$

4.62 Erosion of F255

Figure 4.621 is a plot of wear volume as a function of time. There is essentially a straight line relationship between the two with wear volume increasing with time. However, more information can be obtained by considering the V_u against TEV (Figure 4.622) this serves the same purpose as specific wear rates do in reciprocating tests. It can now be seen that the wear rate decreases with time. There is an initial nucleation period with wear rate at a maximum at 10 minutes, after which the wear rate settles down gradually to a constant value, which is reached after approximately 100 minutes.

4.63 Erosion of LW45

Figure 4.631 shows the volume loss of LW45. There is a near linear relationship between volume of material lost and time up until 180 minutes, above this value there is a significant increase in wear rate. Again, if the information is viewed as V_u against TEV (Figure 4.632), an initial nucleation period can be seen, after which there is a steady decrease until 180 minutes, after which there is a further increase up to 300 minutes.

It is beneficial to look at the comparative erosion of the two materials and Figure 4.633 shows the wear volume produced for each material on the same graph. It can be seen that the wear volume data is given on a logarithmic axis and this shows the great differences in wear rates between the two; a factor of 40 at the start to a factor of 15 after 300 minutes. It can, therefore, be seen that there is a considerable increase in erosion resistance with LW45 as opposed to F255. This is further supported by reference to Figure 4.634 which shows the comparative V_u's of the two materials, again exhibiting the significant improvement offered by LW45.

Analysis of eroded samples was carried out by both 3D profilometry and Scanning Electron Microscopy (SEM).

4.64 Erosion Scar Profiles

The 3D profiles of erosion scars for both materials is given in Figure 4.641. The process consists of taking multiple line traces across the surface, with each line separated by a set distance. A data point is taken every 100 μm of the traverse. The images shown are magnified to X5000 (for LW45) and X500 (for F255) respectively with the data detrended to remove slopes etc. and make interpretation easier. The trace parameters may be altered to suit the particular requirement but it was normally found that twenty traces with an inter-trace distance of 1 mm gave the optimum results with respect to time. Such a trace will take approximately 20 minutes and the duration is directly proportional to the number of data points being collected. It is, therefore, important to keep the amount of data being acquired to a minimum necessary for the individual application.

It can be seen that a great deal more wear has occurred on the F255 than on the LW45, but significantly a distinct change in the shape of the wear scar may also be observed. This difference is viewed more readily by reference to a single traverse across the centre of each wear scar (Figure 4.642). The F255 is relatively unworn in the centre of the scar but shows far greater wear as it proceeds away from the central area and is referred to as a "W" shaped erosion scar.

Conversely, the LW45 shows greater wear as it approaches the centre of the scar and gives what is known as the "U" shaped erosion scar.

Figure 4.643 shows how wear proceeds for the F255 material with respect to time. It can be seen that the "W" shaped scar has formed by 15 minutes. As wear progresses the depth of the "W" valleys become deeper with respect to the centre, leading eventually to the surface seen in the sample that has been eroded for 300 minutes.

With the erosion apparatus used, it was possible to vary the impingement angle on the sample. The effect of changing the impingement angle from 90° to 30° for F255 is shown in Figure 4.644. All other test conditions were similar to the other samples; test duration was 120 minutes. From the 3D profile it can be seen that the central "hump" of the "W" has been offset. Therefore, a single trace through the centre of the scar will change with respect to which direction the trace is taken in. Figure 4.645a shows a trace parallel to the direction of impingement. The "W" is greatly offset towards the direction of the jet, with by far the greatest volume of wear occurring in the part furthest from the jet. Looking in the other direction (Figure 4.645b), perpendicular to the jet, the trace gives a "U" shaped scar. However, the depth found will not be the deepest part of the scar and this shows the value of 3D profilometry in accurate interpretation of results, or if such an instrument is not available, it is essential to take a trace across both axes.

The wear volume produced was significantly greater than that found with an impingement angle of 90° (25.63229 as opposed to 10.3201 mm^3). To fully evaluate the effect of impingement angle would take numerous extra tests and, therefore, it was decided not to continue further testing at different angles due to limited rig availability. It can be said, however, that impingement angle plays a significant role in the erosion F255 and this will be explained in the discussion with reference to the tests conducted at normal impingement angles.

4.65 SEM investigation of erosion scars

Figure 4.651 shows a selection of micrographs taken within the erosion scar of LW45 samples with all samples showing evidence of a brittle, discontinuous surface. Cracks can be seen to be forming throughout and eventually show evidence of interlinking, which leads to large quantities of material being removed. Figure 4.652 shows a differing manner of material removal. In Figure 4.652a individual carbide grains may be seen, corresponding to the removal of binder phase. This is further reinforced by reference to Figure 4.652b which gives a back scattered image of a scar surface, showing clearly the carbide grains standing proud of the surface. Also, note the evidence of transgranular fracture across the large grain on the right of the micrograph. This can be contrasted to Figure 4.653 which shows the eroded surface of a F255 sample. On this occasion wear can be seen to have occurred by a microcutting action.

4.66 Taper Sections

Figure 4.661 shows two taper sections through the eroded surface of LW45. Both microsections show cracks formed running from the worn surface. When these cracks interlink, large scale material removal will result.

5.0 Discussion

The objective of this work was to assess tribological problems experienced in subsea gate valves and conduct laboratory based, simulative tests on the most commonly specified valve face material. The problems of examination of such components have been overcome by use of various replication techniques and the findings have pointed to a complex tribological system present within the valve. In particular, the failure analysis pointed to wear by three-body abrasion and erosion, both caused by the ingress of hard sand particles. In addition, galling of the surface due to high contact pressures is, from experience, also known to be of concern.

An attempt was made to simulate these failure modes in three simplified laboratory tests that could be readily repeated for other candidate materials. A reciprocating pin-on-plate arrangement was chosen as most representative of the operating system and, therefore, two of the wear tests were based around it. Firstly, the action of gate on seat was replicated under dry conditions for LW45 on LW45 at pressures that were similar or greater than those produced in service. Problems are experienced with conducting such tests on LW45 or similar hard coatings and therefore, a pre-test running in process was developed to ensure full contact between pin and plate during the test. Secondly, a diamond pin was used on a LW45 plate to simulate the high stress abrasion that is caused by the entrapment of hard sand particles. Finally, erosion was simulated on a slurry erosion test rig.

By conducting testing in all three wear modes, it was possible to be in a unique position to fully categorise the tribological properties of the coating. In addition, extensive post test examination has helped to reveal the underlying cause of the failure mechanisms seen in service.

Consequently, two major benefits can be drawn from this work. Firstly, the presentation of a *design guide* that will include recommendations for the maximum design pressures that can be tolerated under a sliding regime, either with or without the presence of abrasive particles,

together with the values of kinetic energy of impinging sand particles that can be tolerated and the impact angles that give most resistance.

Secondly, by discovering the underlying cause of the failure mechanism, it is possible to discuss the effects of microstructural parameters upon it and propose methods by which the tribological performance of the coating could be improved.

5.10 In Service Failure Mechanisms

In order to obtain the maximum benefit from a tribological study it is necessary to fully understand the failure mechanisms that may be experienced in service. Sometimes this is not possible, for instance when the component is at the design stage and in-service behaviour has yet to be established. In this case, it may be necessary to commission ranking tests to evaluate suitable candidate materials. Another example, is similar to the one described in this study, where the failure mechanisms, although appreciated, are not fully documented and understood.

One of the reasons for the lack of fundamental work into the wear mechanisms experienced by gate valves is the difficulty experienced in inspection, with the components themselves hard to obtain. If a fault occurs in service the valve is quickly replaced, with the demands placed on operation managers being such that little regard is given to the storage of failed components so that they may be systematically examined at a later date. It should also be remembered that failure is relatively uncommon and this is another factor that makes the supply of failed components difficult. Although gate valve problems are infrequent, when they do occur they are incredibly expensive with replacement of a failed gate valve requiring subsea welding, blocking and waterflood operations. Consequently a high research priority has been placed on valves of this type.

As a result, failure investigation is limited to components that have been evaluated in the BP pipe test loop at Sunbury and it is one such component that has been examined in this study. A further complication arises in that the dimensions and mass of the valve components make

direct examination impossible. The normal response would be to section the component but in this case the component is considered too valuable and, furthermore, the sectioning itself would be extremely difficult. The only method of cutting through the tungsten carbide coating gate is by use of an abrasive wheel. The size of the component dictates that it would not fit into a standard abrasive cut-off machine and therefore, the sectioning would require a specialist clamping arrangement that although far from being impossible, would be extremely time consuming and costly to implement.

It is for this reason that the surface replication methods were pursued and it is considered that they would be suitable for a great deal of similar applications. The results from the replication techniques have clearly shown two predominant failure mechanisms in gate valves, namely erosion and three-body abrasion which could ultimately lead to failure, where failure is the point at which the valve loses its ability to seal as shown in Figure 5.1.

The presence of abrasive particles is responsible for both failure mechanisms and, therefore, it would be advantageous if they could be filtered out of the crude. However, the volume of sand produced would make this impossible. It is possible by good design to minimise the amount of sand entering between the sealing interfaces but this has already been implemented. Therefore, the only method of further improvement available to the design engineer is the use of more wear resistant materials. For instance, to prevent plastic deformation of the substrate it could be made of a harder material or a thicker coating could be specified. To minimise erosion it may be better to specify a tougher coating rather than a harder one. Therefore, the information obtained from surface replicas can lead to ideas for improved materials design.

In conclusion it can be said that the replica techniques used in this investigation have proved invaluable for first stage examination of gate valves, and should prove just as valuable for other service components. A comparison of the usefulness of the various techniques has been given in Table 4.1. The acetate film technique has given the best results for microscopy, especially if a metallic film is evaporated onto the surface, and the PMMA replicas have been best for talysurf traces. The use of the talysurf technique alongside stereological pairs enables quantitative three-

dimensional information to be obtained on specific surface features. If all this information is pieced together it is possible to identify wear mechanisms that have occurred.

The use of replication techniques for failure analysis have not received the attention that they deserve. By choosing the appropriate technique and adapting it, there are few engineering applications that cannot be examined in this way.

5.20 Microstructural Classification

To fully understand the structure of detonation gun deposits of tungsten carbide LW45 it is necessary to first consider the structure of conventional sintered WC-Co alloys.

Tungsten forms two hexagonal carbides - the monocarbide WC and the subcarbide W_2C. The crystal structure of tungsten carbide is a simple hexagonal with lattice constants a = 2.91Å and c = 2.84Å [62 63] as shown in Figure 5.2. Both the monocarbide WC and the sub-carbide W_2C are found in the D-gun deposit and this corresponds with the findings of other workers [35 39 48].

The ratio of intensity levels of the two peaks is indicative of a significantly greater quantity of W_2C present in the deposit in comparison to WC. In comparison, the work of Ramnath and Jayaraman[43] showed that after plasma spraying, WC still remained the dominant phase. This is indicative of a greater carbon loss occurring during D-gun spraying. Ramnath and Jayaraman further pointed out that there were no distinct diffraction peaks corresponding to the cobalt rich matrix, although individual peaks corresponding to metallic cobalt were seen in the starting powders. This is broadly in agreement with the findings of this work although several of the smaller peaks are consistent with that of hcp Co. It has been reported by other workers [64 65] that the compositions of the cobalt matrix in plasma sprayed WC-Co coatings varies, mainly because of the inhomogeneities in the raw material and also because of minor variations in the plasma spray conditions. Ramnath and Jayaraman suggest that this variation in matrix composition could be a contributing factor to the line broadening of the diffraction peaks of cobalt rich matrix. However, the fact that these latter peaks are broad is also indicative of high

residual stresses within the binder. Ramnath and Jayaraman conclude their study by stating that the phase compositions of the coatings are distinctly dependent upon the characteristics of the as-received powders.

Cobalt is the most common binder metal, due to its good wetting, adhesion in the solid state and adequate mechanical properties. At room temperature the equilibrium structure of cobalt is close packed hexagonal (hcp), but above 450°C it modifies to a face centred cubic (fcc) structure. Mixtures normally coexist and pure cubic specimens can be retained at room temperature. The transition is martensitic with $M_s = 388°C$ [66].

In sintered WC-Co the cobalt is predominantly fcc [67], due to the cemented carbides restricting the hcp transformation [68]. The amount of retained fcc is determined by the plastic strain introduced on cooling, the mean free path, the cooling rate and the amount of WC dissolved in the binder [69]. The fcc phase is stabilised by dissolved tungsten and carbide in the lattice with the cobalt binder commonly containing 2-10% WC in solid solution at room temperature[67]. The tungsten substitutes for cobalt atoms whilst the carbon fills the octahedral interstices in the cobalt matrix. The result is that the hardness of the binder is increased by the WC in solution.

For the sintered alloy, the range in which the stable two phase microstructure occurs is narrow - the carbon content must be kept within ± 0.05 wt% of the stoichiometric composition of 6.12 wt% C. Deficiencies of carbon lead to the formation of η carbide (W_3Co_3C), whilst an excess of carbon leads to free graphite. Both graphite and η carbide decrease the strength of the alloy[68]. η carbide is precipitated as hard brittle particles and causes local denuding of cobalt leading to structural weakness.

For the sprayed coating, however, the temperatures reached are much higher than in conventional sintering and cooling is rapid. It is, therefore, perhaps surprising that the cobalt binder in the coating is predominantly in the hcp phase (Figure 4.231) and not retained in the fcc condition. However, the gas temperature will not correspond to that of the coating particles and Simma and Ratnickin's[37] calculations show that the Ni binder particles used in their study

only reach a temperature of 300-600°C at impact, and therefore, this temperature may be insufficient to effect the martensitic transformation.

The binder material will suffer residual stresses as a result of the variation in thermal contraction coefficients between the carbide and the binder. Cobalt shows a volumetric contraction associated with the allotropic fcc → hcp phase transformation. This results in an increase in the tensile stresses in the cobalt further to that imparted by the contraction on cooling, leading to a weakening of the cobalt-carbide bond. In some cases this may lead to debonding and the characteristic cracking visible in the microstructure (Figure 4.204). The broadness of the x-ray diffraction peaks, as seen in Figure 4.231, is also indicative of the high residual stresses that are present within the coating.

5.30 Pin-on-Plate testing

The failure analysis outlined in Section 5.10 has not shown adhesive wear of LW45 to be a problem in gate valves. However, it is considered that the study of the sliding wear behaviour of LW45 is fundamental to this work, as the actual operating regime of the gate valve is most closely simulated by this test. Furthermore, the supply of information on the wear properties of the coating should assist design engineers when specifying LW45, for instance in informing them of the maximum design pressures that can be tolerated. In addition, the type of test conducted may prove ideal as a first stage evaluation technique for other candidate materials.

Although the operating environment of the gate valves is in crude oil, the tests were conducted dry so as to represent a worse case scenario that would occur with no lubrication. Furthermore, the presence of any third body makes interpretation of results significantly more difficult. Therefore, it was decided to conduct these wear tests in as simplified an arrangement as was practical and to attempt to extrapolate these results to the real life application.

The load ramping tests conducted at different speeds effectively showed that over the range of speeds chosen there was no relationship between wear, friction and speed. The findings of this

specific series of tests was significant in that it allowed future effort to be concentrated on the lowest speed available (41 rpm). This was beneficial in two ways. Firstly, it obviously meant that less tests needed to be conducted, but secondly the tribometer operated most effectively at the lowest speed and therefore, the results obtained could be viewed that much more confidently. Several differences in wear rate were experienced as the load was increased for each speed, noticeably when the load was increased from 196.2 N to 294.3 N. The reasons and significance of this will be discussed in depth below with respect to tests conducted at a constant load.

Testing at 98.1 N load was the lowest reported in this work due to the inability to measure wear below this load with the resolution of the instruments that were available (approximately 1 x 10^{-11} m^3). However, for future work, it may be possible by using non-contact profilometry to measure the scar volumes more accurately. By simply considering the scar to have an area of 0.03 m x 0.005 m (wear track length multiplied by pin diameter) then it has taken 2,460 cycles to wear to a depth of 0.33 μm. Therefore, for the coating to wear through to a depth of 100 μm would take 730,000 cycles, which would far exceed the life expectancy of any valve. However, this simplified analysis neglects the fact that wear volume does not increase with sliding distance at 98.1 N load (Figure 4.411) and therefore, it can be stated that pressures occurring at or under those experienced by the 98.1 N series of tests i.e. 3.92 MPa, can safely be tolerated in any design using LW45 in a dry reciprocating sliding application.

The results shown for testing at 196.2 N load are similar, in that the specific wear rate continues to decrease as test duration increases. This is indicative that after an initial high wear period, wear settles into a steady-state regime. However, unlike the first series of tests at 98.1 N load, there is a slight upward trend in wear volume against sliding distance (Figure 4.421). Therefore, it would be expected that the coating would have a finite life, which using a similar calculation to that employed previously, would be in the region of 260,000 cycles. If the coating were to continue to wear in an approximately linear manner, and the maximum allowable wear was known, then the expected lifetime of the component could be estimated. Therefore, it may be said that at this load, wear rates are still very low and unlikely to be of consequence for the gate

valve application. However, it should be remembered that service lifetime is likely to be finite and, therefore, care must be taken when specifying LW45 at likely design pressures of 7.84 MPa, when long distances of sliding are anticipated.

By increasing the test load to 294.3 N there is a corresponding increase in wear rate by approximately a factor of three. This result is clearly significant and marks a transition in wear behaviour. As for the tests conducted at 98.1 N load, there is a flattening off of wear volume with respect to time (Figure 4.431). There is reason to believe that the wear volume produced may be able to be accommodated with good design with a predicted coating life of 124,000 cycles. Nevertheless, in view of the increased wear that is now taking place, it is not recommended that LW45 is specified if pressures of 11.76 MPa are expected. However, in the event of breakdown, it is not expected that LW45 would fail catastrophically under these conditions and should give satisfactory service until a repair is effected.

Further increasing the test load to 392.4 N brought about an order of magnitude increase in wear rate, showing another transition in wear behaviour. With this rapid degree of wear, LW45 should not be specified in applications with contact pressures of 15.68 MPa, as represented at this load, under any circumstances. Complete coating failure is anticipated in less than 3,500 cycles. The amount of wear taking place resulted in very high machine vibrations and consequently no long duration tests were conducted at this load.

The results of the pin-on-plate tests are summarised in Figure 4.451. It can be clearly seen that wear increases with load, but less significantly with sliding distance. As previously discussed, there is a significant increase in wear rate with the introduction of 294.3 N load and then again at 392.4 N load. This is seen more clearly in Figure 4.452 which summarises the specific wear rates versus sliding distance for all of the loads. There is no real difference between the loads of 98.1 N and 196.2 N but again the definition is clear between these loads and those of 294.3 N and 392.4N.

As a result of these wear tests, the wear performance of LW45 in the dry reciprocating mode can be classified into four categories:

1. At or below 3.92 MPa, wear rate is minimal. LW45 may be safely specified under these conditions.

2. At operating pressures of around 7.84 MPa, the wear rate is still low but wear will continue to increase with sliding distance. Ideally LW45 would not be specified under these conditions, however for the majority of applications it would perform quite adequately.

3. At pressures of 11.76 MPa, there is a significant increase in wear rate, corresponding to a different wear regime. LW45 should not be used under these conditions. However, in the event of component failure leading to such pressures, LW45 should perform adequately for a short period prior to replacement.

4. At or above 15.64 MPa, LW45 wears rapidly and should not be used under circumstances involving continuous dry sliding contact.

5.31 Sliding Wear Mechanisms of LW45

The post wear examination of the worn surfaces and subsurfaces of LW45 after testing has helped to classify the performance of the coating into the categories given above. The analysis has basically divided wear into two categories, *mild* and *severe*, with *mild* occurring at or below 7.84 MPa and *severe* occurring at or above 11.76 MPa. The wear mechanisms for the tests conducted at the lower loads would be expected to be similar, as they have near identical specific wear rates. However, it was surprising that there was no discrimination in appearance between the highest two loads, even though there was an order of magnitude difference in their wear rate.

5.311 Mild Wear Regime

The mild wear surfaces viewed in Figure 4.453 show that little wear has taken place in this regime with the polishing marks made by the running-in technique still apparent on the surface, which suggests wear depth is less than 1 μm. Wear that has occurred appears to be the result of a polishing action that serves to flatten the scar surface. Comparison with the as-prepared specimen (Figure 4.453a) highlights that binder removal is the rate controlling step. In particular, Figure 4.453c shows that during sliding the binder has been removed. It is suggested that initially this is by an adhesive mechanism, and upon further sliding particles break away from the two surfaces to form work hardened debris. This subsequently becomes entrapped at the wear interface, leading to three body abrasion and the production of the cutting type debris shown in Figure 4.461c. Following binder removal, the carbide particles are left proud of the surface and minimise further wear. Eventually however, sufficient binder is removed for these particles to become undermined which causes fall-out (Figure 4.453c). The process is presented schematically in Figure 5.3.

The debris formed has a very variable size distribution, as can be seen in Figure 4.461, and this is attributable to the differing stages in the *mild* wear process as discussed above. Several different types may be seen, ranging from a fine agglomerate of *oxide* type particles to coarser cutting type debris. Unfortunately, insufficient debris was produced in the low load tests to be able to perform x-ray diffraction upon it. Analysis of worn wear pins from typical *mild* wear tests have revealed similar failure mechanisms to those experienced by the plate.

5.312 Severe Wear Regime

The typically *severe* wear surface shown in Figure 4.454 is distinctly different from that produced by the *mild* wear process. On this occasion, none of the original polishing marks are visible on the surface and considerable damage may be seen. There is a slight evidence of carbide particles visible in Figure 4.454c, but they are unable to provide the load bearing support as they would in the *mild* mechanism. The rate controlling step for wear is no longer binder removal, although it appears that this still takes place. It would seem that the pressure generated is sufficient to exceed the compressive modulus of the coating, the material is unable

to plastically deform to accommodate the stress and will, therefore, crack in the subsurface. Under repeated sliding, these cracks propagate and possibly link up with cracks that are visible in the coating microstructure. Eventually, when full scale interlinking occurs, large quantities of the material break away. Much of this debris will be re-entrained in the contact zone and will be ground down to smaller sizes as seen in Figure 4.462. X-ray diffraction of this debris shows that the phases present are consistent with those in the virgin coating, suggesting that no oxidation of the surface takes place.

The taper microsection of the pin from a typical *severe* test (Figure 4.471a) clearly shows the crack interlinking mechanism that subsequently caused material removal and the characteristic *severe* wear scar surface. The *severe* wear process is shown schematically in Figure 5.4.

5.32 Frictional Values

The friction coefficients recorded during the tests gave somewhat unusual values in that there appeared to be no real pattern between μ and load. Obviously there is a change in wear mechanism that has previously been discussed. Normally however, such transitions also mirror themselves in the values of μ recorded. The reason that this is not seen in these results may be because of experimental inaccuracy. Normally, it is preferred to use a load cell for reciprocating studies as frictional force may then be measured in both directions and therefore, differences can be measured between the static and the dynamic coefficient of friction. Because of the magnitude of the loads used, it was not possible to utilise a load cell for such experiments and therefore, a traditional arrangement of force post and transducer was employed. To minimise movement of the arm during the test, a relatively thick force post was used and this effectively limits the resolution of measurement of frictional values. Over and Stevens[70] have shown that large variations in μ are experienced in wear testing in general and therefore, with the added limitation of the force post arrangement, values cannot be quoted to a resolution of much greater than 0.1.

However, it is more likely that the reason for the similarities is related to the respective failure mechanisms. Friction is essentially a surface phenomenon and, therefore, there is little difference between *mild* and *severe* values due to the fact that *severe* wear is caused by subsurface defects.

5.33 Test Parameters

The discussion so far in Section 5.30 has concentrated upon the wear data and the failure mechanisms produced during the pin-on-plate test. It should also be considered, however, that the test procedure developed is not a standard one and, therefore, this section discusses the relative merits of this approach and considers other potential methods of testing.

5.331 Geometry

One of the most important factors that needs to be considered in the design of a friction and wear test is the geometry of the contact between the two specimens[54]. Conformal contacts seem on the face of it, to be easier to simulate. All that is necessary is to use specimens and applied loads which give the nominal contact pressure required.

However, there are several problems with this approach. It is very difficult to align the specimens so that true plane contact is achieved, so that, at least in the early part of the test, wear will be concentrated at the few points where the two specimens are in contact and the material experiences higher contact pressures than those expected from simple estimates. Even when alignment is perfect, contact mechanics shows [71] that there will inevitably be concentrations in contact stresses at the edge of the specimen contact area. These may cause chipping or other damage to the edge of the specimens, particularly in brittle materials, and although they may to some extent be alleviated by chamfering the edge of the specimens, some stress concentration will always remain.

The problem is more serious in testing LW45 and other hard coatings, because there will be no mating-in of the two surfaces. For more ductile materials, whenever conformance of the two

surfaces is not complete, they will suffer a short period of high wear (running-in). After this, they will have deformed plastically so that full contact is effected. At this point the contact load will return to normal levels and the wear rate will decrease (steady state). With this type of D-gun coating there is no plastic deformation. The coating will either be breached by a cutting action due to high contact stresses or there will be brittle fracture resulting in large quantities of coating being removed. In either of these cases, the material removal mechanism will not result in conformal surfaces.

A popular alternative approach is to use a non-conformal specimen geometry, where it is recognised that the stress at the contact between the specimens will be changing as the wear takes place, although this is occurring in a controlled way that can be calculated using Hertzian contact equations. However, there may still be unwanted changes in mechanism that occur as the contact pressure drops.

A further complication is that the coating of such geometries can prove difficult with certain processes and can lead to poor coating properties.

Possibly, the most effective solution is to use a large radius spherical pin (e.g. 50 mm) and to try and align the contact so that it is as central as possible. This approach is gaining increasing popularity [72]. However, the pins for this test were designed prior to any work taking place and due to financial considerations it was not possible to change the specification midway through the project.

The approach taken in this thesis, therefore, has several advantages. The first is that a conformal contact is produced, that allows the accurate determination of contact stresses and prevents possible changes in mechanism as the test progresses due to changes in pressure. The post test examination of samples has shown no dependency on the topography of the surface and is therefore suggestive that in these experiments, the pre-test preparation has not influenced results. However, this must be balanced against the fact that a change in surface topography undoubtedly occurs, resulting in a directional surface rather than a randomly orientated one.

Furthermore, this approach limits the resolution of wear measurements, which is particularly noticeable at lower loads. In summary, however, the benefits in this case outweigh the disadvantages and allow the sliding wear of LW45 to be measured in a controlled and reproducible way.

Improvement could be obtained if non-contact surface profilometry was used. The wear plate could be removed after the running-in process has taken place. The profile of the scar could then be determined by non-contact methods, thereby not damaging the surface in any way, before being exactly repositioned on the tribometer. Upon completion of the test, the plate could be removed again and measured, with the difference in the readings computed to be the wear volume. A similar approach could be used to find the wear volume of the pin. This measuring technique would also have the benefit of allowing the significance of surface finish of the wear surfaces to be examined.

5.332 Test Speed

The speed of the test is an area that may require a more detailed examination. It has been shown that an increase in sliding speed has no effect on the wear rates and transitions of LW45 and, therefore, the test programme concentrated on speeds of 41 rpm. However, it might be a suggestion for future work to conduct the tests at lower speeds.

The power that is lost in the test (W) is:

$$W = \mu . P . V \qquad \textbf{5.1}$$

where: μ is the coefficient of friction, P is the applied load and V is the relative speed.

Of course the speed is not as straightforward to determine in reciprocating tests compared to unidirectional ones. The speed follows a sinusoidal pattern with velocity varying from stationary at the ends of the track to maximum speed in the centre of the stroke (Figure 5.5). The coefficient of static friction at the end of the track will also be greater than the coefficient of dynamic friction in the centre and this complicates calculations (Figure 5.5). However, by taking an average velocity and an average friction coefficient the power lost can be readily calculated. These frictional losses are dissipated as heat which must be removed from the interface by conduction into the specimens and cooling by any interfacial medium that is present. However, at only moderate speeds very high local temperatures are generated at the contacting asperities with a relatively high coefficient of friction. Because the properties of many materials, and their reactions, are highly temperature dependent, the relative speed of the test can have a dramatic effect on friction and wear, simply through frictional heating.

5.333 Testing Against Dissimilar Materials

A different approach is to compare the hard coatings against dissimilar counterfaces. This would usually be in the form of a harder material, for example a diamond indenter or a tungsten carbide ball to promote wear of the plate. Conversely a softer pin material could be used and this time the wear of the pin would be measured. It is also possible, but less common, to run pins of the test material against either harder or softer plates. The use of dissimilar wear couples is an ideal way to compare the tribological properties of different materials and reference to the literature shows that wear rating tables are usually constructed in this way. However, they are of only limited use when trying to address a more fundamental study of a failure mechanism that is taking place in a specific environment, as is the case here. Tungsten carbide coated gate valves are coated on both the gate and the seat and, as such, are sliding against each other.

5.34 Sliding Wear of LW45 in comparison with other materials

LW45 is a proprietary coating exclusive to Praxair and, therefore, little information is available with respect to its wear performance. Davis et al [73] have developed a suite of test methods for determining the relative performance of candidate wear resistant materials for the oil industry. A range of materials were investigated including LW45 and two other D-gun coatings LW5 and LW15, as well as cobalt based Stellite alloys, sintered tungsten carbides, ceramics and diamond films. The three ranking tests that were used were different to the ones employed in this study: pin-on-disc with a conformal pin geometry, abrasive wear tests using the same configuration but utilising abrasive papers and a synthetic sandstone disc.

The respective D-gun coated pins were worn against Boart tungsten carbide V7 discs with the specific wear rates produced on the pins in the order of 1 to 3 x 10^{-16} m^3/Nm. LW45 did not perform as well as LW5 and LW15 and, for all three coatings, a higher wear rate was observed on the pin in comparison to the disc. When a V7 pin was worn against a LW45 disc, the wear rates for both materials was lower. This indicates that LW45 performs better when it is in intermittent contact in comparison to continuous contact.

Davis et al [73] have produced a test rating system to facilitate technology transfer from laboratory to component and such a system, using the tests employed in this Thesis as an example, is illustrated in Table 5.1. The full results for dry sliding, adhesive wear as produced by Davis et al is shown in Figure 5.6 and, remembering that the lower the rating number, the better the performance, it can be seen that the D-Gun coatings perform well in comparison to other materials.

The information presented, however, gives no indication of the performance of LW45, or indeed any of the other D-Gun materials when slid against themselves. To address this problem Binfield and Davis conducted pin-on-disc studies wearing the above detonation gun coatings against themselves [74], the results of which are summarised in Table 5.2.

The results shown are similar to the pin-on-flat tests reported in this thesis in that there is a large degree of experimental scatter. The coatings do not perform as well when sliding against each other as they do against sintered tungsten carbide material. The specific wear rates are also similar to those produced for the reciprocating pin-on-flat tests reported in this thesis. These pin-on-disc tests were not run with sufficient repeats to be absolutely confident in their accuracy. However, they prove a useful indicator of the comparative performance of LW45 against other coatings.

5.40 Diamond-on-Plate Testing

Failure analysis has clearly shown three body abrasion caused by the ingress of sand particles to be of concern. This test was chosen as the one that best simulated this mechanism and has the advantage that it represents a single point contact and, therefore, does not experience problems with misalignment. Furthermore, analysis is simplified in comparison to testing in the presence of sand particles in that there will be no element of rolling, a known attack angle and a known counterface angularity.

For all of the above reasons, the reproducibility found in the reciprocating diamond on flat tests is much better than that for the sliding wear tests. The three loads used for the tests were an order of magnitude less than those used for sliding wear due to the nature of the point contact that makes operating pressures greater. Figure 4.501 shows the dependency of wear volume on test load with Figure 4.502 clearly showing that wear volume is proportional to sliding distance at all loads tested.

To clarify whether or not different wear regimes are operating, it is best to consider the specific wear rate in terms of load and sliding distance. Figure 4.503 shows that there are significant differences between loads at low sliding distances, however after approximately 17 m the specific wear rates converge and can be taken as being independent of load. Therefore, it is proposed that the same material removal mechanism predominates at all of the loads tested.

This assumption is supported by reference to the scanning electron micrographs taken from taper sections through the scar (Figs. 4.511 to 4.513) where essentially, the scar appearance is the same regardless of load or sliding distance. It is, therefore, proposed that there are two fundamental and interrelated failure modes for the coating under this test. These mechanisms correspond to the two principle types of abrasive wear; namely by plastic deformation or by brittle fracture.

5.41 Failure Mechanisms

Probably the most appropriate mode of failure to consider with LW45 is brittle fracture. Several models have been proposed for brittle failure [75] [76] and are summarised by Hutchings[11]. However, regardless of which is chosen, the wear rates predicted are inversely proportional to both hardness, H, and fracture toughness, Kc. The quantity H/K_c, sometimes referred to as the *brittleness index*, gives an indication of a material's ability to resist fracture. If the value is low then it will take more force to cause fracture. Nevertheless, a threshold value of hardness must be exceeded before any penetration can occur.

Lawn and Swain [76] have shown that the application of a sharp indenter above a certain load for a brittle material will lead to the creation of a *median vent crack* in the subsurface area. Upon relaxation of this strain, lateral cracking will occur in the vicinity of the deformed region. These lateral cracks can lead to the free surface and result in material removal. However, they will only form if sufficient load is applied and this load can be taken to be inversely proportional to the brittleness index. Certainly these tendencies will exist in a coating such as LW45 and the likelihood of brittle fracture is increased by the presence of microcracks throughout the microstructure. The coating is unable to accommodate the strain by plastically deforming alone and will, therefore, fracture at its weakest point that will correspond to subsurface flaws. The surface produced by such a mechanism can be seen in the centre of the wear track, where stresses are highest, and is shown in Figure 4.515. No plastic deformation dominated abrasion is apparent and wear will ensue by the removal of platelet type debris initiated by lateral cracking.

The coating does not wear in a uniformly brittle manner, however, and examination of the edge of the wear track in Figure 4.514 shows a representative scar worn at 58.86 N load for 1.69 m. Plastic deformation can be seen to have occurred resulting in the material being extruded over the edge of the wear track. However, the strain to failure of the coating is low and therefore, the deformed material will subsequently fracture and result in material removal.

In areas away from the surface of the plate, but still in the region where stresses are less concentrated than at the centre of the scar, the coating material will be unable to deform to the edge of the wear track where it can subsequently be removed. Therefore, an independent but related mechanism controls wear in these areas. It is essentially similar to that experienced in dry sliding tests as discussed in Section 5.31. The compressive strength of the coating is exceeded and this leads to fracture at the weakest points, corresponding to the subsurface cracks apparent in the microstructure. A clear example of this is shown in Figure 4.516.

Throughout the series of diamond-on-flat tests abrasive marks can be seen in the direction of sliding, that result in the removal of a small quantity of material. However, it is suggested that under none of the conditions tested, does this failure mechanism assume any importance in comparison to the fracture mechanism proposed above that controls the rate of material removal.

It can, therefore, be seen that abrasive wear experienced by LW45 in this test is not represented solely by brittle fracture or plastic deformation. In view of this, Figure 4.502 takes on added significance. For plastic deformation it is predicted that wear volume is proportional to load[11] whereas in the case of wear by brittle fracture, material removal should increase more rapidly than linearly with applied load. In Figure 4.502, the relationship between load and wear volume is near linear, suggesting that plastic deformation is the rate controlling step in the wear process. This is reinforced by reference to the micrographs in Figs. 4.511 to 4.513 which show greater wear at the edge of the scar, relating to the plastic deformation mechanism mentioned above, in comparison to the brittle mechanism in the centre of the scar.

Moore and King [77] attempted to assess the roles of plastic deformation and fracture in the wear process and to determine the effect of mechanical properties on wear. Their investigation showed that the mechanism controlling the rate of material removal differed for different materials and wear environments. Importantly they found that fracture mechanisms may cause the rate of material removal to be about ten times greater than that for plastic deformation mechanisms. These fracture mechanisms predominate when the depth of indentation of the abrasive is high, the abrasive is sharp and the ratio of fracture toughness to hardness of the material is low. This is essentially the situation that occurs during the reciprocating diamond-on-flat testing of LW45. According to Moore and King's analysis, a tougher rather than a harder material will reduce abrasion. Basic Griffith theory shows that the fracture toughness of a material is directly related to flaws in its microstructure and therefore, their elimination may lead to significant increases in both toughness and consequently wear resistance.

Because of the fact that there is no change in wear mechanism with load or sliding distance, it is proposed that with this thickness of coating (approximately 100 μm) the hardness of the substrate plays no part in the failure mechanism. There appears to be no evidence of deformation in the coating that may be attributable to substrate collapse.

5.42 Comparison with tests on the substrate material

No directly comparable work with other wear resistant materials or coatings was conducted and, therefore, the only material with which comparison can be made is the substrate material AISI 410 ferritic stainless steel.

Reference to Figure 4.521 shows that for 410 wear volume increases with applied load. However, unlike LW45, there is no increase in wear volume with respect to sliding distance for any of the loads tested. Consequently, tests were conducted for shorter durations (Figure 4.523) and showed that wear occurred rapidly up to approximately 3 m of sliding, after which no further material was displaced. This is explained by reference to the failure mechanism attributable to these alloys, which is purely by plastic deformation. Because of their lower

hardness, they are less able to resist indentation and the diamond tip will rapidly penetrate to cause large wear volumes. However, repeated sliding will lead to work hardening and prevent further deformation. In comparison, no such work hardening can occur on the LW45 coating and therefore, wear rates remain approximately constant. Nevertheless, wear rates for the substrate material are approximately 100 times greater than those for LW45 and it is suggested that the additional hardness that the coating imparts is responsible for this improvement.

5.43 Test Limitations

The diamond-on-flat test reported in this study is designed to simulate the high stress abrasion that is likely to occur due to the ingress of foreign hard particles. Nevertheless, it should be remembered that in a real life application, it is unlikely that a particle would continually slide against a particular area (unless, of course, it had become embedded in the counterface). Furthermore, it would not be as hard or as large as the Rockwell diamond, would probably not possess such a sharp incident angle and would also be likely to experience some rolling element in its motion. All of these factors will have a significant influence on the wear of LW45. However, consideration of particle hardness and size are perhaps the most pertinent and need to be discussed before proceeding further.

Perhaps the greatest deviance from service conditions is the fact that diamond has a hardness of 6,000 - 10,000 H_v in comparison to that for silica of around 800 H_v. The particle hardness has been shown to have a profound effect on the abrasion of all materials, it is known[11] that unless the ratio of hardnesses of the abrasive, H_a to the surface H_s exceeds 1.2 then no plastic deformation will occur. Therefore, as LW45 has a bulk hardness of around 900 H_v it can be seen that it would normally be expected to resist abrasion by silica particles. Consequently, the regime generated by this test may not be strictly applicable to the application.

Furthermore, the size of the abrasive particle has been shown to be of significance in the abrasive wear performance of sintered cermets [78]. If the dimension of indentation is substantially greater than the size of the carbide particles and their separation, then the material

will behave in a similar manner to a homogeneous solid. If, on the other hand, the hard phase particles are comparable in size to the indentation then the material will perform heterogeneously (Figure 5.7).

For such reasons it has been found that the best abrasion performance is found in grades that have a small carbide grain size and a low binder content [79]. Furthermore, increasing the hardness of the binder will help to reduce the amount of preferential binder removal.

It can be seen, therefore, that the test represents a scenario that is likely to far outstrip, in terms of severity, the conditions that are encountered in service. Consequently, it is not possible to comment on potential service lifetimes from the data produced. Nevertheless, for the same reasons mentioned above the particle variables such as hardness, angularity and size will be completely removed from the test and the H_s/H_a value can be discounted for all engineering materials. Therefore, regardless of the provisions already stated relating to the suitability of the diamond-on-flat test in simulating this particular set of operating conditions, the test is excellent at producing comparative material data.

5.50 Erosion

The results of the replication studies given in Section 4.11 and the subsequent failure analysis have shown that erosive effects are amongst the most important failure mechanisms for gate valves. Therefore, the results of the simulative erosion tests conducted on candidate materials are of considerable significance in the overall scheme of this work.

5.51 Flow through the gate valve

The failure analysis also showed that erosion is concentrated at the pinch point of the valve and the reason for this is relatively straightforward if the analysis given in Section 2.23 is considered. Regardless of whether the material is susceptible to either ductile or brittle erosion characteristics, the erosion rate is directly proportional to the kinetic energy of the impinging particles which, in turn, is proportional to their velocity. When the valve is closed, there will be

zero velocity and therefore, zero erosion. On the other hand, when the valve is fully open, although flow is occurring, there will be no interaction of the erosive particles with the valve itself. Therefore, erosive damage has to occur during the opening and closing of the valve.

It has already been shown in Section 2.11 that the velocity through the valve is dependent upon the degree of opening, with the maximum velocity occurring at around 5% open, below which cavitational effects prevent further velocity increases. Therefore, the area of erosive damage occurs when the valve is in the nearly closed condition and results in the marks seen around the pinchpoint.

Figure 5.8 shows the influence of area of flow through a gate valve on particle velocity for two representative flow rates, with Figure 5.9 showing the corresponding influence on kinetic energy. These values, however, remain somewhat arbitrary in that flow rate may vary significantly between fields of service. Nevertheless, values for testing were selected to mirror the worse case scenarios that were likely to occur.

The detailed analysis of fluid flow is not yet fully understood and is beyond the scope of this work, however reference to Figure 5.10 clearly shows that the valve will be subjected to a range of attack angles by erosive particles as it flows through the gate. It is, therefore, important to review the performance of candidate materials under the influence of various attack angles.

5.52 Test Dynamics

The erosive performance of various materials has already been shown to highly dependent on attack angle in Section 2.23, with materials being grouped into two general categories of having either brittle or ductile erosion characteristics. The slurry erosion test used in this work is excellent at determining which group a material belongs to, in one test alone, negating the need to test at differing impingement angles.

The reason for this can be explained by reference to Figure 5.11 which schematically illustrates the slurry of erosive particles contacting the wear surface. In such liquid-borne streams, particle trajectories at an obstructing surface are governed by the combined effects of forward momentum and sideways viscous drag. For a jet normal to the surface, particles at the centre of the jet remain unaffected by viscous forces and hence strike the surface at normal incidence. Viscous drag rises as the distance from the centre of the jet increases, progressively reducing the angle of incidence. Therefore, all angles from 0° to 90° may be experienced across the diameter of a wear scar.

Hence, consideration of Figure 5.11 and the differing angle of impact across the wear surface can lead to an understanding of whether or not a material is wearing by ductile or brittle erosion mechanisms. It has already been stated that hard materials are susceptible to fracture and maximum wear occurs at normal degrees of incidence, i.e. at the centre of the jet. Conversely ductile materials suffer the most severe damage towards the edge of the scar where impingement angles are around 15° to 30°. This effect is manifested in the shape of a section through the middle of the wear scar which will either be 'U' shaped for brittle materials or 'W' shaped for ductile materials.

5.53 Failure Mechanisms

Such scars are clearly exhibited in this work with a contrast between the F255 which shows a 'W' shaped scar (Figure 4.642), corresponding to a predominantly ductile failure mechanism and LW45 which shows a 'U' shaped scar, corresponding to a brittle failure mechanism.

Reference to the eroded surfaces further reinforces this argument. Figure 4.653 shows the eroded surface of F255 taken from the lowest point of the wear scar in the 'W' valley (i.e. the point of most wear). It is evident that material has been removed by a microcutting action in the direction of fluid flow in the valley of the wear scar.

This is in clear contrast to the eroded surface of LW45 (Figure 4.651). The images taken are from the centre of the wear scar, where damage is greatest, however the manner of material removal remains constant across the whole wear surface. The discontinuous nature of the surface is clear evidence of brittle failure. Surface cracks have formed and these will subsequently interlink, giving rise to large scale material removal.

There is, therefore, a contradictory requirement for materials to be able to withstand erosion dependent upon whether the environment gives rise to low or high incidence angles. For low angles of attack, a high surface hardness is the best way to combat wear since fracture is unlikely at low impact angles unless the particle velocity is high. To this end, LW45 with its hardness of 900 H_v would appear eminently suitable. This is supported by examination of the wear scar which shows no evidence of cutting type failure. Therefore, it may be said that the wear occurring in service, highlighted by the failure analysis, is overwhelmingly comprised of damage occurring at normal impingement angles.

At such angles wear is caused by the interlinking mechanism mentioned above. The ability of a material to resist high impact angle erosive wear depends on the amount of energy it can absorb before fracture, as indicated by the area under its stress-strain curve. Thus, tough ductile materials are superior to hard brittle materials when the impact angle is high.

5.54 Mathematical Treatments

Impact erosion phenomena are difficult to describe in precise terms due to the complexity of the wear mechanisms. Nevertheless, simplified treatments provide a useful guide to the behaviours to be expected. The original ductile mechanism envisaged by Finnie[19], for example, predicts wear quite satisfactorily. The influences predicted for particle mass and velocity are:

$$V_u \propto \rho . d^3 . v^2 \qquad \textbf{(5.2)}$$

or

$$V_u \propto E_k \tag{5.3}$$

where V_u = the volume lost to one sand particle

ρ= the particle density

d = the mean particle diameter

v = particle velocity

and E_k = the kinetic energy of the impinging particles

A more detailed analysis of cutting wear by Hashish [80] yields the slightly higher velocity exponent of 2.5, corresponding to:

$$V_u \propto E_k . v^{0.5} \tag{5.4}$$

The analysis for hard materials prone to fracture is more complex. An analysis by Sheldon and Finnie [81] predicts that the influence of each wear-controlling parameter is itself a function of the brittleness of the wearing surface. Conclusions of the analysis can be simplified to:

$$V_u \propto E_k^{f(m)} \tag{5.5}$$

and

$$f(m) = \frac{1.2m}{m-2} \qquad \textbf{(5.6)}$$

where *m* is the Weibull flaw parameter characterising the fracture properties of the surface in flexure. Exponents for highly flawed materials differ little since *f(m)* tends to a limiting value of 1.2. For alumina, the value of 14.5 for m indicated by flexure tests corresponds to an energy exponent of 1.39. The value determined directly from erosion studies is 1.30 [82].

The effect of particle energy on the erosion of LW45 is shown in Figure 5.12 where V_u is plotted against E_k. It can be seen that there is a clear dependence of wear rate upon kinetic energy of the impinging particles. It is possible to determine the Weibull flaw parameter as 4.26 by taking the gradient from this graph and substituting in Equation 5.6, which implies that LW45 is not as highly flawed as alumina. Normally, the Weibull Flaw Parameter is derived from a series of values taken from flexure tests on samples of a material with different flaw levels and, therefore, it was not possible to calculate the parameter by conventional methods as part of this work.

It can, therefore, be seen that to minimise the effects of wear at normal impingement angles, it is necessary for a material to have as few internal flaws as possible, corresponding to a high toughness. The detonation gun process is characterised by its high density and low porosity, when compared to other thermally sprayed coatings. However, the microstructural analysis of the coating has shown that a significant quantity of microcracks are present and this leads to nucleation points for the brittle failure mechanism.

To increase the toughness of the material would involve changes in the spraying parameters or material composition. There is a gap in the literature concerning the erosive performance of

tungsten carbide coatings in comparison with their composition. Therefore, the most appropriate work to consider is the erosive performance of various grades of sintered tungsten carbide.

5.55 Erosion of Sintered WC-Co

Because of the two phase nature of these alloys, WC-Co is considered to undergo a mixed mode of erosion. Both brittle fracture of the tungsten carbide grains and ductile deformation of the cobalt binder have been observed [83] [84]. Therefore, it can be seen that microstructural properties play an important role when considering the erosion of WC-Co alloys.

Both hardness and fracture toughness are considered to be important properties affecting erosion. As both are dependent on the binder content, work has been conducted on the study of erosion rate as a function of cobalt content.

There are contradictory findings on the influence of cobalt content on erosion resistance, Conrad et al [85] found that solid particle impact erosion rate generally increases with increasing binder content and the result for slurry erosion tests has been found to be similar[86]. However, Pennefather[83] found that for solid particle impact erosion at high impact angles, erosion rate did not increase monotonically with binder content. A maximum in erosion rate was found at 10 wt% cobalt and a minimum was found at 20 wt% cobalt.

Generally, two types of failure are proposed: Most workers point to cobalt removal as being the initial and rate controlling step. It is suggested that the binder is preferentially removed, followed by pull-out of WC grains when there is no longer sufficient binder to hold them in place. The removal of cobalt is initiated at binder-carbide interfaces and a considerable amount of cobalt is removed prior to WC pull-out.

The maximum at 10 wt% was explained in terms of microstructure. Below 10 wt% erosion is controlled by the WC skeleton. As the contiguity increases, the skeleton becomes more rigid and the erosion rate decreases. A more rigid skeleton is, however, usually associated with brittle

erosion, which would normally correspond with an increase in wear volume. This indicates that an underlying mechanism, which is not immediately apparent, must be responsible for the decrease in erosion. Above 10 wt%, erosion is controlled by the strength and microstructure of the binder. At 10 wt% the WC skeleton is fragile and discontinuous, and the cobalt has low toughness. The minimum in erosion at 20 wt% cobalt was explained as the result of an optimum combination of hardness and toughness of the binder.

Pennefather extended this model by dividing it into three regions according to the method of material removal. Below 10 wt% cobalt, the load is transferred through the rigid WC skeleton; cobalt extrusion is predominant and little WC grain fracture occurs. As the binder content increases and the skeleton weakens, more carbide fracture occurs. Between 10 and 20 wt% binder there is a structural change towards more embedded grains. The decrease in contiguity means that less grains touch, resulting in a reduction in WC grain fracture, which leads to a decrease in erosion rate. Above 20 wt% cobalt, the WC grains are mainly embedded and erosion occurs predominantly by a ductile mechanism. Limited carbide grain fracture, however, still occurs. The three modes of material removal, cobalt extrusion, WC cracking and ductile cutting, were all considered to occur at any binder level, however the predominant mode was dependent upon the binder content.

The tungsten carbide grain size has also been shown to affect the erosion rate of WC-Co alloys. Conrad et al[85] observed a maximum in particle erosion rate at a grain size of 1.5 μm. However, Pennefather[83] found a higher particle erosion rate for smaller grain sized alloys, for tests conducted at high attack angles.

Hankey [87] has suggested that the transformation of the binder from the metastable *fcc* phase to the *hcp* phase seems to play a role in the erosion of the alloys. As a result he has split the alloys into two groups; those containing less than 23 vol% cobalt and those containing more.

For the higher percentage binder alloys, the WC grains are essentially embedded in the binder and large amounts of cobalt must be removed before WC grains become unbound and are lost

from the surface. The total strain absorbed by the transformation of the binder increases with increasing binder content, thus reducing the erosion rate.

5.56 Comparative Erosion of LW45 and Sintered WC-Co

In the light of the previous discussion upon the erosion of sintered WC-Co alloys, it is interesting to view the comparison between erosion performance of sintered tungsten carbide (Boart V7) and LW45. Table 5.3 gives comparative performance of the two[88].

At the lower test energy there is no difference in the weighting of the two materials with both materials having V_u values of approximately 5×10^{-3} mm^3/impact. However, when the test energy is increased by an order of magnitude, there is now a very significant difference in performance. The V_u for LW45 is recorded as approximately 50 times greater than that for the sintered material. Therefore, it can be seen that the likely impingement kinetic energy of eroding particles plays a crucial role in determining whether or not LW45 is fit for purpose. Further work is required to find the threshold value at which the sprayed deposit starts to perform worse than the sintered material.

The typical eroded surface of the V7 tungsten carbide material is shown in Figure 5.13. In comparison to the LW45, the microstructure is far more consistent. Individual carbide grains can be seen to be standing clear of the surface showing that the cobalt binder material has been preferentially removed. The underlying material removal mechanism, therefore, is likely to be binder removal followed by carbide fall-out.

5.57 Erosive Failure Mechanisms of LW45

It can be seen from Figure 4.652 that preferential binder removal also occurs on LW45, but on a much smaller scale. It is suggested that a more brittle failure mode is exhibited which is the rate controlling step, particularly at higher energies. This involves the linking of microcracks by a fatigue action of the eroding particles, resulting in large scale material removal. This mechanism

can clearly be seen by reference to the taper microsection in Figure 4.661 and is illustrated schematically in Figure 5.14.

The presence of fatigue is supported by reference to Figure 4.631 which shows the variation in volume loss with test time for LW45. It can be seen that volume loss increases linearly with time up to 180 minutes. After this, wear accelerates and it is argued that this is a result of microcracks gradually becoming interlinked by the fatiguing action of the erosive particles.

Figure 4.632 shows how V_u is related to total erodent volume for a series of tests conducted under identical conditions but for different durations. It shows that material removal is relatively high at the beginning of the test and drops with time to a minimum at 0.04 m^3 before increasing rapidly. It can be seen that material removal is more easily facilitated earlier in the test and this may be explained by subsequent work hardening of the binder, reducing the wear rate. However, after a set time it is proposed that the effects of fatigue will take over, leading to the higher removal rates as previously outlined.

The failure mechanism outlined shows that the erosive wear performance of LW45 could be improved by making its microstructure more closely resemble that of the traditional sintered material. In particular, the elimination of microcracking from the coating would, above all else, lead to significant improvements. In high energy testing, the discontinuous microstructure leads to rapid material removal, whereas for low energy testing, the microcracks act as nucleation sites for subsequent fatigue damage. To better resist brittle type erosion, the toughness of the coating will need to be increased and this may be achieved by increasing the binder content. The binder content of the LW45 alloy is not known, but further work is recommended to review its significance.

5.58 Erosion of F255

It has been shown by reference to the appearance of wear scars, both by SEM and by profilometry that F255 erodes in a ductile manner. Testing was only conducted at one energy

for this alloy, and Figure 4.621 shows a near linear relationship between test duration and the volume of material removed. Consideration of the influence of total erodent volume on V_u (Figure 4.622) shows that after a short nucleation period, the wear rate increases by approximately 30% for a short period, before settling at a steady value. It is suggested that the initial low wear rate corresponds with a short period of oxide removal after which the resultant higher wear rates are reduced by the influence of work hardening.

The progressive erosion of F255 is shown in Figure 4.643. The typical 'W' shaped profile is already visible after 15 minutes of testing. The influence of attack angle is shown by the profiles of the scars as the test duration increases. There is very little increase in the wear that is occurring at the centre of the jet, i.e. at normal impingement angles, whereas wear continues to increase in the outer areas of the scar that correspond to the lower attack angles.

The effect of incident angle is quantified in Figure 4.644. For this test the jet has impinged upon the sample at a 30° angle. The typical 'W' shaped profile is still apparent, however, it has been skewed off centre, with the majority of the wear occurring in that part of the scar furthest from the jet. The wear volume has increased by a factor of 2.5 for this test and it can, therefore, be concluded that the erosion of F255 is highly dependent on impingement angle, with greatest wear recorded at lower angles.

5.59 Comparison of Erosion of LW45 and F255

A comparison between the erosive characteristics of LW45 and sintered tungsten carbide has already been made. However, the improvements offered by the use of such a coating are considerable when viewed in respect of the Ferralium F255 alloy.

Both Figure 4.633 and Figure 4.634 respectively, show that the erosive performance of LW45 is between fifteen and forty times better than that of F255. It should also be considered that the test conditions chosen, i.e. 90° impingement angles would represent a worse case scenario for LW45 and a best case for F255. Therefore, the differences given in this study are likely to be

more favourable to F255 than would be expected in most real-life applications in which it may have to perform.

5.60 Methods of Coating Improvement

Regardless of the type of test used, failure of LW45 in this work has occurred by a brittle failure mechanism, that is aided by microcracking inherent in the microstructure. To improve the tribological characteristics, therefore, it will be necessary to control composition, spraying or subsequent heat treatment.

5.61 Composition

It has been shown that the overriding failure mode of the coating is by brittle fracture and consequently the fracture toughness of the material is probably the most important single mechanical property to control. Work involving traditional sintered WC-Co materials have shown that microstructural parameters such as binder content, carbide grain size, mean free path and contiguity have an important influence on mechanical properties. Definitions of these parameters are given in Appendix I. In particular, increasing binder content is known to confer increased fracture toughness. However, to do so will also decrease hardness which may, in turn, lead to more *ductile* abrasion and erosion, and an increase in adhesive tendencies. It is clear, therefore, that further testing of different coatings to assess their dependence on these microstructural characteristics is necessary.

Some workers have suggested that the use of a nickel binder may be beneficial to cobalt in that it is not subjected to the allotropic phase change that results in a volume contraction and subsequently high tensile stresses within the coating [89]. On the other hand, Barbezat et al[31] argue that although the highest toughness can be obtained with a nickel matrix, the relatively low work hardening of the nickel under the attack of abrasive particles cannot protect the hard tungsten carbide particles from pull-out. Therefore, the hardening properties of the cobalt can be considered to be an advantage in obtaining high abrasion resistance. They also point out that the

presence of certain brittle carbide phases decreases the abrasion resistance of sprayed tungsten carbide coatings. Therefore, strict regulation of carbon content is recommended to control this.

Barbezat et al believe that the fracture toughness of sprayed carbide coatings is paramount in obtaining a better understanding of the mechanism of damage by abrasion or erosion and requires further investigation.

5.62 Spraying velocity

Detonation gun deposits are amongst the most coherent coatings available and they owe this to the high deposition velocity generated by the process. This means that the high kinetic energy generated enables the particles to completely deform on impact and so result in high density, extremely low porosity coatings. The energy is converted into heat on impact and can lead to metallurgical as well as mechanical bonds in the resultant coating. Therefore, it follows that the greater the heat after impact then the greater will be the tendency for individual particles to form metallurgical bonds with their neighbours. As heat is generated by the kinetic energy of the impinging particles, then if the velocity is increased, then so ultimately will particle to particle bonding. Praxair have taken steps to increase particle velocity by the introduction of their patented Super D-Gun™ process and it will be interesting to review the wear performance of such coatings.

5.63 Post Coating Treatments

If a cobalt binder is specified there will, of course, still be the contraction following the fcc to hcp phase transformation and therefore, benefit might be gained by subsequently heat treating the deposit. Subrahmanyam et al [39] heat treated plasma sprayed deposits at 1373 K where WC and tungsten react with Co to form Co_3W_3C. In spite of the presence of the brittle Co_6W_6C type compound at the interface, the diffusion treatment improved the bonding between the coating and the substrate and also its wear resistance in a diamond scratch test.

5.70 Design Guidelines

To date, the failure mechanisms under the differing wear modes have been discussed and suggestions for improvements have been made in terms of the coating's microstructure. However, the overall objective of this, or any similar work, could be viewed as providing tribological guidelines, upon which the correct choice of material for the particular application can be made.

The work conducted has further emphasised that a systems approach to tribology is necessary to obtain maximum benefit from a design standpoint. Wear, of course, differs from other material properties such as hardness and tensile strength in that it is not an intrinsic material property. Therefore, the production of design guidelines is complicated in that it is not possible to quote an all-embracing material parameter to quantify wear.

Kato [90] has commented on the selection procedure for an optimum surface treatment to meet the required wear properties. He states that although surface treatments and coatings are now being increasingly considered at the design stage, it remains very difficult to select treatment techniques properly, due in part to the extensive range of surface treatments and coatings currently available, and partly because a large number of factors should be considered from mechanical, tribological and economical points of view. Kato highlights the lack of a widely accepted procedure to aid in the selection of an optimum surface treatment with current selection policies often being based on experience and information gleaned from suppliers' guides and internally produced company data which normally does not allow meaningful comparison between different techniques. It is clear, therefore, that a more systematic programme in the area of wear of surface treatments is required.

Kato's studies use the "wear mapping approach" to point to the performance of nitrided steels over a range of speed and load and relate this to failure mechanisms in different areas of the map. Significant advances have also been made with respect to suitable database and computer expert systems which would be the ideal in the selection of the most appropriate surface treatment.

Kato also points out the limitations of this approach.

> "Although these systematic approaches yield useful design guides for selection, they are not perfect tools. In some cases, empirical knowledge or case studies may still be of more direct use in practical engineering than the systematic database, which needs so much data and experience on tribology and surface engineering that there is no hope of constructing a universal database which describes all aspects of all surface treatments."

There are four further points of relevance to consider concerning the creation of such design guidelines. The first is the resource necessary to produce the data and consequently maintain it. The second is that large variations in wear data are often reported in interlaboratory exercises. Accuracy and repeatability of wear test results is a matter that receives a great deal of attention that is beyond the scope of this work. However, it is a fact well worth considering in the production of design guidelines and recent moves towards standardised practices may help considerably with this. The third point is that the test chosen may not be truly representative of the operating condition and, as such, the guideline information given may be misleading. Finally, difficulty may be experienced with some materials for certain tests, a good example being LW45 in this study.

In comparison, although not as fundamental as the "wear mapping approach", the ideas presented by Davis et al [73] have benefits from a designers standpoint, as they give a likely indication of the performance under a range of wear conditions and form the basis upon which most computer databases operate.

This alternative approach is based on a fundamental study of the failure analysis and reproducing it in a controlled test. At the one end of this approach lies test rigs that are virtually a copy of the machine being studied, these sort of tests are normally expensive to conduct and often have limited relevance to other applications. On a laboratory scale, an existing standard test can be modified to suit the individual application. This is often the most cost effective way

to proceed but again it may not be possible to easily transfer this information to other areas of application for the material. As a result, it is often necessary to conduct a large number of tests for different materials for useful comparative data to be found.

It can be seen that if tests are carried out on all candidate materials for each different application, it will take considerable time and will involve a great deal of replication of effort if each material is evaluated using each test.

Therefore, it can be seen that a dilemma is reached when developing tribological guidelines between keeping the required work down to an acceptable level yet still producing information that is of genuine relevance to the problem in hand. This problem will escalate as the range of tribological materials, particularly surface coatings and treatments continue to grow at a rate that far outstrips our understanding of their wear properties.

The author believes that the best solution is an approach similar to that adopted by Davis et al, whereby a range of tests is conducted on candidate materials where the tests simulate a particular failure mechanism. Rating tables can then be used as a first stage filtering process for subsequent simulations that more closely mirror the real life application.

In this study, the erosion tests and the reciprocating diamond-on-flat tests are examples where it is relatively straightforward to obtain comparative information between different materials. The reciprocating studies involving LW45 on LW45, however, is more complex and any comparison would have to be done using an equivalent pin geometry, which could lead to alignment problems similar to that experienced by LW45.

Part of the approach used by Davis et al is a weighting procedure showing the percentage of each type of failure that is expected. This matter can, unfortunately, be very subjective and the author believes that great care must be exercised for their approach to be most effective.

Taking into account the previous comment, a similar rating system to that employed by Davis et al can be employed for gate valves, bearing in mind that failure investigation has been based on only one valve. The results of this failure analysis and comments of experienced operators have suggested that the percentage wear produced by each failure type could be broadly considered as follows:

Adhesion	30%
Abrasion	40%
Erosion	30%

The next step is to give a rating value to the different wear rates. For this to be sensible, it is best to conduct tests on several different materials to get a feel for the values. Nevertheless, the rating is purely arbitrary and, therefore, if the example given in Table 5.4 is taken, LW45 has a relative performance factor of 4.7. Purely for reasons of comparison (and substituting in values of F255 for the erosion studies) the rating factor for the substrate material is 7.1. This does not mean that LW45 is 7.1/4.7 times better than AISI 410 for this application; it will, in fact, be significantly better than this. To obtain such comparisons it would be necessary to conduct tests on many different materials and also, in this instance, the test conditions are not strictly equivalent for the substrate material. Nevertheless, this simplified design guide readily shows that the specification of LW45 leads to significant improvements over AISI 410.

Kato's concluding remark is perhaps the most significant. He states that one of the most important things is to produce "well-organised" data, for example, which describes clearly a relationship between wear properties and the characteristics of surface treatments. The author endorses this view and has attempted to follow it in this work. Its application allows the wear data produced to be used as a baseline from which more specific tests can be conducted on LW45. Similarly, it permits comparative testing of other candidate materials under a range of conditions that simulate the gate valve application.

5.80 Summary

The aim of this work has been to take an in-service tribological problem and simulate it in such a way in the laboratory that meaningful guidelines in the selection of a material *fit for purpose* can be made. The failure analysis has pointed to a complex tribological system that cannot be reproduced by one test alone.

To test the whole range of candidate materials for this application is an immense task and one that is beyond the scope of this work. Therefore, this study has concentrated upon only the one coating, LW45, which is currently the most frequently specified for gate valves and aimed to develop testing methodology that is most suitable for this application.

Throughout, the approach has been to simplify tests as much as possible, which may to some extent lead to a deviance from service conditions, in order to allow a fundamental interpretation of underlying material failure mechanisms to be made. Out of the three failure mechanisms identified, erosion is perhaps the easiest to simulate, and no adaptation of the existing technique has been deemed necessary. Similarly, high stress abrasion has been simulated by a diamond-on-flat test, which deviates from service conditions but eliminates many of the parameters usually associated with abrasive testing.

To maintain this *simplistic* approach a conformal contact geometry was adopted for the reciprocating pin-on-plate test. However, this highlighted a fundamental problem with alignment that is present with hard surfaces such as LW45. Therefore, a test procedure was developed, involving running-in of the surfaces with 1 μm diamond paste that enabled full contact over the whole area of the pin.

Regardless of the test used, the extensive post-test analysis has revealed that under severe conditions of loading or impact LW45 fails predominantly by a brittle type mechanism caused by an interlinking of microcracks within the microstructure. Examination has also revealed that at lower loads, the rate controlling step is binder removal, followed by carbide pull-out, resulting in a significant reduction in wear rate. Therefore, two important conclusions can be

determined from these findings regarding the specification of LW45. Firstly, it must be specified in an operating regime that results in contact conditions at or below those required for *mild* wear, which will be the case for the majority of engineering applications. Secondly, if performance is required under more severe conditions, the tribological performance of the coating can be improved by the reduction or elimination of microcracking within the microstructure.

Methods of doing so have not been assessed in this work but probably the same principles of tribological behaviour will apply to sprayed deposits of WC-Co as they will to the sintered material. It is suggested, therefore, that areas to be assessed, in particular, include the binder content and the carbide grain size. Furthermore, the increase of spraying velocity may result in a denser, less cracked microstructure.

The production of design guidelines for the selection of optimum surface technologies for the gate valve application are complicated by the wide range of wear mechanisms prevalent in the system, the lack of a real knowledge of the underlying importance of each and the lack of comparative data for other materials. Nevertheless, an attempt has been made to mirror the approach of Davis et al in producing a ranking number for the performance of the material for each test and relating this to its relative importance in the application. In doing so, the vast improvement offered by the specification of LW45 in comparison to standard substrate materials can be seen.

6.0 Conclusions

1. A complex tribological system exists in a gate valve that cannot be represented by any single laboratory test. Failure analysis using replication techniques has pointed to abrasion, erosion and adhesion being the dominant wear mechanisms. The replication techniques used in this study have not received the attention they deserve in identifying failure mechanisms and it is suggested that they could be used successfully on many similar components.

2. Three standard tests have been developed to most closely simulate the application, replicating the three principle failure modes. A reciprocating diamond-on-flat test has been used to simulate abrasive wear, a reciprocating pin-on-plate for adhesive wear and a slurry erosion test for erosive wear.

3. X-ray diffraction analysis has shown a higher level of W_2C compared to WC in the D-gun coating, indicative of carbon loss during spraying. The broad diffraction peaks disclose a high level of residual stress within the coating.

4. Problems involving alignment when conducting conformal pin-on-plate tests on the hard D-gun coatings have been overcome by use of a running-in technique.

5. Wear of LW45 occurring during the pin-on-plate test is not affected by test speed over the range selected, but is highly dependent upon load. Four different categories ranging from minimal wear to catastrophic wear have been identified. Conditions involving continuous sliding under operating pressures of above 7.84 MPa should be avoided.

6. Sliding wear can be divided into two categories, at or below 7.84 MPa termed *mild* wear and at or above 11.76 MPa termed *severe* wear. In the *mild* wear regime, wear occurs by preferential removal of the binder phase, which is minimised on further sliding by protruding carbide particles. Eventually, sufficient binder is removed for carbide fall-out to occur, upon which the cycle is

repeated. A greater wear volume is associated with the *severe* wear mechanism which is caused by interlinking of cracks present within the microstructure of the coating.

7. Abrasive wear simulated by the diamond-on-flat test increases with load. The failure mechanisms produced are independent of load and consist of a combination of plastic deformation and brittle fracture. It is proposed that plastic deformation represents the rate controlling step in the wear process.

8. Slurry erosion tests have shown that LW45 wears by a brittle erosive mechanism, whereas Ferralium F255 wears by a ductile erosive mechanism. Therefore, LW45 is best able to resist erosion at low impingement angles. The volume loss per particle impact for LW45 is proportional to the kinetic energy of the impinging particles.

9. In all three tests, failure has occurred by a brittle failure mechanism aided by microcracking inherent in the microstructure. The removal of such cracks, therefore, should lead to significantly improved wear resistance. Potentially, this may be achieved by varying coating composition, spraying parameters or subsequent heat treatment.

10. A simplified design guide has been produced which gives the performance of a material under each test and then weights the contribution of the differing failure types in the gate valve. LW45 gives a significant improvement in wear resistance in comparison with the substrate material. No comparison was made with competitive wear resistant materials in this work but reference to the literature shows that LW45 performs favourably.

7.0 Recommendations for Further Work

The approach of this work has been to produce simplified laboratory tests that mirror the in-service failure mechanisms experienced by gate valves. Therefore, wear testing has concentrated upon LW45 alone and comparison with other potential seal-facing materials is necessary to gain ideas for improvements in valve performance. Other candidate materials include diamond like carbon (DLC), silicon nitride or sialon, sintered tungsten carbide and advanced nitriding processes. It is hoped that the test methodology developed in this study may form the foundation for such work.

Furthermore, the influence of coating variables such as composition, spraying parameters and heat treatment have not been assessed for detonation gun deposits of tungsten carbide. It is thought that significant improvements in wear performance may be brought about if the alteration of such variables leads to the removal of microcracking from the coating microstructure.

Pin-on-plate test methodology may be further improved by adoption of a non-contact wear measurement principle. In addition, for more accurate simulation, it would be beneficial to run the tests at lower speeds immersed in the processing fluid in the presence of abrasive silica particles. Running at lower speeds in the presence of lubricant may lead to significantly higher maximum pressures being recorded.

Although the reciprocating diamond-on-plate test is excellent for producing comparative data, it does not closely simulate conditions encountered in the gate valve, most noticable in terms of hardness and size of the abrasive. As both of these parameters are known to significantly affect abrasion resistance, it is recommended that future work is conducted using a more appropriate abrasive.

The results of this work suggest that LW45 behaves in a brittle manner under erosive conditions. This also indicates that it is sensitive to impingement angle and it is recommended that further work is undertaken to examine its influence.

Finally, it must be remembered that the values stated for maximum allowable operating pressures etc. are those determined under laboratory conditions. Unfortunately, these tests can never be an exact simulation for service trials and therefore, confidence in the wear test methodology used can only be gained by comparison with results obtained from in-service behaviour.

8.0 References

1. Vivian, B. "Selecting process valves for in-service reliability", *Process Engineering*, April 1988, pp33-36.

2. Tabor, D., Wear - a critical synoptic view, *Trans. ASME, J. Lubr. Tech.*, **99**, 1977, 387-395.

3. Eyre T.S., The mechanisms of wear, *Tribology Int.*, **11**, 1978, 91-96.

4. Wood R.J.K., Private correspondence, 1992.

5. Czichos, H., Tribology, Elsevier, Amsterdam, 1977.

6. Burwell, J.T., "Survey of possible wear mechanisms", *Wear* **1**, pp119-141, 1957/58.

7. Eyre, T.S., "Wear mechanisms", *Powder Metallurgy*, **2**, pp 57-63, 1981.

8. Macmillan, N.H., "Wear of Materials". *Proceedings of the 10th Riso International Symposium on Metallurgy and Materials Science*, Roskilde, Den. p153-173, Publ. by Riso Natl. Lab., Riso Library, Roskilde, Denmark (1989).

9. Bowden F.P., Tabor D., "Friction, an introduction to tribology", 1973, Heinemann, London.

10. Moore M.A., *Materials in Engineering Applications*, **1**, 97-111, 1978

11. Hutchings I.M., "Tribology, friction and wear of engineering materials, Edward Arnold, London, 1992.

12. Oberle, T.L., "Properties influencing wear of metals", *J. Metals*, **3**, 438-39, 1951.

13. Spurr, R.T. and Newcombe, T.P., "The friction and wear of various materials sliding against unlubricated surfaces of different types and degrees of roughness", *IMechE Conf. Lubrication and Wear, London*, 269, (1957).

14. Halling, J., "Principles of Tribology", Macmillan, London, 1975.

15. Bowden F.P., Tabor D., "The friction and lubrication of solids", 1., (1950), 2., (1964), Oxford Press.

16. Archard, J.F., "Contact and rubbing of flat surfaces", *J. appl. Phys.*, **24**, 981-88, 1953.

17. Rabinowicz, E., "Compatibility criteria for sliding metals", Friction and lubrication in deformation processing., Am. Soc. Mech. Eng., N.Y., (90-102), 1966.

18. Welsh, N.C., *Philos. Trans. R. Soc.*, **11**, 435-39, 1965.

19. Finnie I., "The mechanism of erosion on ductile metals" *3rd US National Congress of Applied Mechanics*, 1958.

20. Sheldon G.L., *J. Basic Engineering*, **92**, (1970), 619

21. Bitter, J.G.A., "A study of the erosion phenomena", *Wear*, **6**, pp 51-69, 1963.

22. Bell T., *Eur. J. Eng. Educ.*, 1987, **12**, (1)

23. Chagnon P., Fauchais P., "Thermal Spraying of Ceramics", *Ceramics International*, **10**, No. 4, (1984), pp.119-131.

24. UK Department of Trade and Industry, "Wear Resistant Surfaces in Engineering", HMSO, 1986.

25. Grainger S. ed., "Engineering Coatings - Design and Application", 1989, Abington Publishing, Cambridge, U.K.

26. Budinski K.G., "Surface Engineering for Wear Resistance", Prentice Hall, New Jersey, 1988.

27. Cooper D., Davis F.A., Wood R.J.K., "Selection of wear resistant surfaces for the petrochemical industry", *J. Appl. Phys.*, **25**, A195-A204, 1992.

28.Booth M, "A resume of commercially significant thermochemical surface treatments" at Surface Treatments and Coatings for Wear Resistance, Cranfield 1985.

29. Jack, K.H., "Nitriding", Heat Treatment '73, pp39. The Metals Society, London, 1975.

30. Barbezat G., Moens J.R., Nicholl A.R., "Chromium and carbide-containing coatings using the CDS process, *Proc. Natl. Thermal Spray Conf., Long Beach, CA, May 21-24, 1990*, ASM, Metals Park, OH, 1990.

31. Barbezat G., Nicoll A.R., Sickinger A., "Abrasion, erosion and scuffing resistance of carbide and oxide ceramic thermal sprayed coatings for different applications", *Wear*, **162-164** (1993) 529-537.

32. Poorman R.M., Sargent H.B., Lamprey H., "Method and apparatus utilizing detonation waves for spraying and other purposes"' U.S. Patent 2,714,553, August 2, 1955

33. Guest, C.J.S. "Plasma and detonation gun coatings", *Trans. Inst. of Metal Finishing*, **64**, , pp. 33-38, Feb 1986.

34. "Putting A Hard Face On The World", published in *Metallurgica*, July (1983), pp 299-301.

35. Tucker R.C., "Plasma and Detonation-Gun deposition techniques and coating properties" from "Deposition Technologies for Films and Coatings, Developments and Applications", Rointan F. Bunsah et al. eds., 1982, Noyes Publications, New Jersey, USA.

36. Quets J.M., Tucker R.C., "The high temperature impact-sliding wear and oxidation resistance of several cobalt-based oxide-containing detonation gun coatings", *Thin Solid Films*, **84** (1981), pp. 107-118.

37. Simma, L.I. and Ratnichkin, S.V., "Formation of Detonation-Deposited Tungsten Carbide-Base Coatings." Translated from *Poroshkovaya Metallugiya*, No.11 (227) pp 64-68, (1981).

38. Wigren J., "Grit blasting as surface preparation before plasma spraying", *Surface and Coatings Technology*, **34**, (1988) pp 101-108.

39. Subrahmanyam J., Srivastava M.P., Sivakumar R., "Characterisation of plasma-sprayed WC-Co coatings, *Materials Science and Engineering*, **84** (1986) pp. 209-214.

40. Union Carbide Standard on finishing, Union Carbide Corporation, 1986.

41. "Finishing - UCAR Metal and Ceramic Coatings", Union Carbide Corporation, 1989.

42. Wang, Y., "Friction and wear performances of detonation-gun and plasma-sprayed ceramic and cermet hard coatings under dry friction", *Wear*, **161**, 1993, pp 69-78.

43. Ramnath V., Jayaraman N., "Characterisation and wear performance of plasma sprayed WC-Co coatings", *Materials Science and Technology*, **5**, (1989), pp.382-388.

44. De Bessett, R.P. and Schwarz, E., "The Detonation Gun Coating Process", *International Colloquium on Hard-Facing Materials in Nuclear Power Plants*, Avignon, France, 25-26 Sept. 1980, Societe Francaise d'Energie Nucleaire, pp7.

45. Zaat J., Proceedings of the 9th International Thermal Spraying Conference, La Haye, 23-29 May 1980.

46. Wilms V., Herman H., "Plasma spraying of Al_2O_3 and Al_2O_3-Y_2O_3", *Thin Solid Films*, **39**, (1976), pp.251-262.

47. Binfield M.L., "Wear of plasma sprayed ceramics on steel", M.Sc. Thesis, Brunel University, 1990.

48. Levinstein, M.A., Eisenlohr A., Kramer B.E., "Properties of plasma sprayed materials", *Weld. J.; Weld. Res. Suppl.*, **40**, 8s (1961).

49. Kitahara S, Hasui A., "A study of the bonding mechanism of sprayed coatings", *J. Vac. Sci. Technol.*, **11**, (1974) pp. 747-754.

50. Marynowski C.W., Halden F.A., Farley E.P., *Electrochem. Technol.* **3** (3-4), 109, (1965).

51. Narayanasamy K., Radhakrishnan V., Narayanamurthi R.G., "Analysis of surface reproduction characteristics of different replica materials" *Wear*, **57** (1979) 63-69.

52. George A.F., "A comparative study of surface replicas", *Wear*, **57** (1979) 51-61.

53. Eyre T.S., "The use of a replication technique to study wear", *Tribology Int.*, August 1978, pp 241-242.

54. Gee M.G., "Guidelines for unlubricated sliding wear tests: Part 1, general approach" DMM(A)96, April 1993.

55. Eyre T.S., "Friction and wear control in industry", *Metals and Materials*, **7**, No. 3, pp. 143-148, March 1991

56. Gee M.G., "Wear Metrology: The art of determining a material's performance", *Materials World*, (1993), **1**, No.5, pp. 281-283

57. Davis F.A., Private communication, January 1991.

58. Gee M.G., "Effect of test machine dynamics on the sliding wear of alumina", Wear Testing of Advanced Materials, ASTM STP 1167, R. Divakar and P.J. Blau, Eds., American Society for Testing of Materials, 1992, pp. 24-44.

59. Wood R.J.K., Binfield M.L., Henderson J.P., "Sand Slurry Erosion Testing of Oilfield Materials", to be published in Wear.

60. "UCAR® Metal & Ceramic Coatings Physical Characteristics", Union Carbide Corporation, 1990

61. Bousfield B., Bousfield T., "Progress towards a metallographic standard", *Metals and Materials*, **6**, No. 3, pp. 146-148, March 1990.

62. Hibbs M.K., Sinclair R., *Acta Metallurgica*, **29**, 1981, pp. 1645-1654

63. Luyckx S.B., *Acta Metallurgica*, **16**, 1970, pp. 233-236.

64. Milewski W., *Proc. 7th Int. Thermal Spray Conf.*, Welding Research Institute, London, 1974, p.24.

65. Basinska-Pampuch S., Gibas T, *Ceramurgia Int.*, 1977, **3**, 152.

66. Troiano and Tokich, Trans. AIME **175** 728 (1948).

67. Exner H.E., *Int. Metals Review*, No.4, 1979, pp. 149-173.

68. Exner H.E., Gurland J., *Powder Metallurgy*,.**13**, No. 25, 1970, pp. 13-31.

69. Almond E.A., Roebuck B., *High Temperature and High Pressures*, **14**, 1982, pp. 143-154.

70. Over A., Stevens K., "Friction: The Ubiquitous Coefficient: Can it be Controlled" Surface Engineering, **9**, No.4, 1993, pp.305-311.

71. Johnson K.L., Contact mechanics, Cambridge University Press, 1985.

72. Marlow R., National Centre of Tribology, Warrington, U.K., CAST and QUEST programmes, January 1994.

73. Davis F.A., Cooper D., Wood R.J.K., "Engineering of wear resistant surfaces for the oil industry", *Tribologia*, **11**, (1992) No.3, pp.107-116.

74. Binfield M.L., Davis F.A., Pin-on-disc testing of detonation gun coatings, Unpublished work, BP Research Centre, Sunbury, U.K., 1992.

75. Evans A.G., "Abrasive wear in ceramics in an assessment", *NBS Spec. Publ. 562*, 1979, pp. 1-14 (National Bureau of Standards, Washington DC).

76. Lawn B.R., Swain M.V., *J. Mat. Sci.* **10**, 113-122, 1975.

77. Moore M.A., King F.S., "Abrasive Wear of Brittle Solids", *Wear* **60**, 1, Apr 1980, paper presented at the *Int. Conf.on Wear of Mater.*, Dearborn, Mich, Apr 16-18 1979, p 123-140.

78. Hutchings I.M., *Proc. 2nd European Conf. on Advanced Materials and Processes*, **2**, Institute of Materials, pp. 56-64, 1992.

79. Zum Gahr K.H., Eldis G.T., *Wear*, **64**, 175-194, 1980.

80. Hashish M., "An improved model of erosion by solid particle impact" *Proceedings of the 7th International Conference on Erosion by Solid and Liquid Impact*, Cambridge, 1987.

81. Sheldon G.L. & Finnie I., *J. Eng Ind,* **88**, (1966) 393.

82. Moore A.J. & Wood R.J.K. "Erosive wear mapping of pipe materials" *Plastic Pipes VIII, Konigshof,* September 1992.

83. Pennefather R.C., M.Sc. Thesis, *University of Cape Town*, 1986

84. Wright I.G., Shetty D.K., Clauer A.H., *Proc. 6th Int. Conf. on Erosion by Liquid and Solid Impact*, 1983, pp. 63.1-63.8

85. Conrad H., Shin Y., Sargent G.A., *Proc. Int. Conf. in Recent Developments in Special Steels and Hard Metals*, Pretoria, South Africa, 1982, pp. 423-429.

86. Shetty D.K., Wright I.G., Stropki J.T., *Trans ASLE*, **28**, 1984, pp.123-133.

87. Hankey S.E., M.Sc. Thesis, *University of Cape Town*, 1987.

88. Binfield M.L., Davis F.A., "Selection of Wear Resistant Materials for the Oil Industry", taken from a poster presentation at "Wear of Materials" Conference, San Francisco, 1993 - Unpublished.

89. Heathcock C.J., Ph.D. Thesis, *University of Cape Town*, 1980.

90. Kato H., Ph.D. Thesis, Brunel University, 1993.

Appendix I - Summary of terms used in describing the microstructure of WC-Co alloys

Microstructural Features

Microstructural features that are of importance in the production of the sintered alloy and which may have relevance to the sprayed alloy are dictated by the nature of the starting powders and are developed during sintering. These features include grain size, mean free path and contiguity.

Grain Size (d_{WC})

The WC grain size is dependent on the size and distribution of the starting powders, milling and sintering conditions and the composition of the alloy. A few large grains occur due to discontinuous grain growth during oversintering.

Mean Free Path (λ)

The mean free path is a measure of the thickness of the cobalt layers and is dependent upon binder content and particle size. It can be evaluated by the following expression.

$$\lambda = d_{WC} \cdot \frac{v_{CO}}{(1-v_{CO})(1-C)}$$

Where v_{CO} is the vol% binder and C is the contiguity.

Contiguity (C)

Contiguity is defined as the fraction of the total internal surface area of a phase shared by particles of the same phase. There is difficulty in calculating the number of WC-WC grain contacts as there may be a thin layer of cobalt between the grains. Normally a continuous carbide skeleton is assumed in alloys containing up to 10-15 vol% cobalt. However, some workers believe that contiguity, while decreasing with increasing binder content, still exists in grades containing over 30 vol% cobalt.

Mechanical Properties

Toughness and hardness of WC-Co are both strongly dependent on the microstructural properties.

Hardness

Hardness decreases with increasing binder content and increasing grain size. An apparently simple function between hardness and mean free path has been observed, but on closer analysis it was found that additional parameters such as particle size and composition are necessary to describe the relationship precisely. The precipitation of η carbide has been associated with an increase in hardness.

Toughness

Fracture toughness is very important for WC-Co alloys as they generally fail by brittle fracture at normal temperatures. It is found that the fracture toughness increases linearly with increased mean free path.

Tables & Figures

Table 2.1 - Properties of UCAR® Metal and Ceramic Coatings

Coating Designation	Principal Constituent(s)	Nominal Composition (Weight %)	Hardness (HV .3) (kg/mm²)	Hardness (Rc)	Tensile Bond Strength* (psi)	Metallographic Apparent Porosity (Volume %)	Density (gm/cm³)	Modulus of Rupture (10³ psi)	Modulus of Elasticity (10⁶ psi)	Coefficient of Thermal Expansion 10⁻⁶ in/in/°F	Maximum Operating Temperature (°F)	Maximum Operating Temperature (°C)	Main Features
LW-1	Tungsten Carbide	89W 7Co 4C	1300	72	10,000 min	0.50 max	14.2	72	21	4.0	1000	550	Excellent wear and erosion resistance
LW-1N30	Tungsten Carbide	85W 11Co 4C	1150	70	10,000 min	1.0 max	11.5	110	20	4.1	1000	550	Good wear, impact and thermal shock resistance
LW-1N40	Tungsten Carbide	83W 14Co 3C	1075	69	10,000 min	1.0 max	13.1	120	25	4.7	1000	550	Excellent resistance to severe impact sliding wear
LW-2A	Tungsten Carbide	90W 6Co 4C	1350	74	10,000 min	0.50 max	14.2	58	23	4.0 Estimated	900	475	Similar to LW-1. Has smoother as-deposited surface
LW-2B	Tungsten Carbide	84W 12Co 4C	1250	72	10,000 min	0.75 max	11.5	85	22	4.1 Estimated	900	475	Similar to LW-1N30. Has smoother as-deposited surface
LW-2C	Tungsten Carbide	81W 16Co 3C	1100	70	10,000 min	0.75 max	11.2	98	22	4.7 Estimated	900	475	Similar to LW-1N40. Has smoother as-deposited surface
LW-5	Tungsten Chromium Carbide	70W 19Cr 5Ni 4C	1000	70	7,000 min	1.5 max	10.4	40	18	4.0	1200	650	Recommended where corrosion or oxidation may be factors contributing to wear
LW-15	Tungsten Carbide	81W 8Co 3Cr 5C	1000	69	10,000 min	1.5 max	12.5	19	17	4.3	800	425	Improved resistance in acidic environments
LW-26	Tungsten Carbide	WC based	1100	70	10,000 min Diffusion Bond	0.5	11	100	32	5.0	Not established		Excellent abrasion resistance, uniform wear, good strength. Thick coating possible
LW-45	Tungsten Carbide	W Co Cr C	900	67	10,000 min	2 max	12.0	19	10		800	425	Good in high pressure applications
LC-1B	Chromium Carbide	65(92Cr 8C) + 35(80Ni 20Cr)	700	60	10,000 min	1 max	6.4	100	21	6.4	1400	760	Excellent wear and impact resistance at elevated temperature. Resists flame impingement
LC-1C	Chromium Carbide	80(92Cr 8C) + 20(80Ni 20Cr)	775	61	10,000 min	1 max		77	18	5.8	1400	760	Excellent sliding wear resistance at elevated temperature. Resists flame impingement
LC-1H	Chromium Carbide	90(92Cr 8C) + 20(80Ni 20Cr)	800	61	10,000 min	1.5 max	6.1	83	13	5.8	1400	760	Good wear resistance for seals and sliding surfaces in sodium cooled nuclear reactors
WT-1	Tungsten Titanium Carbide	83(W Ti) Carbide + 17Ni	1200	71	10,000 min	1.0 max	12.1	55	20	4.4	1000	550	Smooth as-coated surface. Excellent galling resistance to steel. Good sand abrasion resistance
LA-2	Aluminum Oxide	Al_2O_3	1000	69	9,000 min	2.0 max	3.3	22	14	3.9	1800	975	Good resistance to wear, chemical attack and high temperature deterioration. Good dielectric
LA-6	Aluminum Oxide	Al_2O_3	700	60	6,500 min	1.0 max	3.1	17	7.9	3.9	1800	975	Good resistance to wear, chemical attack and high temperature deterioration. Good dielectric
LA-7	Aluminum Oxide + Titanium Dioxide	60(Al_2O_3) + 40(TiO_2)	850	66	9,000 min	1.0 max	3.6	21	11		1300	700	Excellent resistance to yarn abrasion. Nodular surface provides low coefficient of friction. Semi-conductor
LC-4	Chromium Oxide	Cr_2O_3	1150	71	5,000 min	1.0 max	5.0	19	15	3.7	1300	700	Excellent resistance to sliding wear in acid, base, solutions. Compatible with metallic and non-metallic packing materials
LC-19	Chromium Oxide + Aluminum Oxide	70(Cr_2O_3) + 30(Al_2O_3)	700	60	6,000 min	4.0 max	4.3			3.8	1000	550	Good resistance to sliding wear and thermal shock
LN-28	Nickel	Nickel	200		5,000 min	1.5 max				8.9	1000	550	Dense machinable material for build up of worn parts
LN-3	Nickel Chromium	80Ni 20Cr	400	48	10,000 min	0.5 max	8.1	190	26				Repair material. Resistant to salt spray corrosion
LCO-17	Cobalt based alloy with Alumina dispersion	90(54Co 25Cr 10Ta 7.5Al 0.8Y 0.7Si 2C) + 10Al_2O_3	800	64	10,000 min (heat treatment develops a diffusion bond)	1.0 max				8.2	2000	1100	Good high temperature oxidation resistance
LDT-400C	Tribaloy 400™	52Co 32Mo 7Cr 1Si 1C	730	51	10,000 min	1.0 max	8				1300	700	Good corrosion resistance and high temperature wear resistance
LDT-800	Tribaloy 800™	52Co 28Mo 17Cr 3Si	750	62	8,000 min	1.0 max	8	18		7.3	1500	800	Good wear resistance at elevated temperatures. Good oxidation resistance up to 1500°F
LSR-1	Titanium Carbide	Titanium Carbide	3000	—	Metallurgical Bond	Non-measurable	4.31		45-60	4.5	750	400	Applies extremely hard, thin coating to difficult shapes. Substrate limited

All data [illegible]

UCAR and Union Carbide [illegible]

* [illegible]

* Maximum operating temperature in an oxidizing atmosphere. [illegible]

Table 4.1 - Comparisons of Replicas

	Acetate	PMMA	Silicone Rubber
Cost	Lowest	Low	Low
Time	20 min	30 min	2 hours
Ease of Use	Good	Good	Good
Optical	Good	Fair	Fair
Coated	Excellent	Very Good	---
SEM	Excellent	Very Good	---
Talysurf	Fair	Excellent	Poor

Table 4.310 - Friction and Wear Data for Ramp Tests

Load (N)	Friction Coefficients (μ)			Transducer Wear (μm)		
	Speed (m/s)			Speed(m/s)		
	0.035	0.07	0.14	0.035	0.07	0.14
98.1	0.4	0.45	0.43	0	9	4
196.2	0.42	0.5	0.42	3	11	7
294.3	0.39	0.5	0.42	20	20	18
392.4	0.4	0.54		35	33	

Table 4.410 - Friction and Wear Data For LW45 (Pin-on-Flat Tests)

Load (N)	Duration (min)	Sliding Distance (m)	Wear Volume (m^3)	Wear Vol-As Prepared (m^3)	Specific Wear Rate (m^3/Nm)	Av μ
98.1	60	98.4	1.42E-10	5.05E-11	5.24E-15	0.4
98.1	120	196.8	2.19E-10	1.28E-10	6.63E-15	0.4
98.1	180	295.2	2.21E-10	1.30E-10	4.49E-15	0.32
98.1	300	492	2.37E-10	1.46E-10	3.03E-15	0.3
98.1	420	688.8	2.11E-10	1.20E-10	1.78E-15	0.41
196.2	30	49.2	2.51E-10	1.60E-10	1.66E-14	0.38
196.2	55	90.2	2.21E-10	1.30E-10	7.35E-15	0.29
196.2	90	147.6	2.61E-10	1.70E-10	5.87E-15	0.32
196.2	120	196.8	3.01E-10	2.10E-10	5.44E-15	0.31
196.2	180	295.2	3.51E-10	2.6E-10	4.49E-15	0.42
196.2	300	492	3.69E-10	2.78E-10	2.88E-15	0.28
196.2	360	590.4	2.84E-10	1.93E-10	1.67E-15	0.21
196.2	420	688.8	3.01E-10	2.1E-10	1.55E-15	0.33
294.3	60	98.4	4.55E-10	3.64E-10	1.26E-14	0.43
294.3	150	246	9.49E-10	8.58E-10	1.18E-14	0.31
294.3	300	492	9.86E-10	8.95E-10	6.18E-15	0.2
294.3	420	688.8	7.97E-10	7.06E-10	3.48E-15	0.39
392.4	6	9.84	9.5E-10	8.59E-10	2.22E-13	0.34
392.4	10.4	17.056	3.66E-09	3.57E-09	5.34E-13	0.37
392.4	33	54.12	7.09E-09	7E-09	3.3E-13	0.31

Table 4.501 - Wear Test Data for Diamond-on-Flat Tests for LW45

Actual Load (N)	Sliding Distance (m)	Wear Volume (m^3)	Specific Wear Rate (m^3/Nm)
19.62	1.69	3.76E-12	1.14E-13
19.62	3.39	1.72E-11	2.58E-13
19.62	8.49	4.14E-11	2.49E-13
19.62	16.96	8.46E-11	2.54E-13
19.62	34.00	1.09E-10	1.63E-13
39.24	1.69	4.99E-11	7.54E-13
39.24	3.36	8.53E-11	6.46E-13
39.24	8.46	1.76E-10	5.32E-13
39.24	16.94	2.33E-10	3.51E-13
39.24	33.70	2.99E-10	2.26E-13
58.86	1.67	1.30E-10	1.32E-12
58.86	3.36	1.80E-10	9.10E-13
58.86	8.45	2.99E-10	6.01E-13
58.86	16.84	3.81E-10	3.85E-13
58.86	33.67	4.73E-10	2.39E-13

Table 4.600 - Erosion Data

Erodant Grade	Mean Part Dia (µm)	Test Mat	Time (min)	Density (mg/mm)	Nozzle Dia (mm)	Flow R (kg/min)	Nozzle Vel (m/s)	Mass Loss (mg)	Vol Loss (mm^3)	TEV (m^3)	Vs (x 10E9)	Vu (um^3)	Ek (J)	EkV 0.5 $J(m/s)^{-1}$
110	135	F255	5	7.81	6.15	30.95	17.36253	3.3	0.422535	0.001222	345.8554	0.445606	5.17E-07	2.15E-06
110	135	F255	10	7.81	6.15	30.0375	16.85063	8.6	1.101152	0.002371	464.3506	0.598277	4.87E-07	2E-06
110	135	F255	15	7.81	6.15	30.0375	16.85063	12.2	1.5621	0.003557	439.1532	0.565812	4.87E-07	2E-06
110	135	F255	30	7.81	6.15	30.95	17.36253	25.1	3.213828	0.00733	438.4329	0.564884	5.17E-07	2.15E-06
110	135	F255	45	7.81	6.15	30.95	17.36253	33.5	4.289373	0.010995	390.1063	0.502619	5.17E-07	2.15E-06
110	135	F255	60	7.81	6.15	30.95	17.36253	45.2	5.787452	0.014661	394.7643	0.508621	5.17E-07	2.15E-06
110	135	F255	120	7.81	6.15	30.0375	16.85063	80.6	10.3201	0.028457	362.6614	0.467259	4.87E-07	2E-06
110	135	F255	180	7.81	6.15	30.0375	16.85063	123.9	15.86428	0.042685	371.6604	0.478853	4.87E-07	2E-06
110	135	F255	240	7.81	6.15	30.0375	16.85063	130.3	16.68374	0.056913	293.1438	0.377691	4.87E-07	2E-06
110	135	F255	300	7.81	6.15	31.8625	17.87443	209.1	26.77337	0.075464	354.7842	0.45711	5.47E-07	2.31E-06
110	135	F255 (30°)	120	7.81	6.15	30.0375	16.85063	200.2	25.63229	0.028457	900.7509	1.160542	4.87E-07	2E-06
50	235	LW45	10	11.95122	6.15	48.288	27.08891	20.5	1.715306	0.003812	449.9505	3.0579	6.63E-06	3.45E-05
50	235	LW45	30	11.95122	6.15	48.288	27.08891	78.6	6.576735	0.011437	575.0587	3.908145	6.63E-06	3.45E-05
50	235	LW45	300	11.95122	6.15	31.863	17.87471	55	4.602041	0.075465	60.98245	0.414442	2.89E-06	1.22E-05
50	235	LW45	300	11.95122	6.15	55.5875	31.18383	653.8	54.70571	0.131655	415.5245	2.823938	8.79E-06	4.91E-05
110	135	LW45	15	11.95122	6.15	30.0375	16.85063	0.8	0.066939	0.003557	18.8185	0.024246	4.87E-07	2E-06
110	135	LW45	30	11.95122	6.15	30.0375	16.85063	1	0.083673	0.007114	11.76156	0.015154	4.87E-07	2E-06
110	135	LW45	45	11.95122	6.15	29.5812	16.59465	1.8	0.150612	0.010509	14.33159	0.018465	4.72E-07	1.92E-06
110	135	LW45	120	11.95122	6.15	29.5812	16.59465	3.3	0.276122	0.028024	9.852967	0.012695	4.72E-07	1.92E-06
110	135	LW45	180	11.95122	6.15	30.0375	16.85063	4.2	0.351429	0.042685	8.233095	0.010608	4.87E-07	2E-06
110	135	LW45	300	11.95122	6.15	31.8625	17.87443	21.3	1.782245	0.075464	23.61721	0.030429	5.47E-07	2.31E-06
HH	62	LW45	360	11.95122	6.15	30.038	16.85091	9.8	0.82	0.085371	9.605117	0.001199	4.71E-08	1.93E-07

Table 4.61 - Mean Particle Diameters of Different Test Sands

Sand Type	Mean Particle Diameter (μm)
Redhill 50	235
Redhill 65	216
Redhill 110	135
Redhill HH	62

Table 5.1 - Typical Weighting System (after Davis et al[73])

		Weighting Factor					
		0	**2**	**4**	**6**	**8**	**10**
Pin-on-plate - Adhesive	m^3/Nm	10^{-17}	10^{-16}	10^{-15}	10^{-14}	10^{-13}	10^{-12}
Diamond-on-plate - Abrasive	m^3/Nm	10^{-15}	10^{-14}	10^{-13}	10^{-12}	10^{-11}	10^{-10}
Slurry Erosion	μm^3/ impact	10^{-4}	10^{-3}	10^{-2}	10^{-1}	1	10

Table 5.2 - Pin-on-disc wear tests specific wear rates (x 10^{-17} m^3/Nm) [74]

Load (N)	**LW5**		**LW15**		**LW45**	
	Pin	**Disc**	**Pin**	**Disc**	**Pin**	**Disc**
5	172	Transfer	2870	0	612	0
10	371	533	423	130	480	232
20	253	133	378	280	362	140

Table 5.3

(a) Comparative wear of sintered tungsten carbide (Boart V7) and detonation gun sprayed tungsten carbide (LW45). Also shown Stellite S6.[88]

MATERIAL	DRY SLIDING ADHESIVE		SAND EROSION	
	PIN	DISC	HIGH ENERGY	LOW ENERGY
LW45	3	3	7	3
S6	6	7	6	4
WC-V7	3	1	4	3

(b) The test rating system

WEAR TEST	WEAR UNIT	TEST RATING					
		0	2	4	6	8	10
Dry Sliding, Adhesive	m^3/Nm	10^{-17}	10^{-16}	10^{-15}	10^{-14}	10^{-13}	10^{-12}
Low Energy Sand Erosion	mm^3/ impact	10^{-4}	10^{-3}	10^{-2}	10^{-1}	1	10
High Energy Sand Erosion	mm^3/ impact	10^{-2}	10^{-1}	1	10	10^2	10^3

Table 5.4 - A Simplified Selection Procedure (after Davis et al [73])

		LW45		AISI 410*	
Wear Mechanism	Weighting Factor (WF)	Test Rating (TR)	WF x TR	Test Rating (TR)	WF x TR
Adhesive	0.30	5	1.5	6†	1.8
Abrasive	0.40	5	2.0	8	3.2
Erosive	0.30	4	1.2	7	2.1
Weighted Average Rating Σ (WF x TR)			**4.7**		**7.1**

---

* F255 for erosion tests

† Not strictly comparable as tests were conducted at different loads

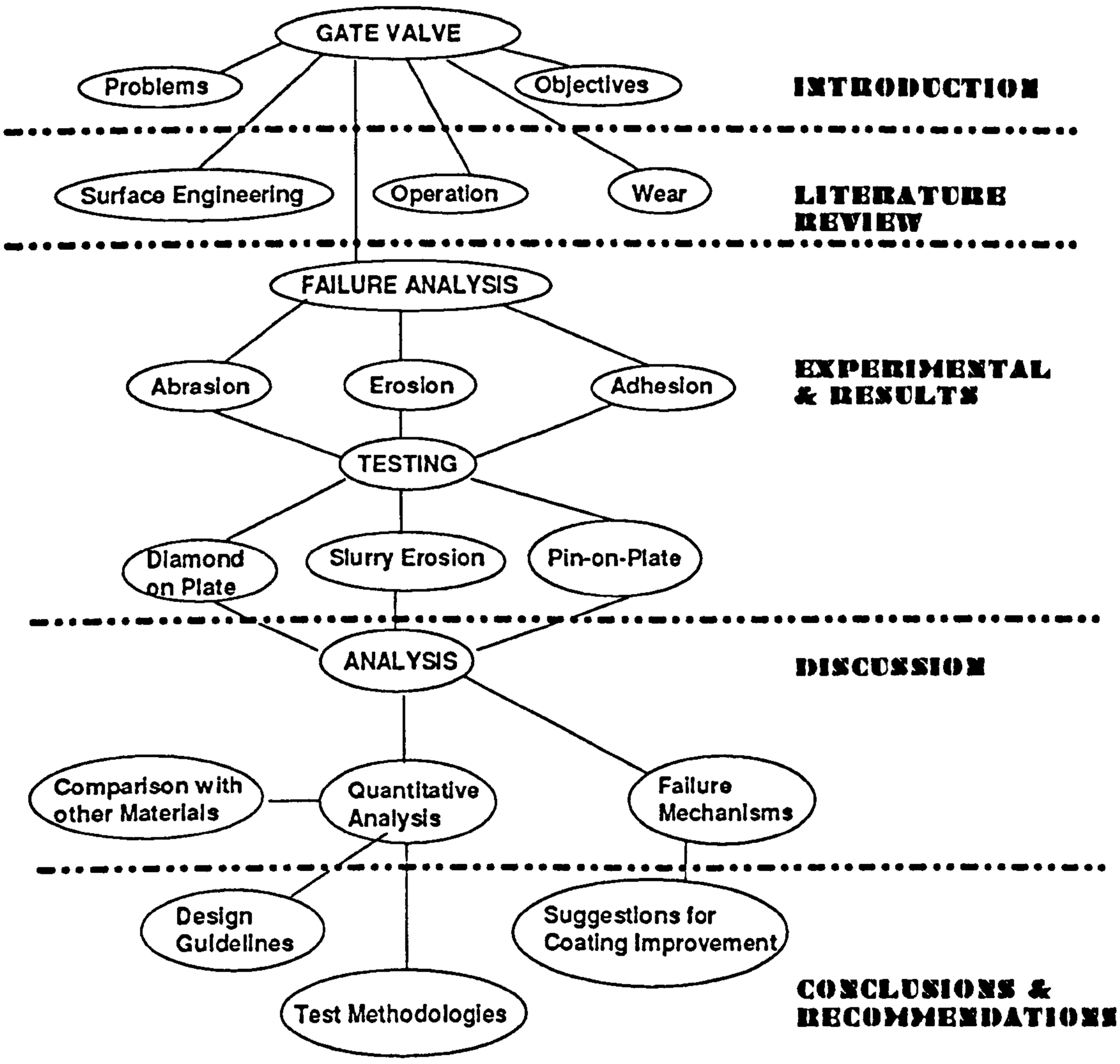

Figure 1 - Thesis Outline

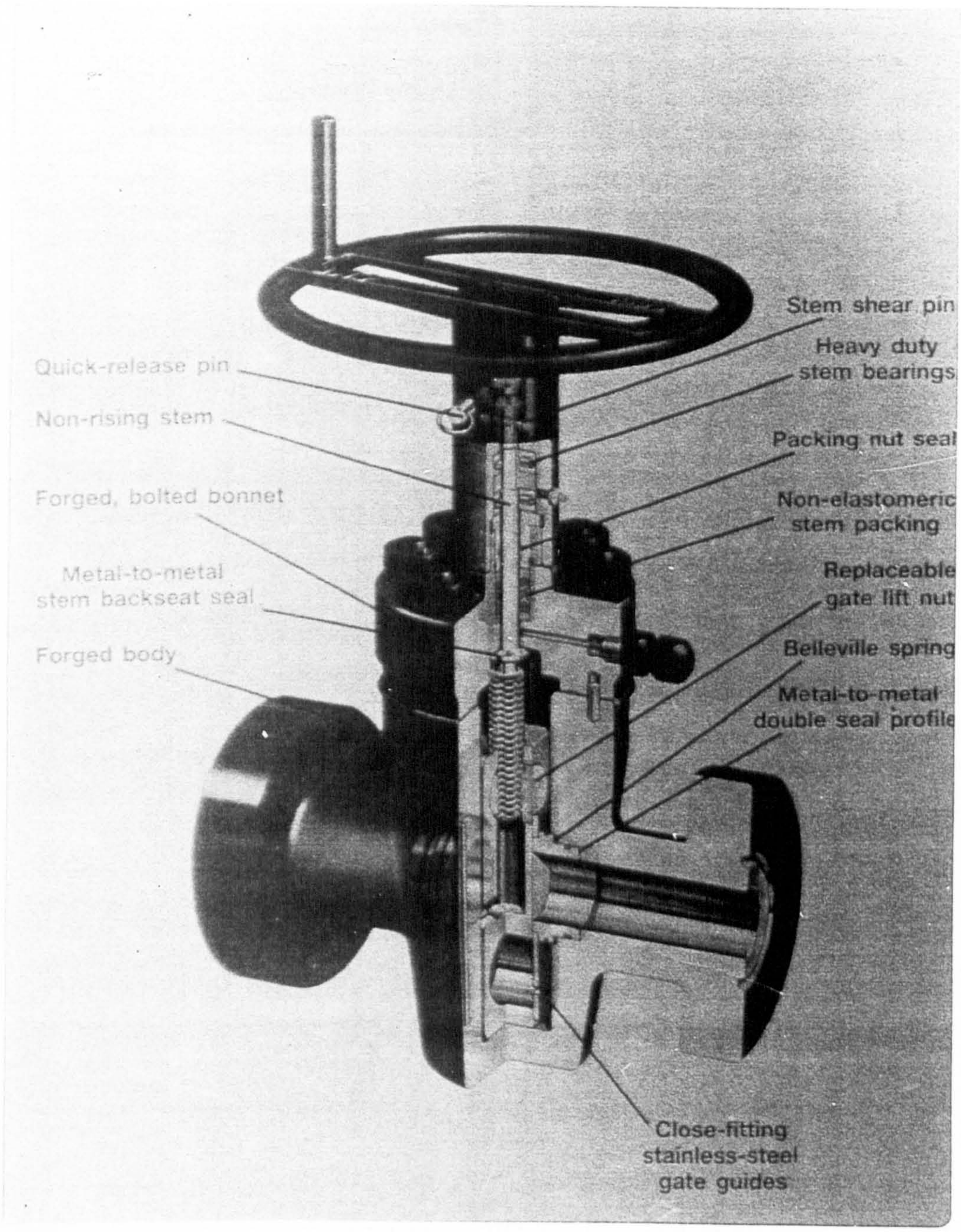

Figure. 2.1 - Schematic diagram of a typical manually operated gate valve

(a) Open: flow normal

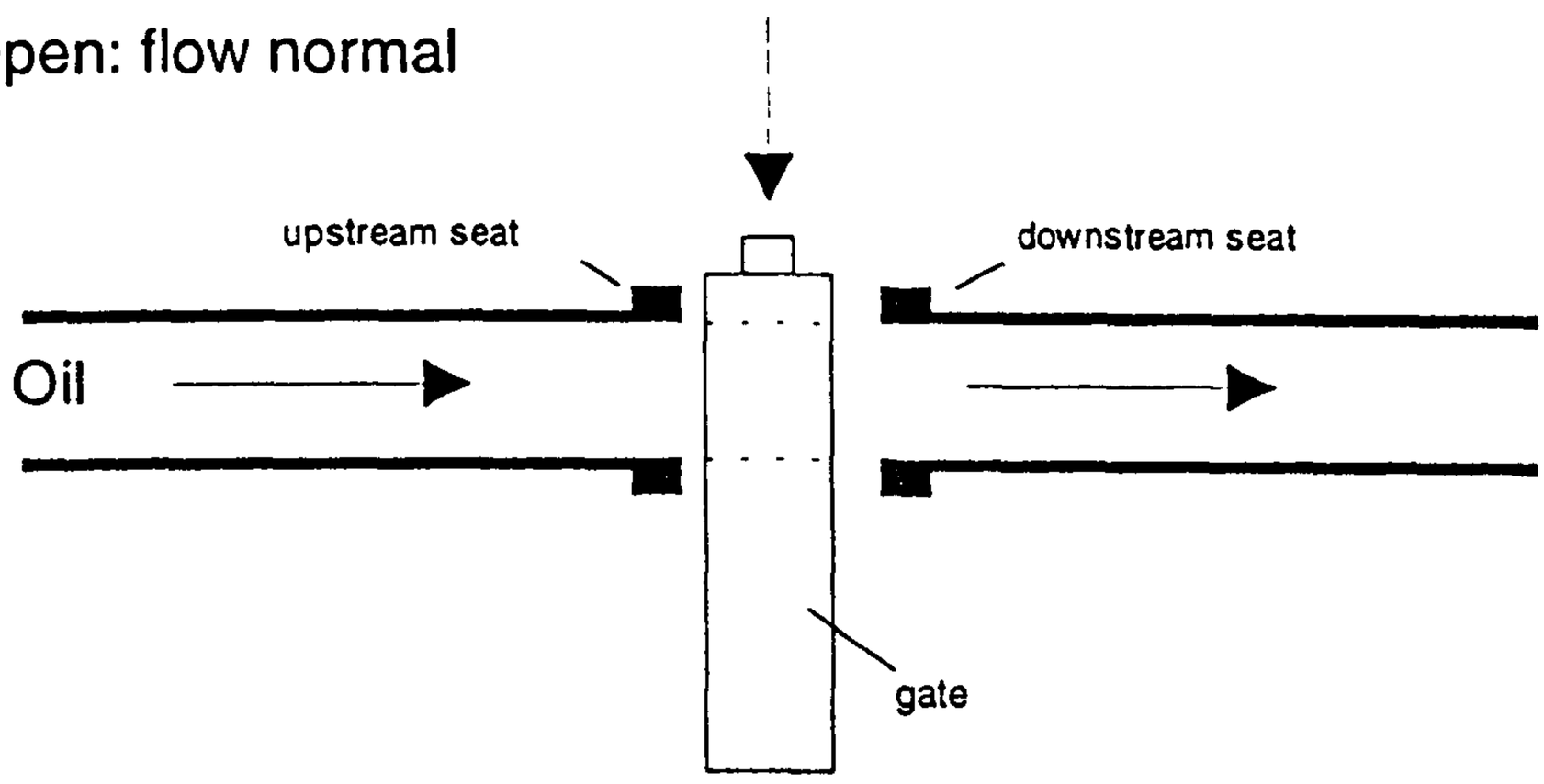

(b) Closed: Liquid pressure forces sealing on downstream seat

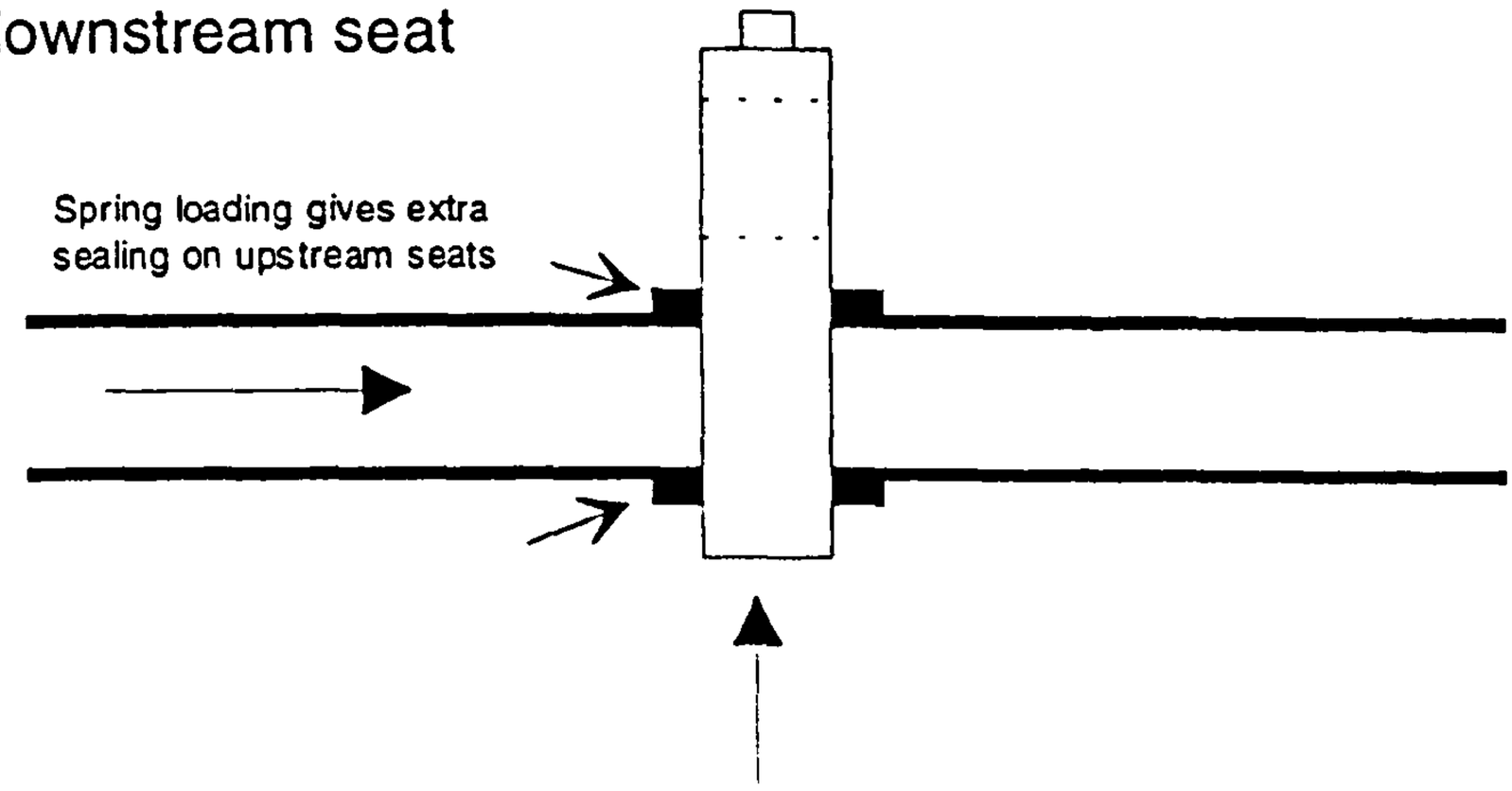

Figure 2.2 - Schematic diagram showing gate valve sealing principle

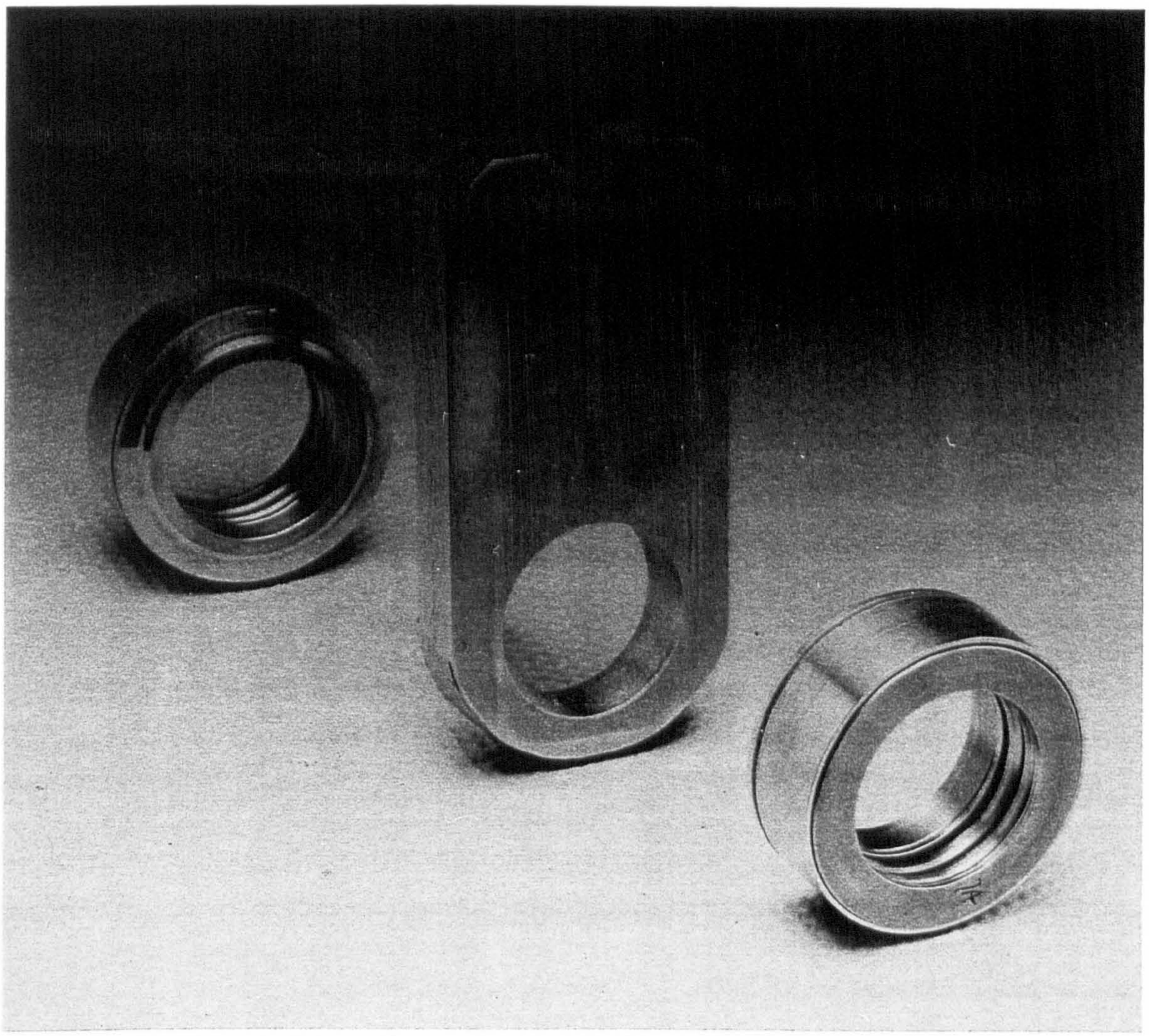

Figure. 2.3 - Typical gate and seats

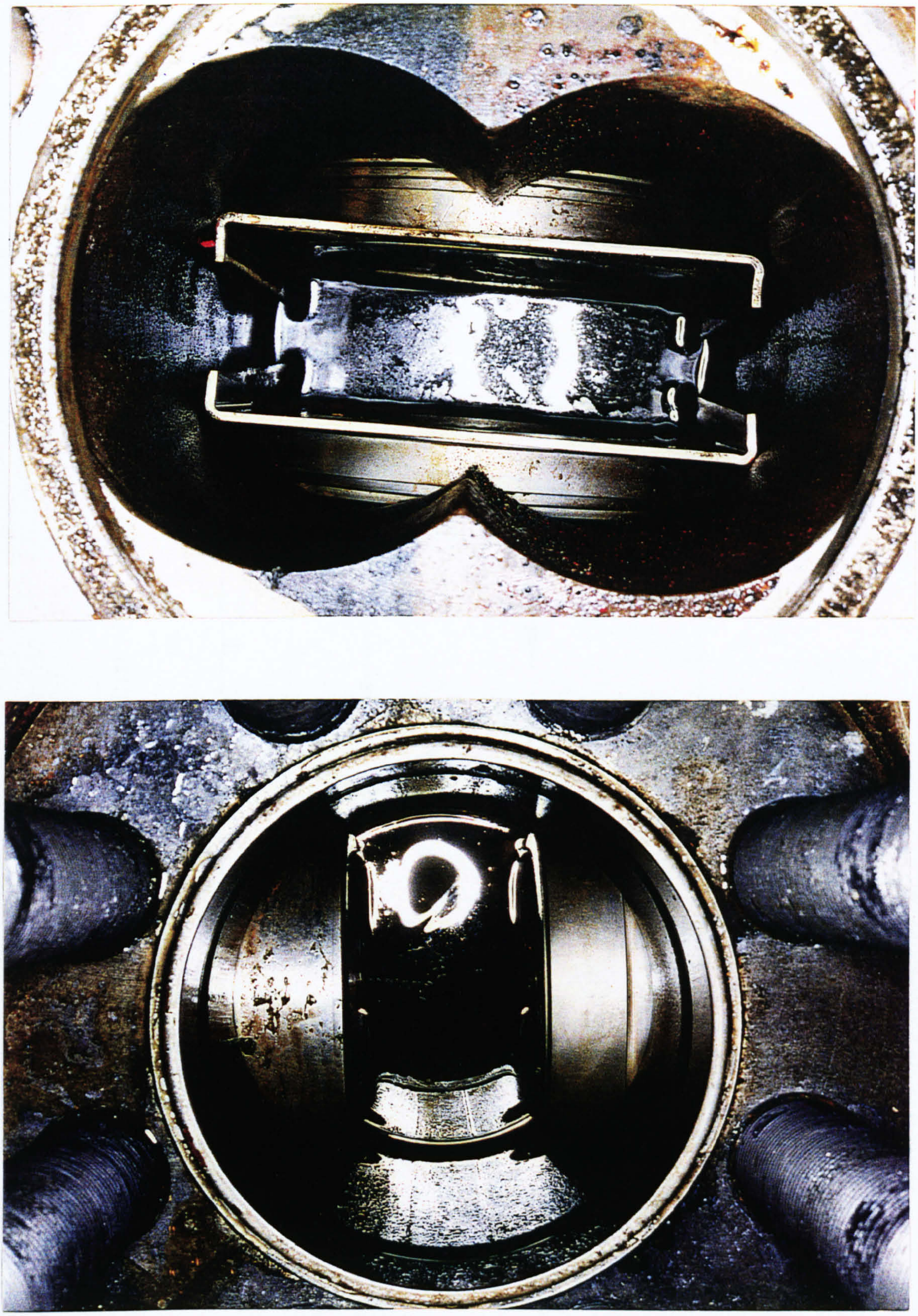

Figure. 2.4 - Seats in situ following pipe loop test

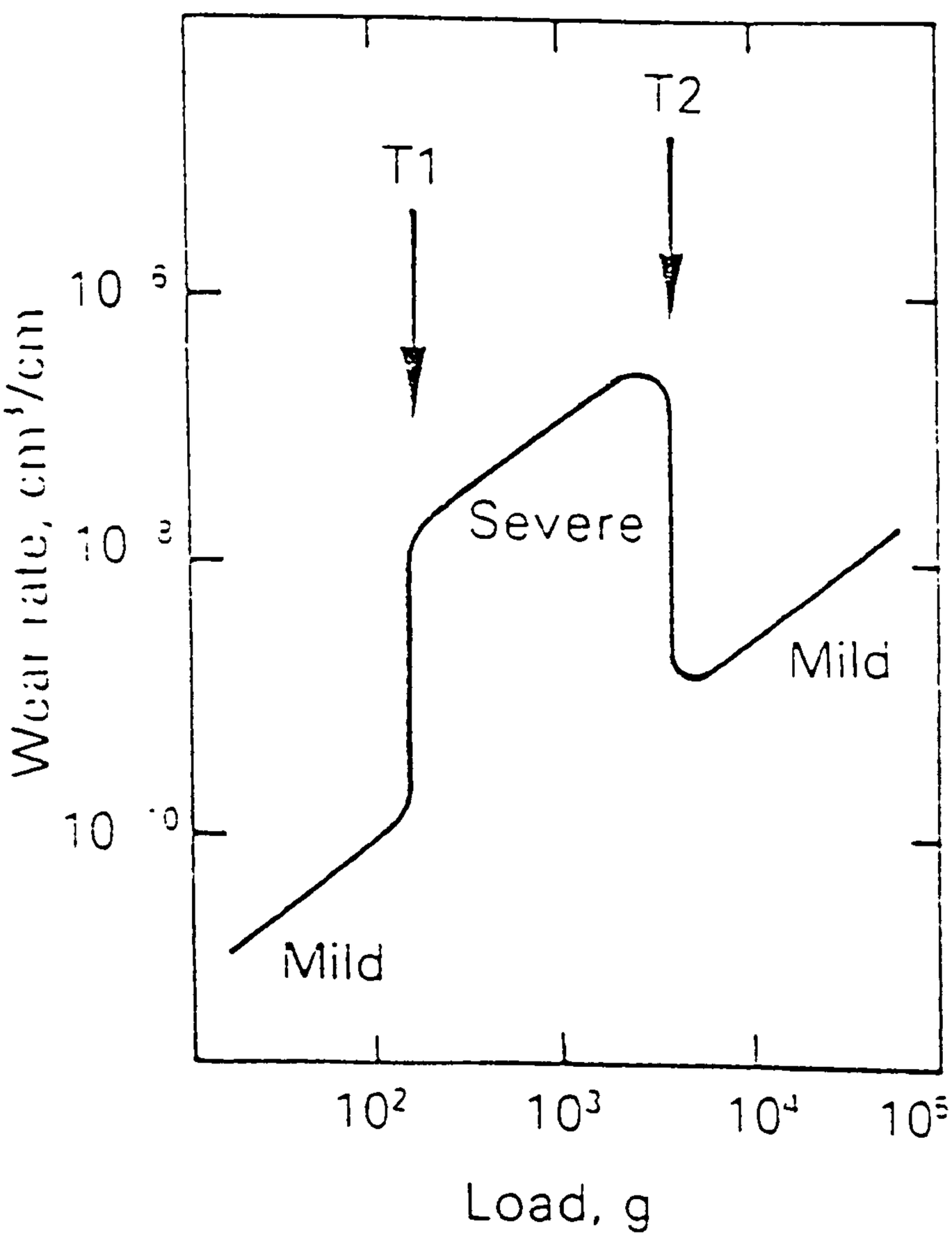

Figure 2.5 - Transition wear behaviour for steel (after Welsh[18])

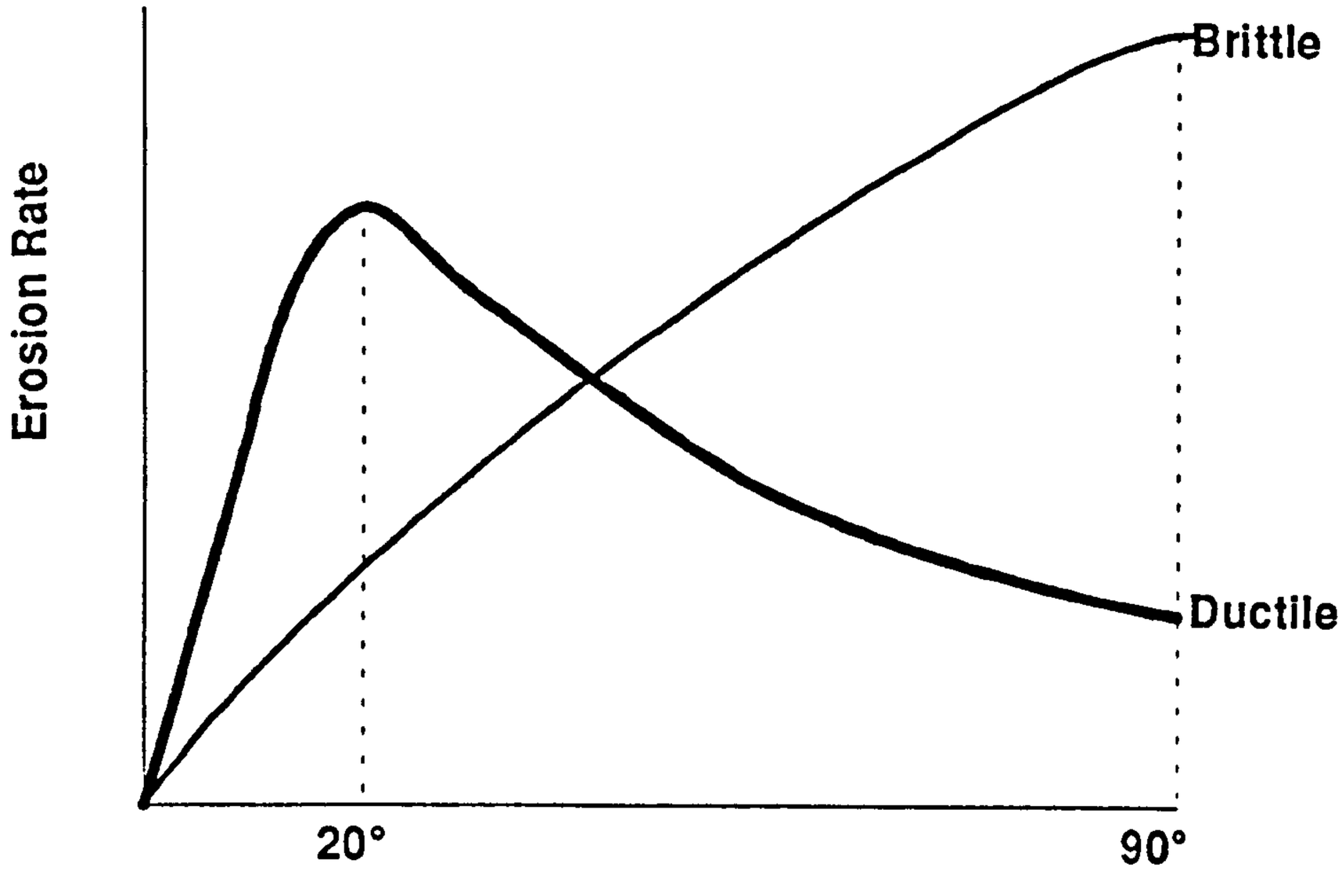

Figure 2.6 - Erosion Rates for Ductile and Brittle Solids

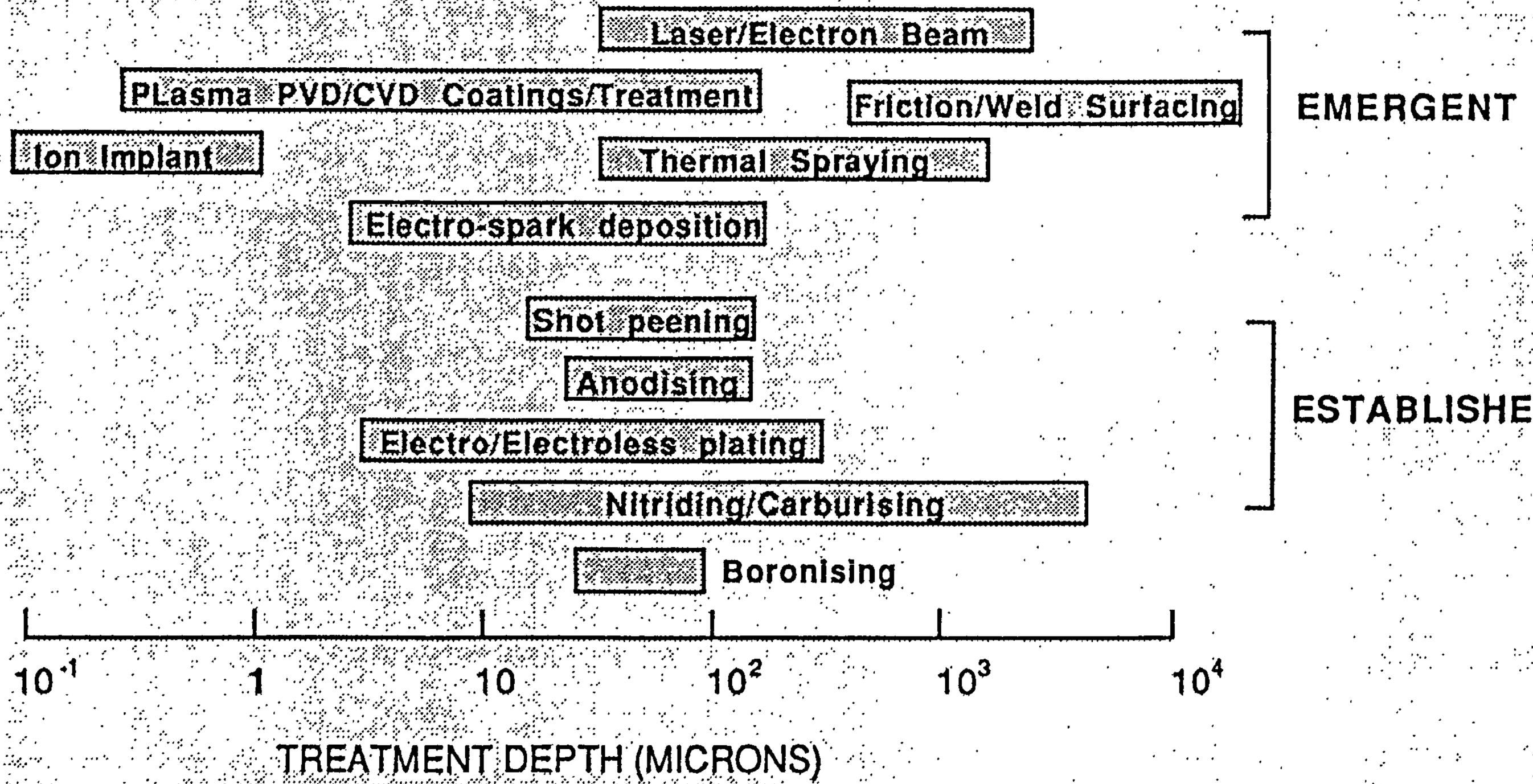

Figure 2.7 - Some Surface Engineering Techniques

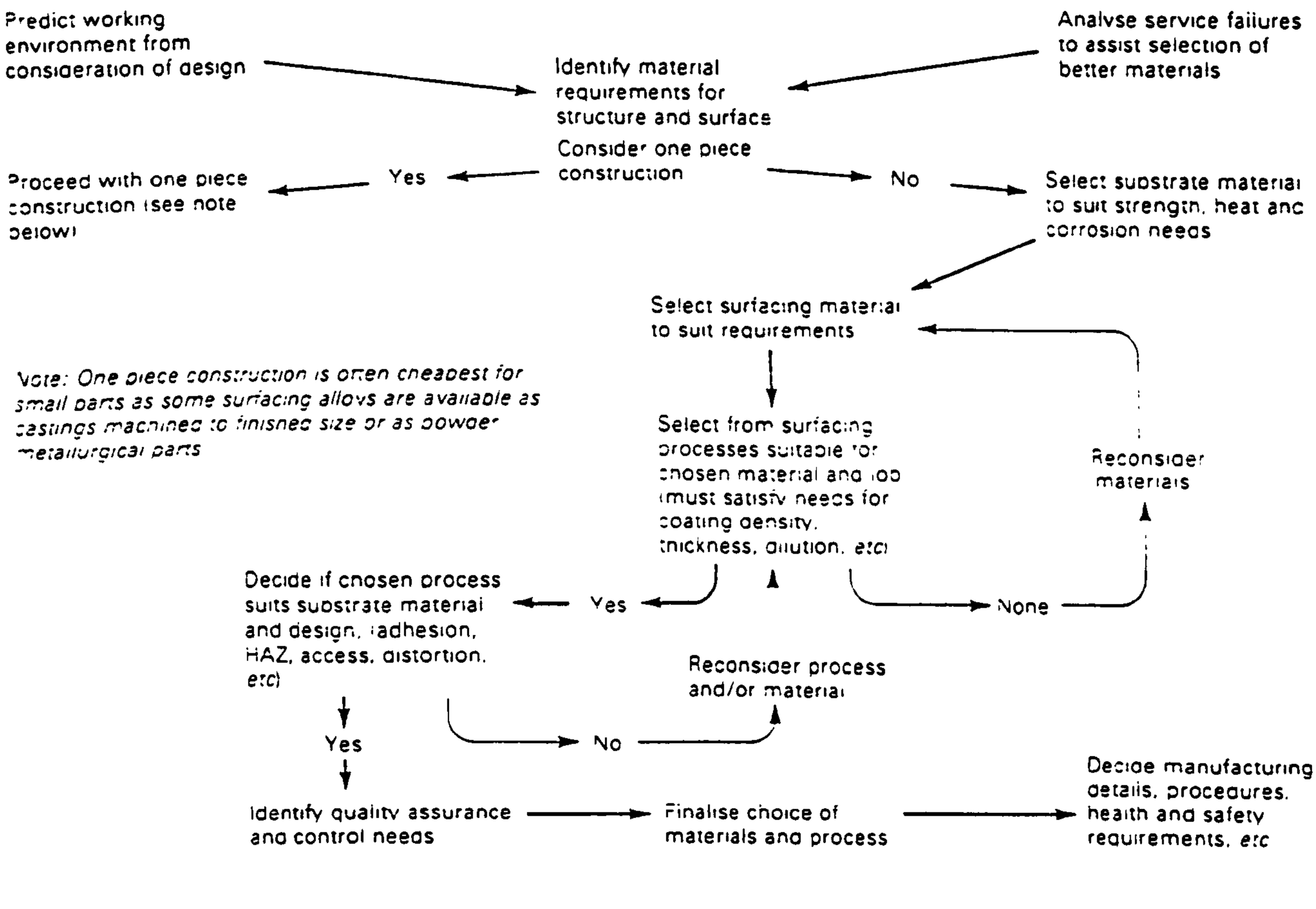

Figure. 2.8 - A typical selection procedure for surface treatments and coatings

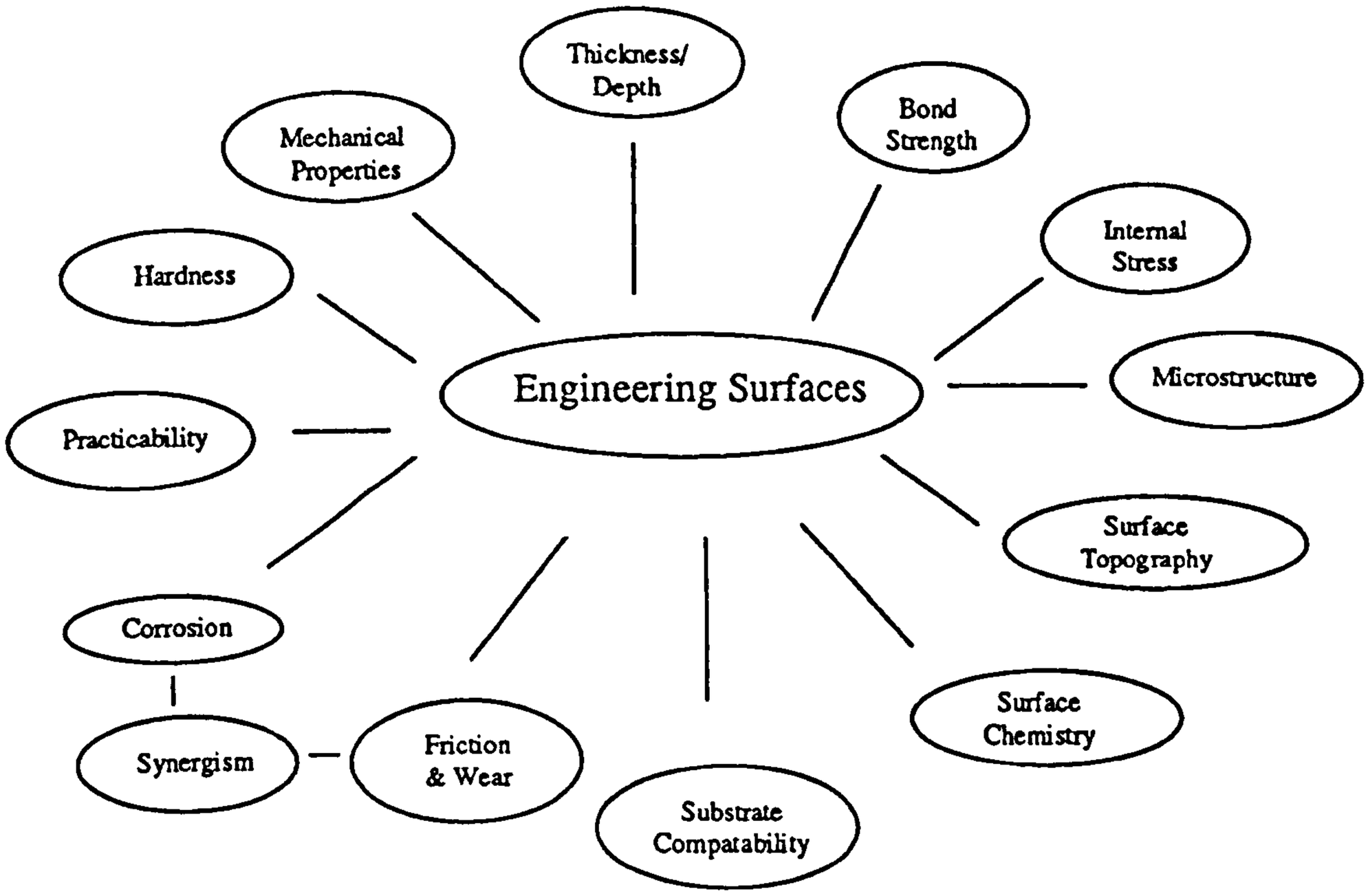

Figure 2.9 - Fundamental Points to Consider when Specifying a Surface Treatment or Coating

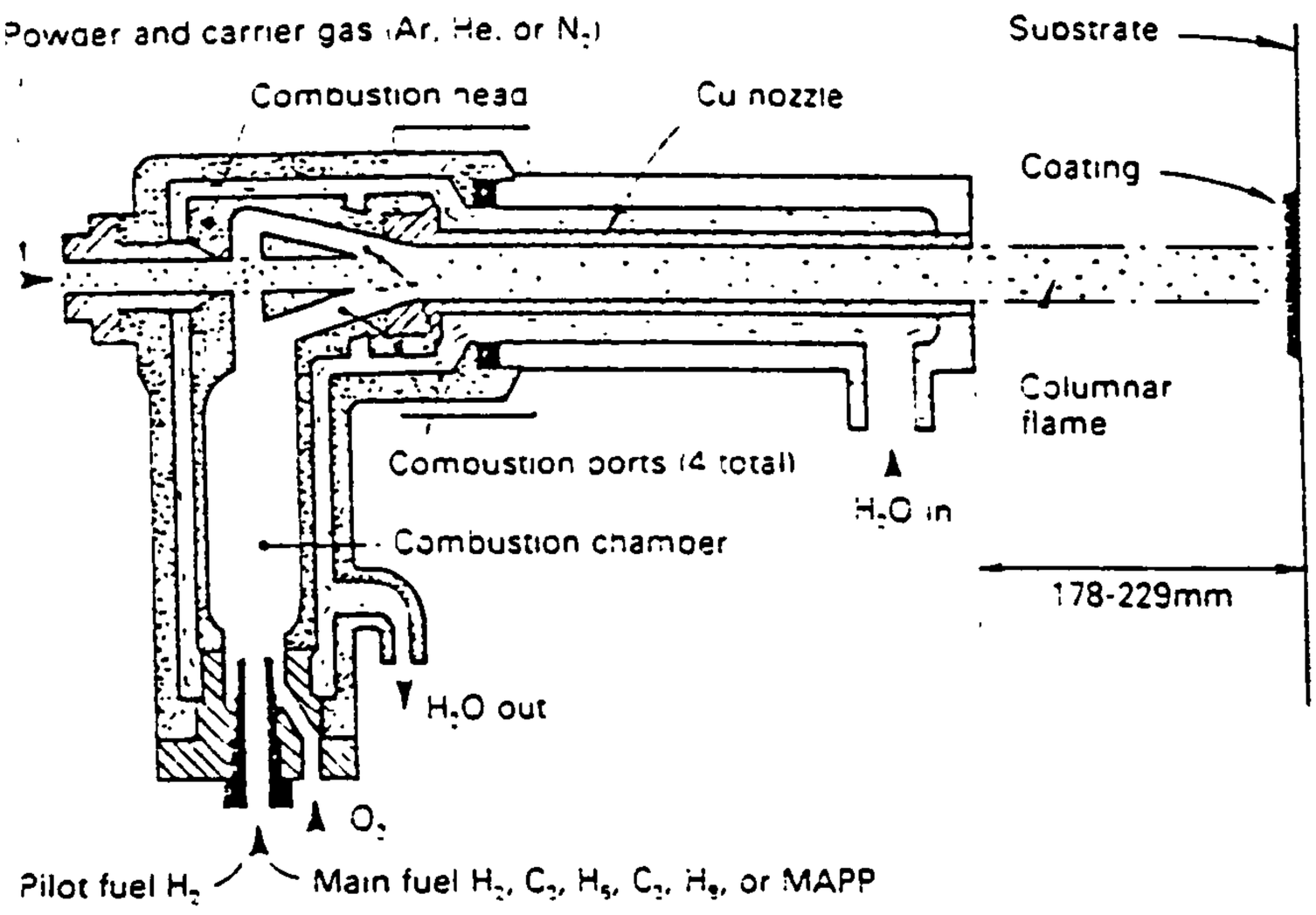

Figure. 2.10 - Schematic diagram of a HVOF gun

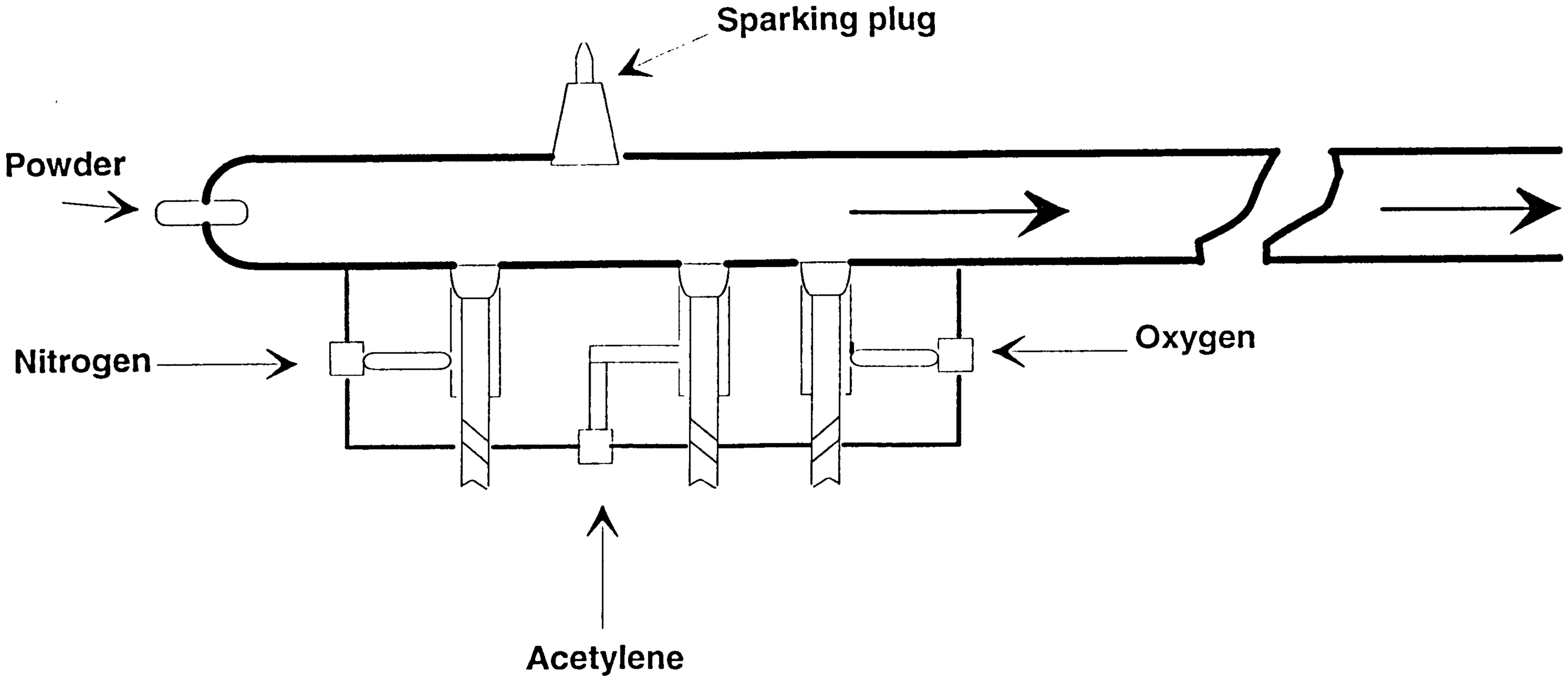

Figure 2.11 - The Detonation Gun

Figure 2.12 - Variation of temperature of particles with their size

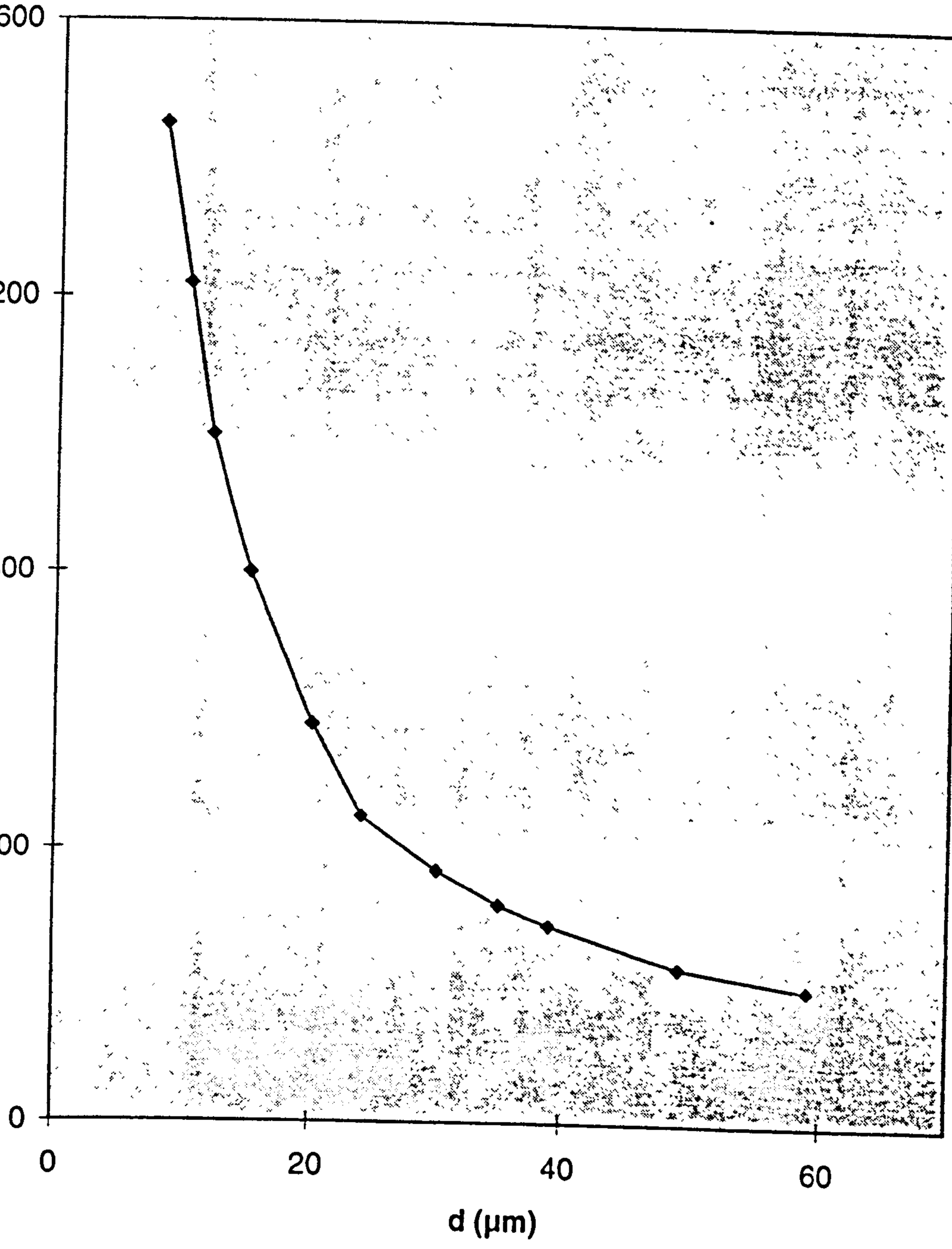

Fig. 3.1(a) Typical gate from test valve (downstream face)

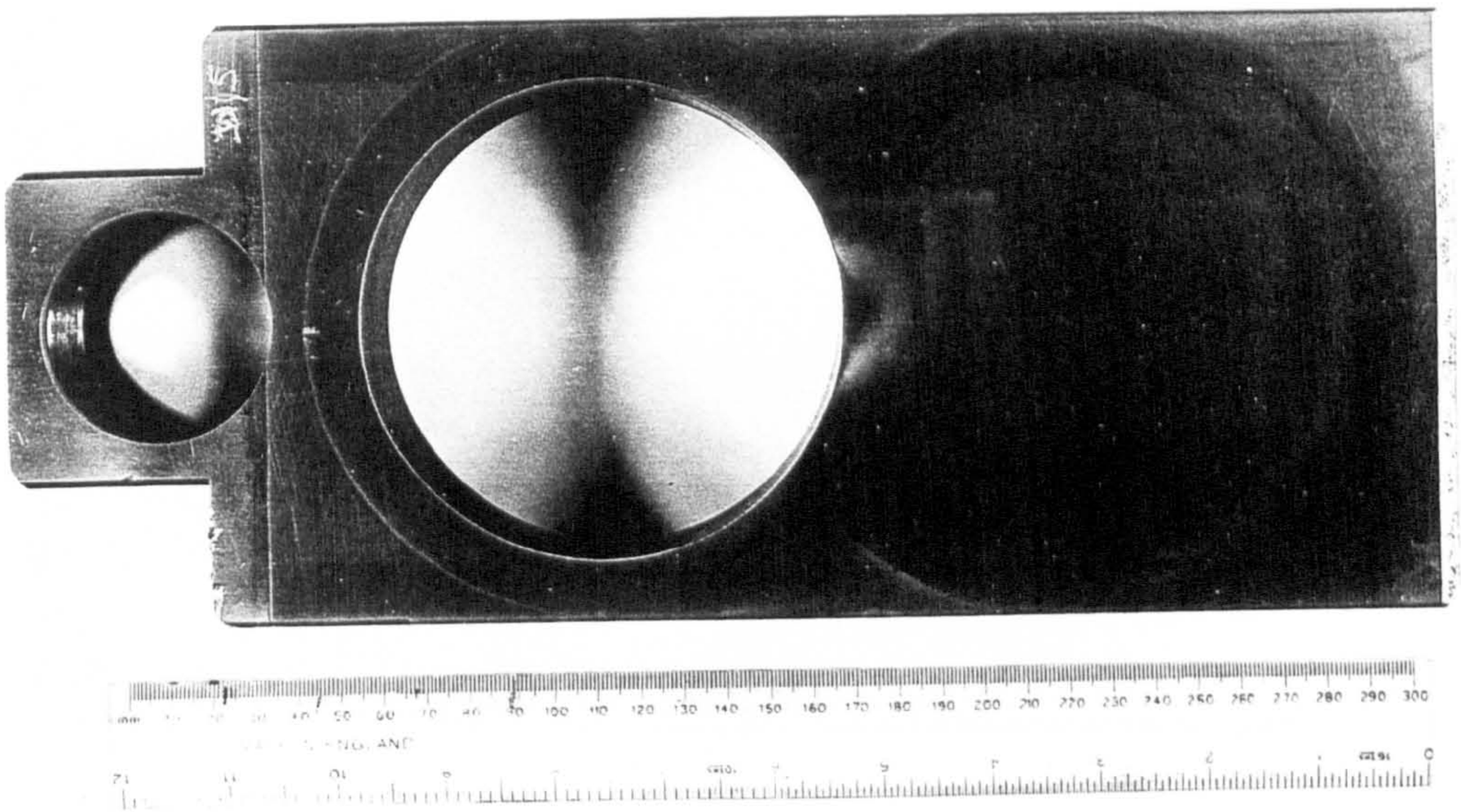

Fig.3.1 (b) Areas of gate examined

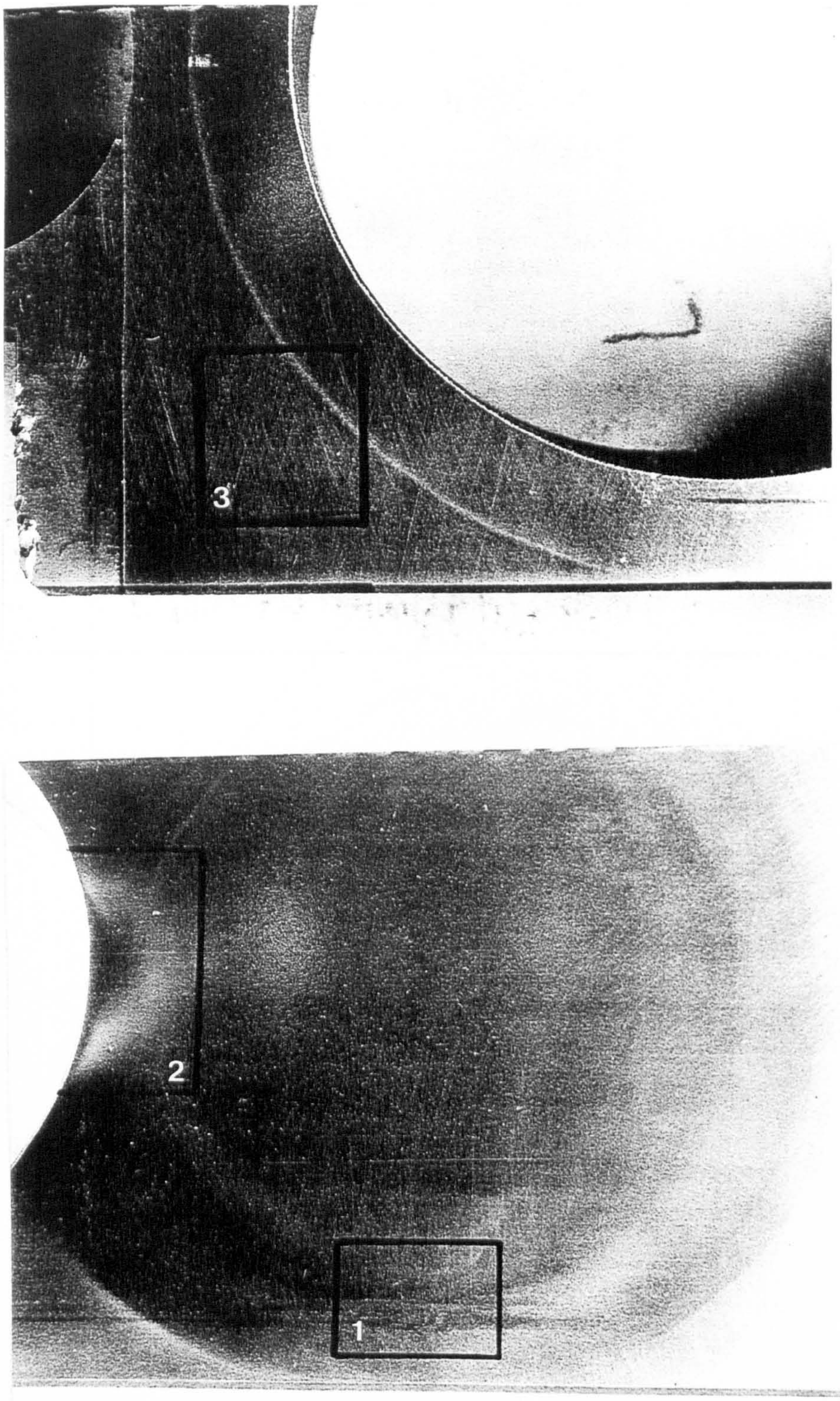

$$Zc = \frac{x_L - x_R}{2\sin\alpha/2} = \frac{P}{2\sin\alpha/2}$$

$$\_\ TrueHeight = \frac{P}{M.2\mathrm{SIN}\alpha/2}$$

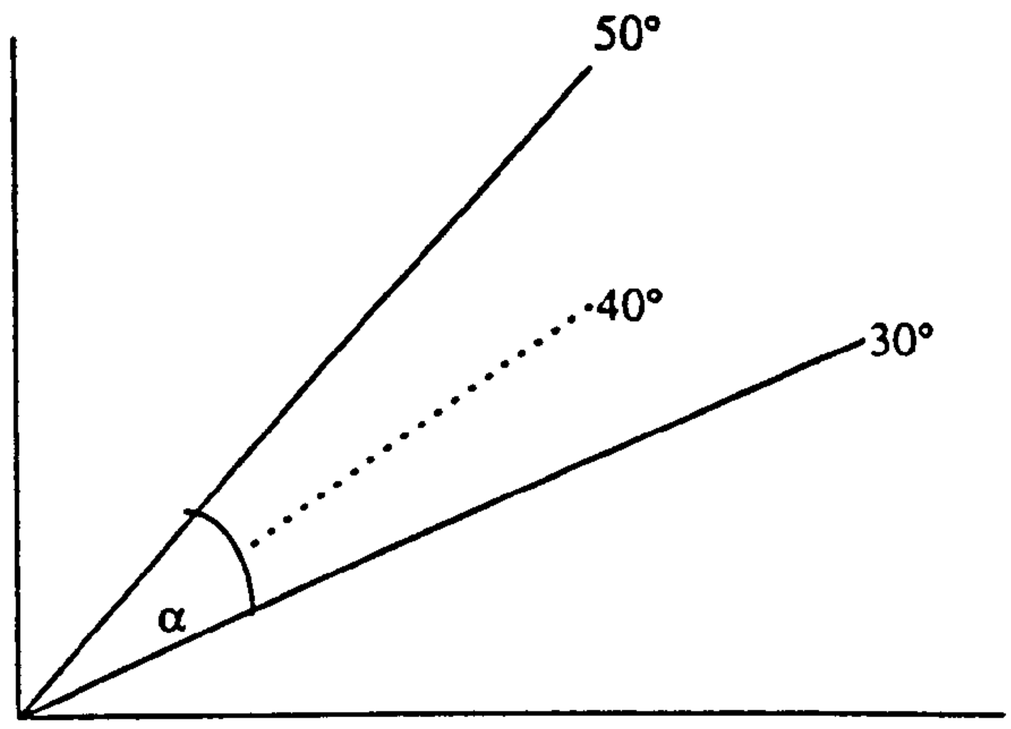

Figure 3.2 - Measurement of Z by Parallax

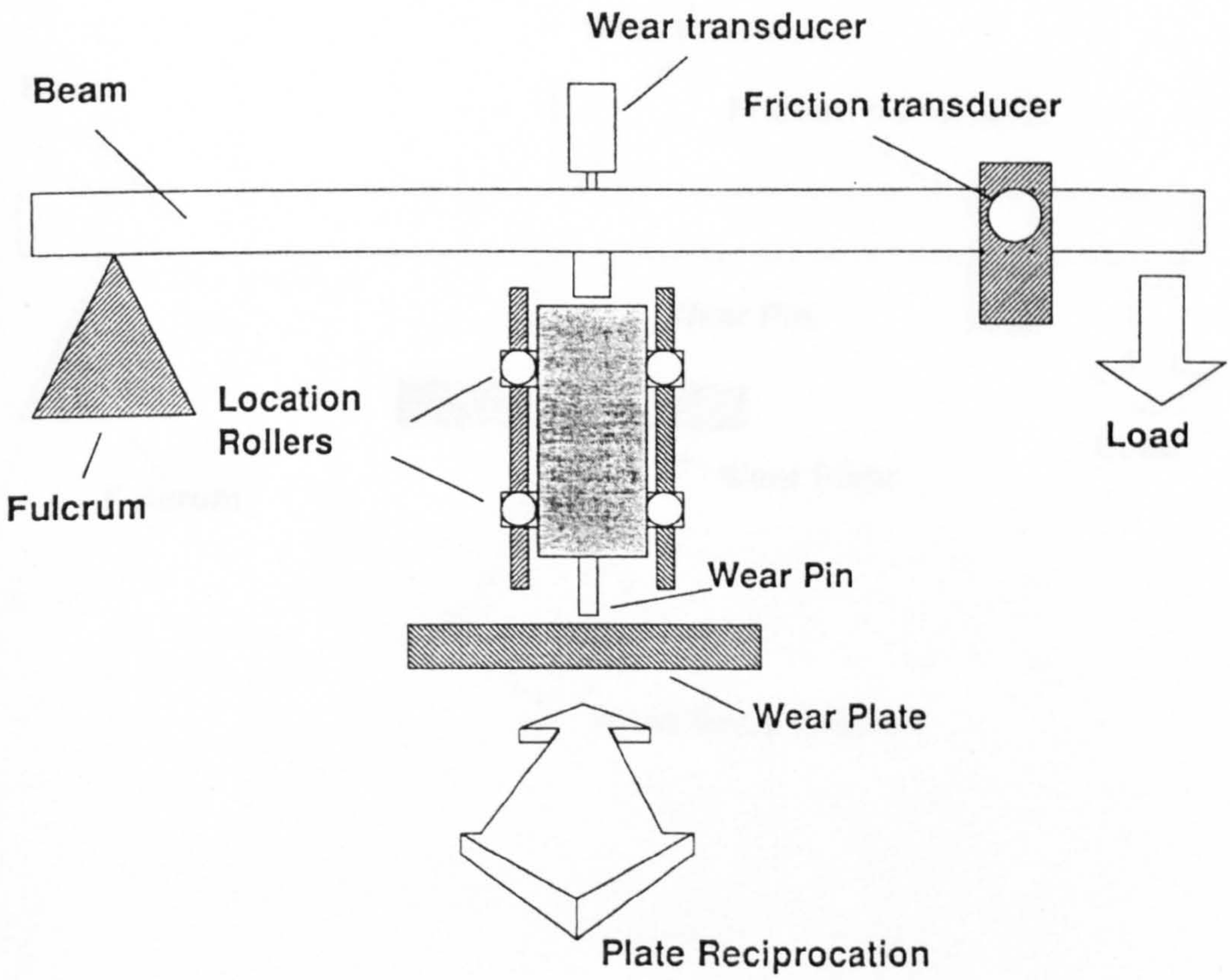

Figure 3.3 - Schematic Representation of "Gantry Style" Tribometer

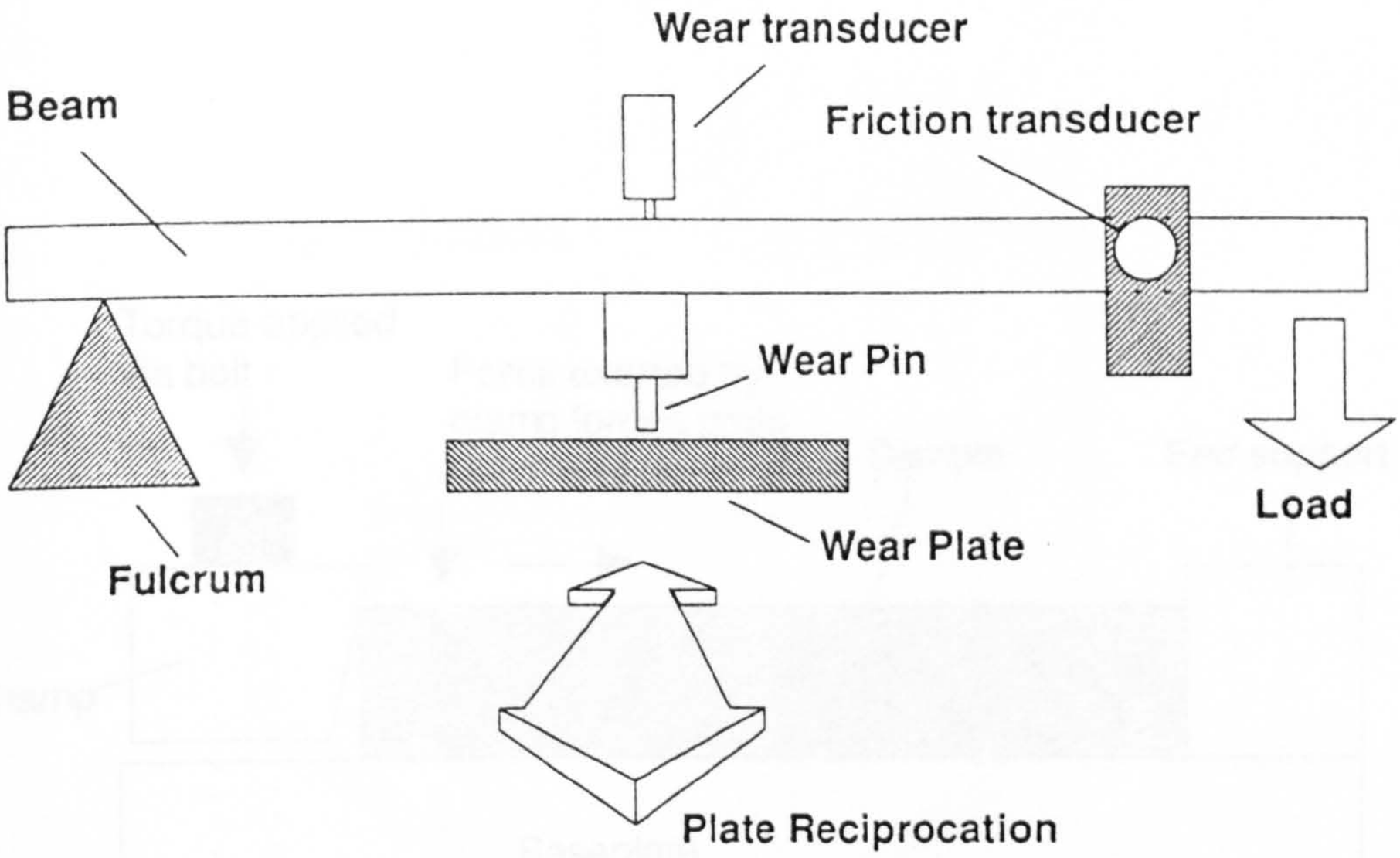

Figure 3.4 - Schematic Representation of Conventional Tribometer

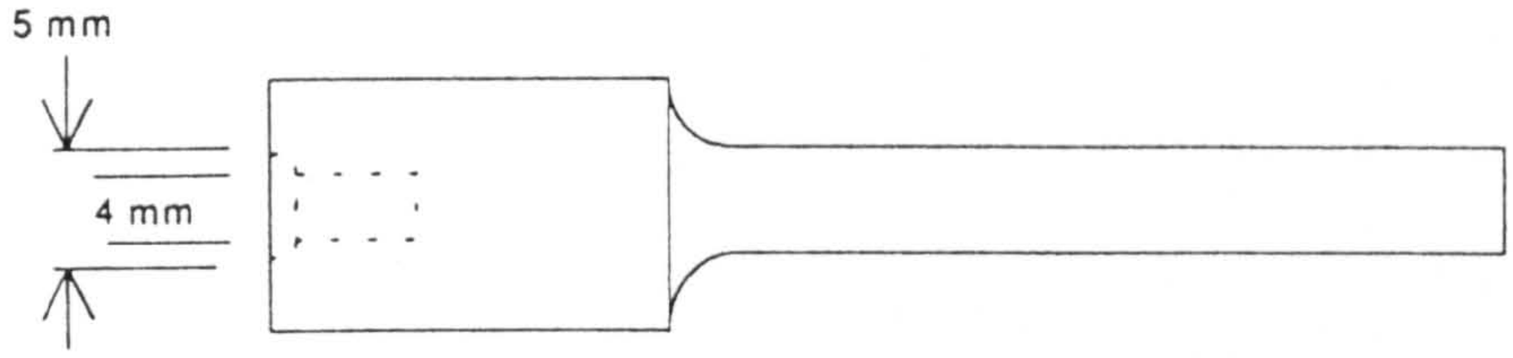

(a) Wear pin holder - material BS 970 817M40

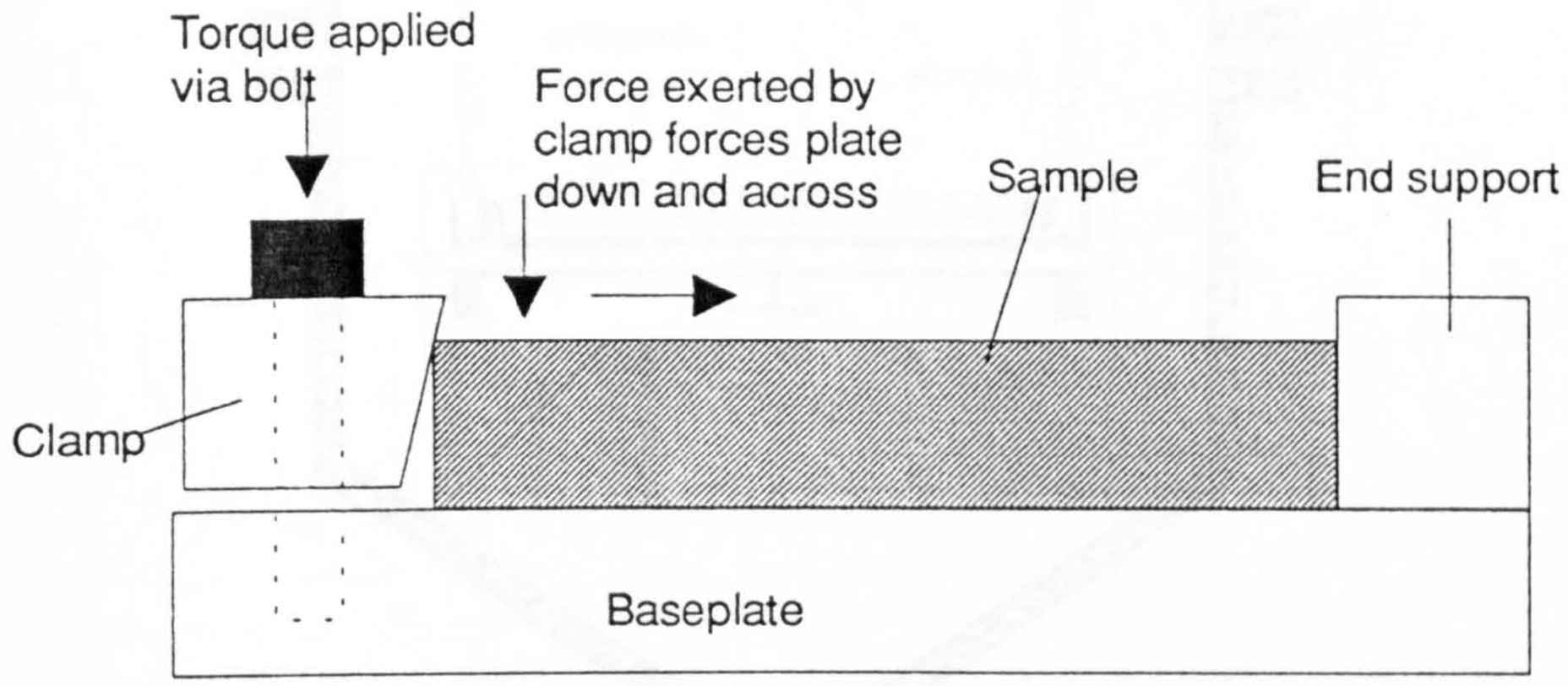

(b) Plate holder - principle

Figure 3.5 - Schematic representation of sample holders for reciprocating pin-on-plate tests

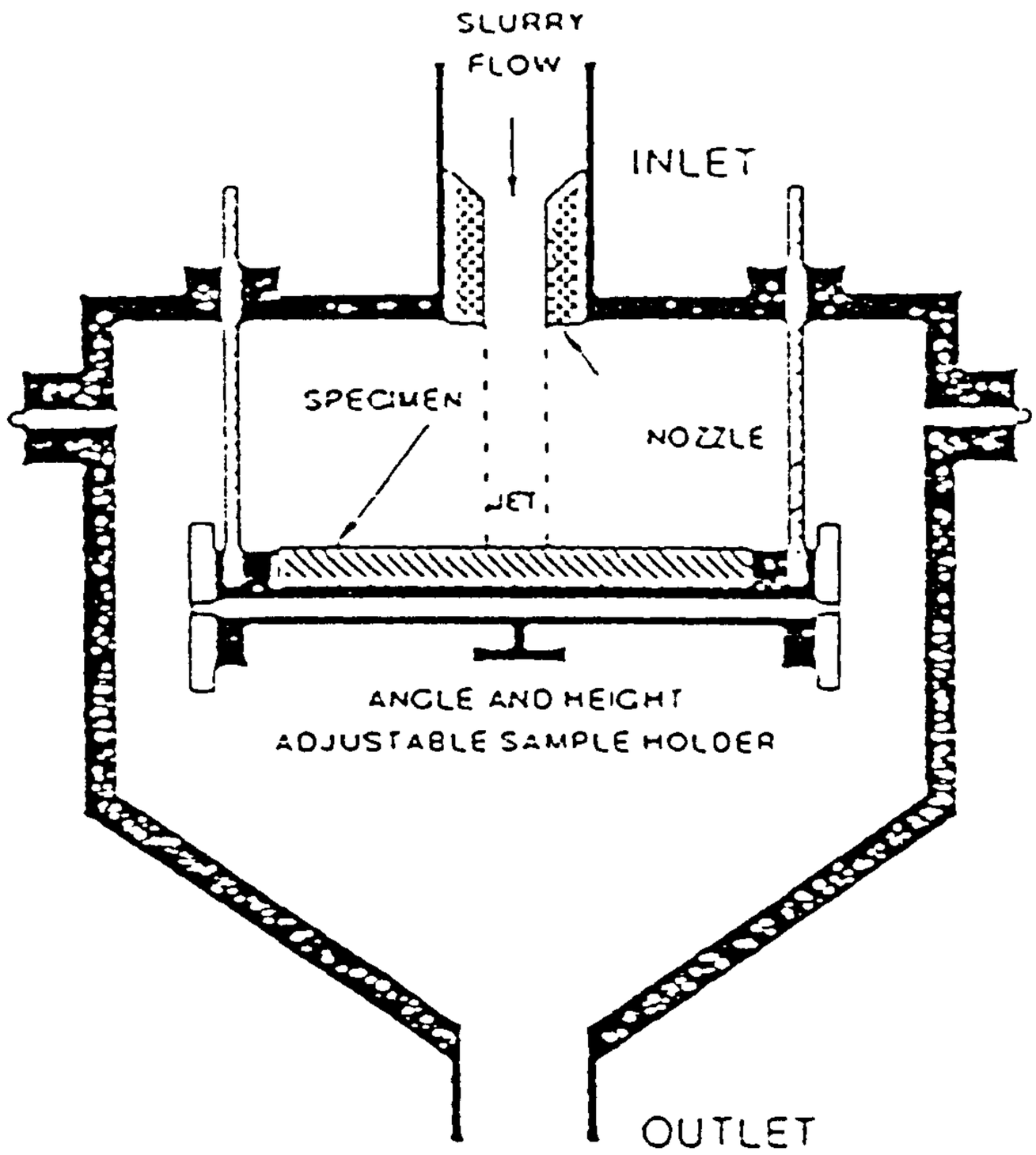

Figure 3.6 - Schematic Representation of the Erosion Chamber

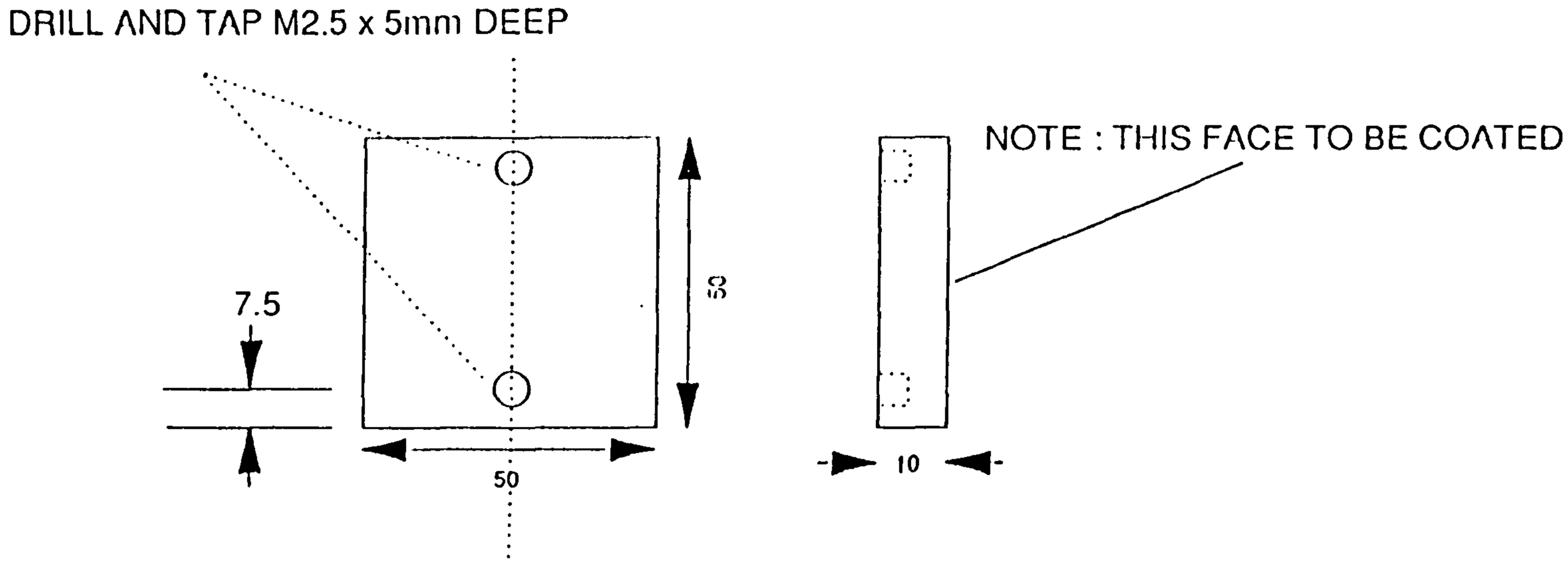

TITLE:	EROSION RIG SAMPLES		
SCALE:			MATERIAL:
TOLERANCES:	+/- 0.5 mm	ALL DIMENSIONS IN MM	SURFACE FINISH: GROUND FINISH
DATE:	5/4/91		BP RESEARCH TRIBOLOGY TEAM / T116
DRAWING NO.	116/1		

Figure 3.7 - Erosion Samples

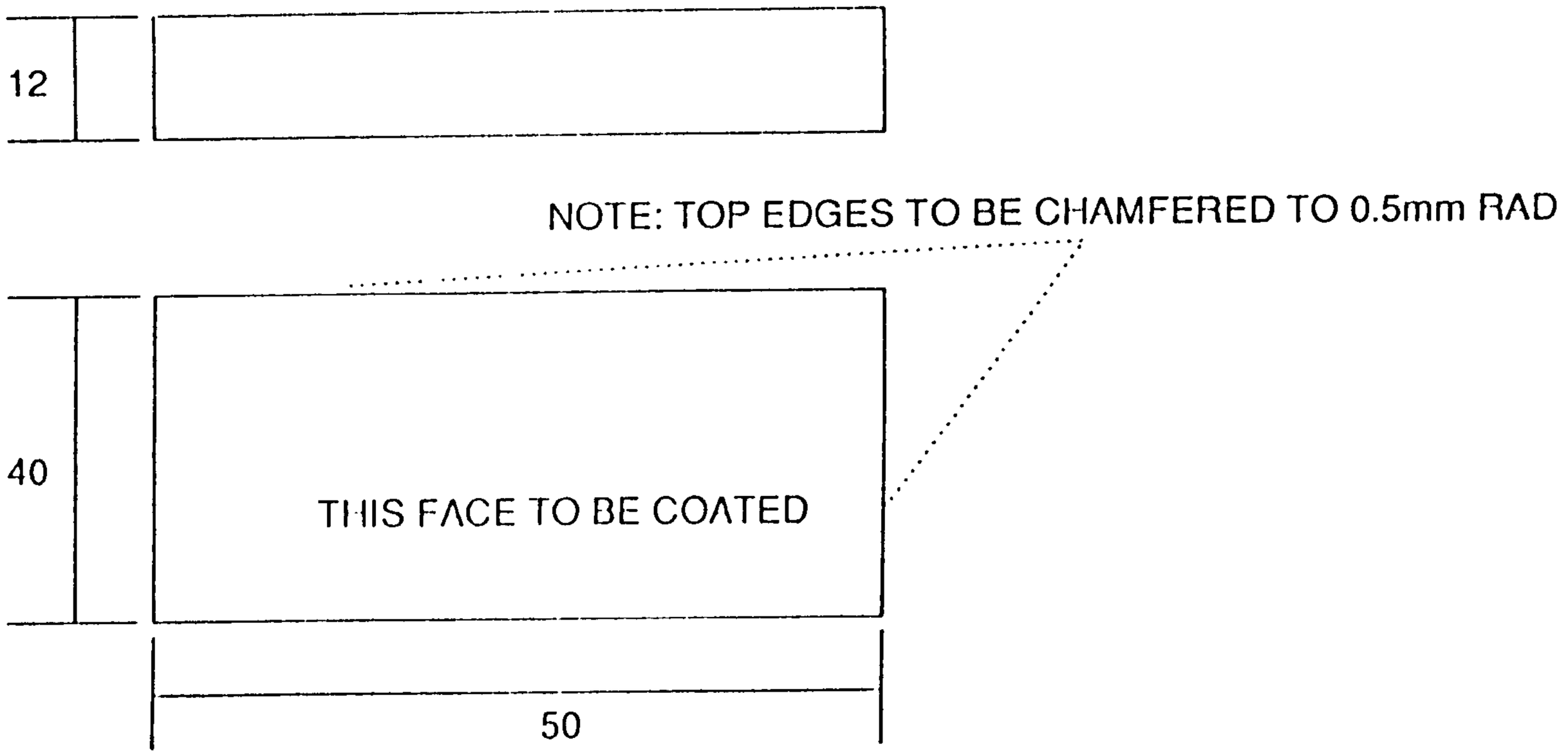

TITLE:	WEAR PLATE		
SCALE:		MATERIAL:	stainless 410
TOLERANCES:	+/- 0.5 mm | ALL DIMENSIONS IN MM	SURFACE FINISH:	GROUND FINISH
DATE:	5/4/91	BP RESEARCH TRIBOLOGY TEAM / T116	
DRAWING NO.	116/1		

Figure 3.8 - Wear Plate Samples

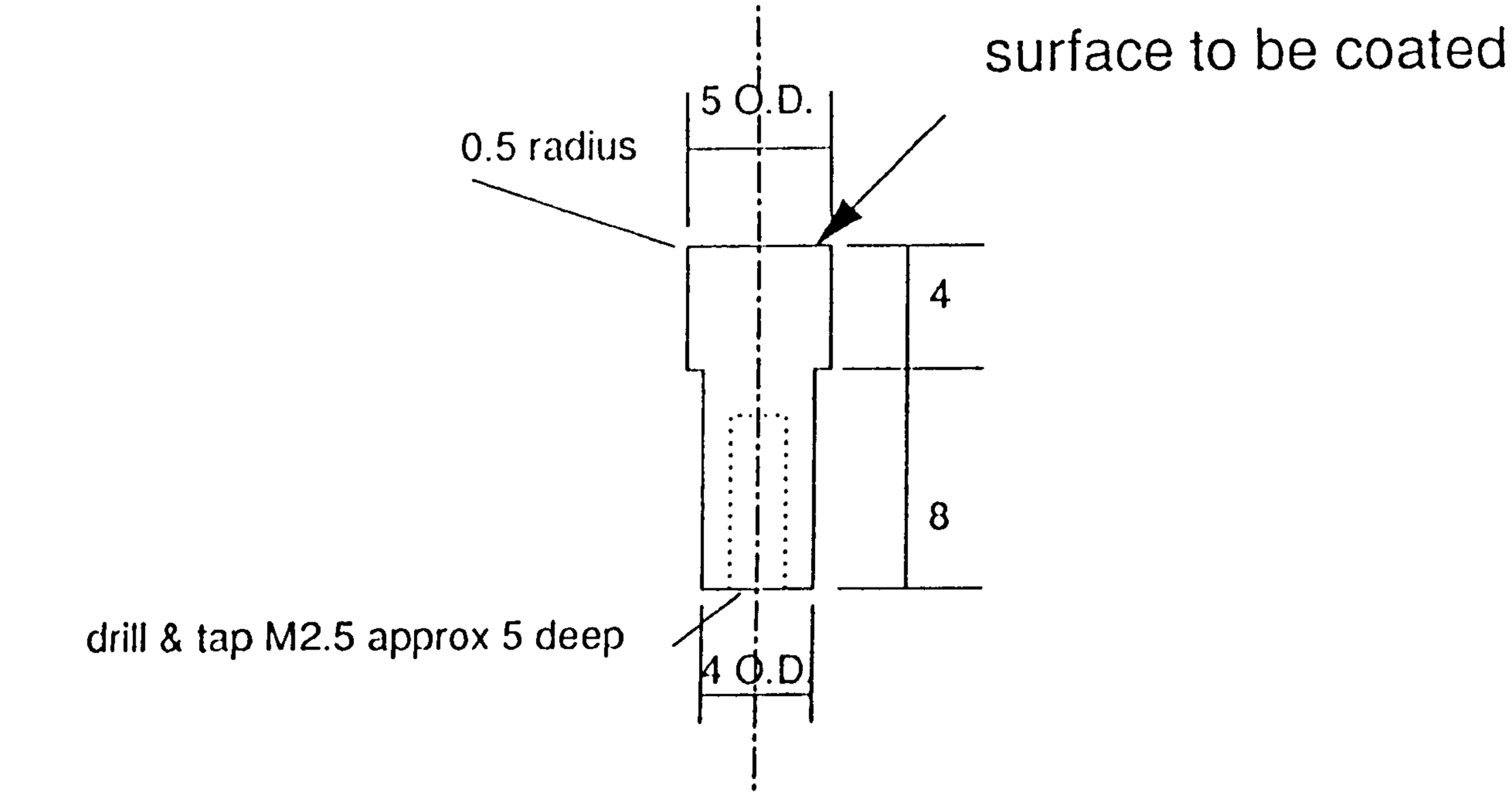

TITLE:	WEAR PIN		
SCALE:			MATERIAL: stainless 410
TOLERANCES:	+/- 0.1 mm	ALL DIMENSIONS IN MM	
DATE:	5/4/91		BP RESEARCH TRIBOLOGY TEAM / T116
DRAWING NO.	116/2		

Figure 3.9 - Wear Pin Samples

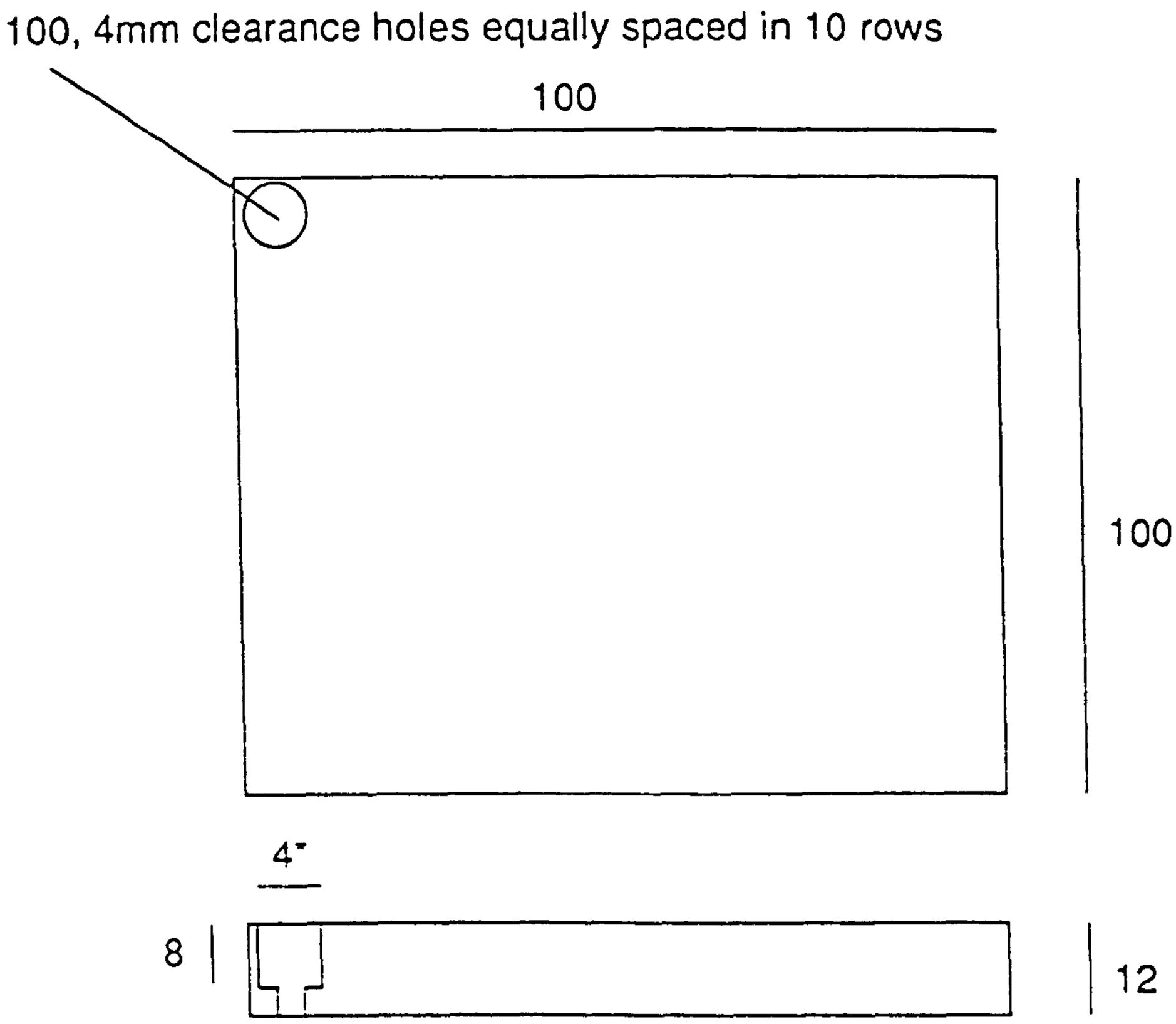

NOTE : * INDICATES CLEARANCE HOLES

GRINDING BLOCK

MATERIAL : MILD STEEL

ALL DIMENSIONS IN mm

Figure 3.10 - Grinding Block

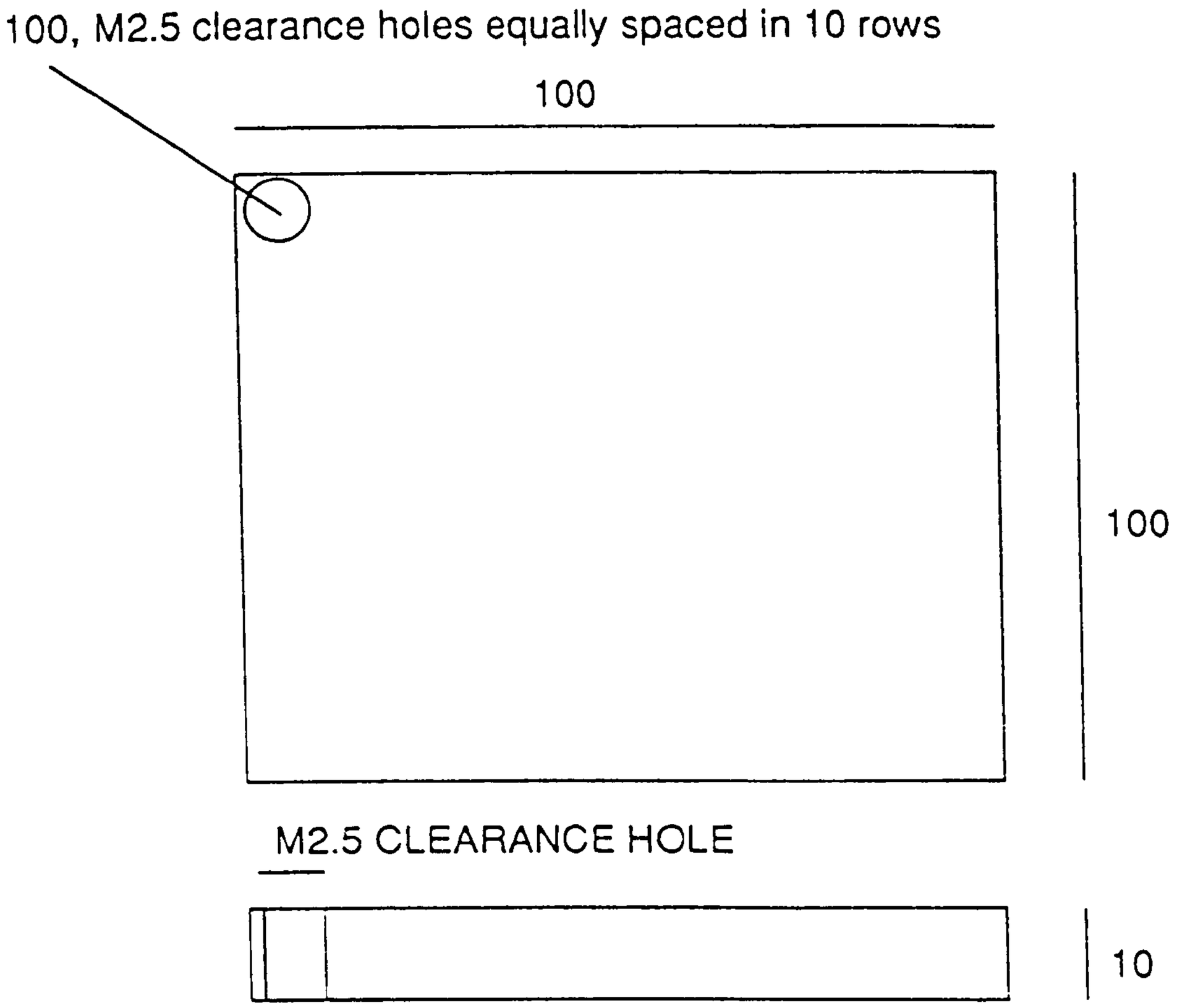

ALSO REQUIRED 100 OFF PROTECTION TUBES
4mm O.D. WITH A M2.5 CLEARANCE BORE
LENGTH OF TUBE 10mm.

SPRAYING BLOCK

MATERIAL : MILD STEEL

ALL DIMENSIONS IN mm

Figure 3.11 - Spraying Block

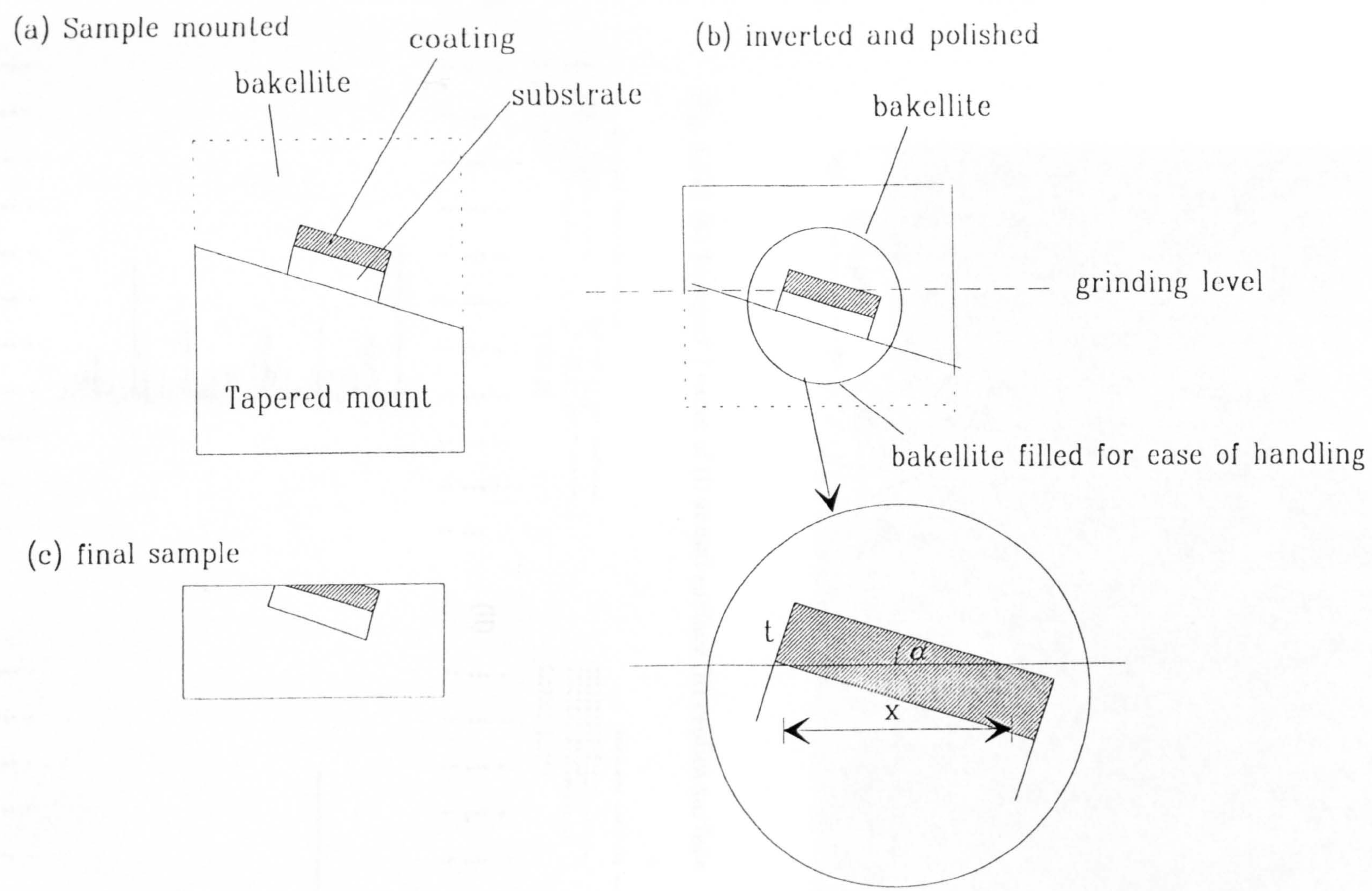

Figure 3.12 - The taper mounting technique

Fig. 4.111(a) Coated PMMA replica of the typical as-supplied finish from Area 3

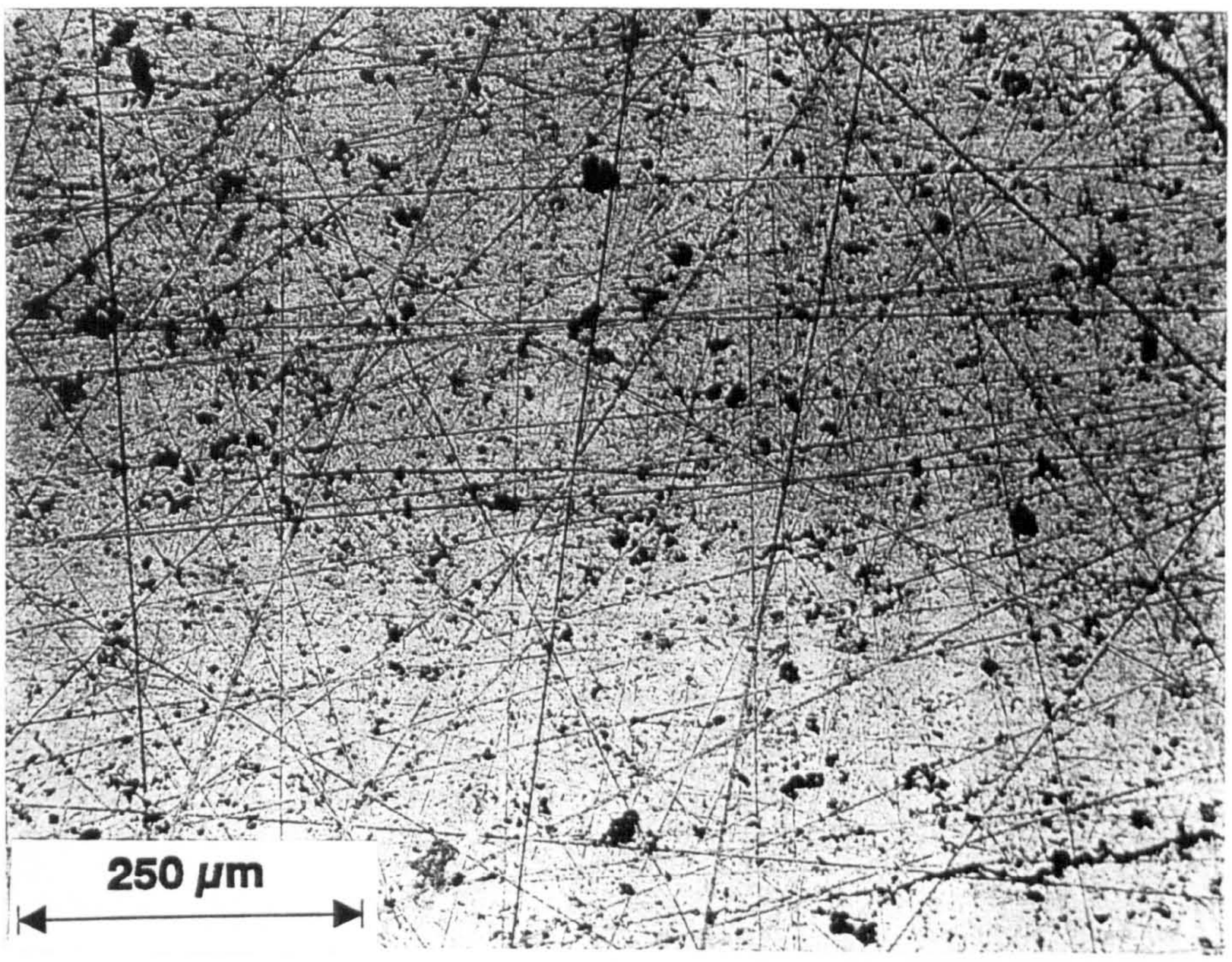

Fig. 4.111 (b) Talysurf Traces of (i) actual surface (ii) replica surface

(i)

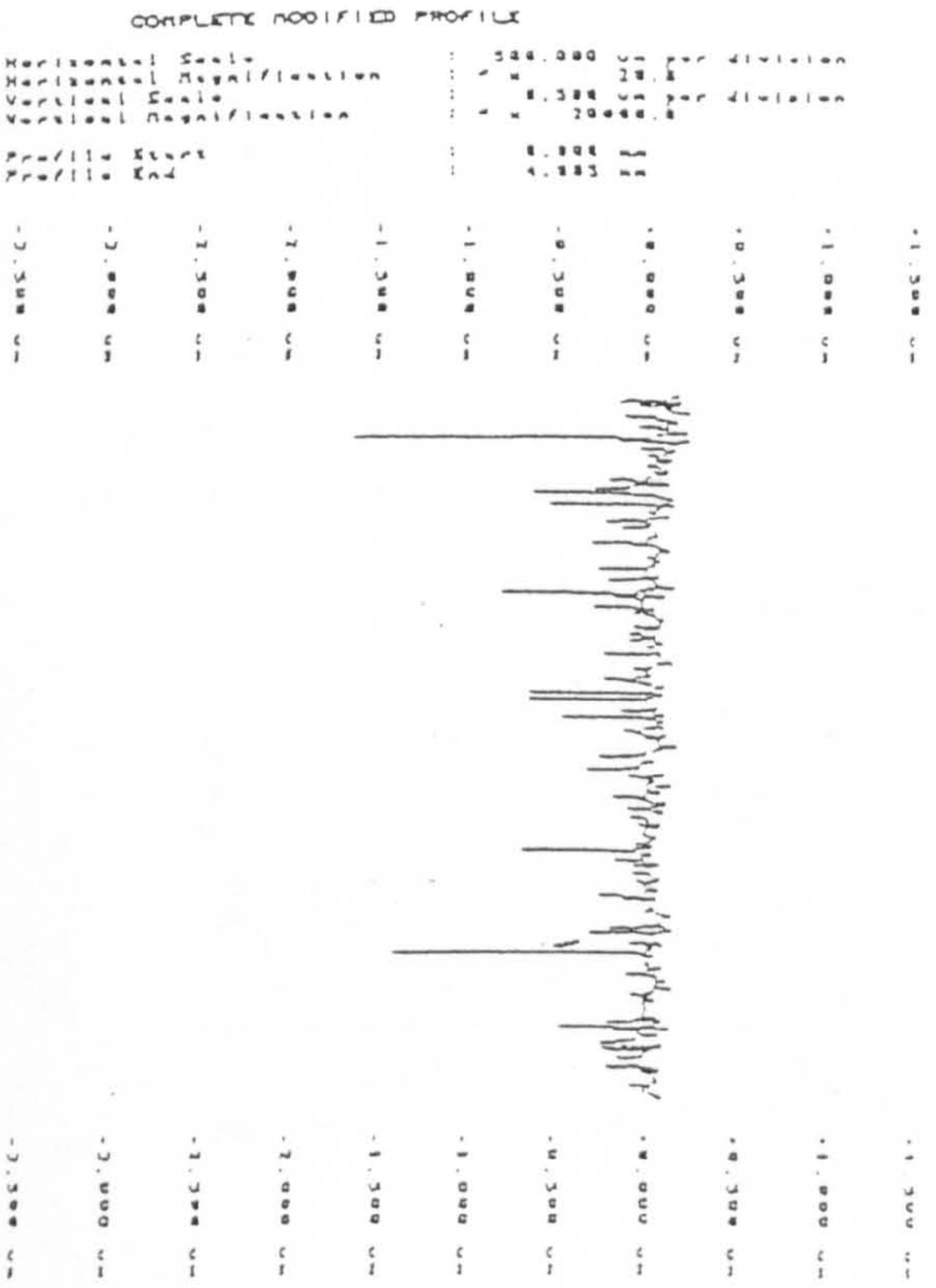

(ii)

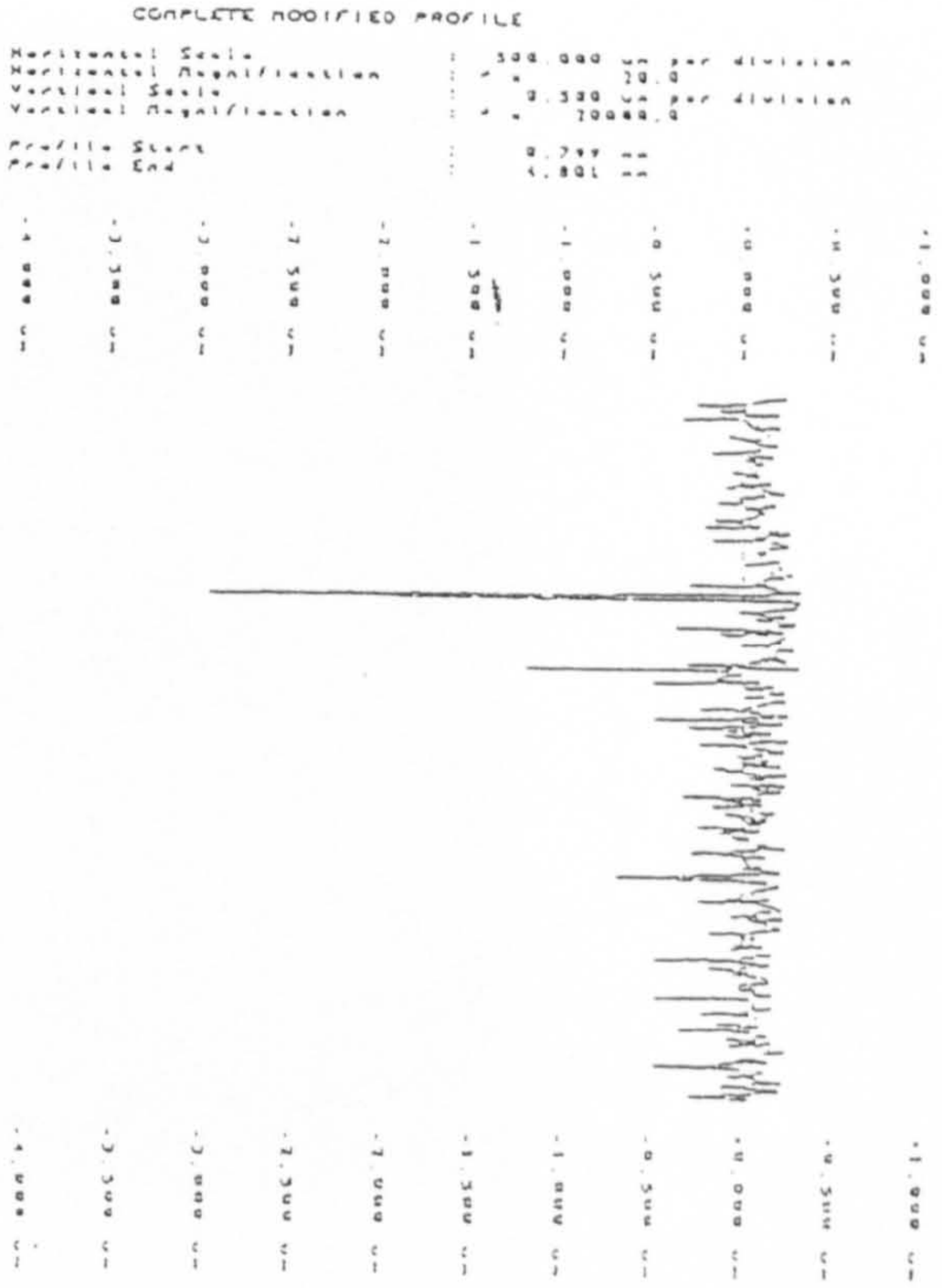

Fig. 4.112 Micrographs of gouge initiation from Area 1
(a) Actual surface

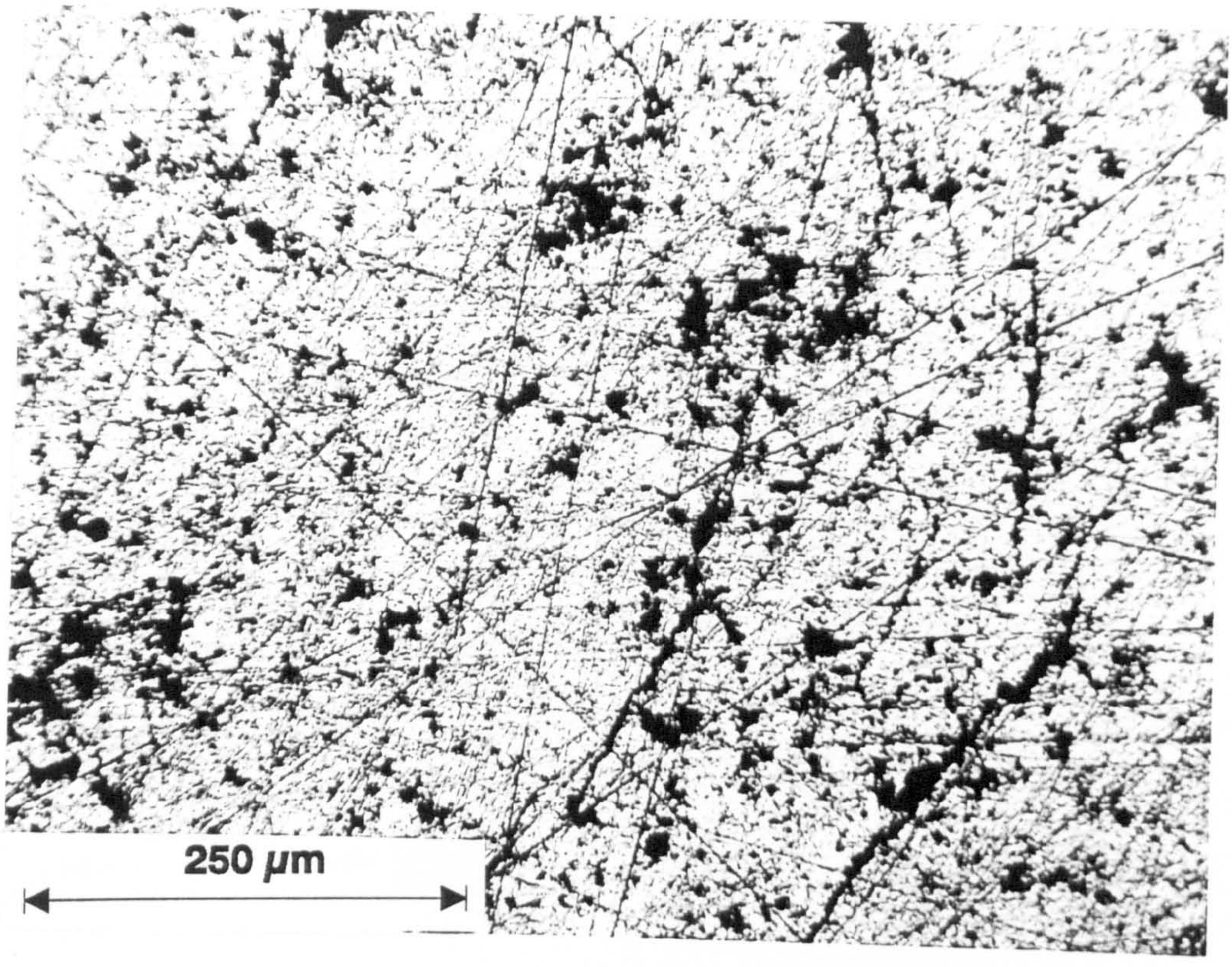

(b) Uncoated acetate replica

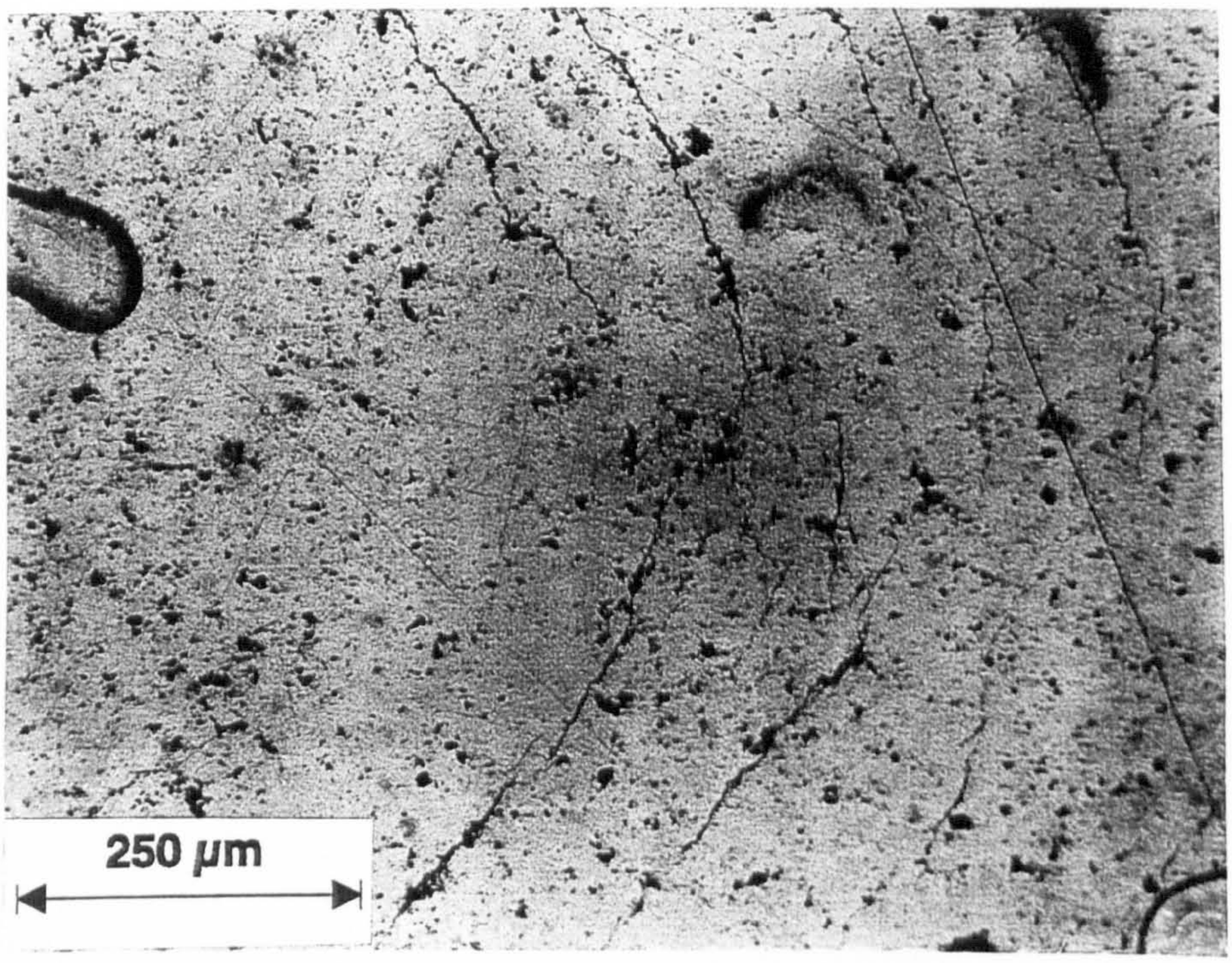

Fig. 4.112...

(c) Coated Acetate Replica

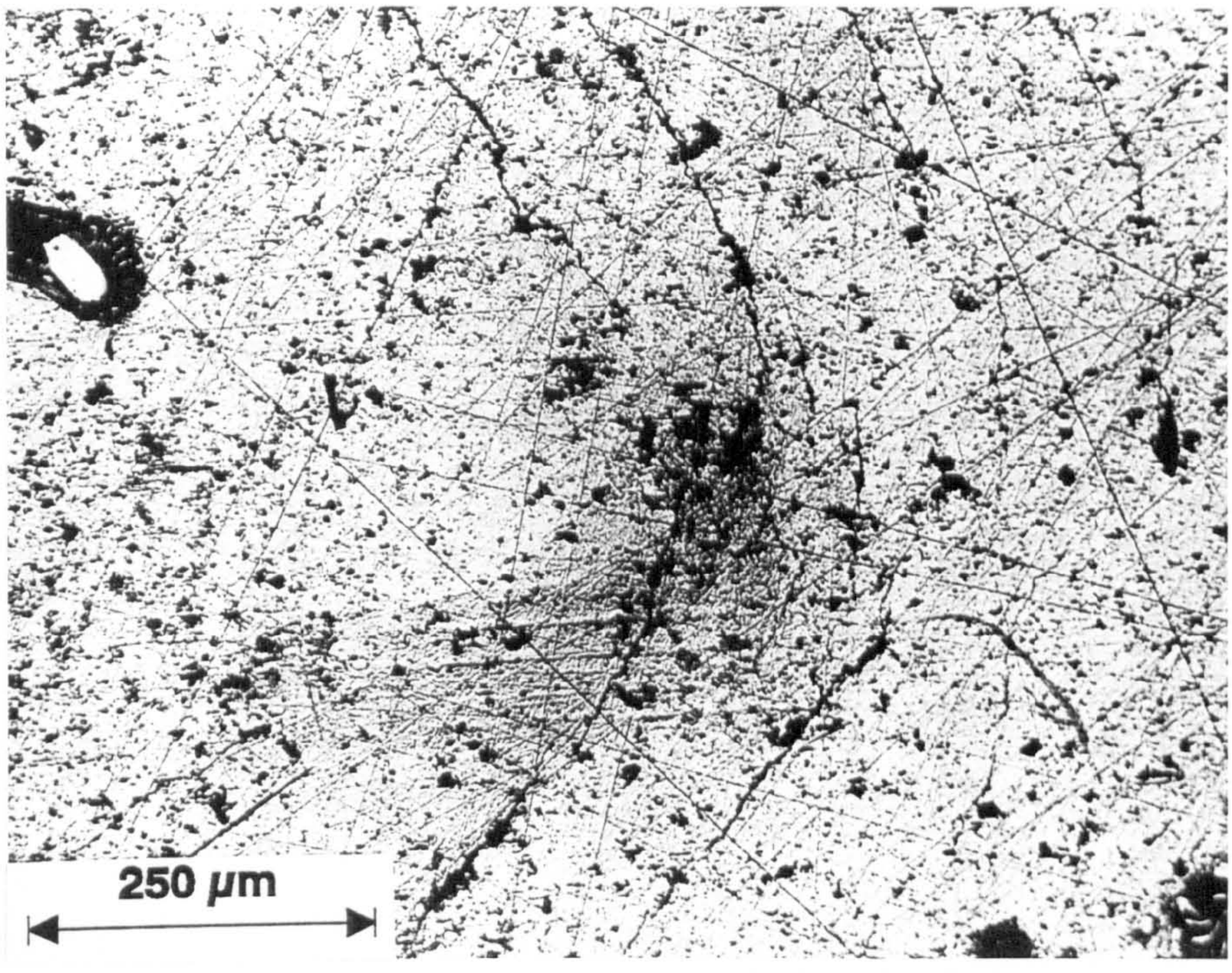

Fig. 4.113 Three-dimensional profile of Area 1 taken from a PMMA replica

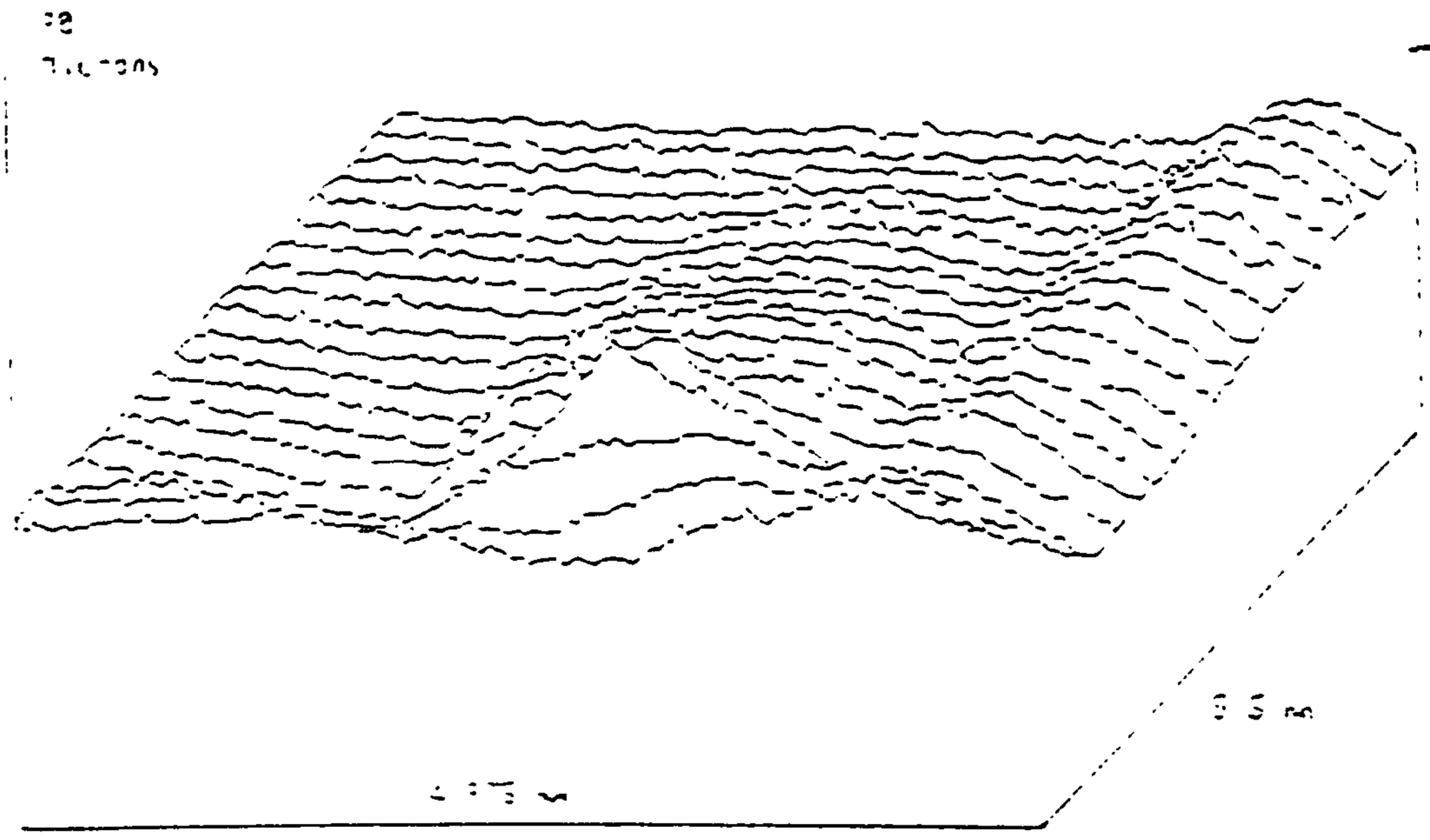

Fig. 4.114 - Problems with Inversion of Replicas

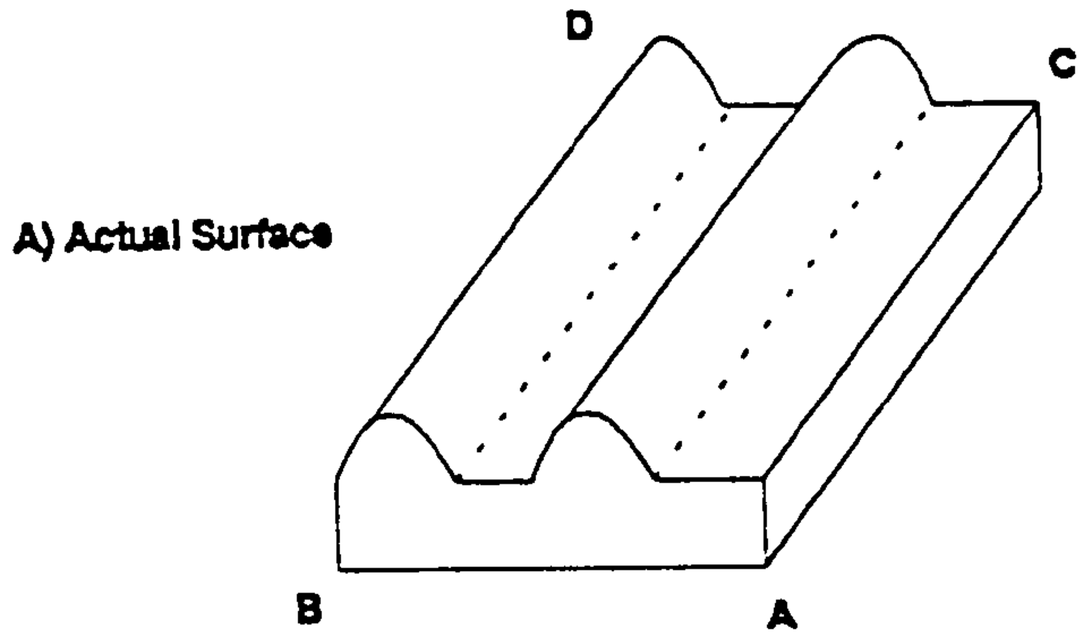

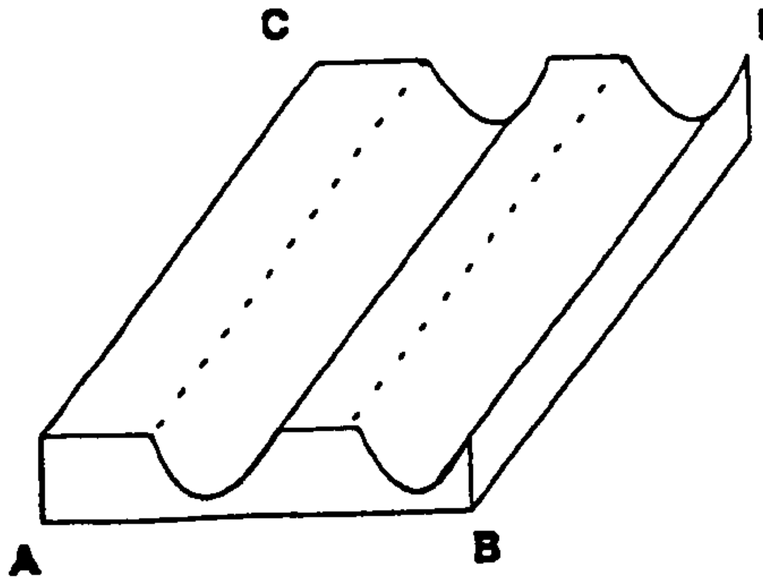

B) Replica

Fig. 4.115 (a) Coated acetate replica of area 2 showing erosion

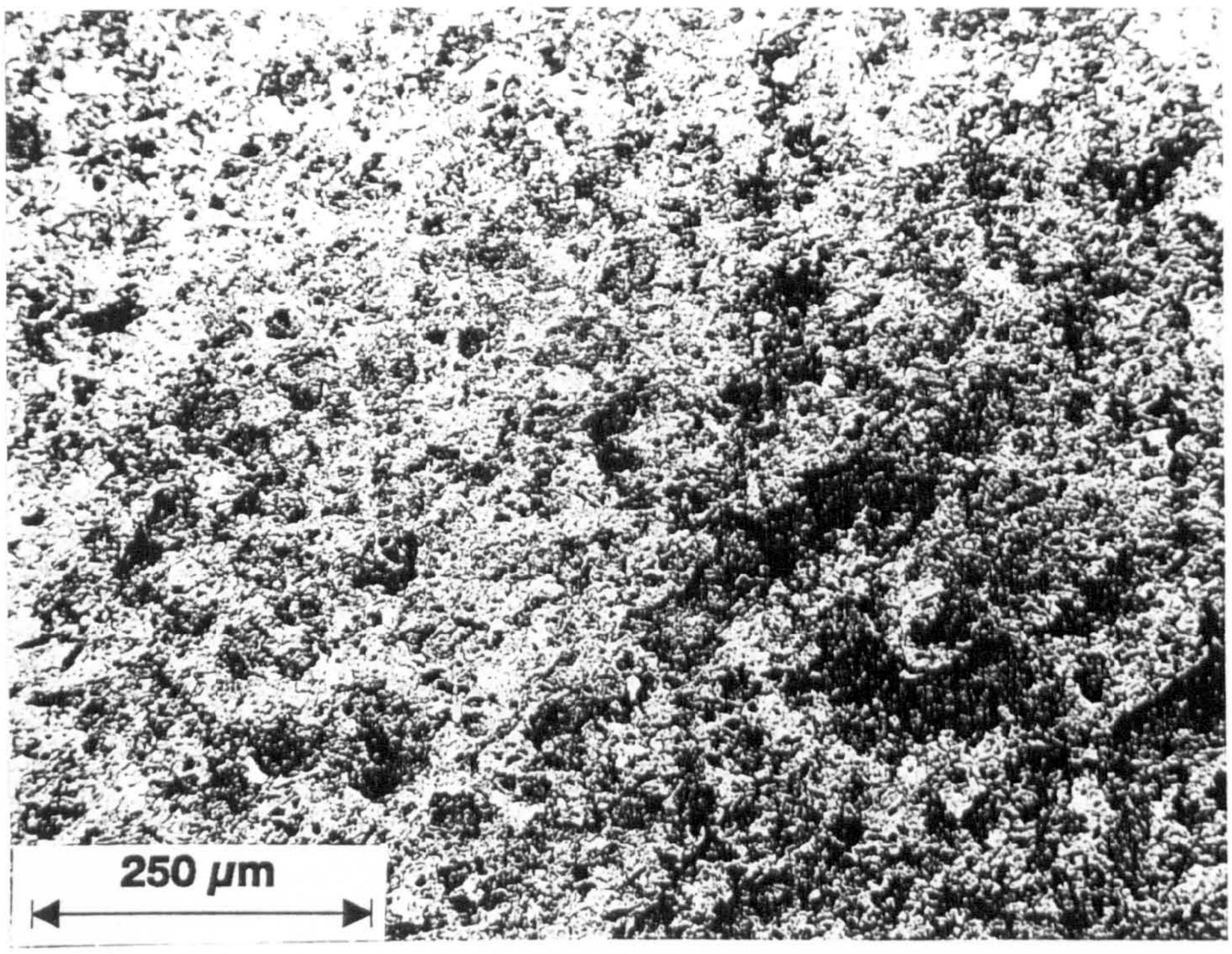

(b) Profile of eroded area

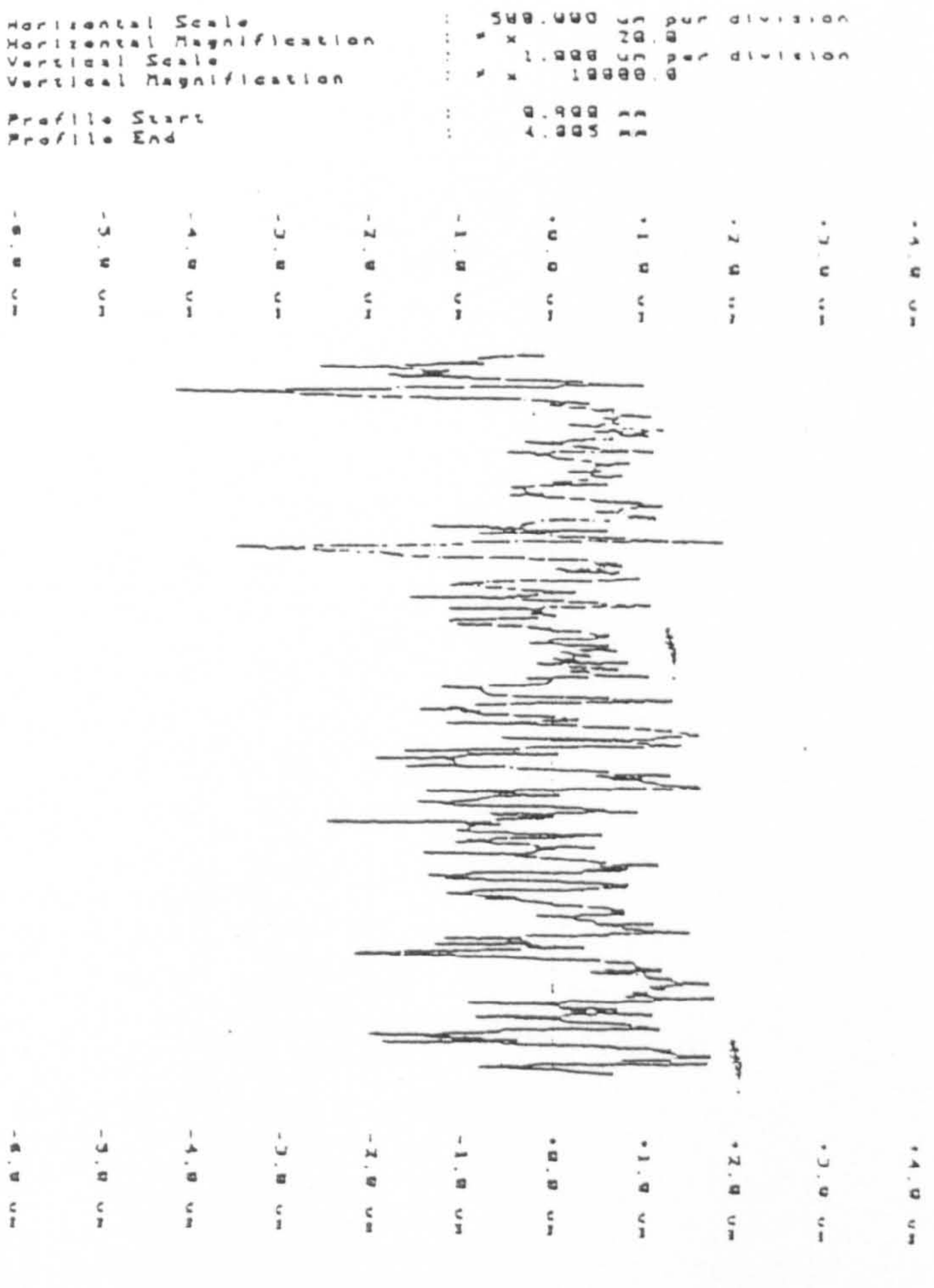

Fig. 4.115...

(c) SEM micrograph of an individual erosion scar

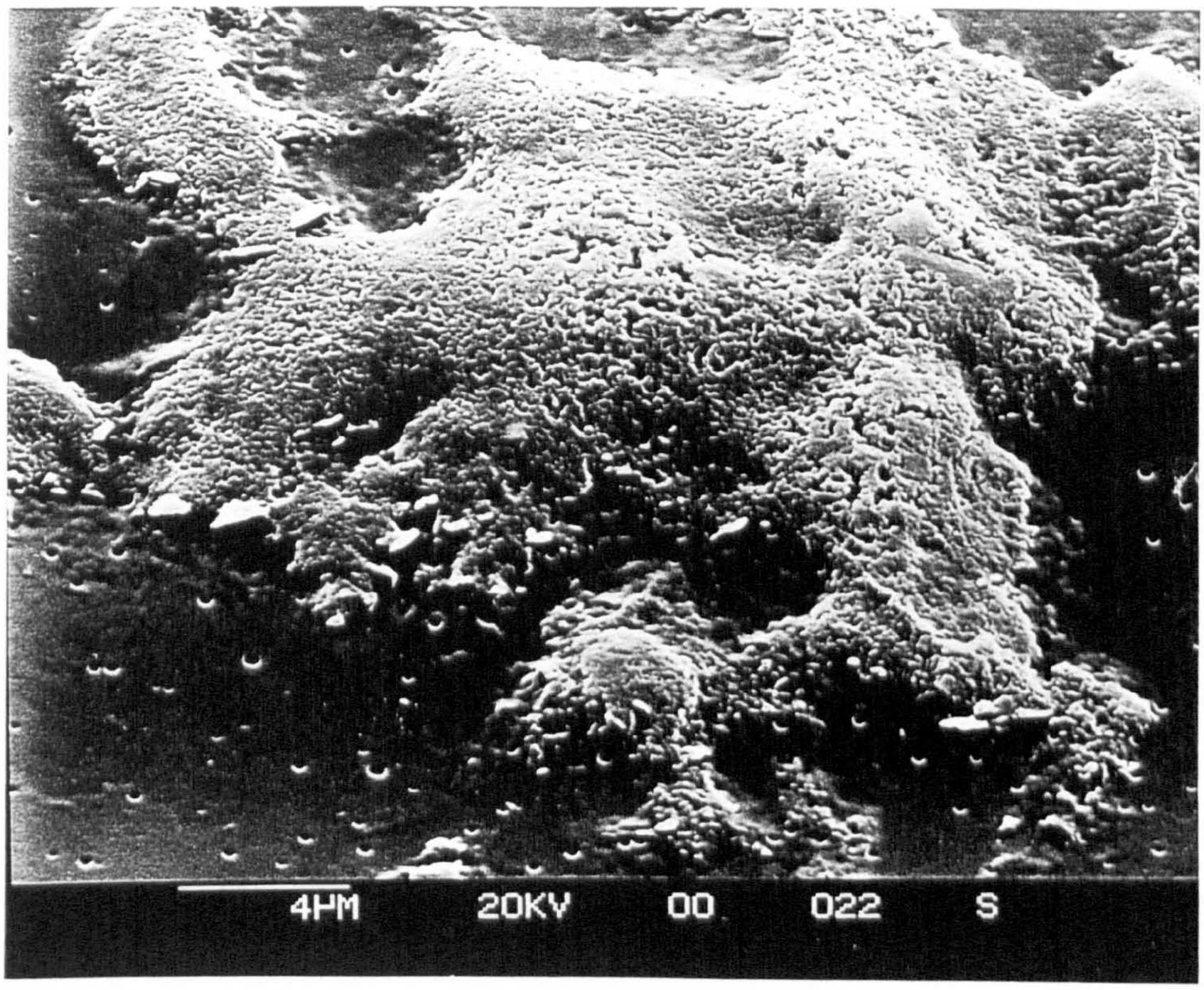

Fig. 4.201 - As-supplied quality control test sample - unetched using differential interference contrast (DIC)

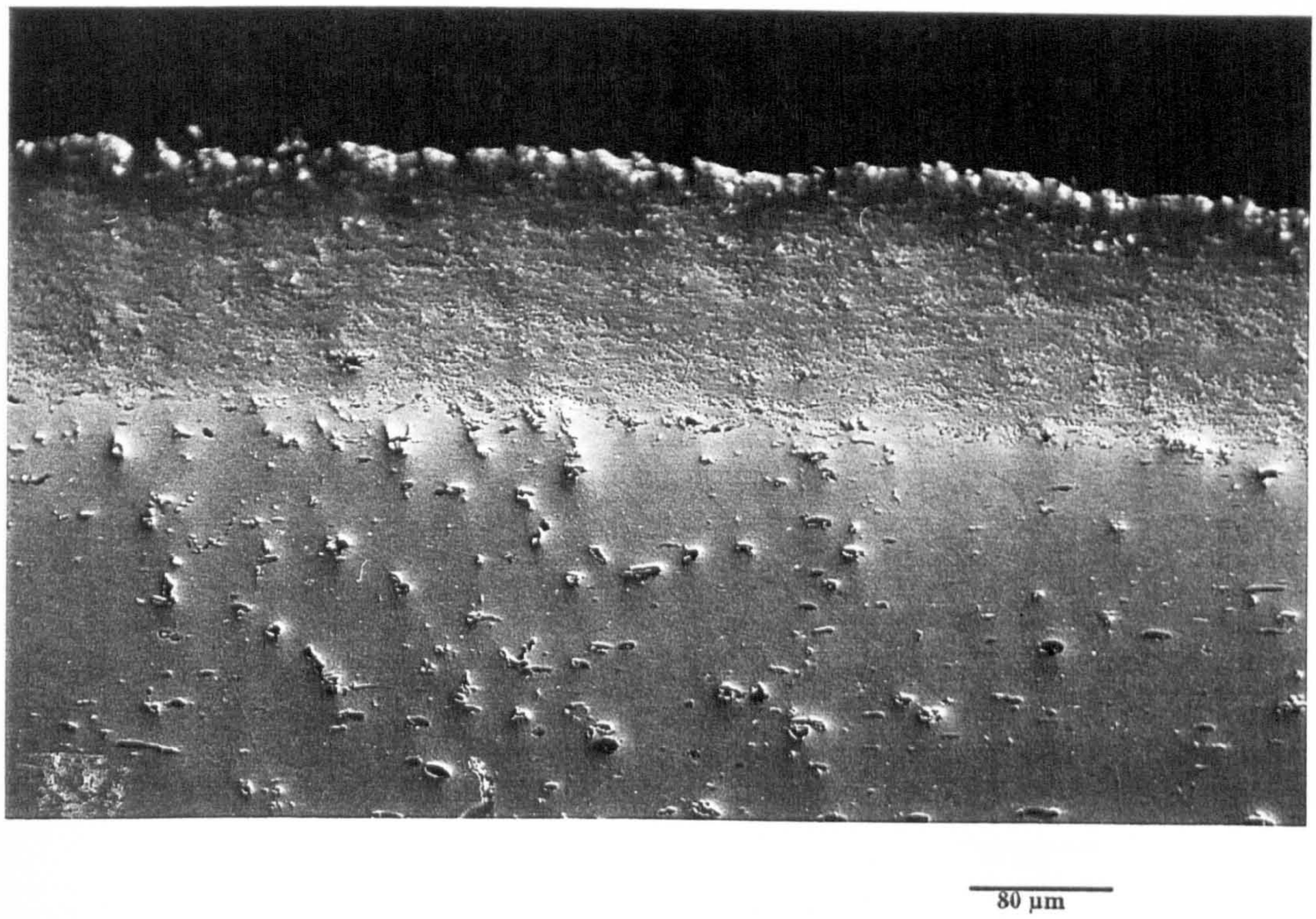

(b) Pin sample - unetched x 300 DIC

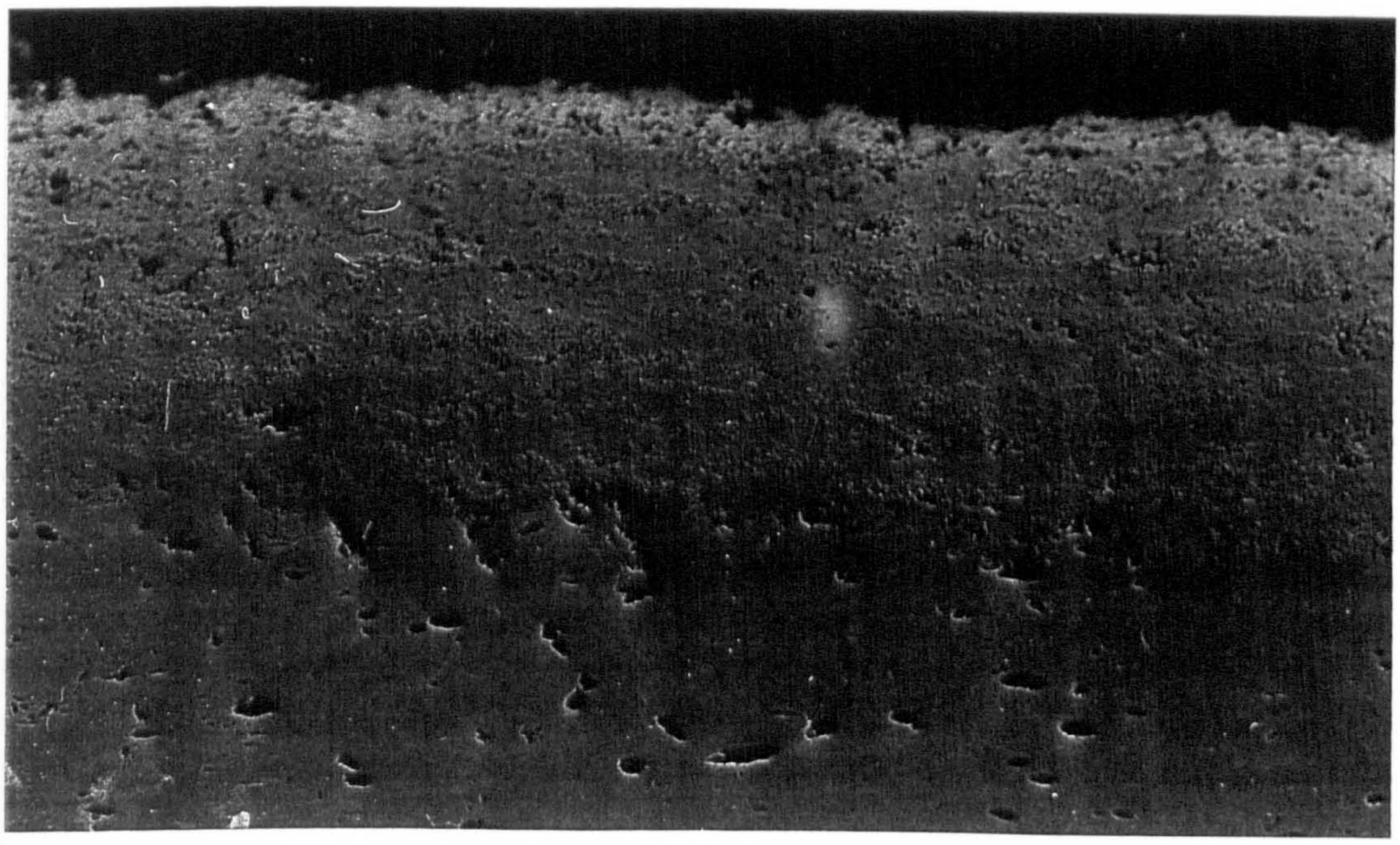

Fig. 4.202 - Sectioned pin - unetched using oblique illumination

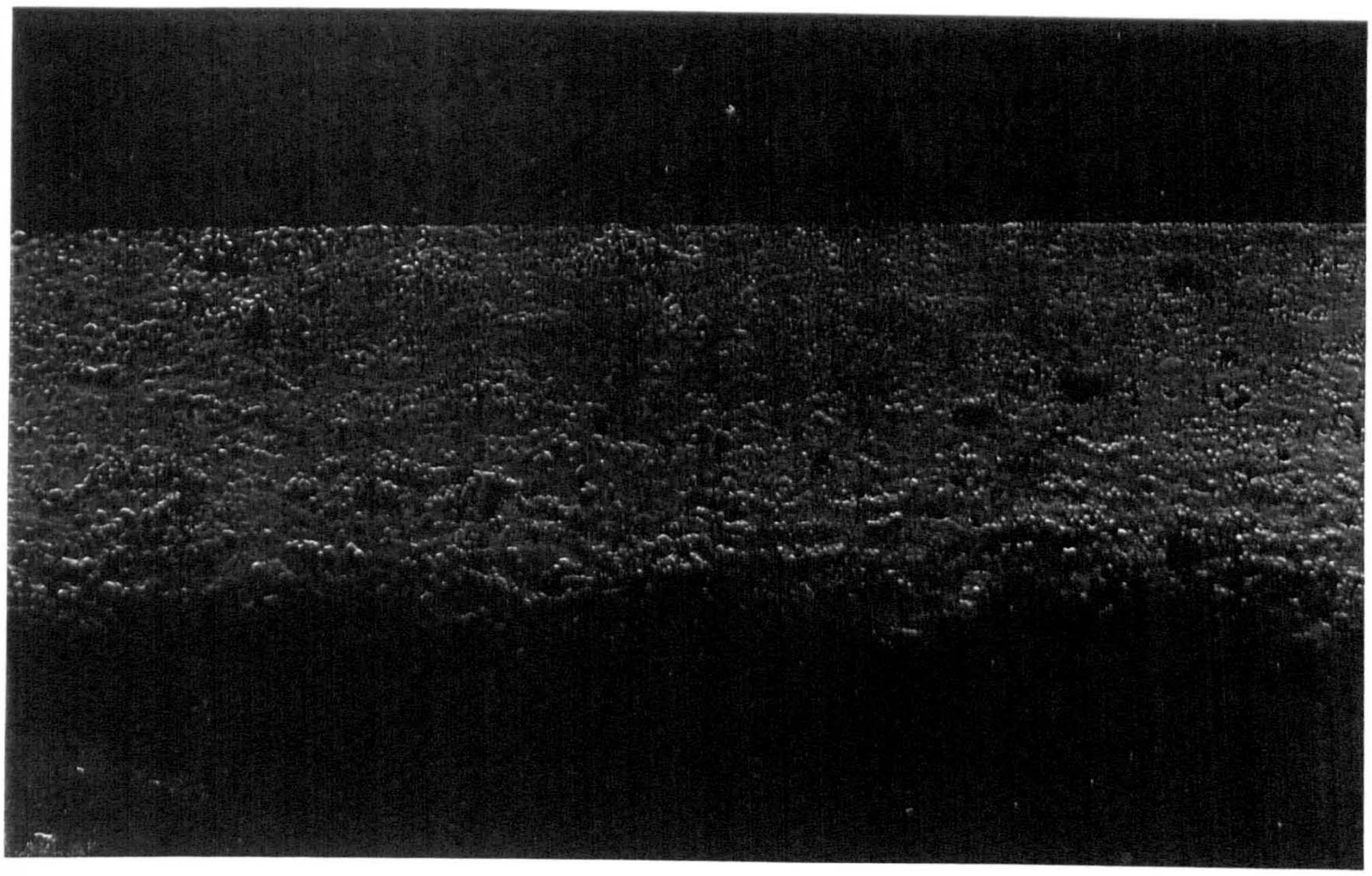

Fig. 4.203 - Schematic Representation of *Shadowing*

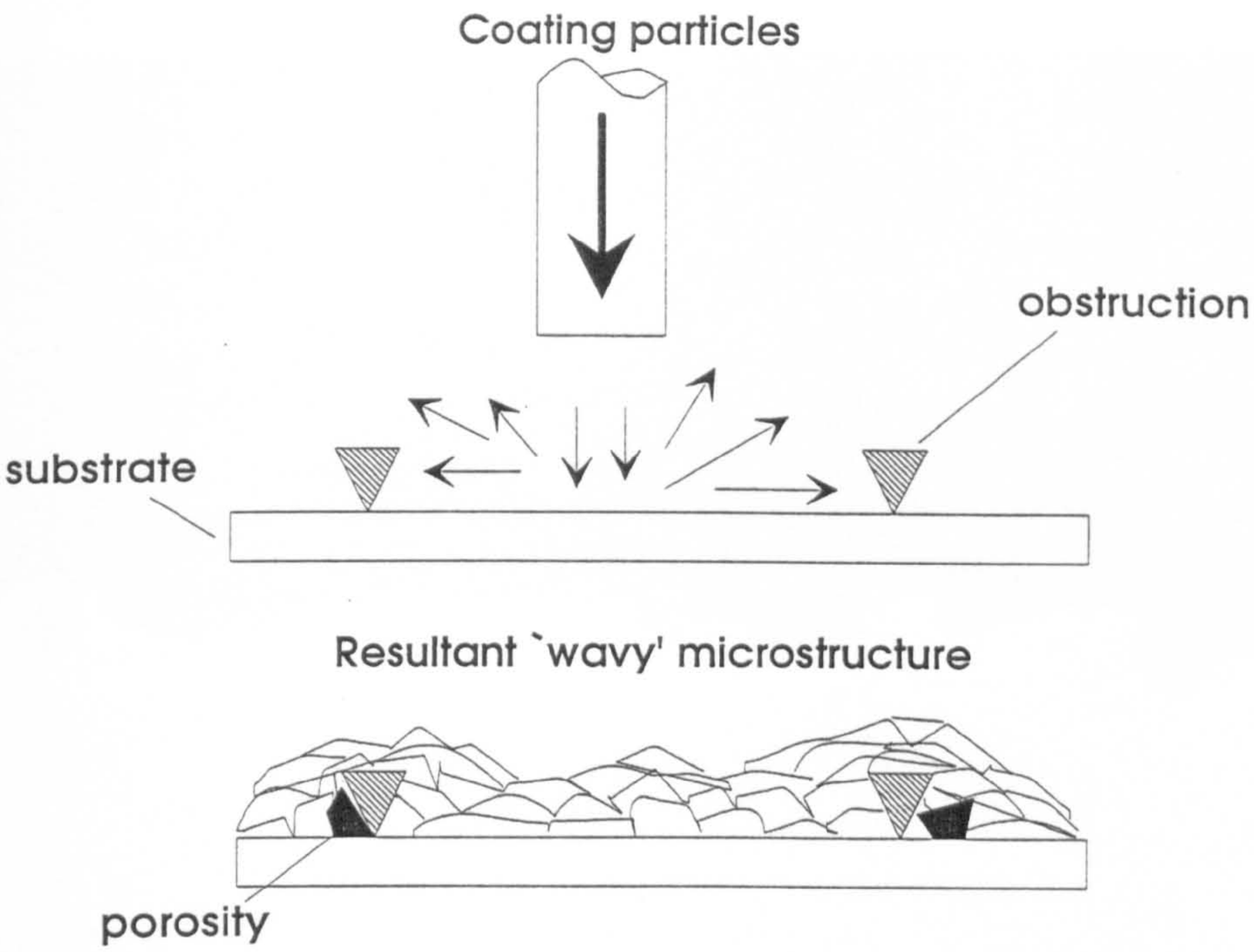

Fig. 4.204 - Sectioned pin - unetched DIC x 1000

Fig. 4.205 - Sectioned pin - etched (DIC)

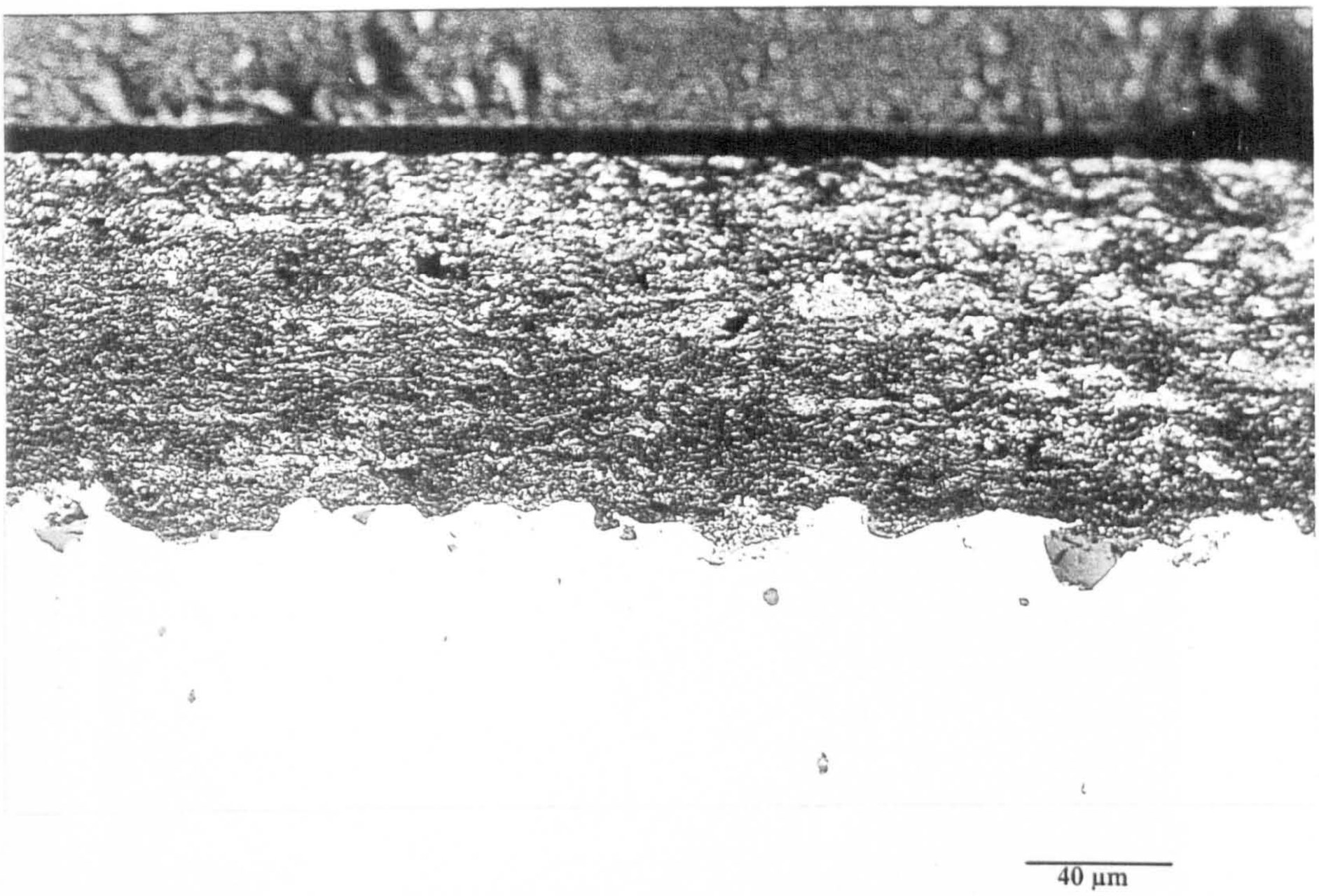

Fig. 4.206 - Sectioned pin - etched, normal contrast

Fig. 4.211 - SEM images of microstructure of coated pin

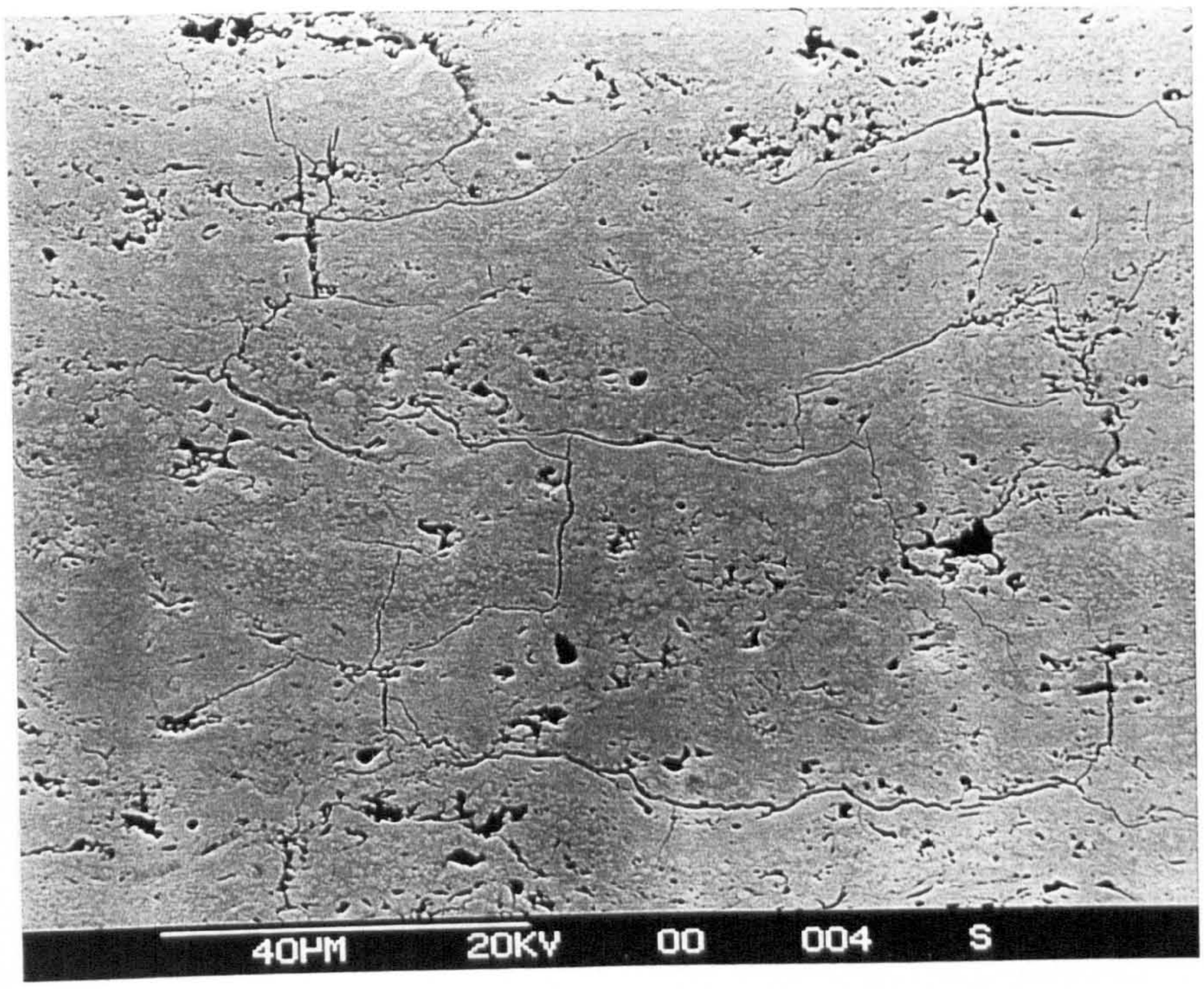

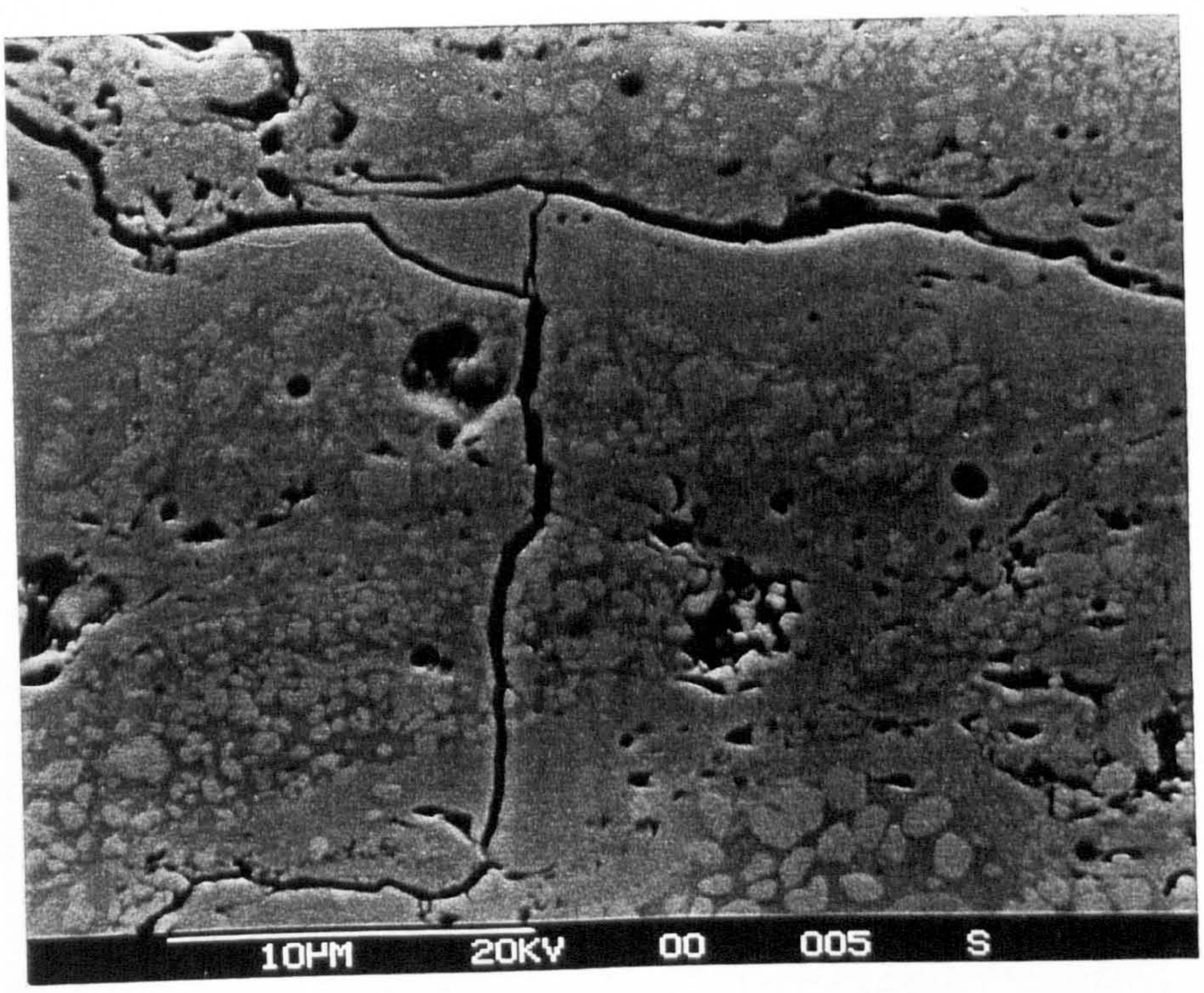

Fig. 4.212 - SEM micrographs of etched pin microstructure

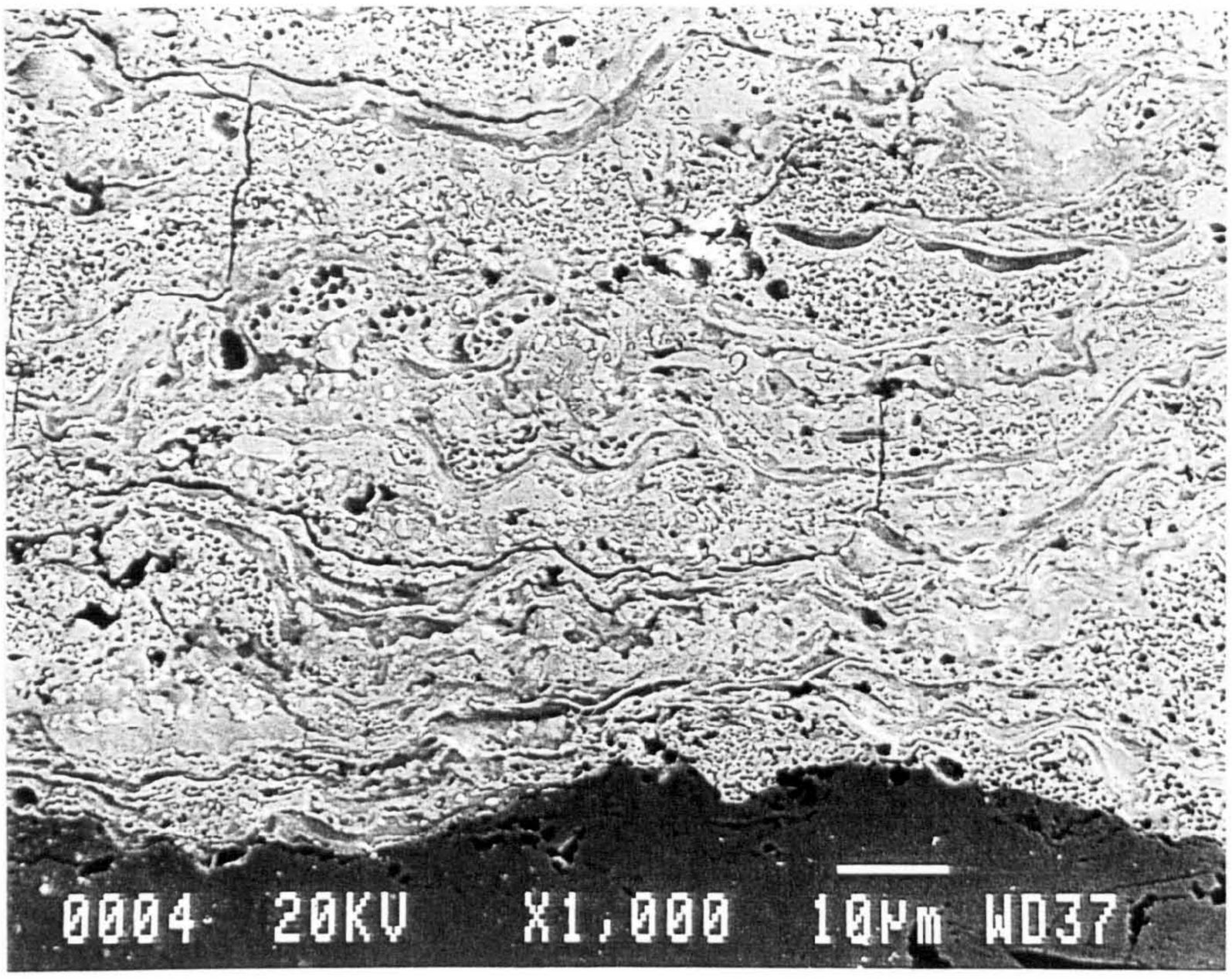

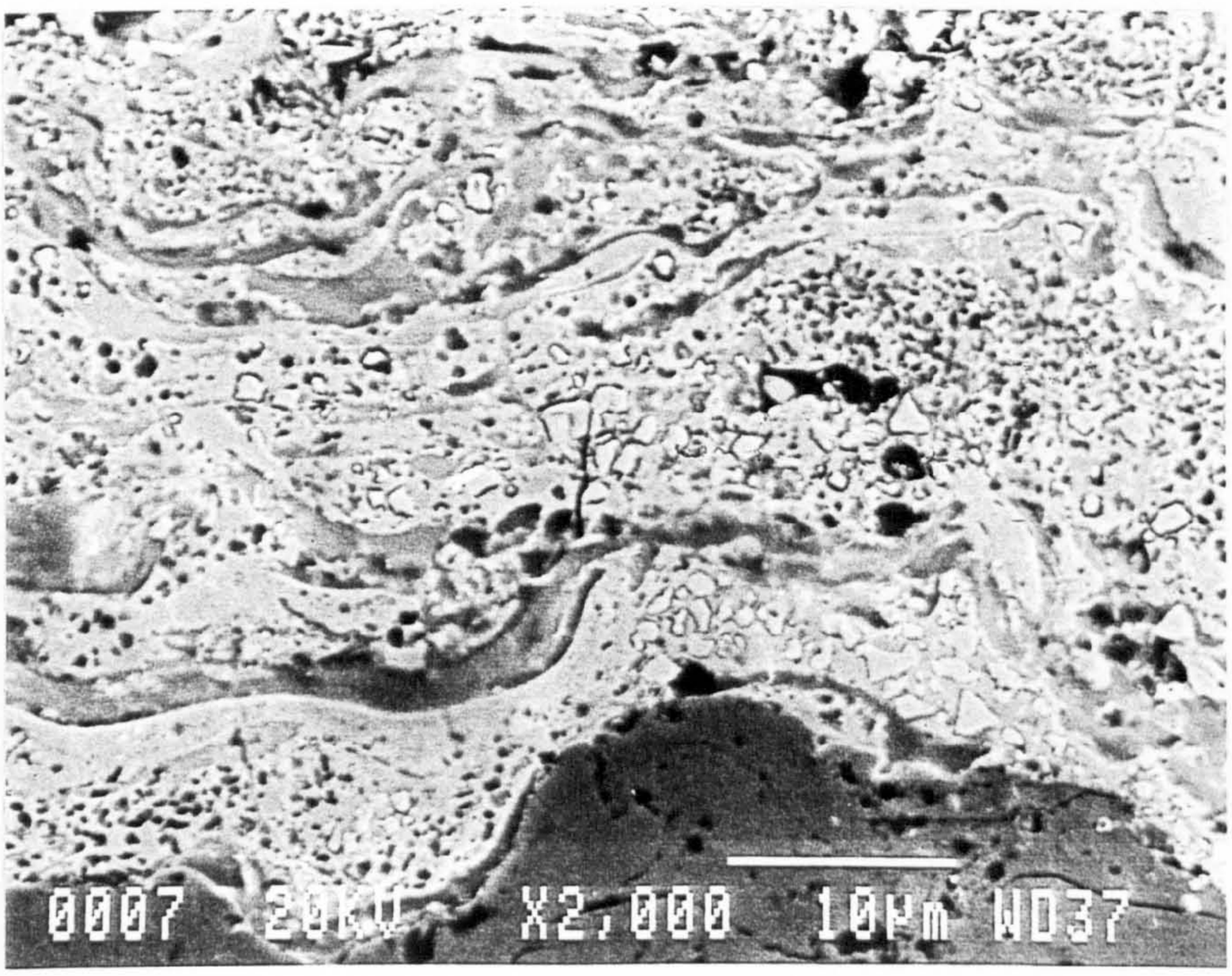

Fig. 4.212 cont... - SEM micrographs of etched pin microstructure

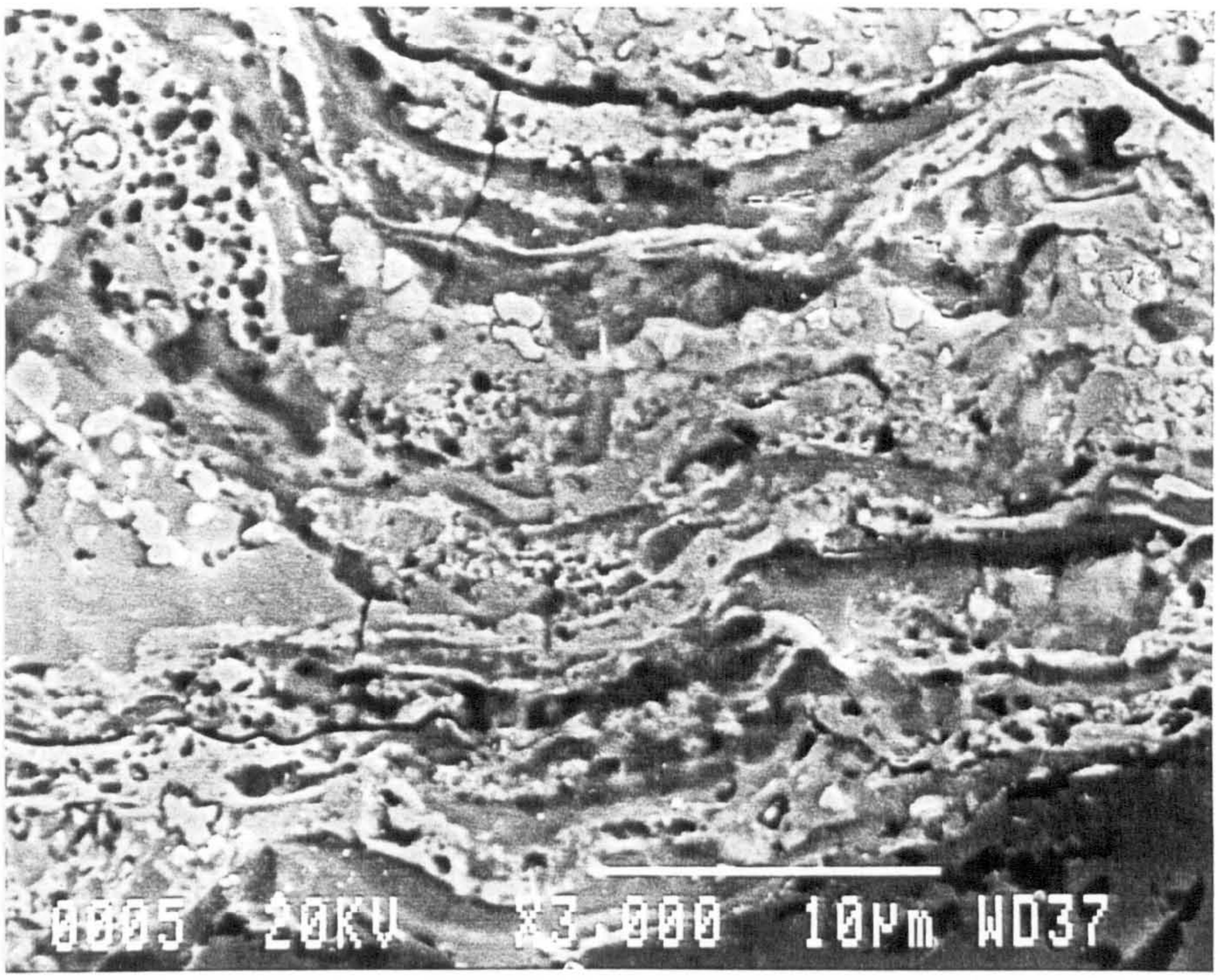

Compositional contrast

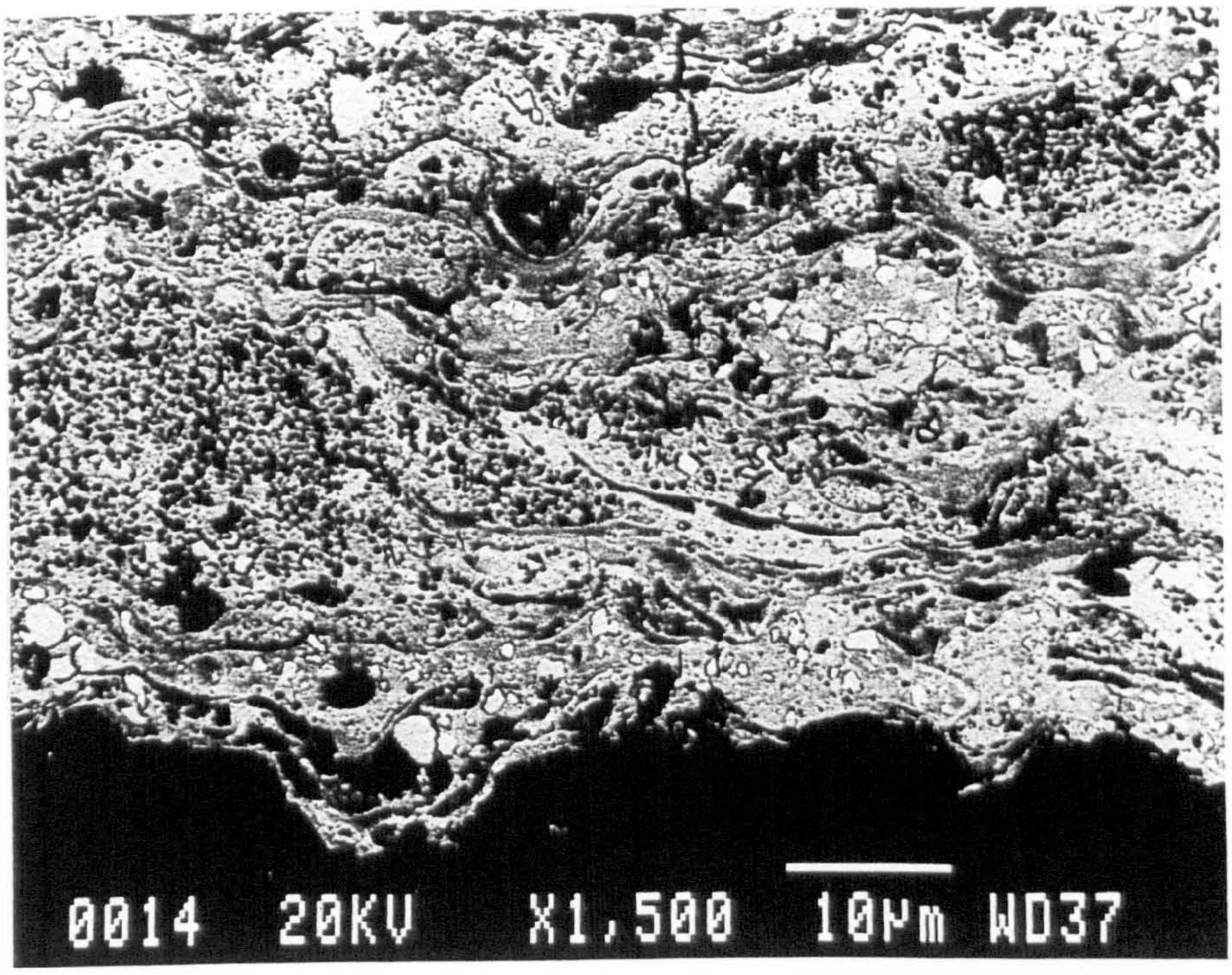

Fig. 4.213 - SEM micrographs of coated pin - coating/substrate interface

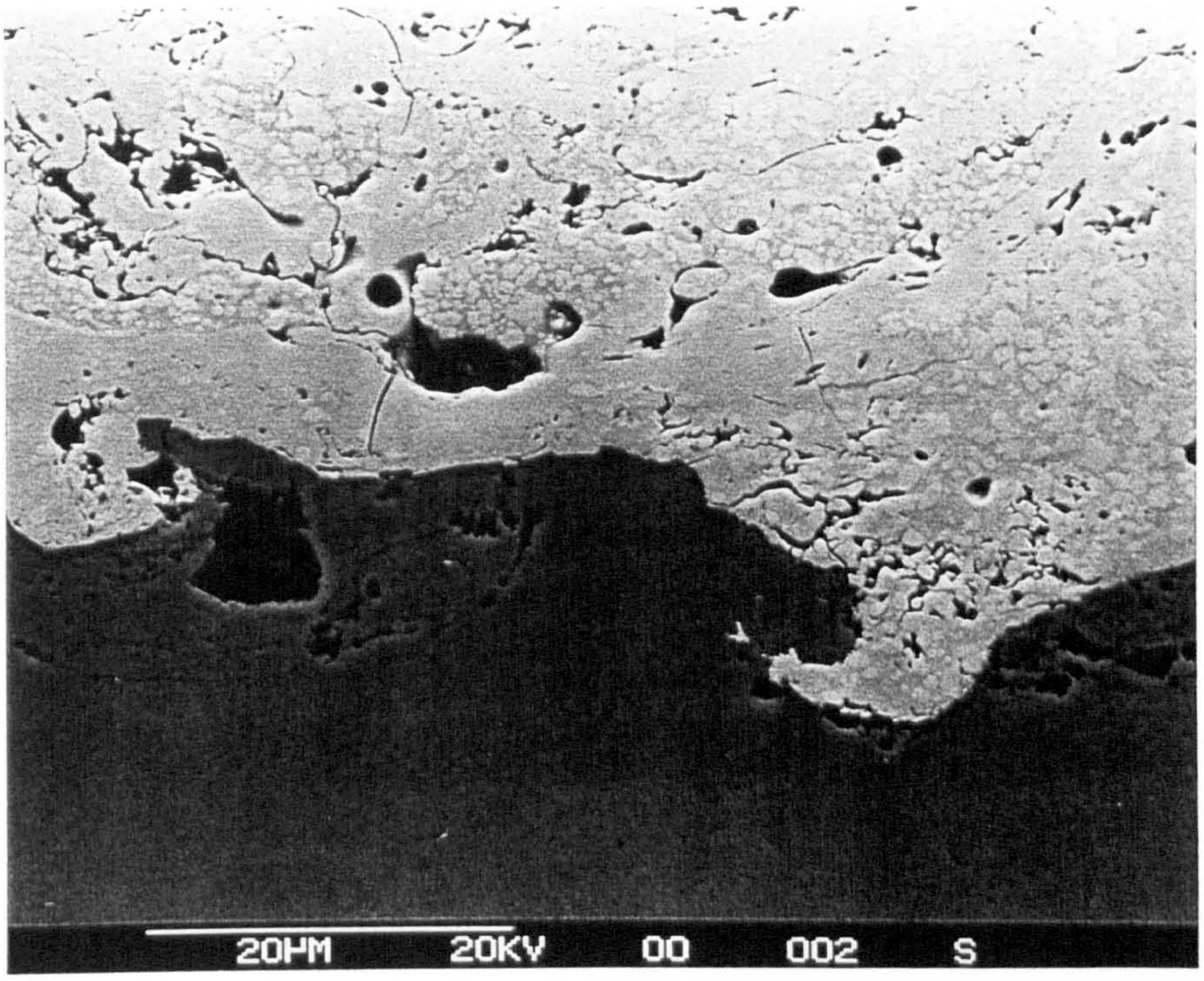

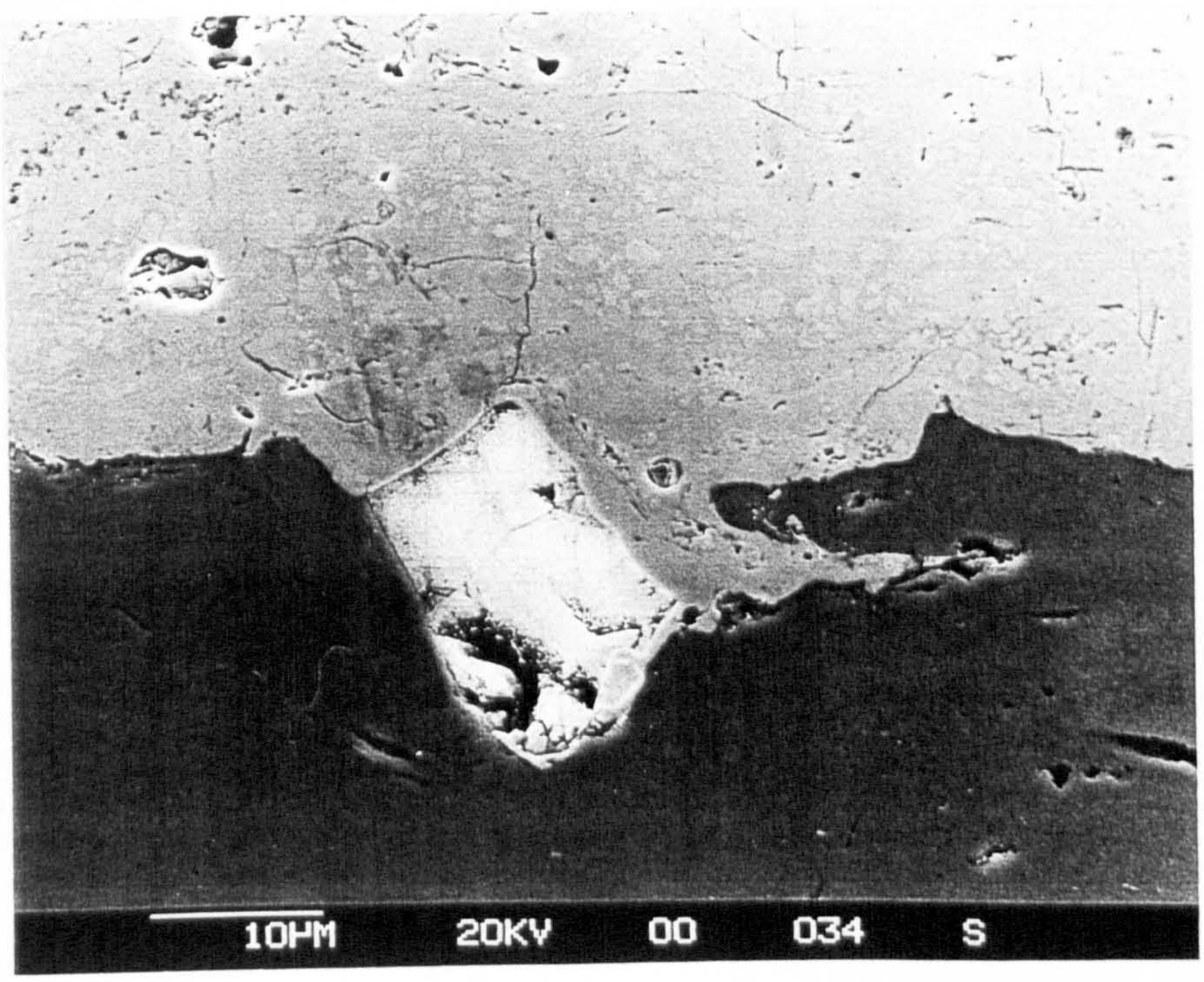

Fig. 4.214 - Elemental dot map showing trapped alumina particle at interface

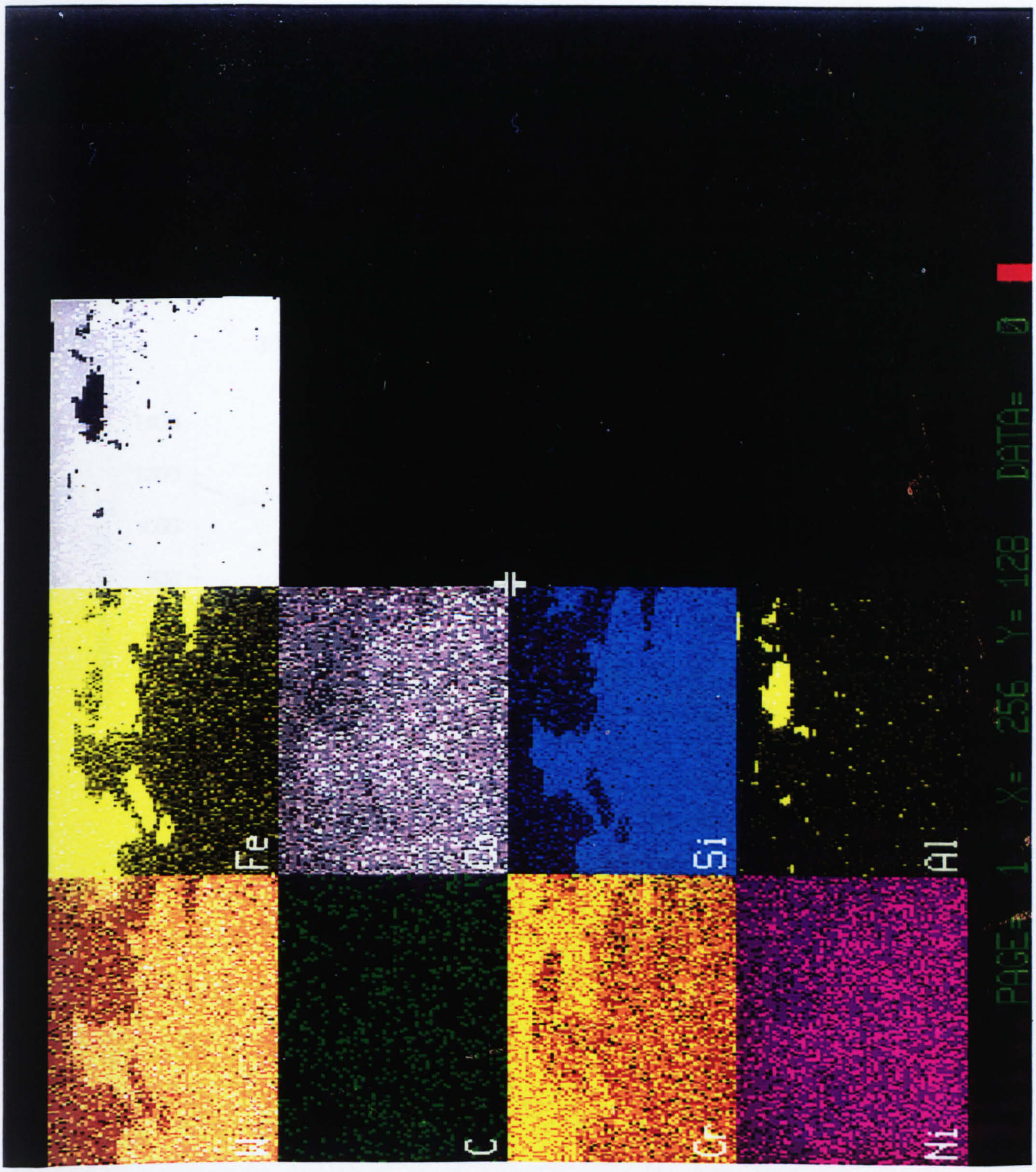

Fig. 4.221 - Microhardness profile of LW45

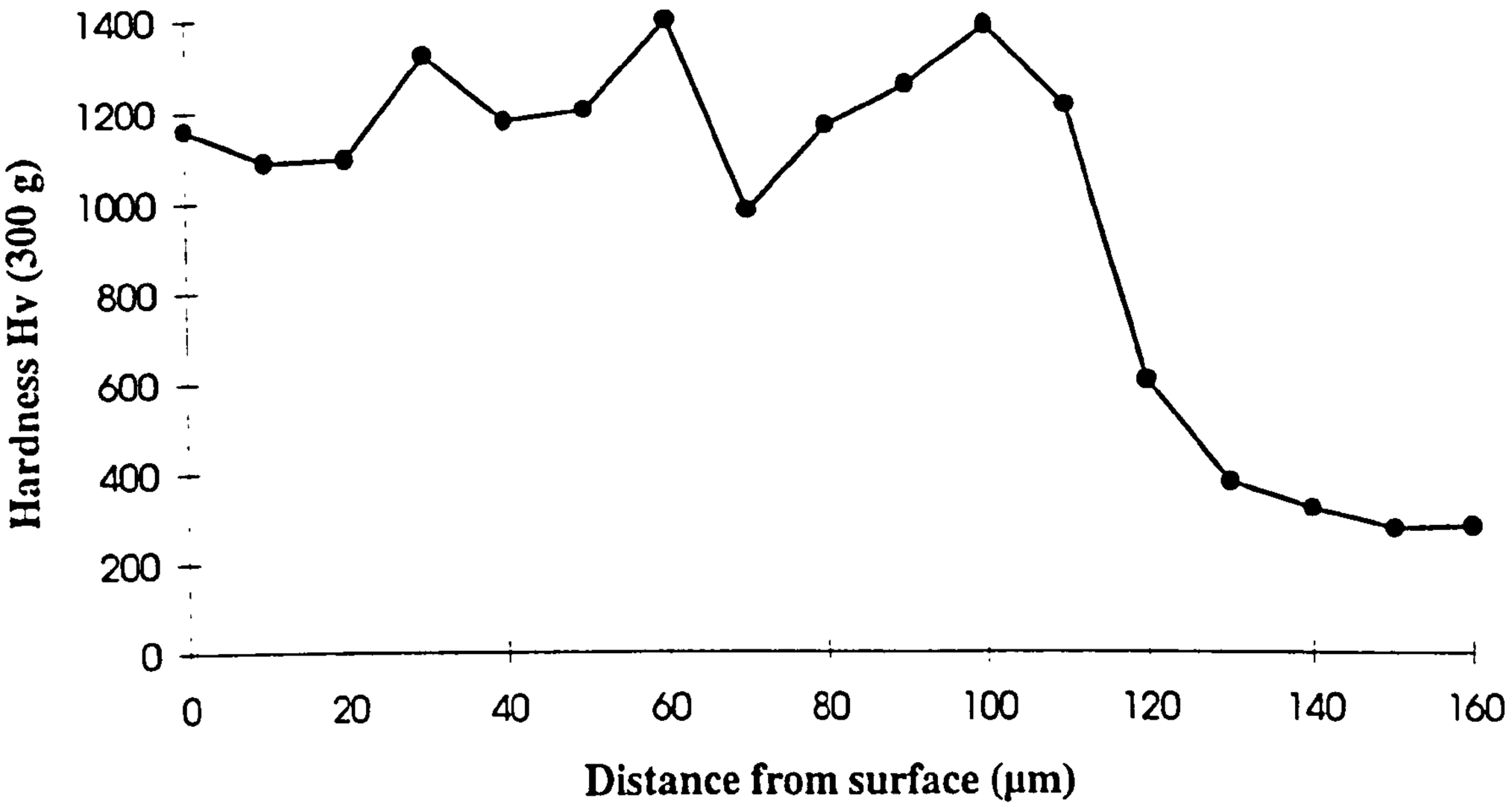

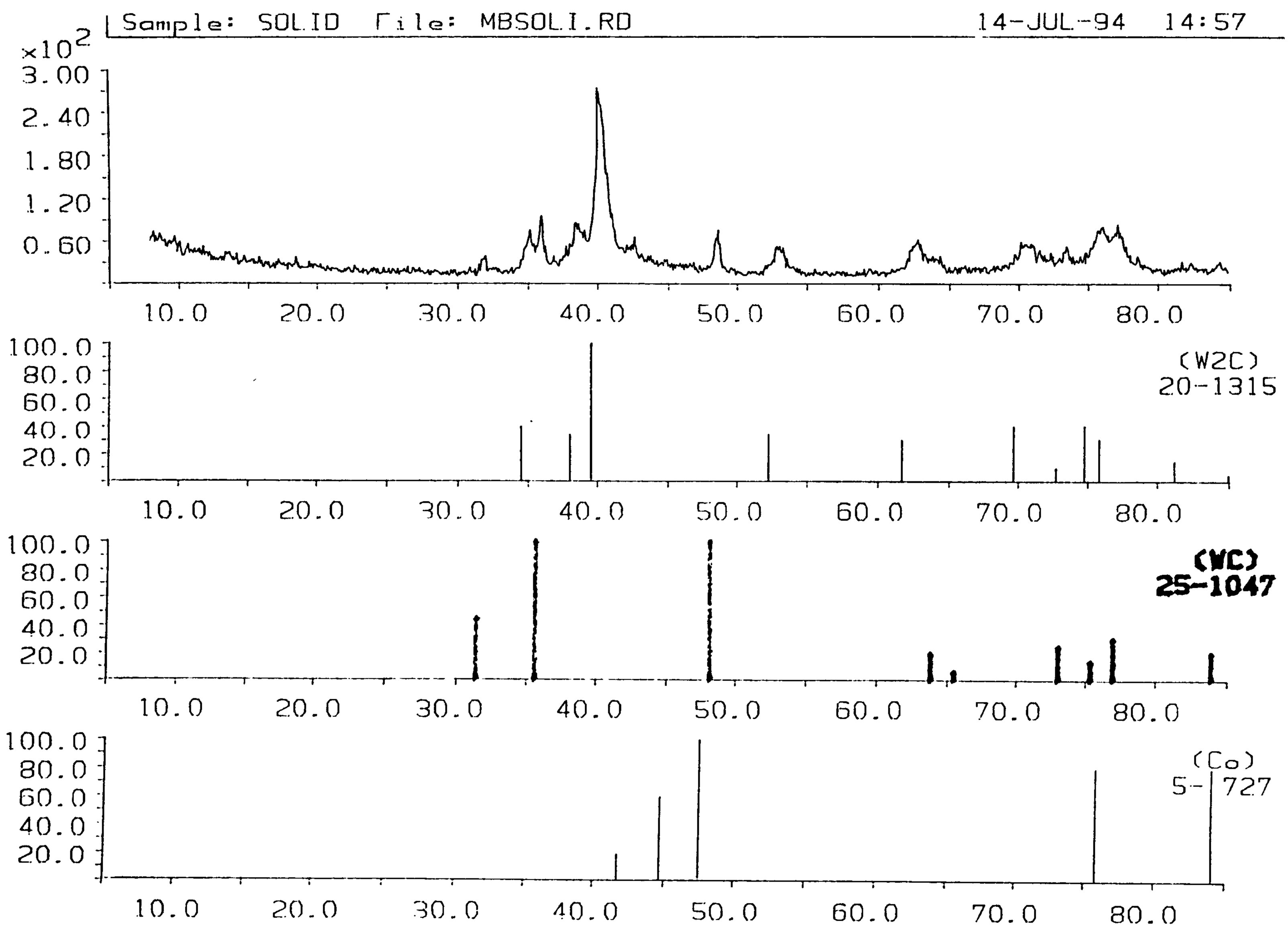

Figure 4.231 - X-ray diffraction trace for the as-coated sample

Fig. 4.311 Wear Depths for Ramp Tests

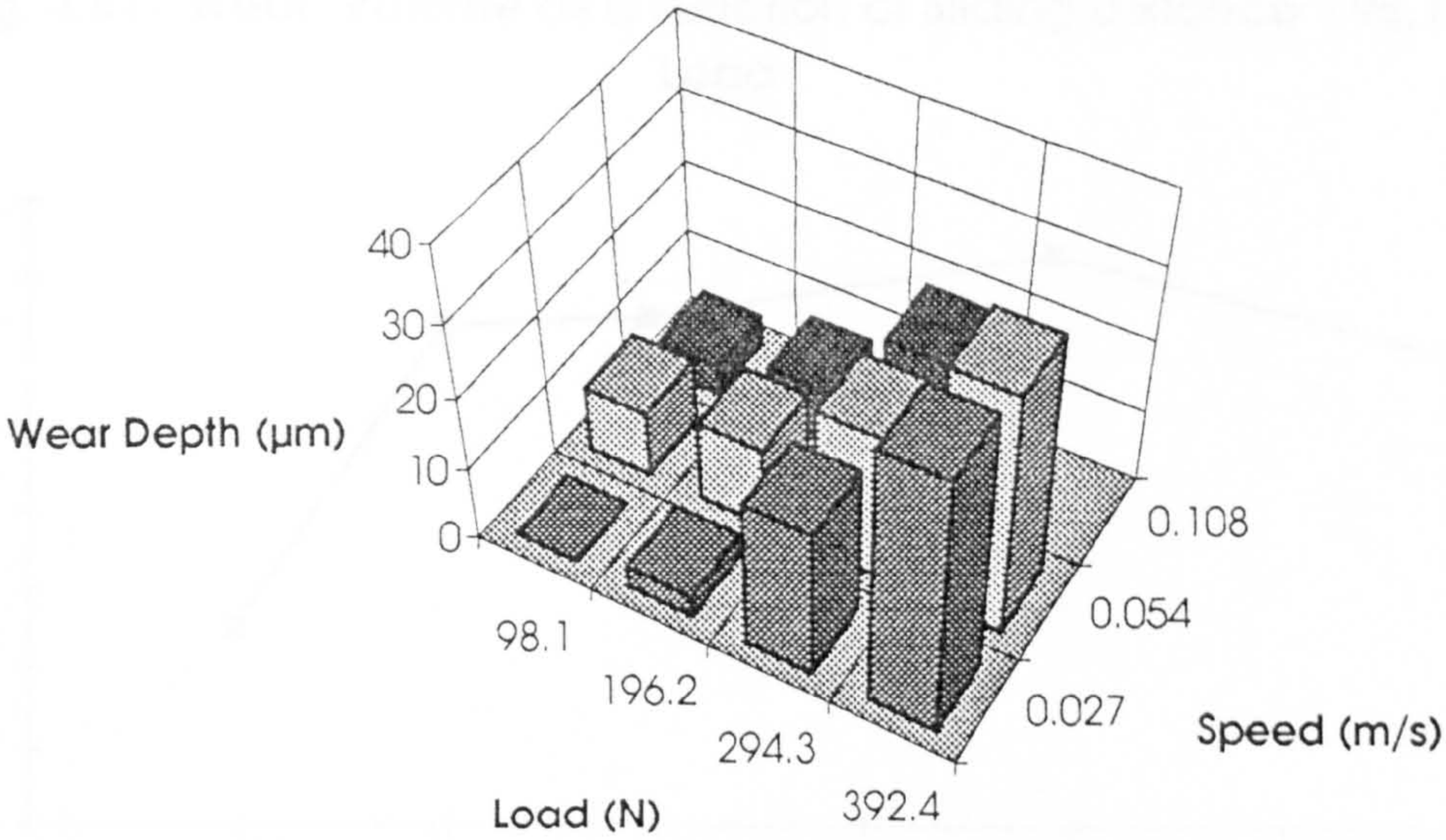

Fig. 4.312 Friction Coefficients (Ramp Tests)

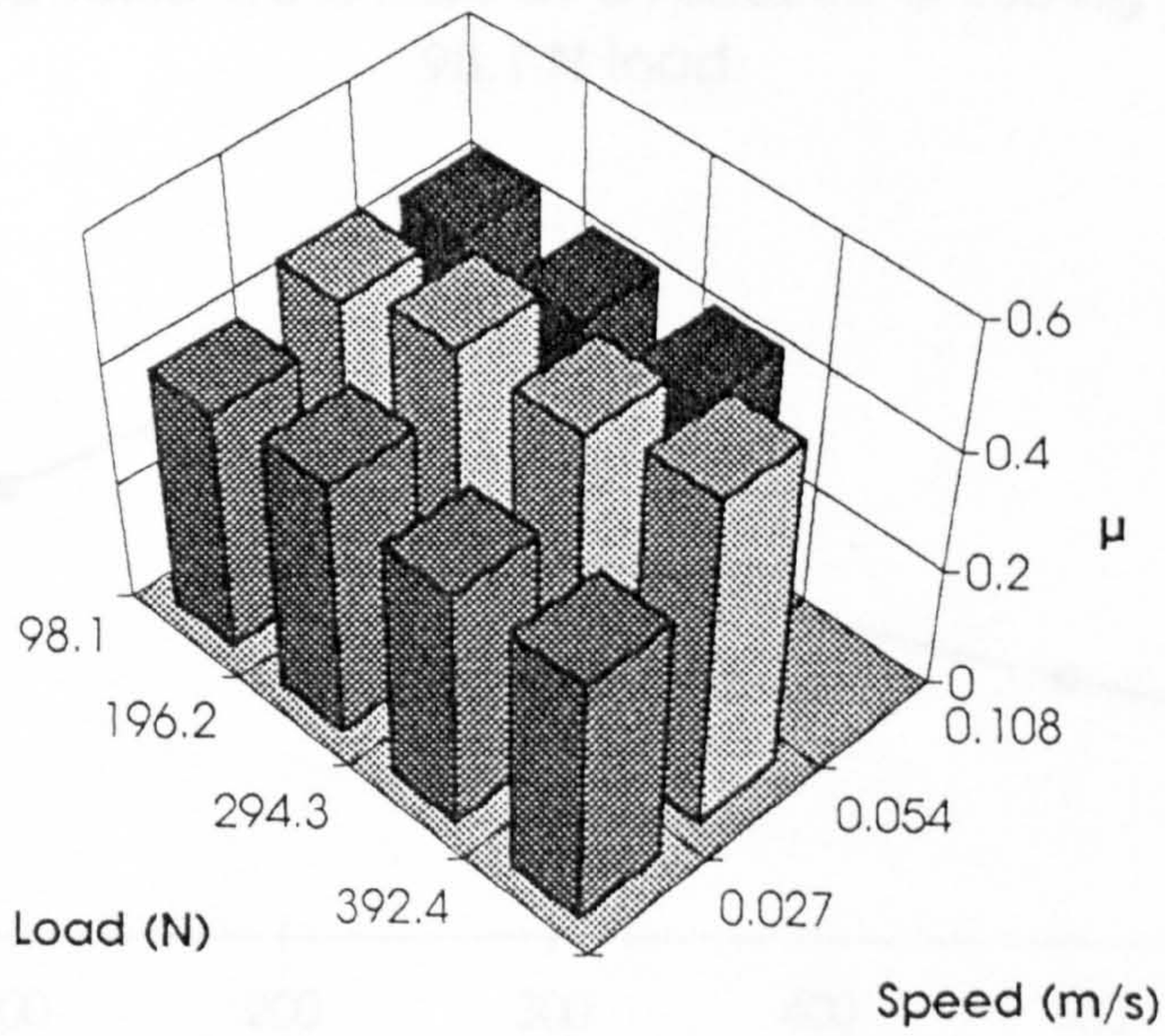

Fig. 4.411 Wear Volume as a Function of Sliding Distance - 98.1N Load

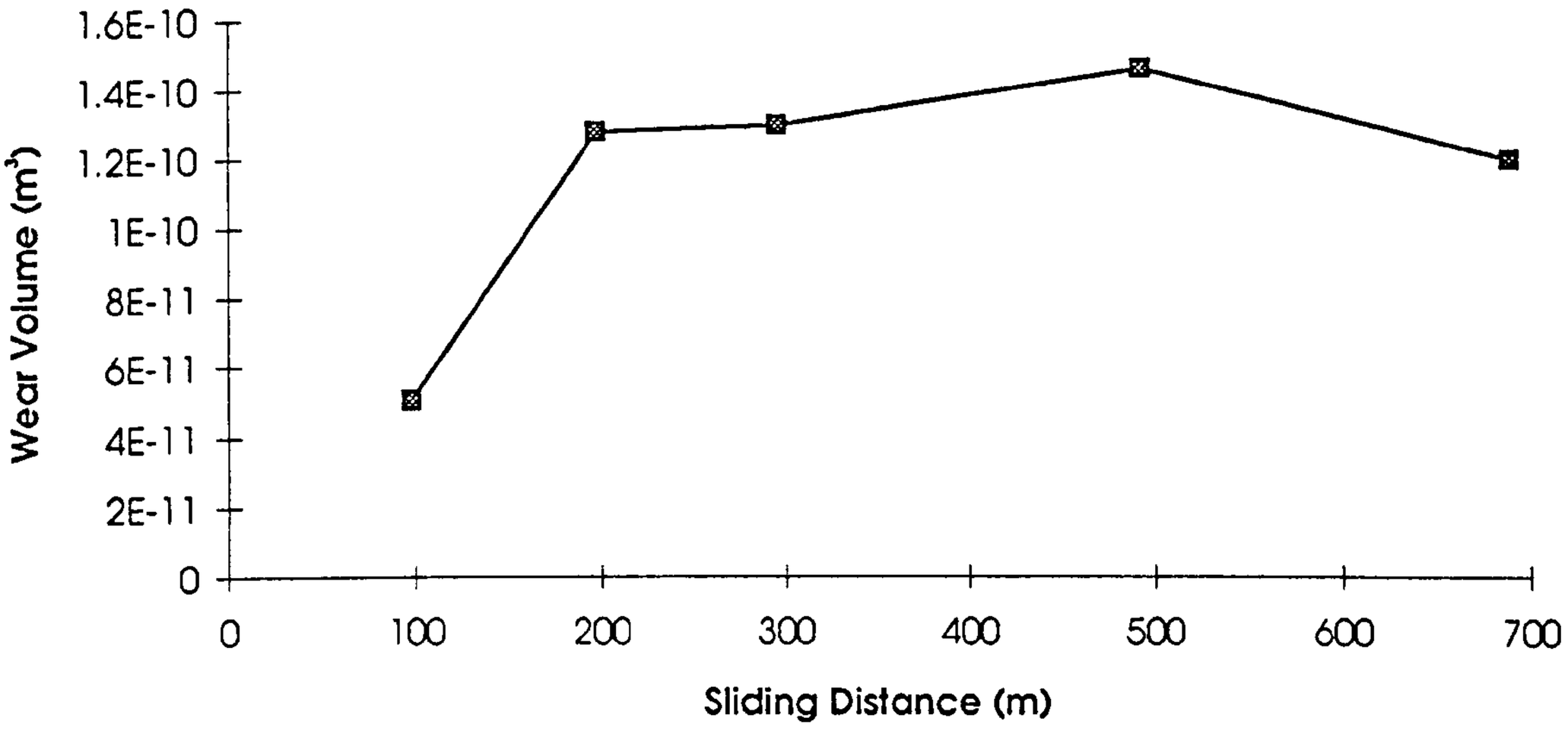

Fig. 4.412 Specific Wear Rate as a Function of Sliding Distance - 98.1 N load

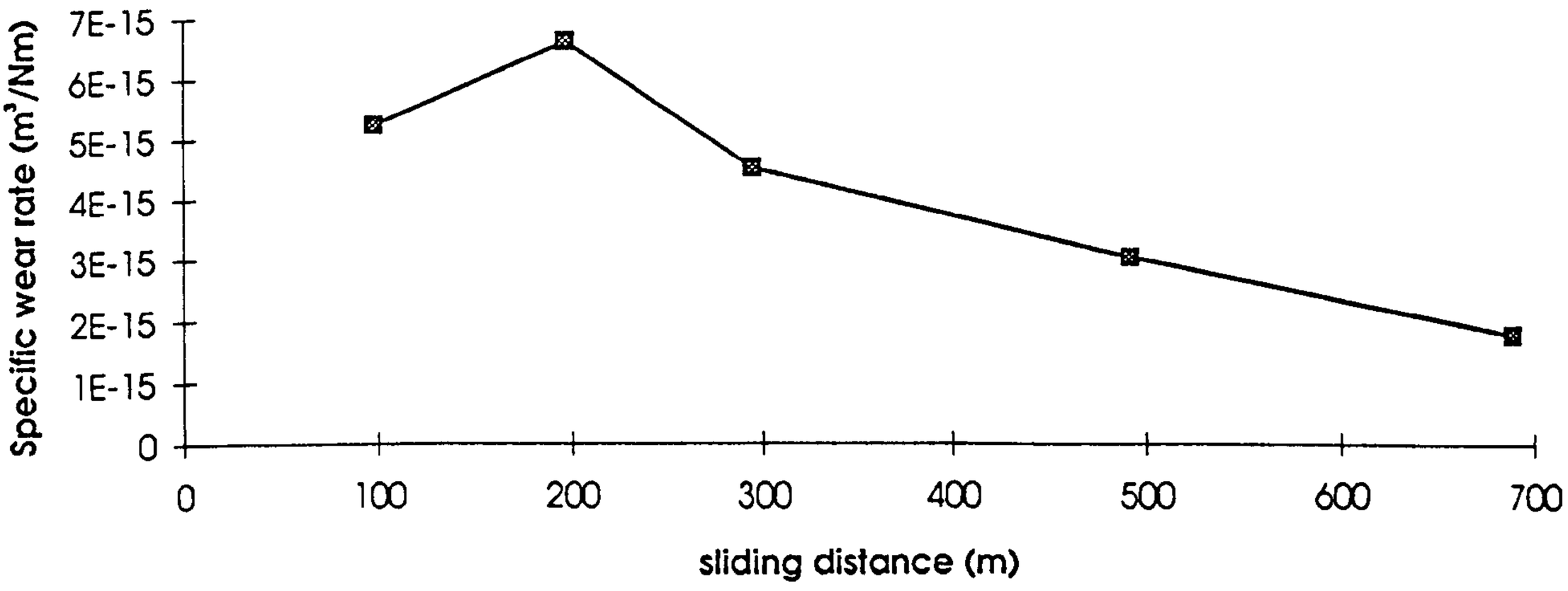

Fig. 4.421 Wear Volume as a Function of Sliding Distance -196.2N Load

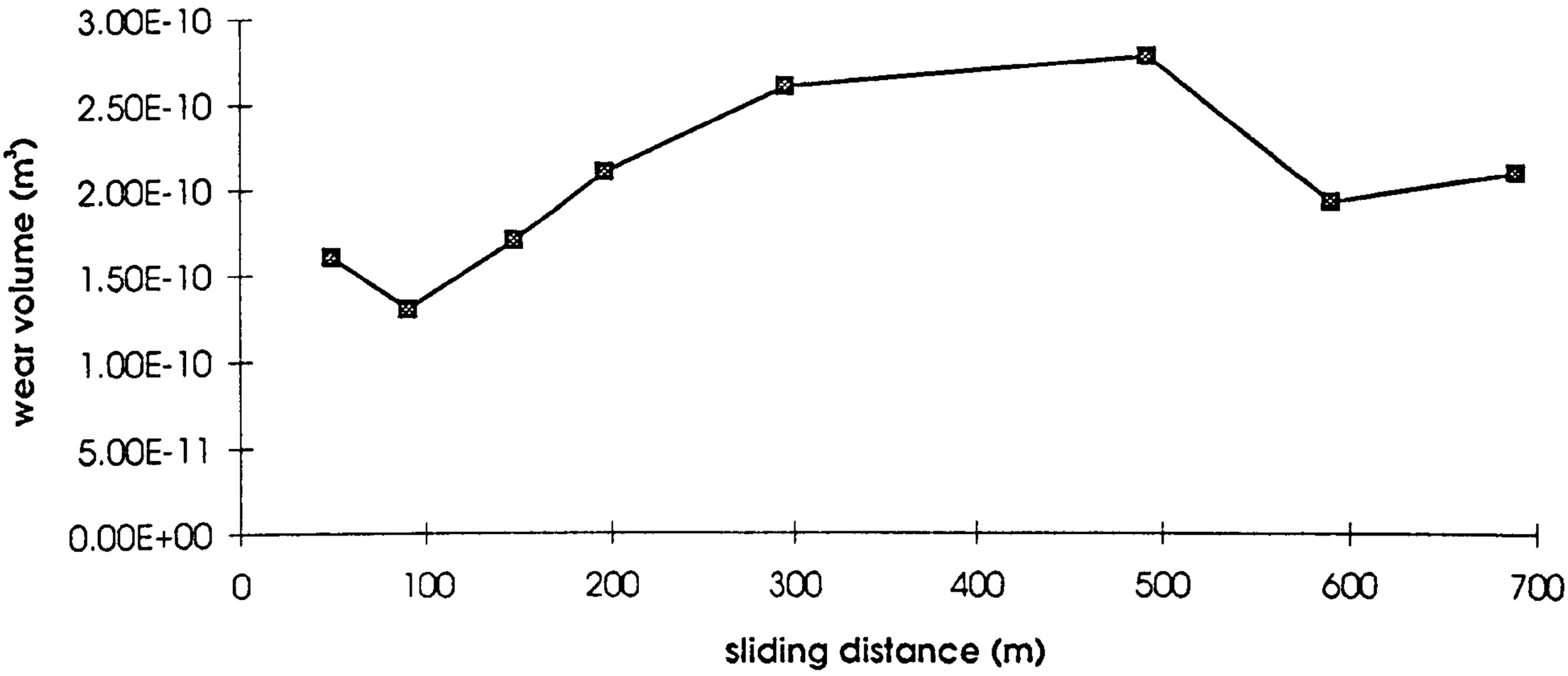

Fig. 4.422 Specific Wear Rate as a Function of Sliding Distance - 196.2N load

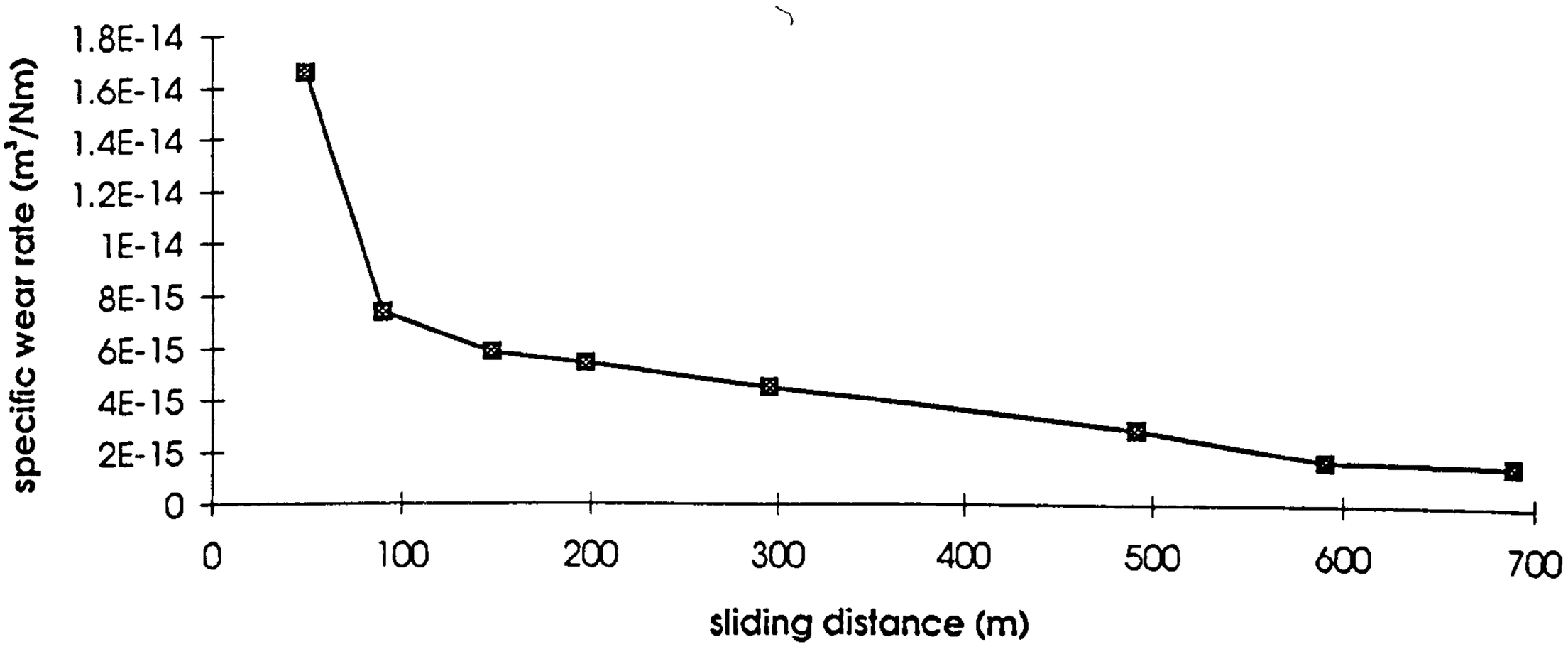

Fig. 4.431 Wear Volume as a Function of Sliding Distance - 294.3N Load

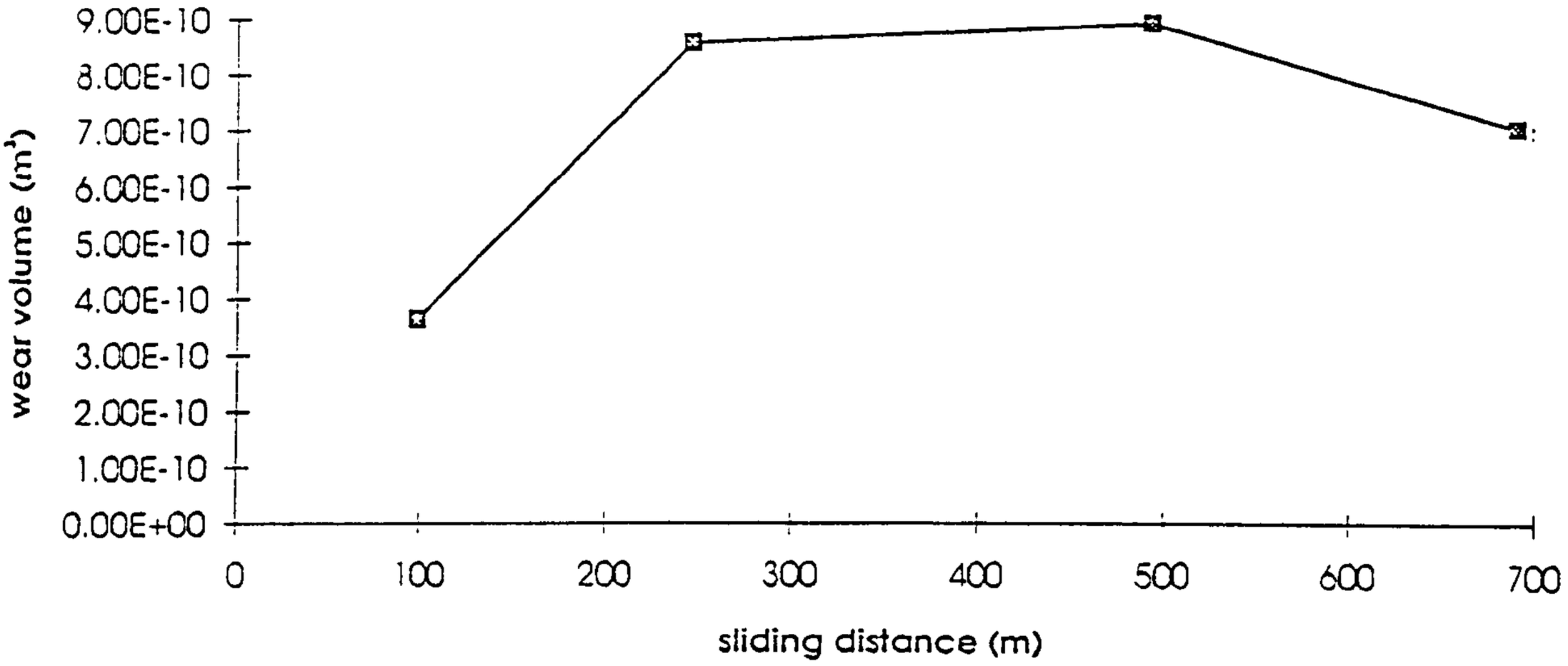

Fig. 4.432 Specific Wear Rate as a Function of Sliding Distance - 294.3N load

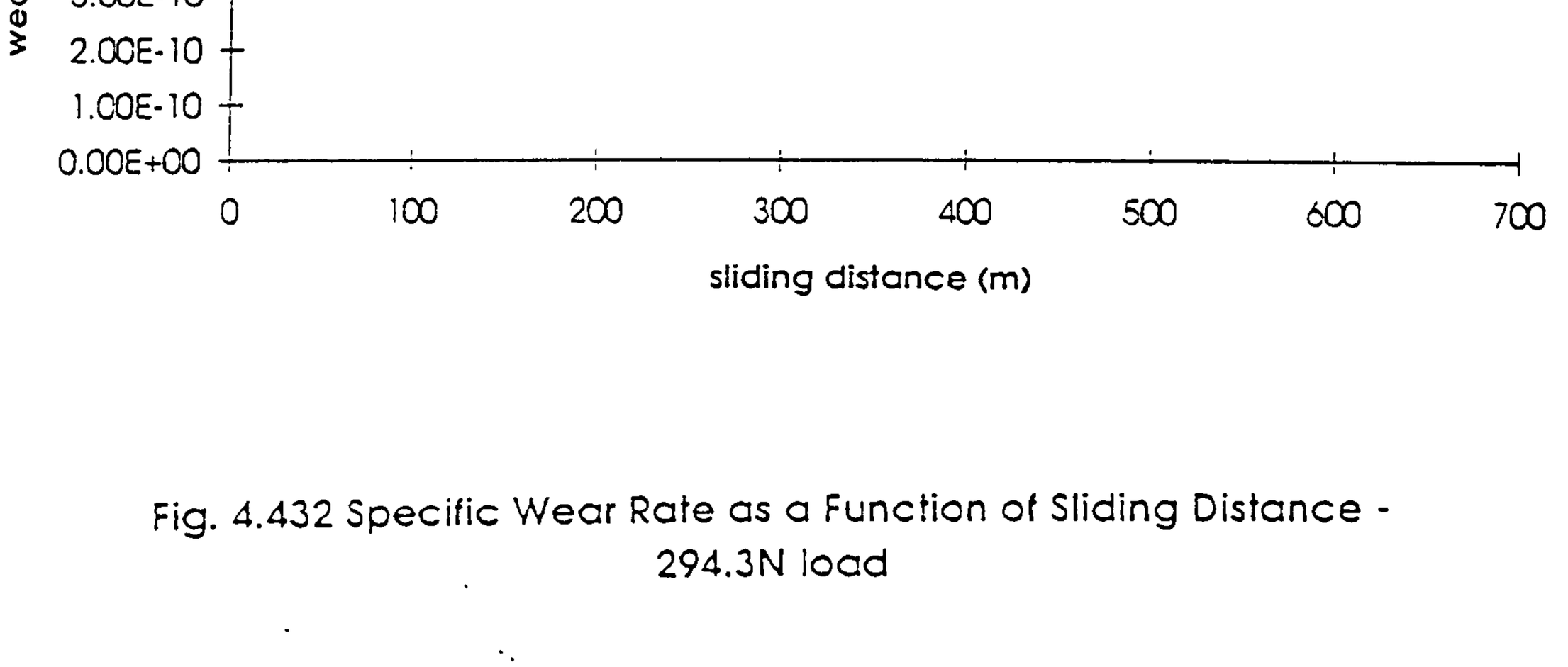

Fig. 4.441 Wear Volume as a Function of Sliding Distance - 392.4 N Load

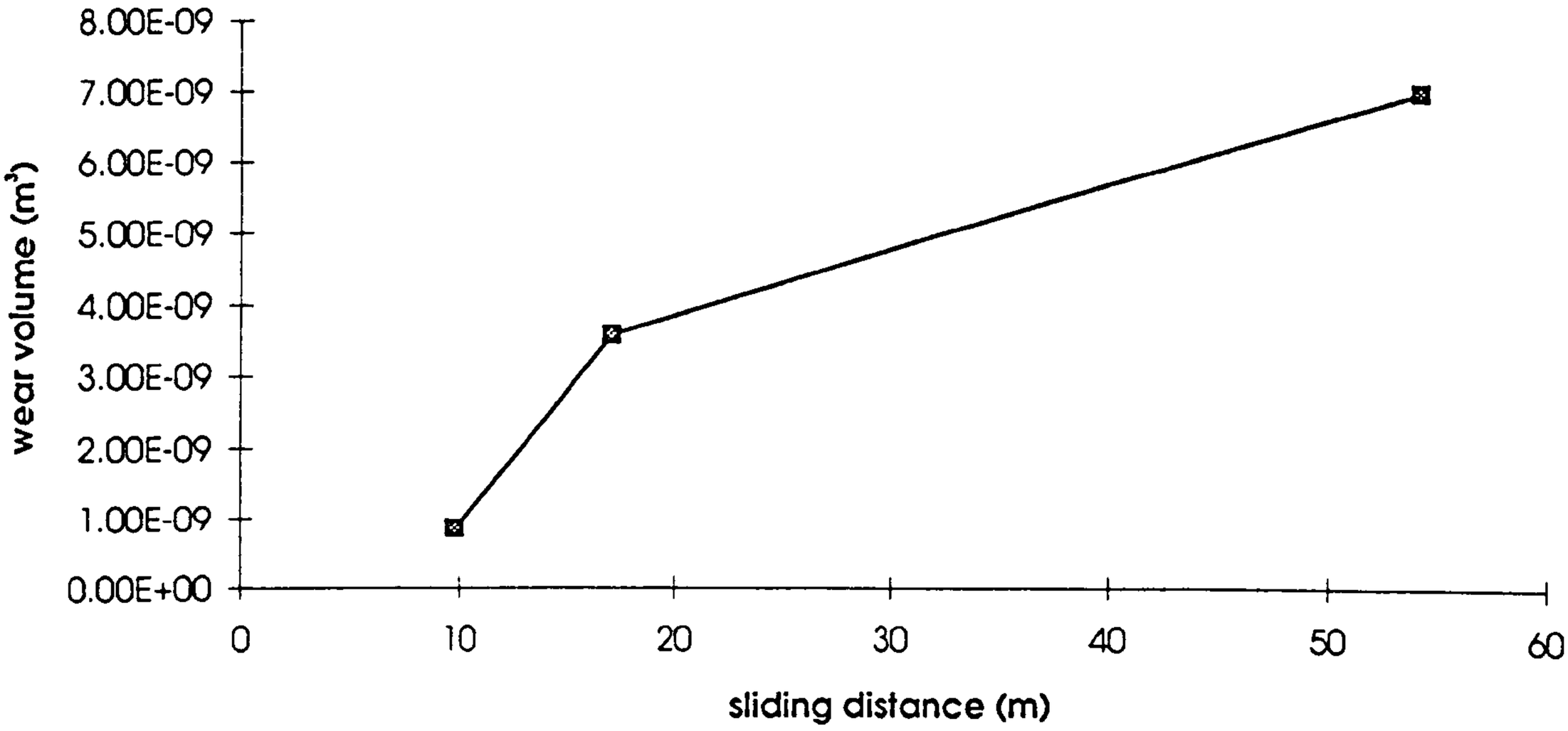

Fig. 4.442 Specific Wear Rate as a Function of Sliding Distance - 392.4 N Load

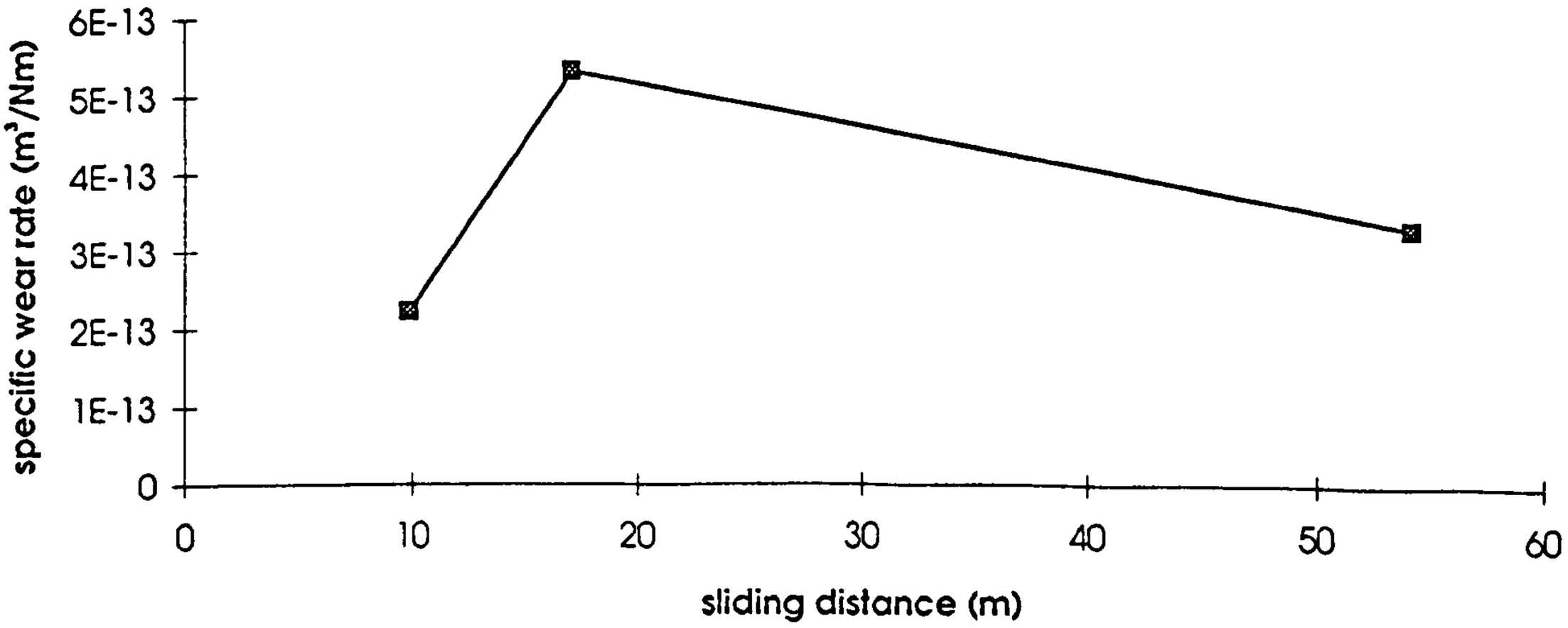

Figure 4.451 - Wear volume as a function of sliding distance for pin-on-plate tests

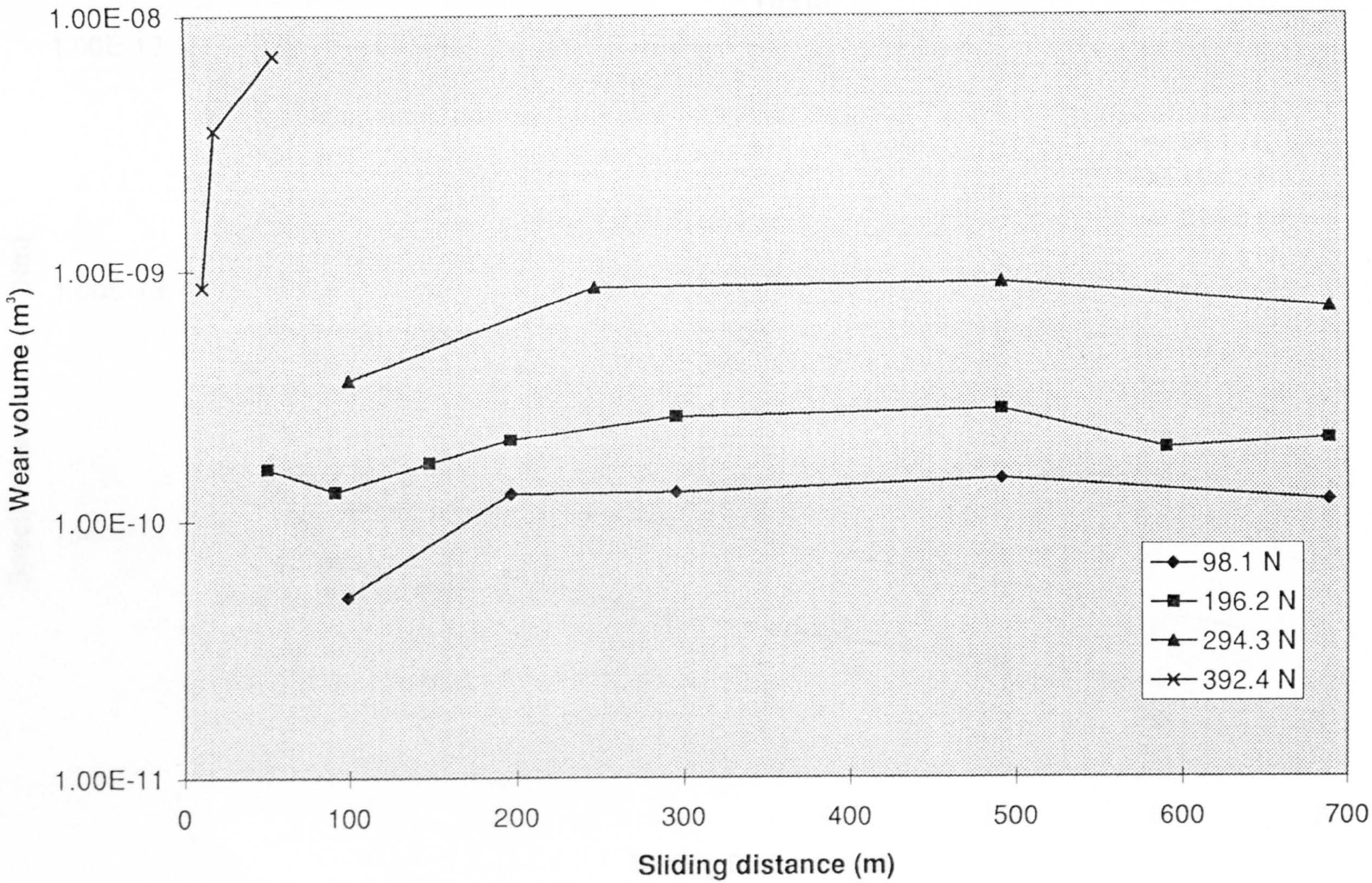

Figure 4.452 - Specific Wear Rate as a Function of Sliding Distance for Pin-on-Plate Tests

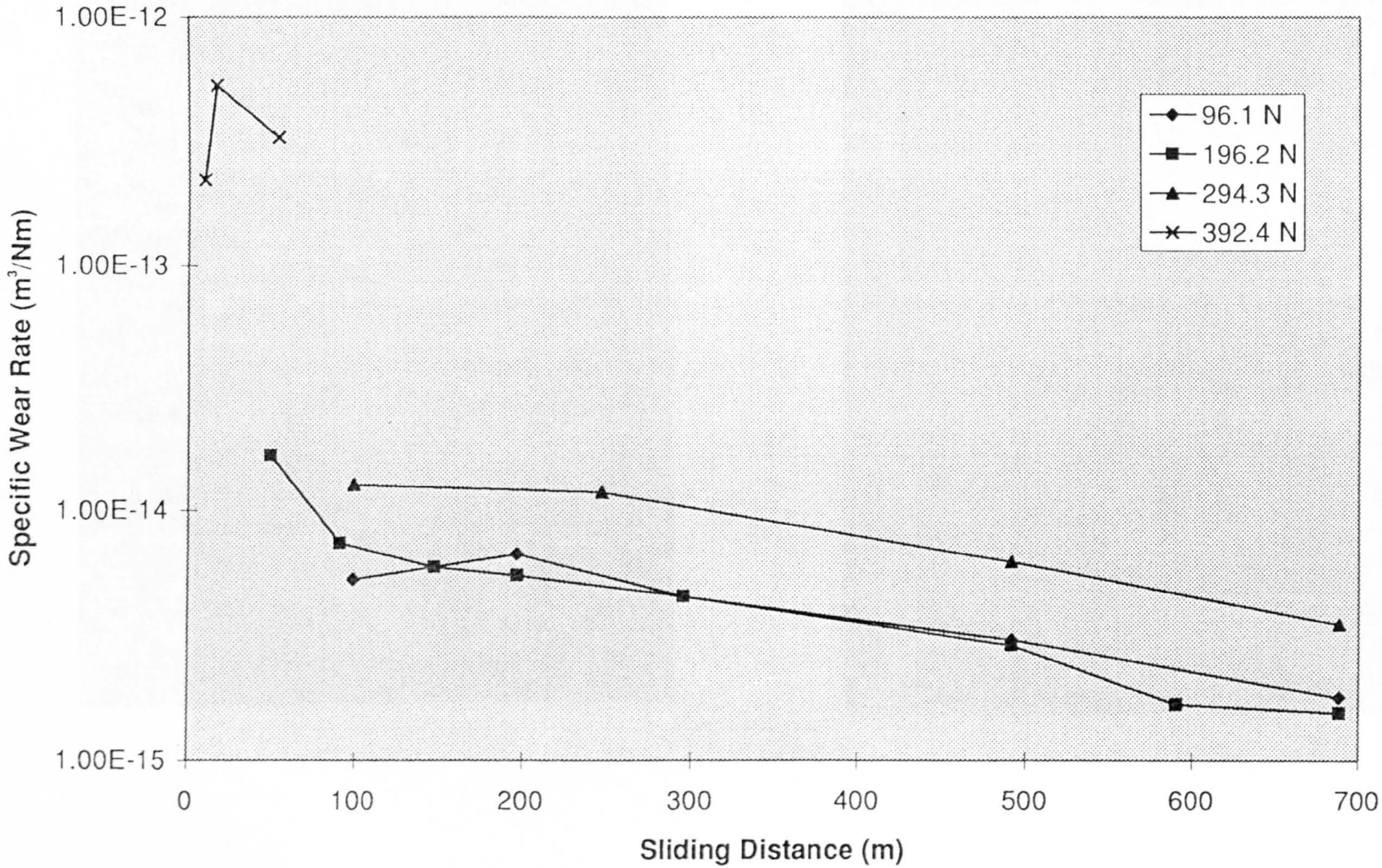

Fig. 4.453 - SEM micrographs of "mild" wear tracks - 196.2 N, 728 m

(a) Surface after running-in procedure X 1000

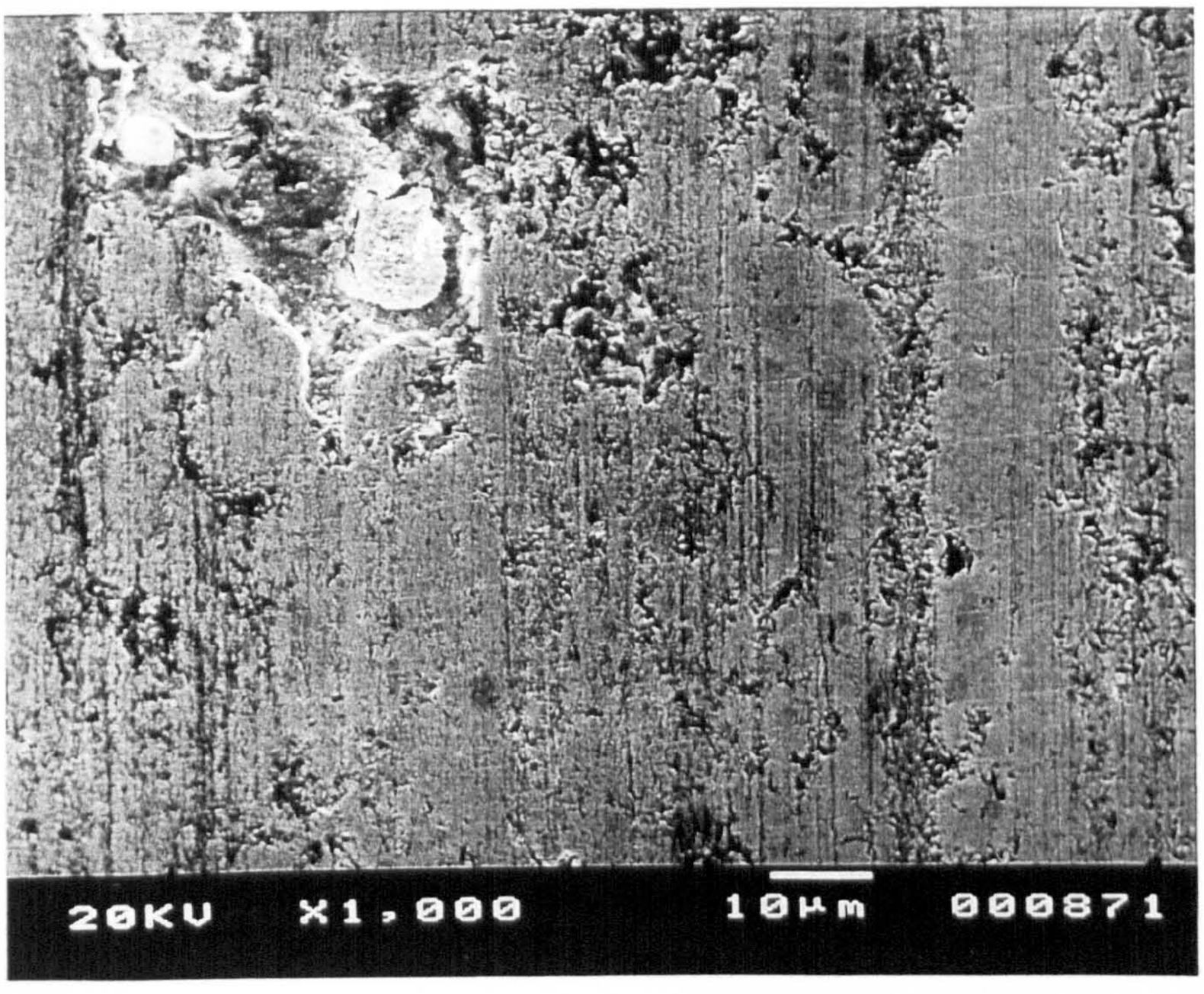

(b) x 1000

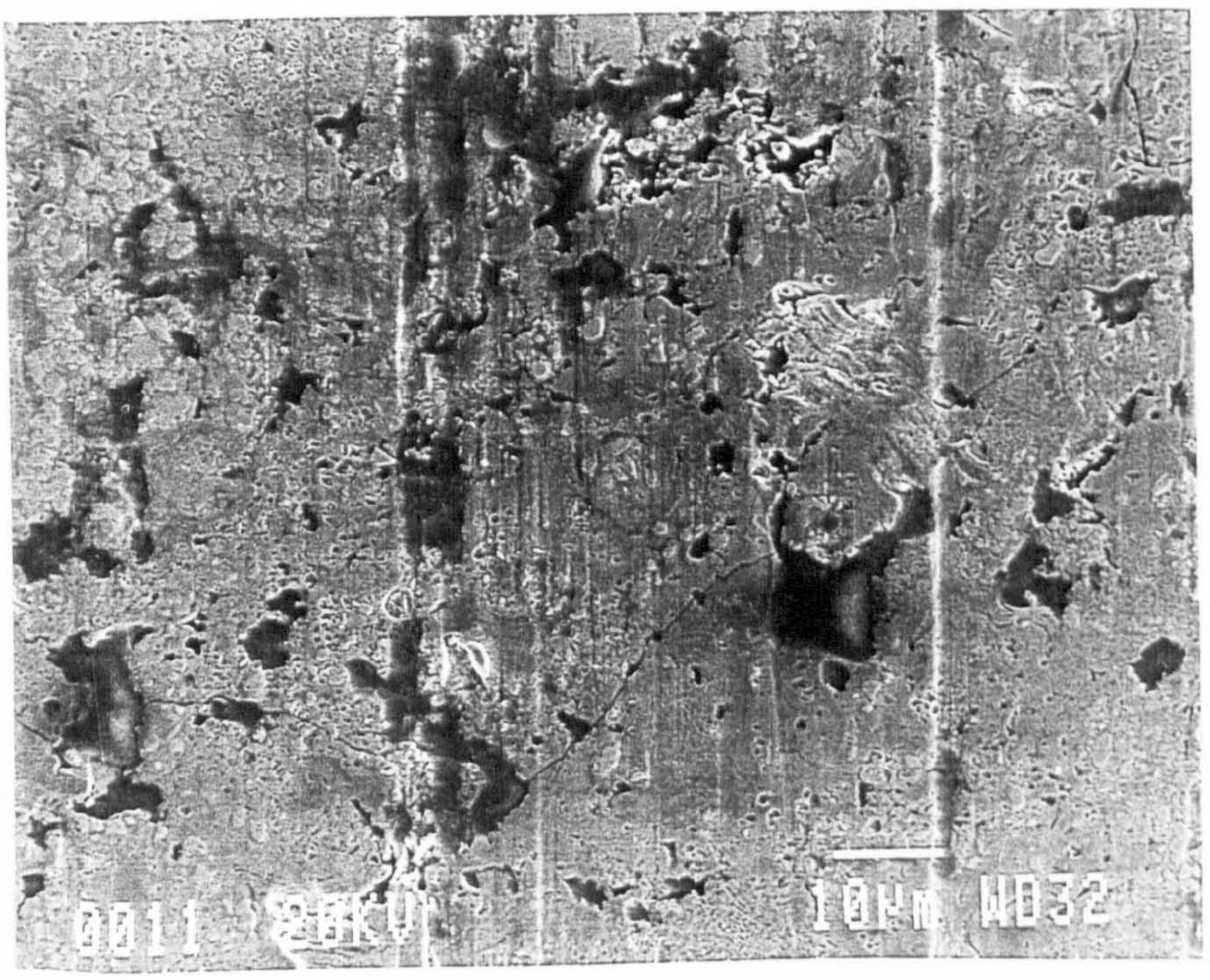

Fig. 4.453 cont...

(c) x 4000

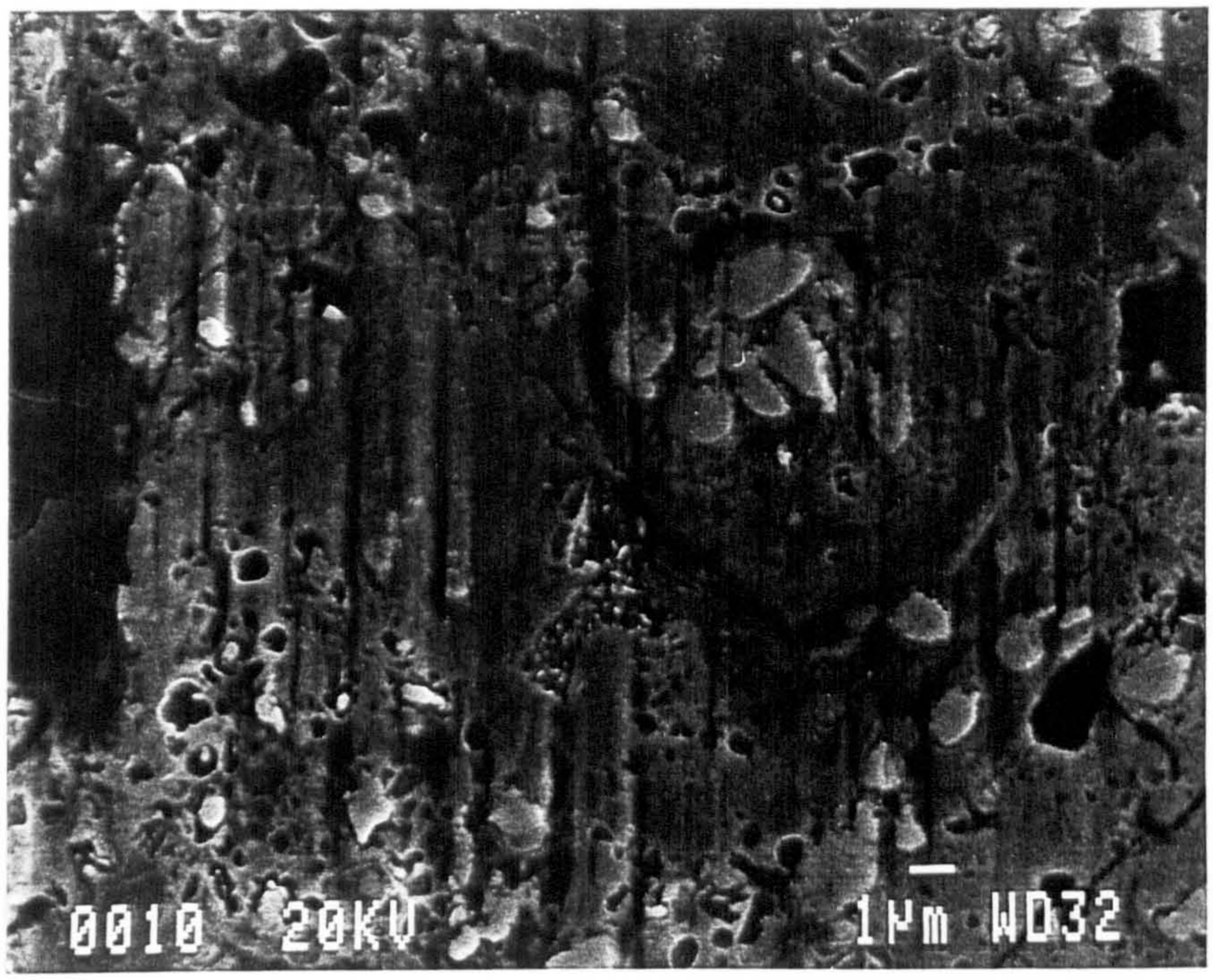

Fig. 4.454 - SEM micrographs of "severe" wear surface - 294.3 N, 590 m

(a) x 200

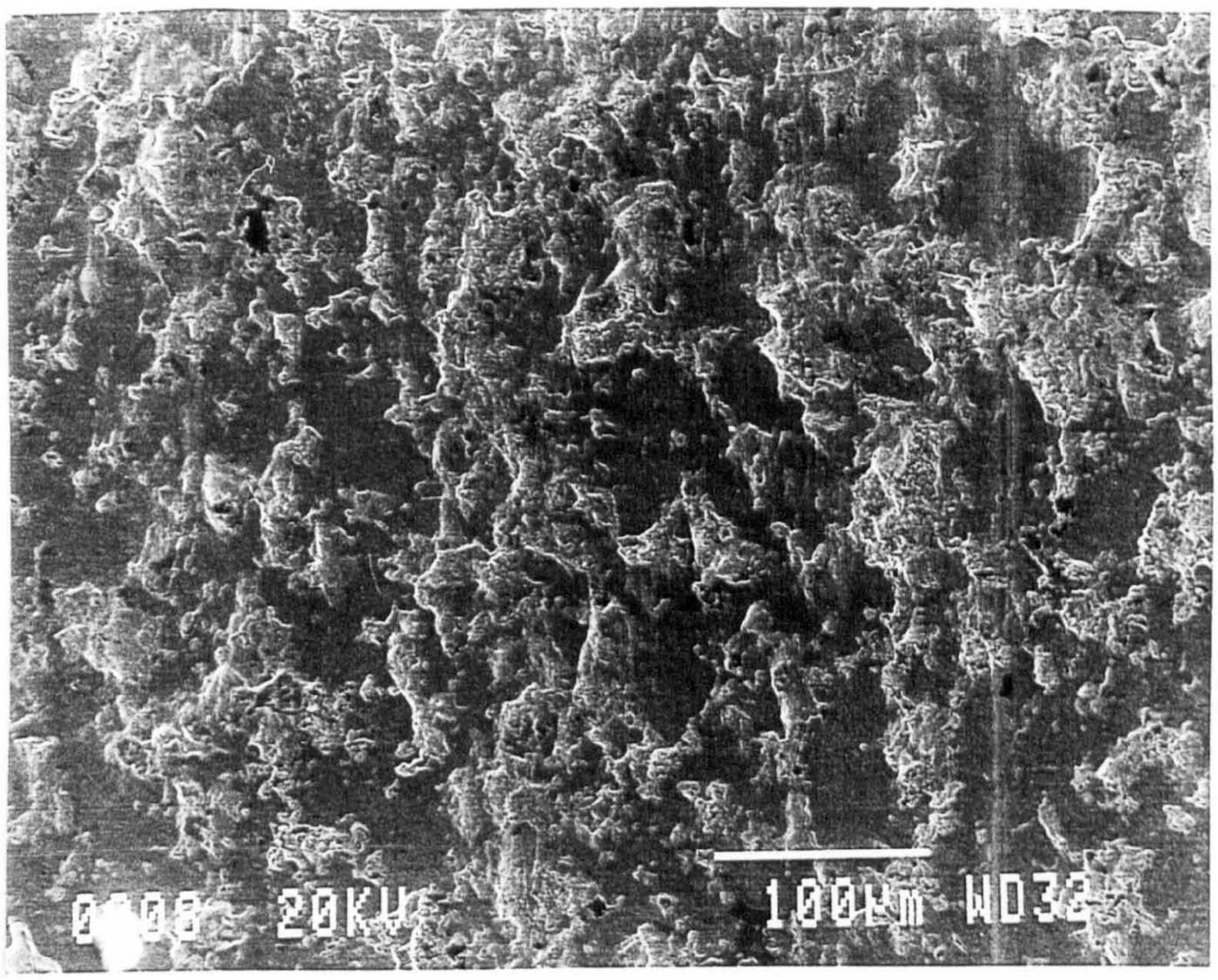

(b) x 500

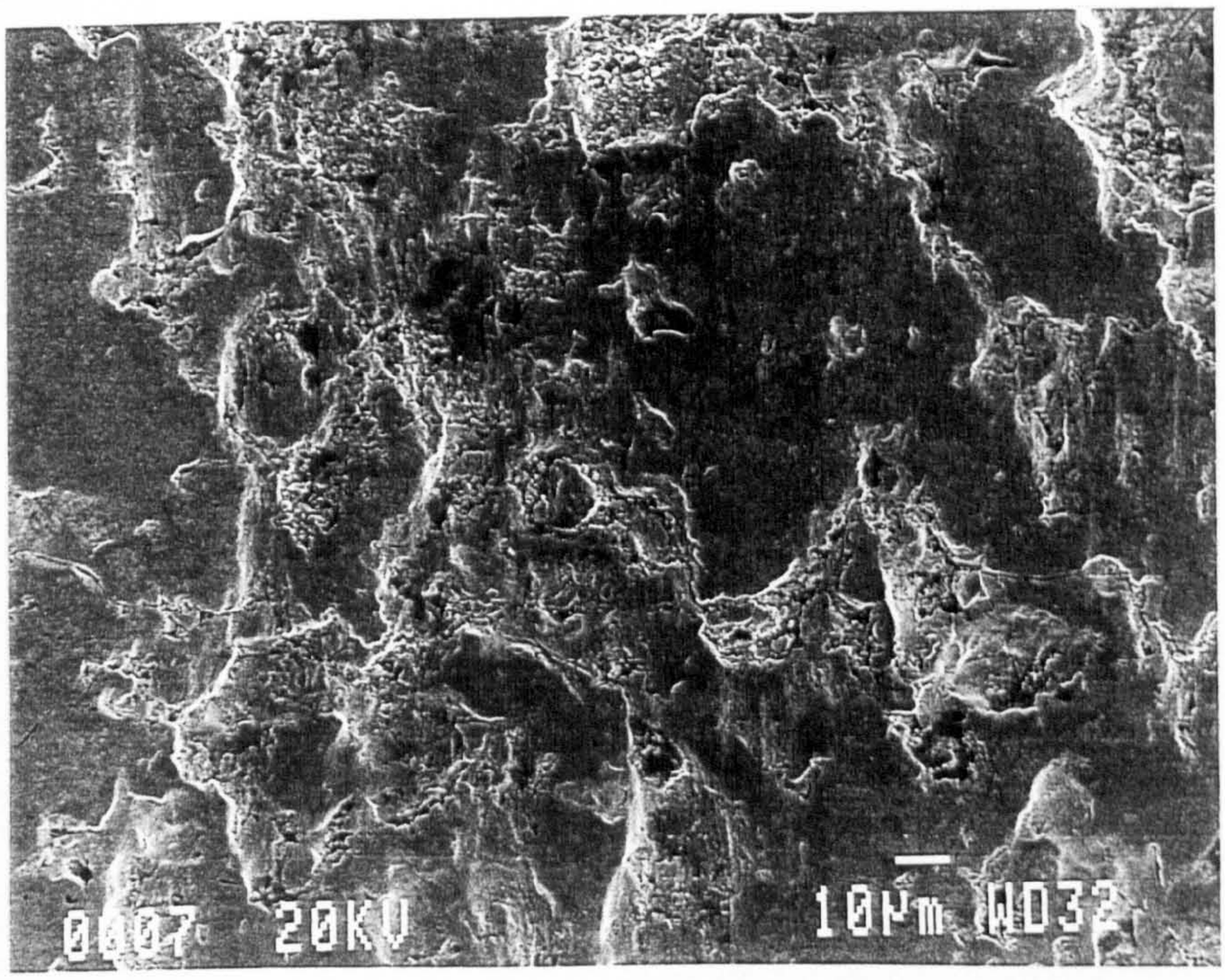

Fig. 4.454 cont...

(c) x 1000

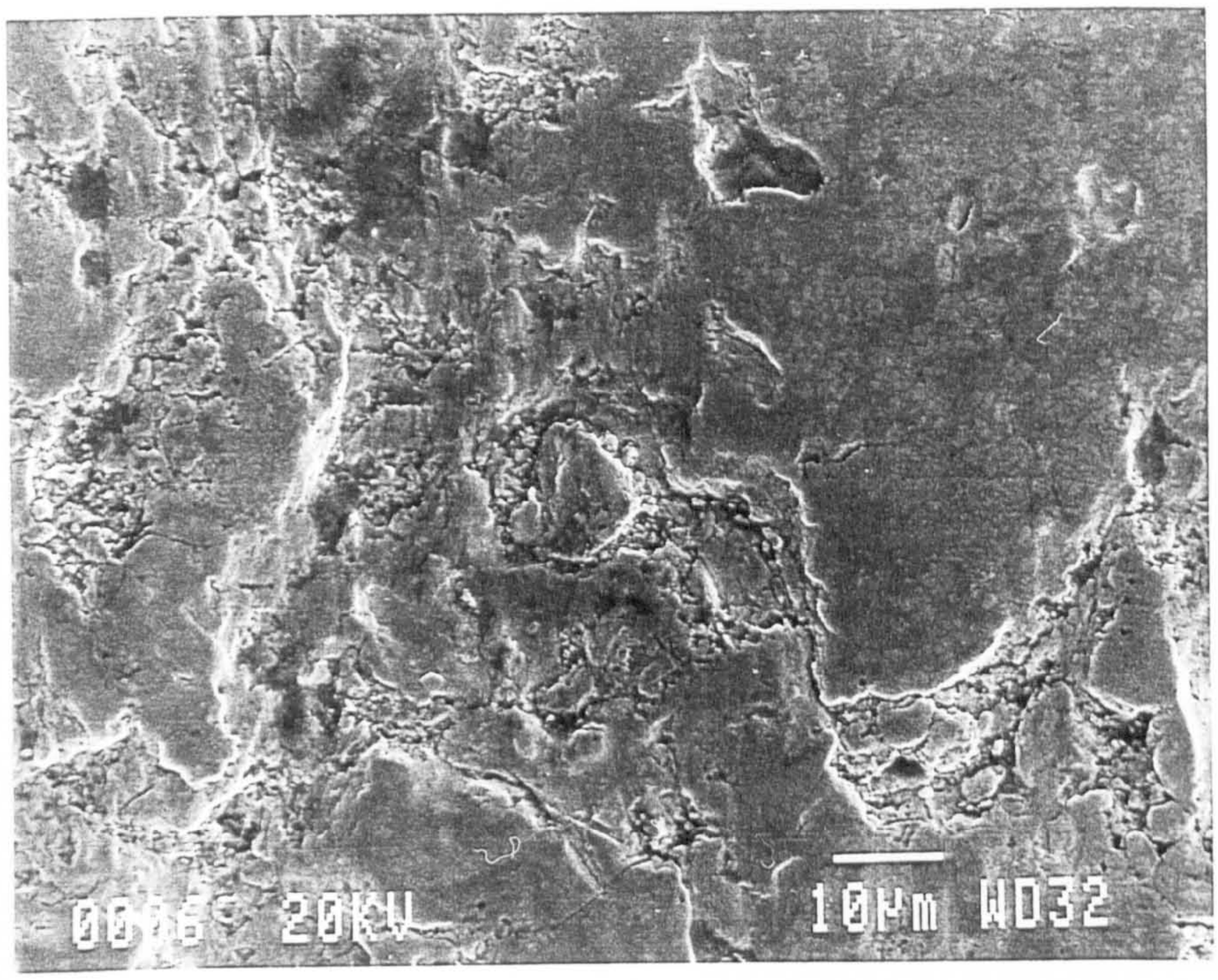

(d) x 4000

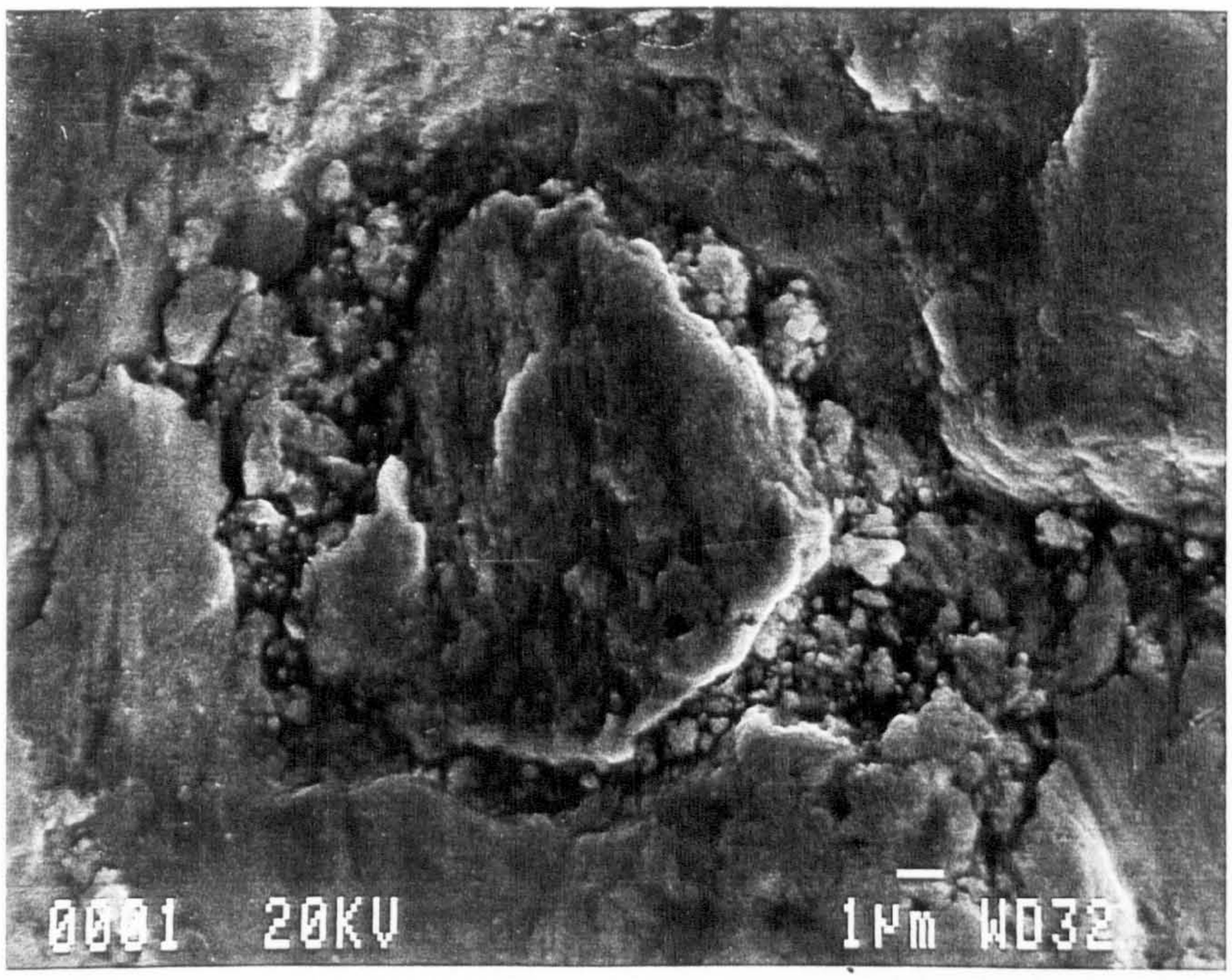

Fig. 4.461 - "Mild" wear debris

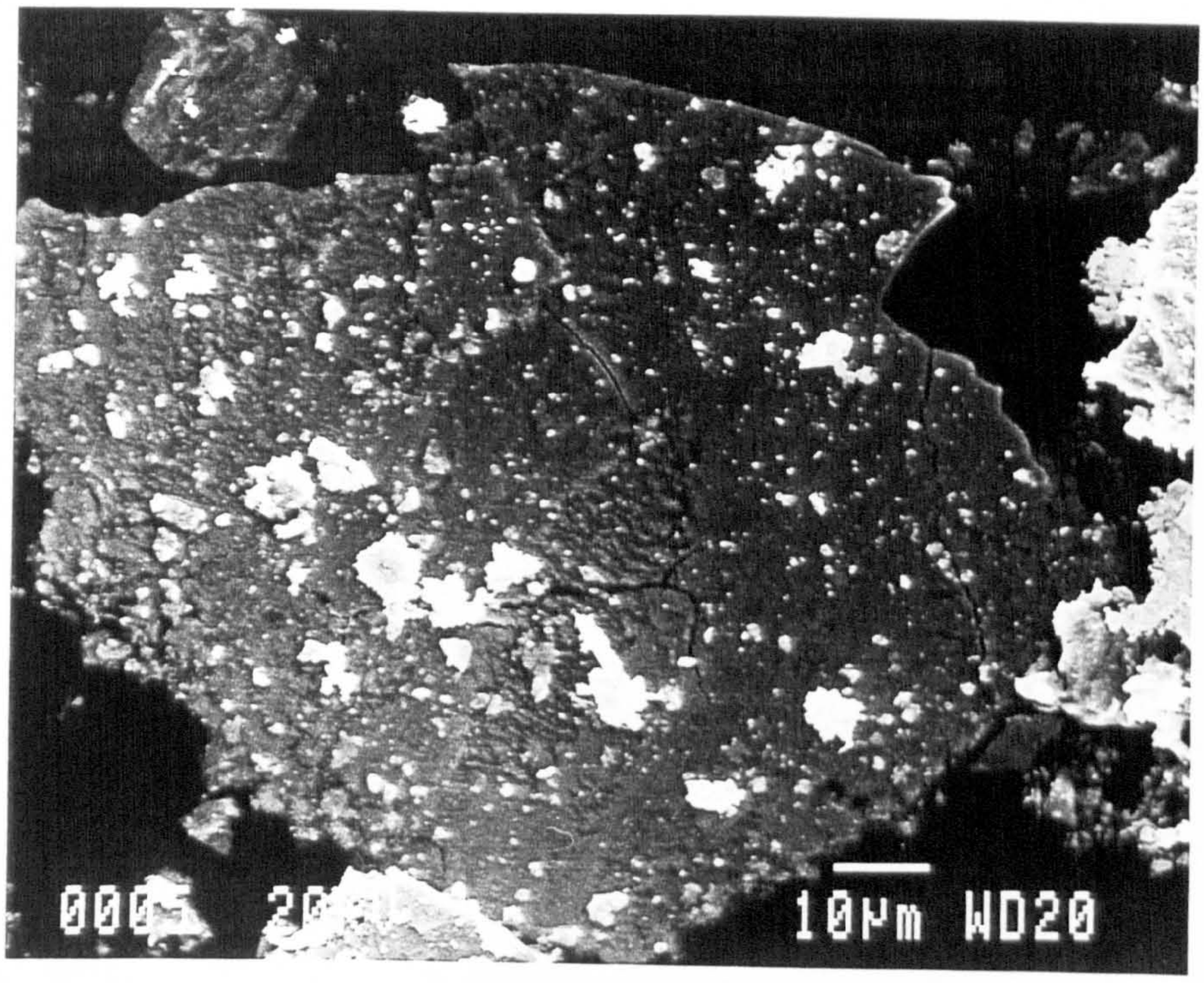

(b)

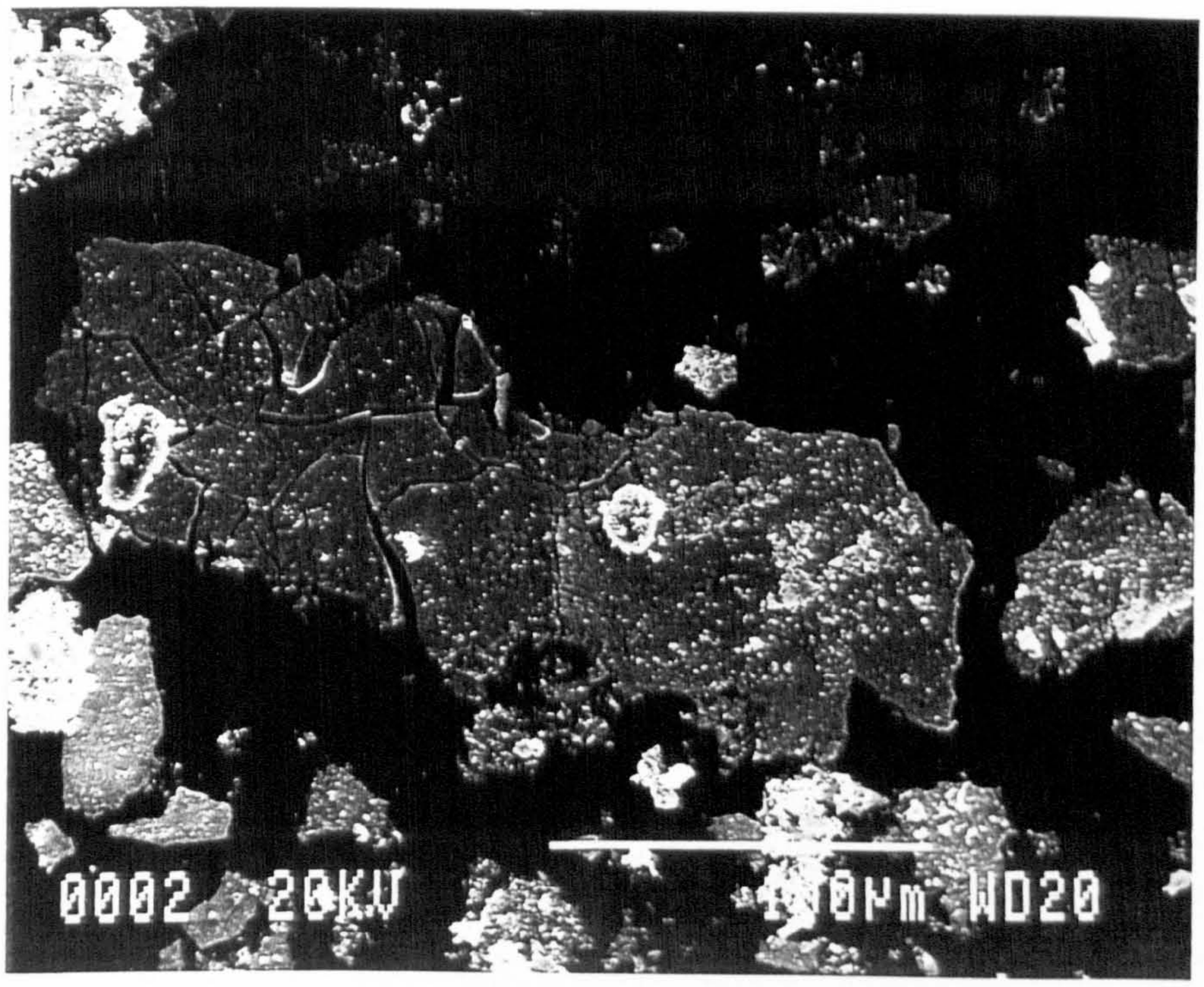

Fig. 4.461 cont...

(c)

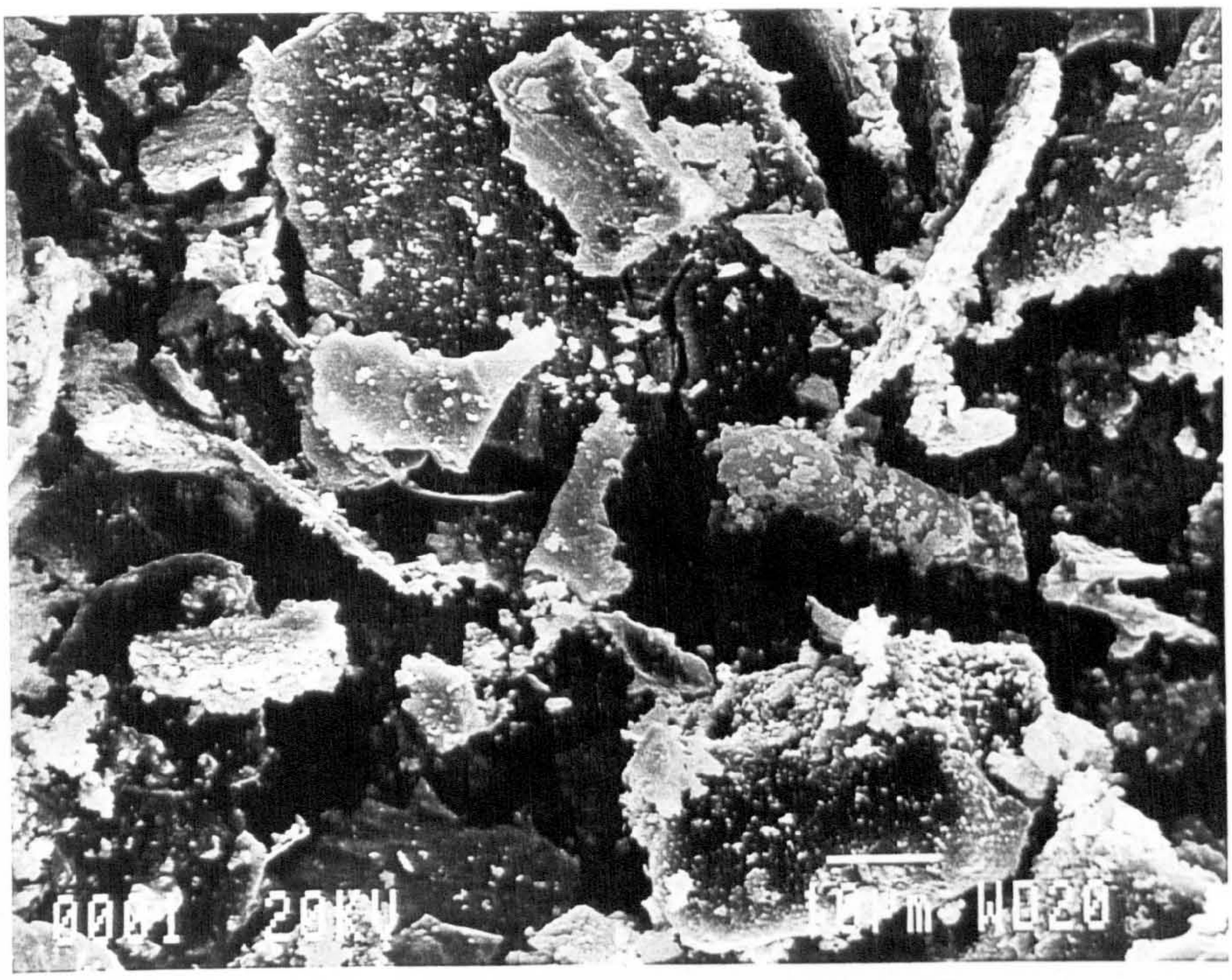

(d)

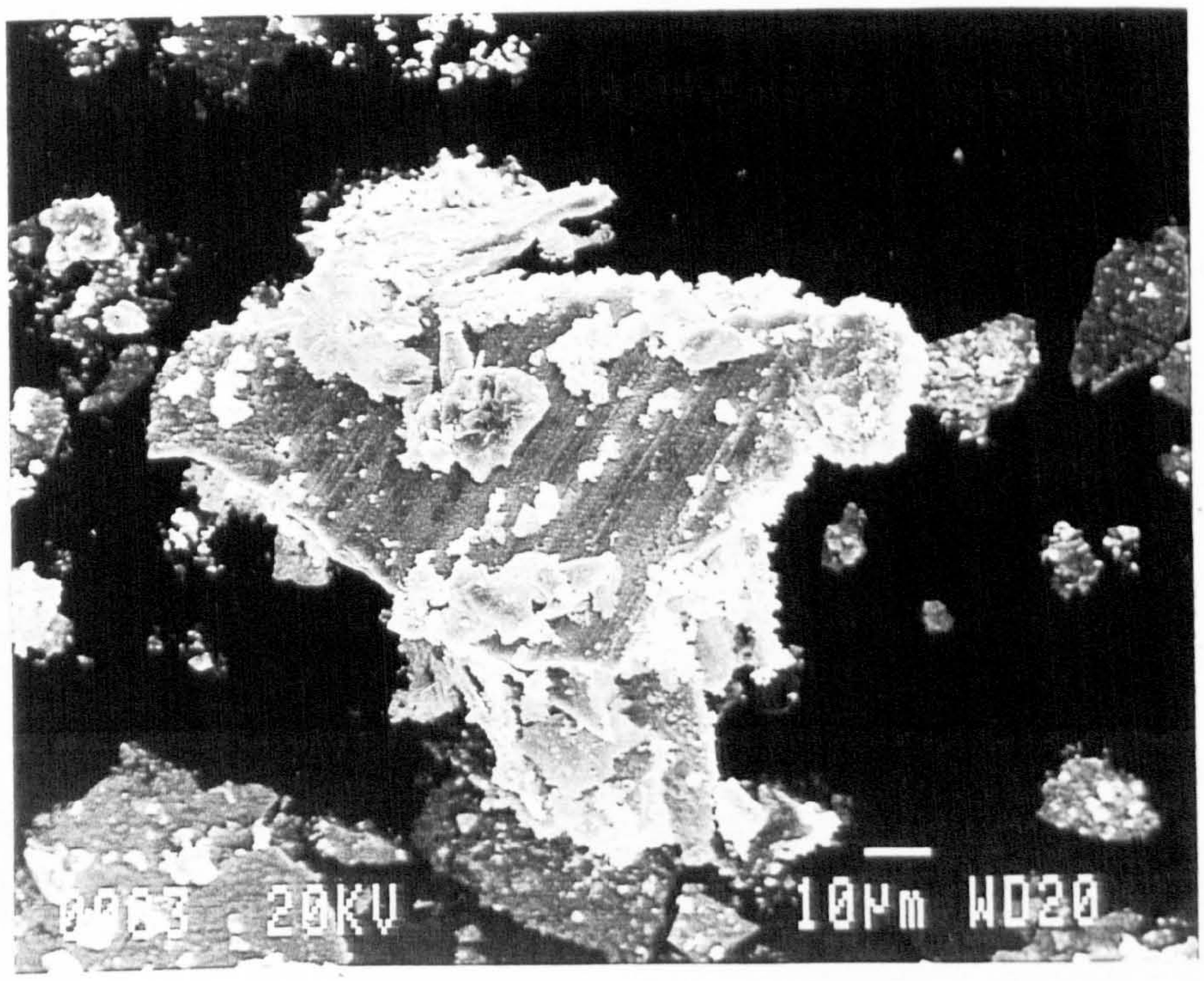

Fig. 4.462 - Severe wear debris

(a)

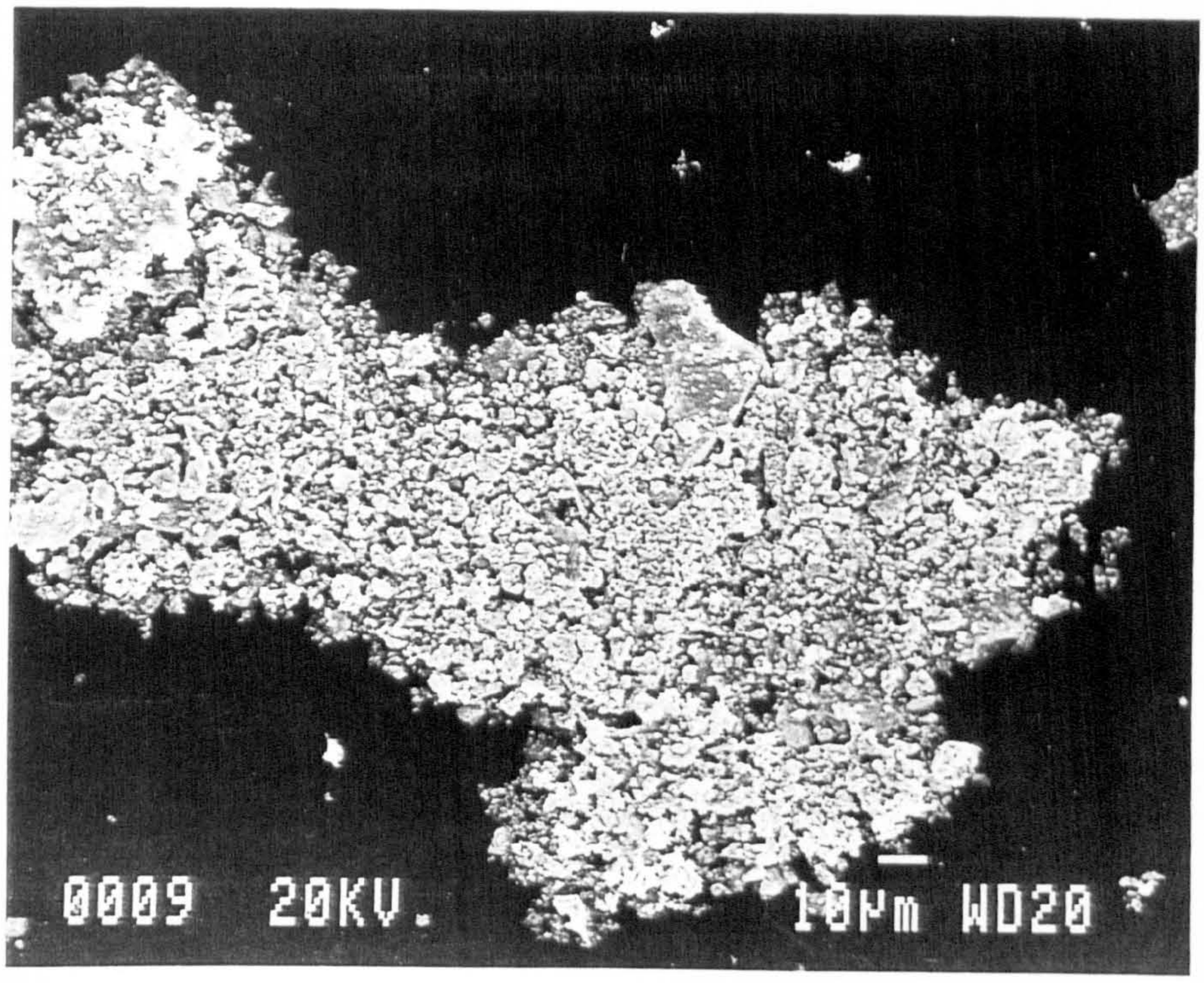

(b)

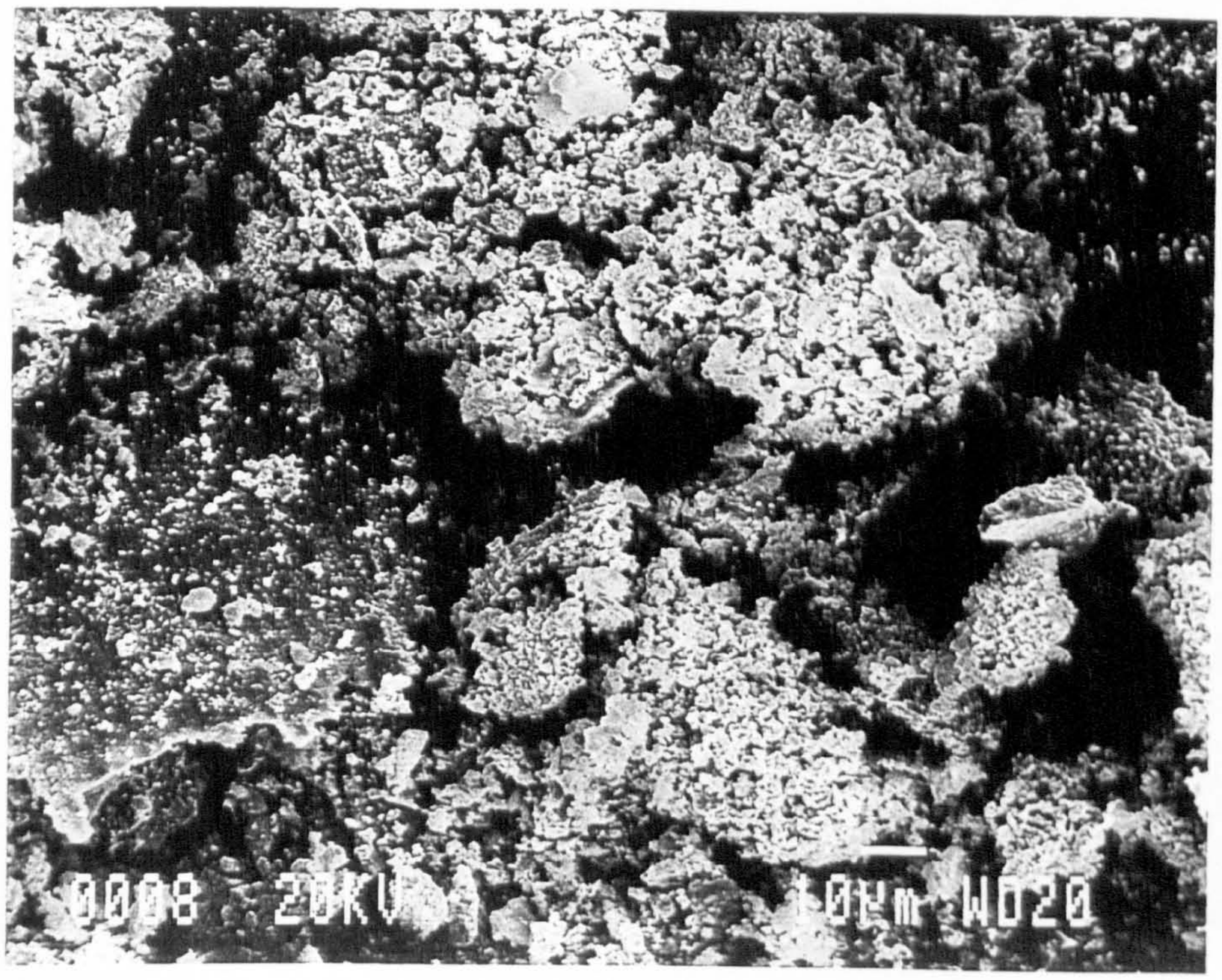

Fig. 4.462 cont...

(c)

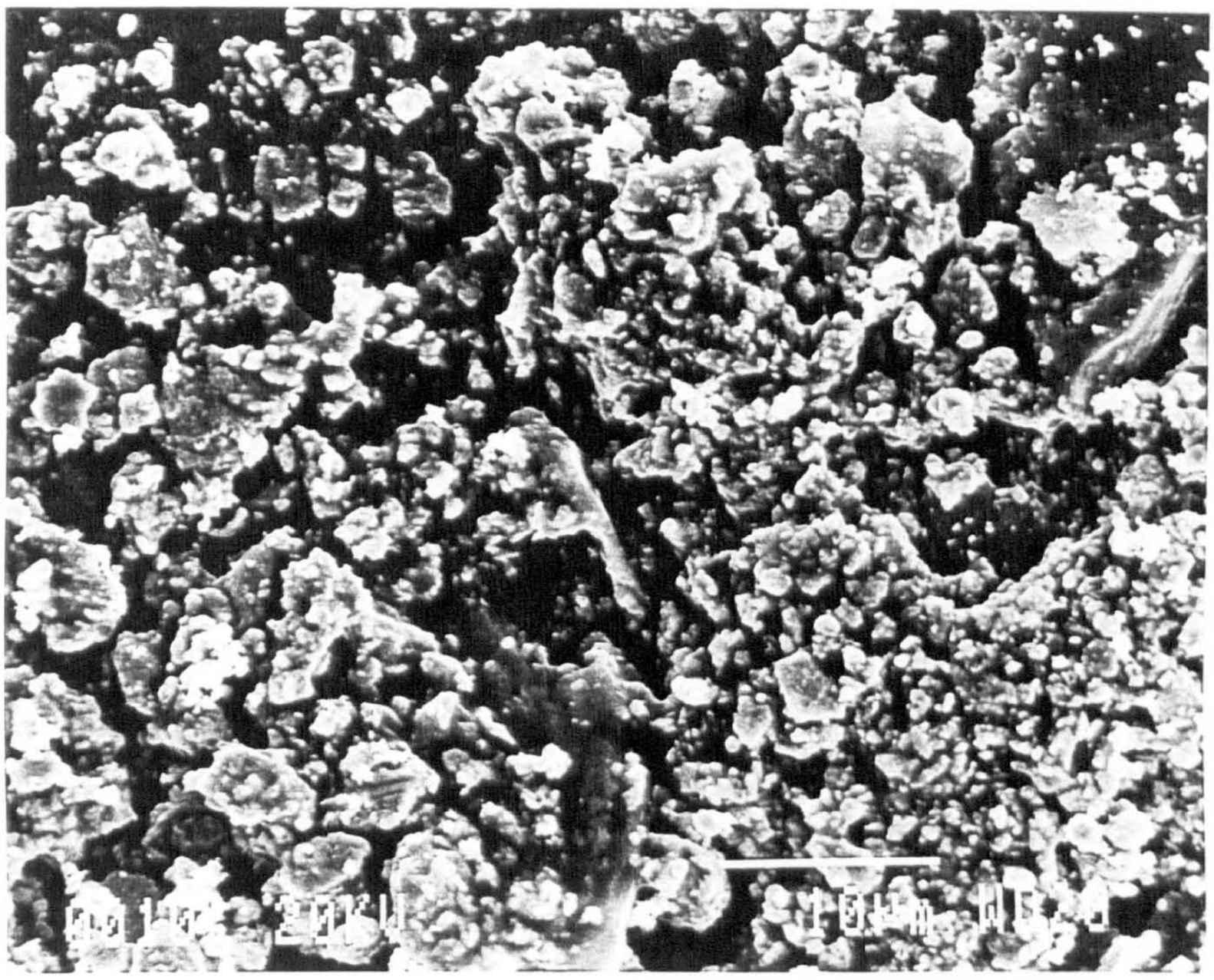

(d)

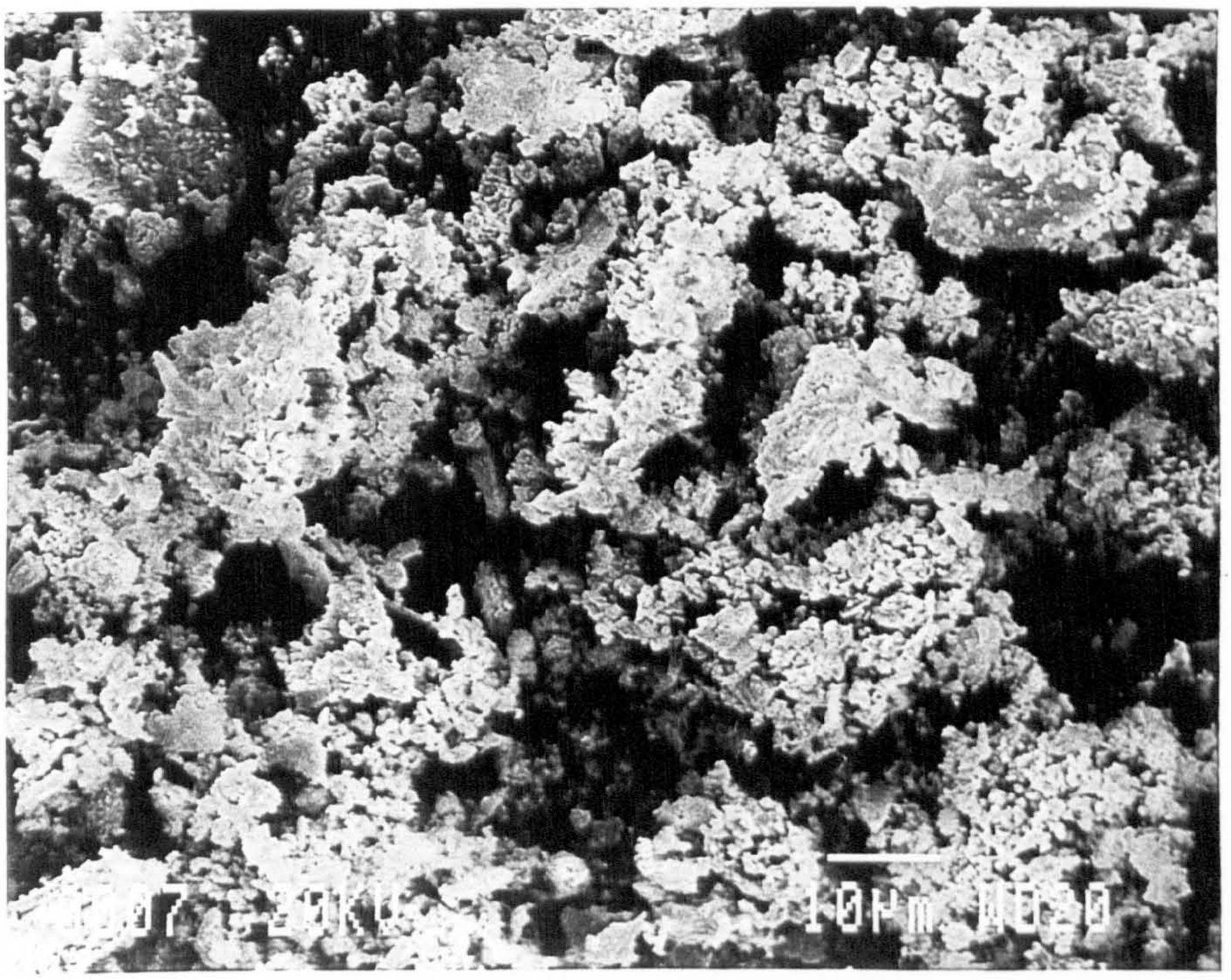

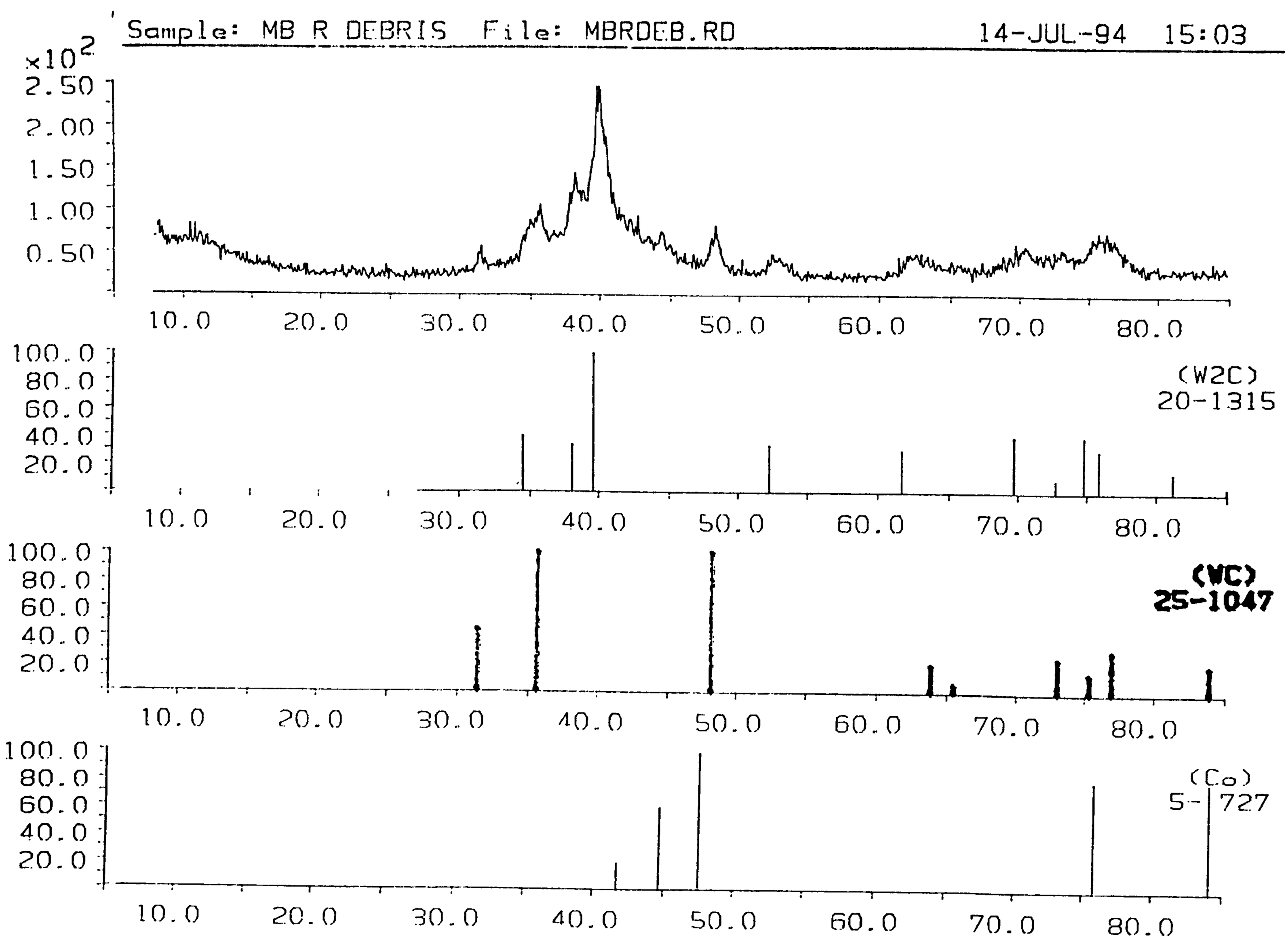

Figure 4.463 - X-ray diffraction trace for severe wear debris

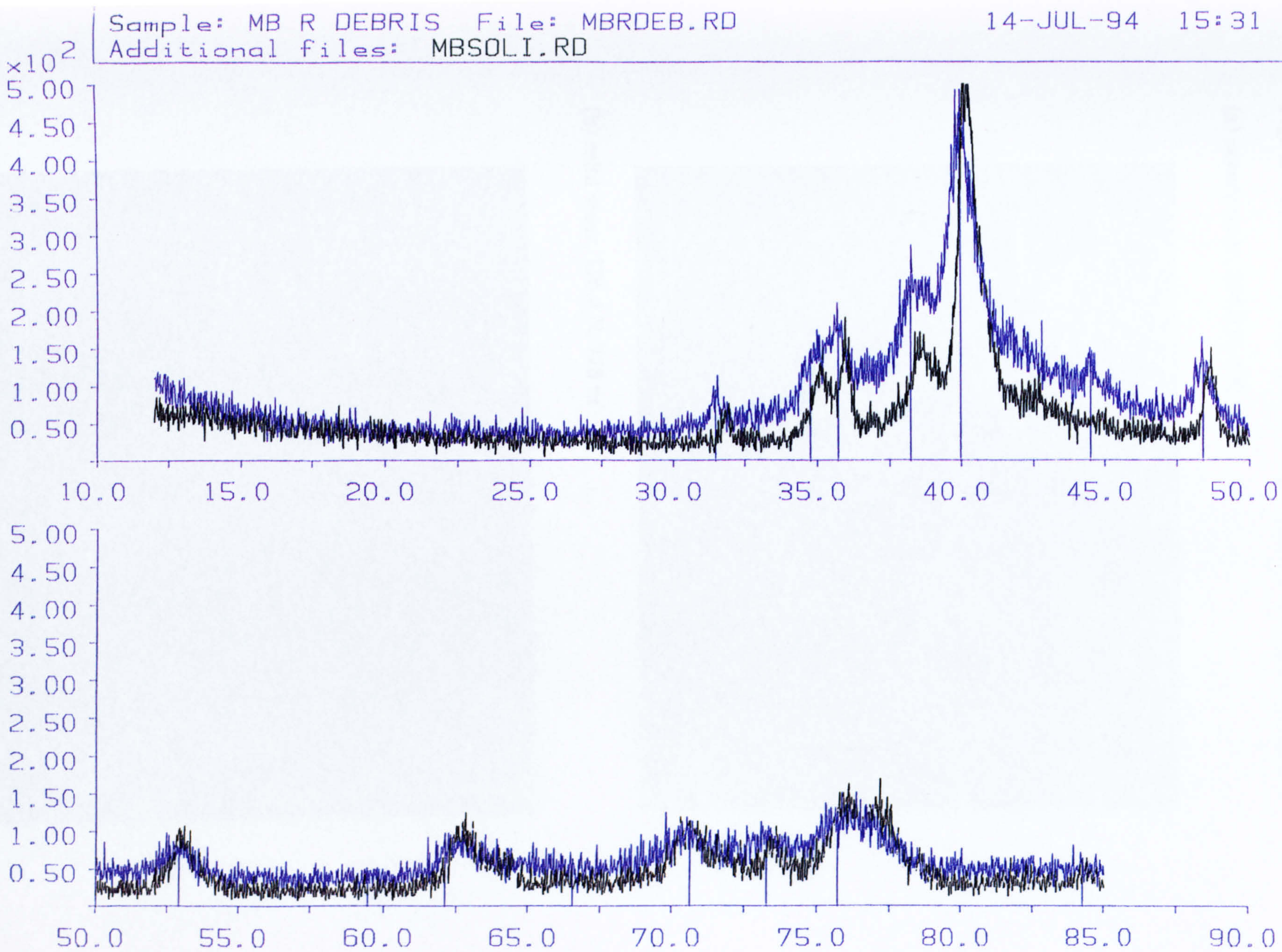

Figure 4.464 - X-ray diffraction trace showing severe wear debris (blue) in comparison to the as-coated sample (black)

Fig. 4.471 - SEM micrographs of a taper section through wear pins

(a) severe wear, 294.3 N, 590 m

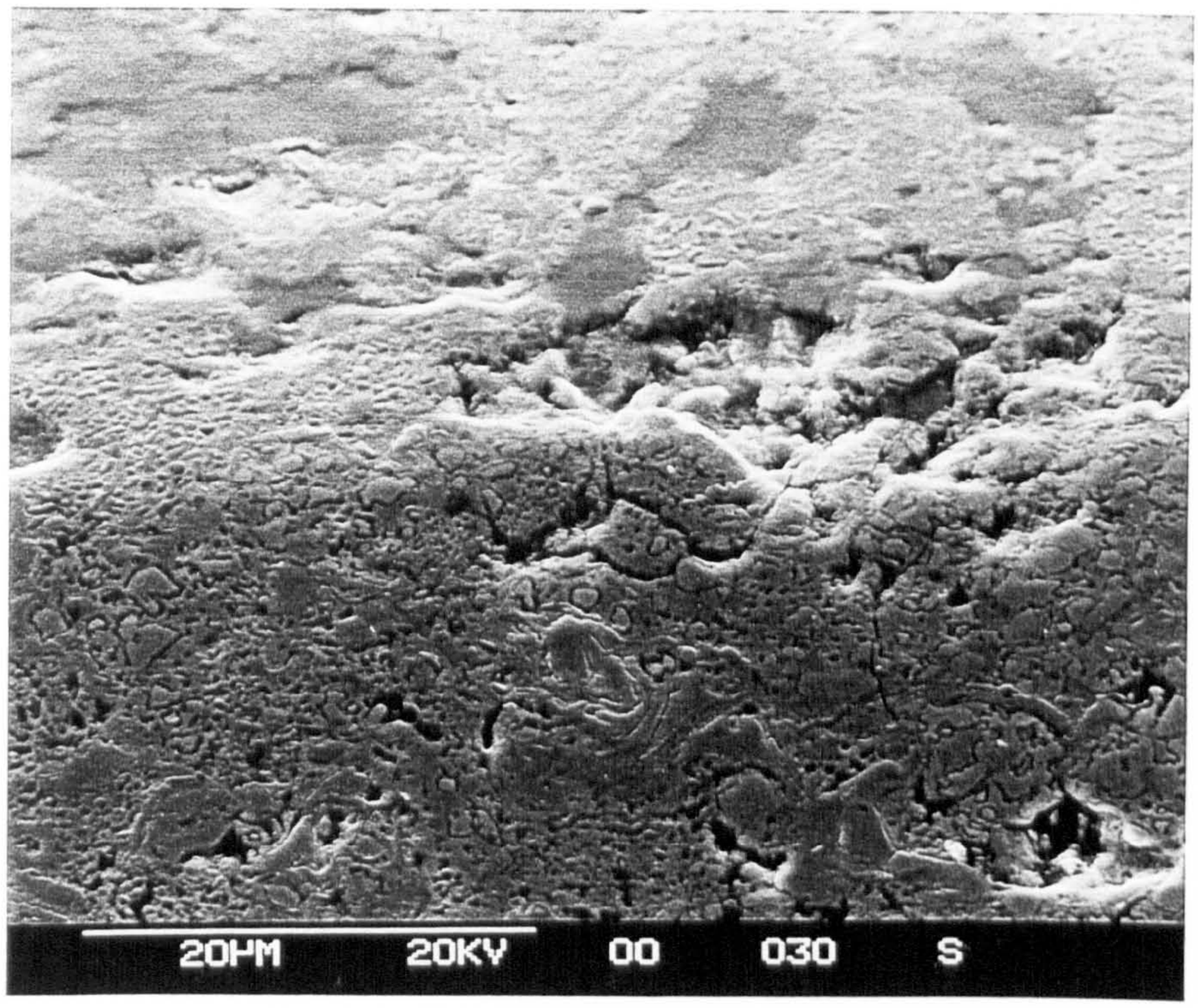

(b) mild wear, 196.2 N, 728 m

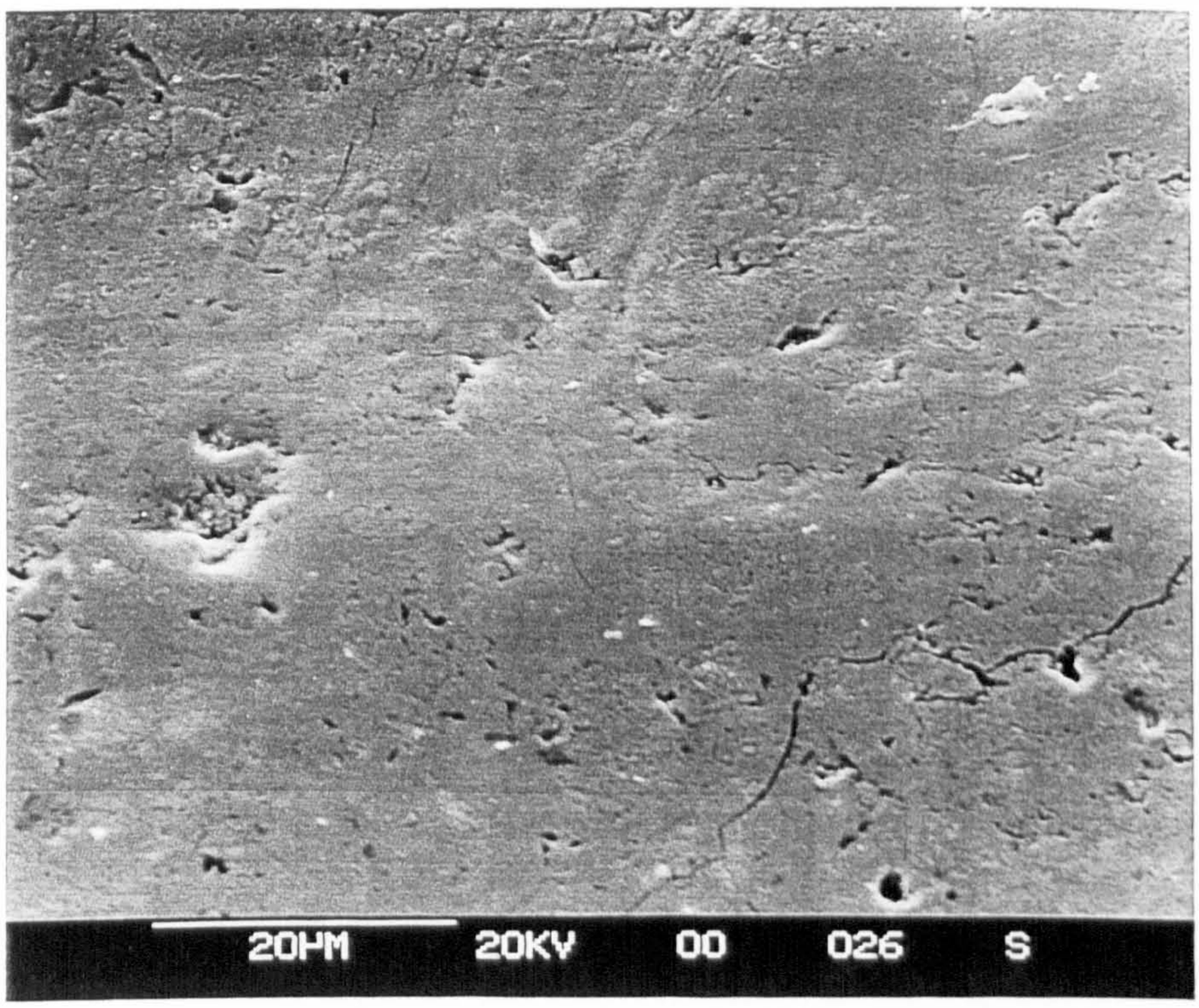

Fig. 4.481 Ball Wear Volume with respect to Sliding Distance for Substrate Material

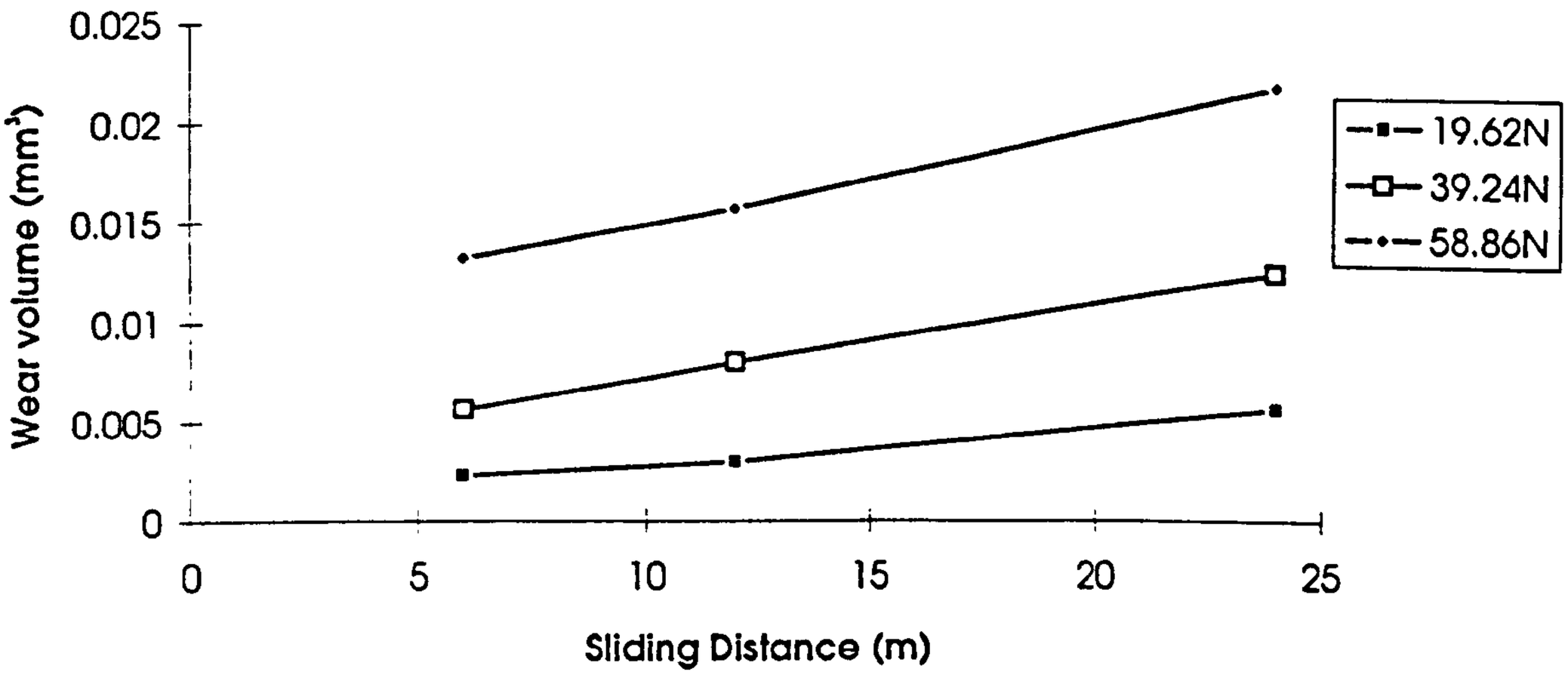

Fig. 4.482 Ball Specific Wear Rates for Substrate Material

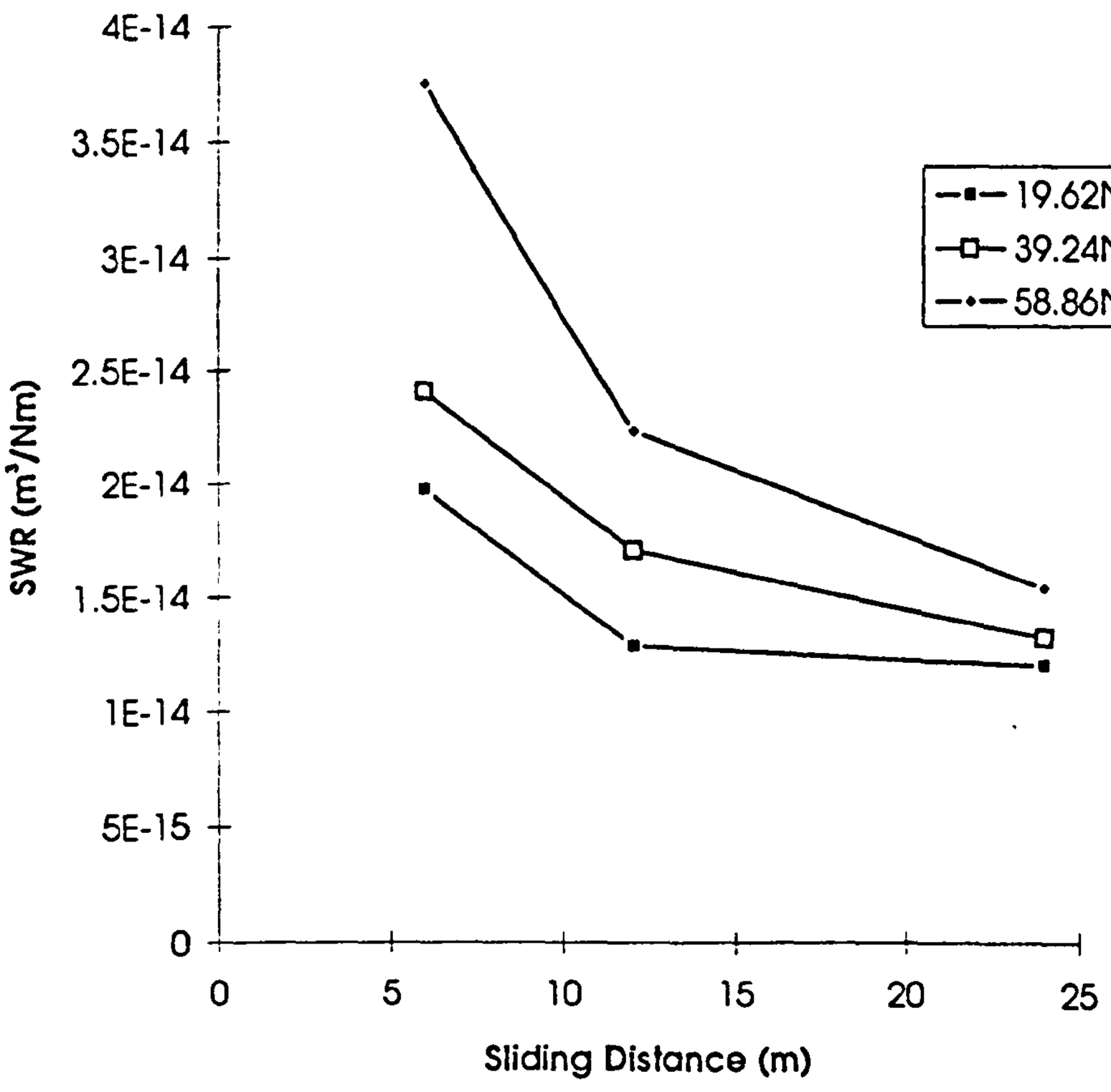

Fig. 4.483 - SEM micrographs of sliding wear of AISI 410 substrate material

(a) Edge of wear track

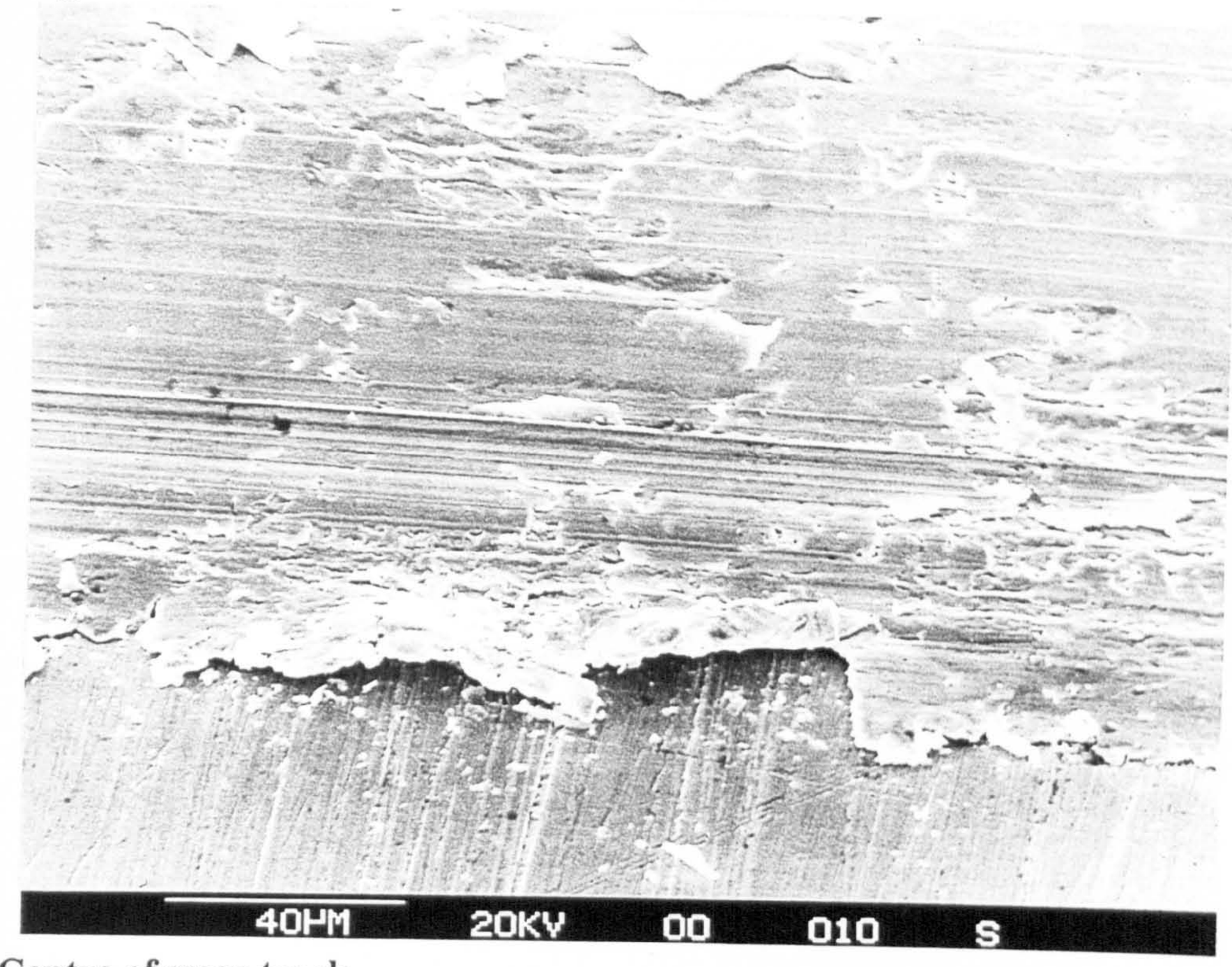

(b) Centre of wear track

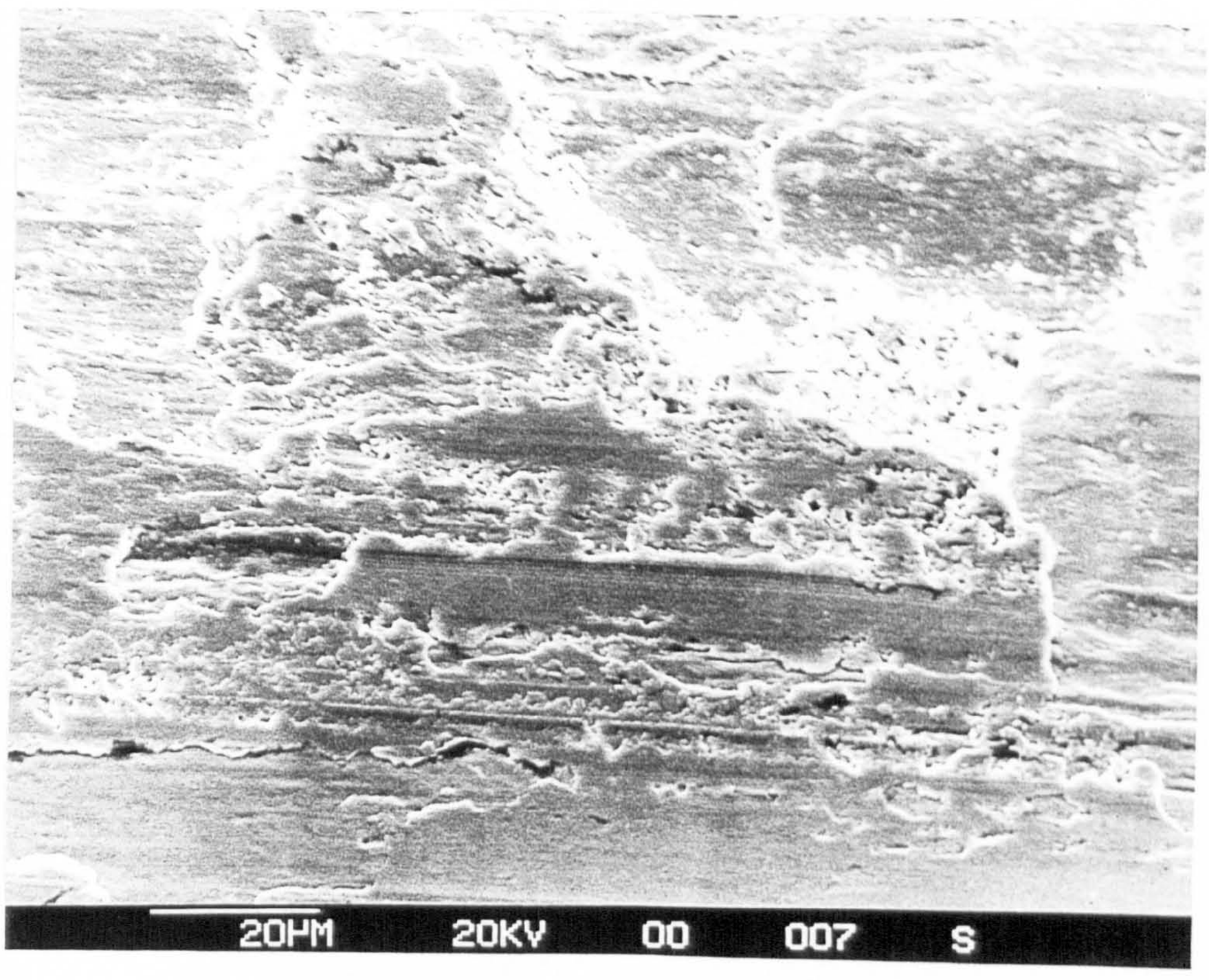

Figure 4.501 - Diamond-on-flat wear volumes with respect to load

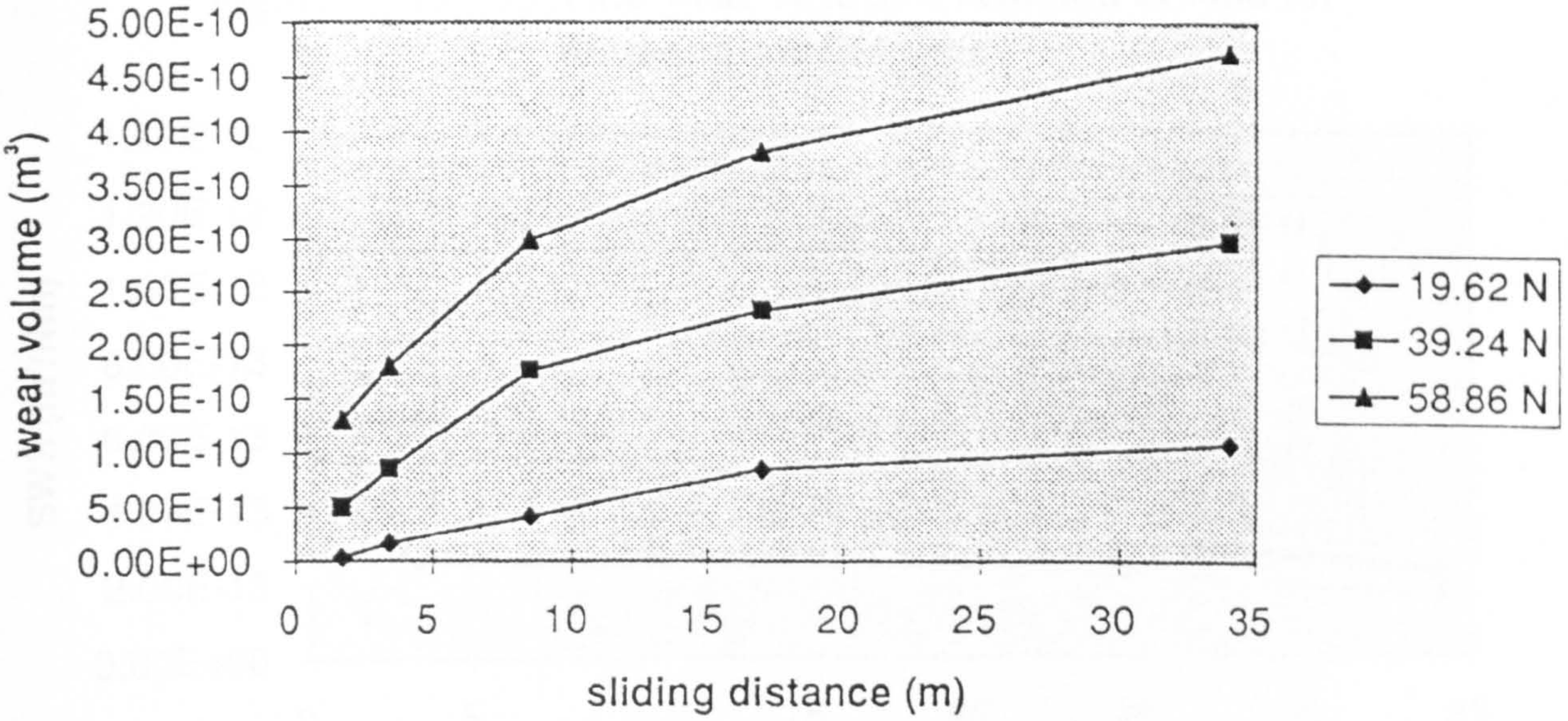

Figure 4.502 Diamond-on-flat wear volumes as a function of sliding distance

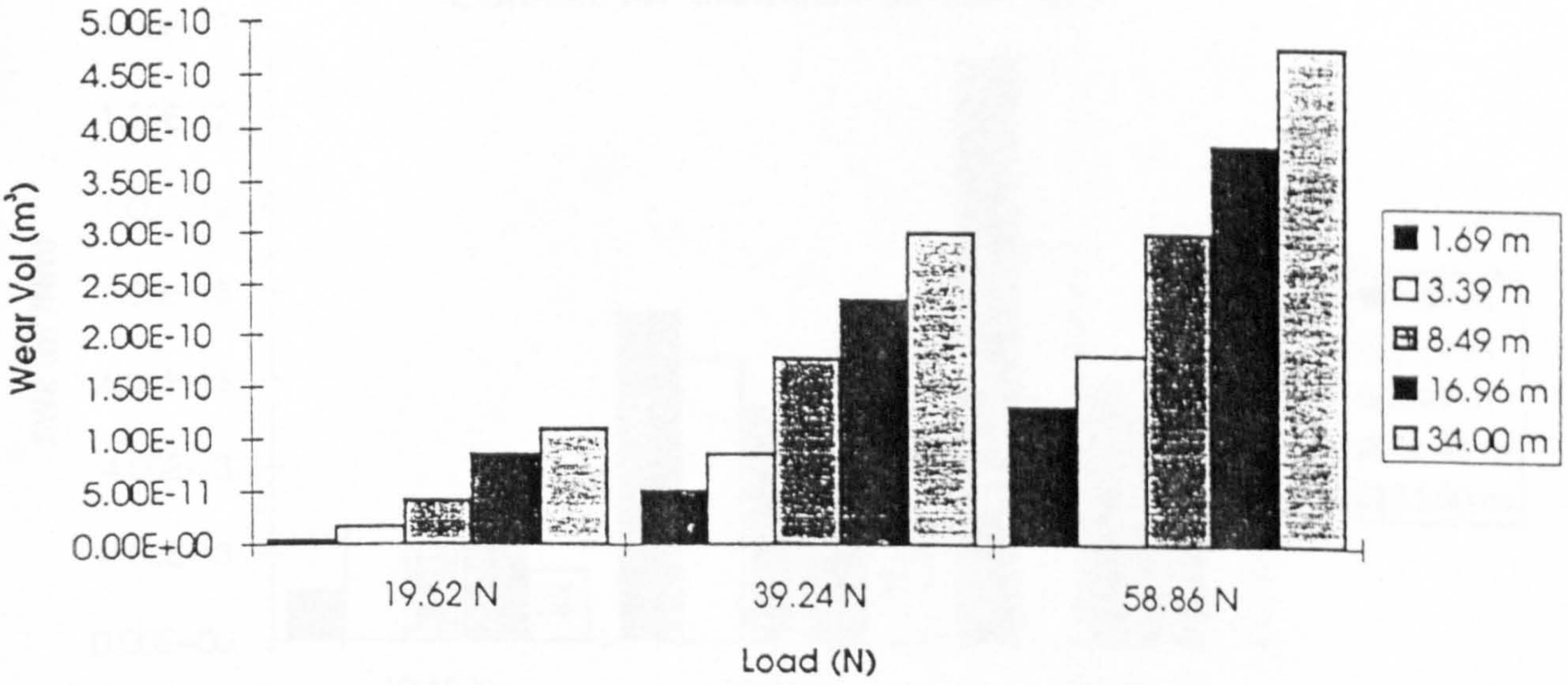

Figure 4.503 - Specific wear rate as a function of load for diamond-on-flat tests

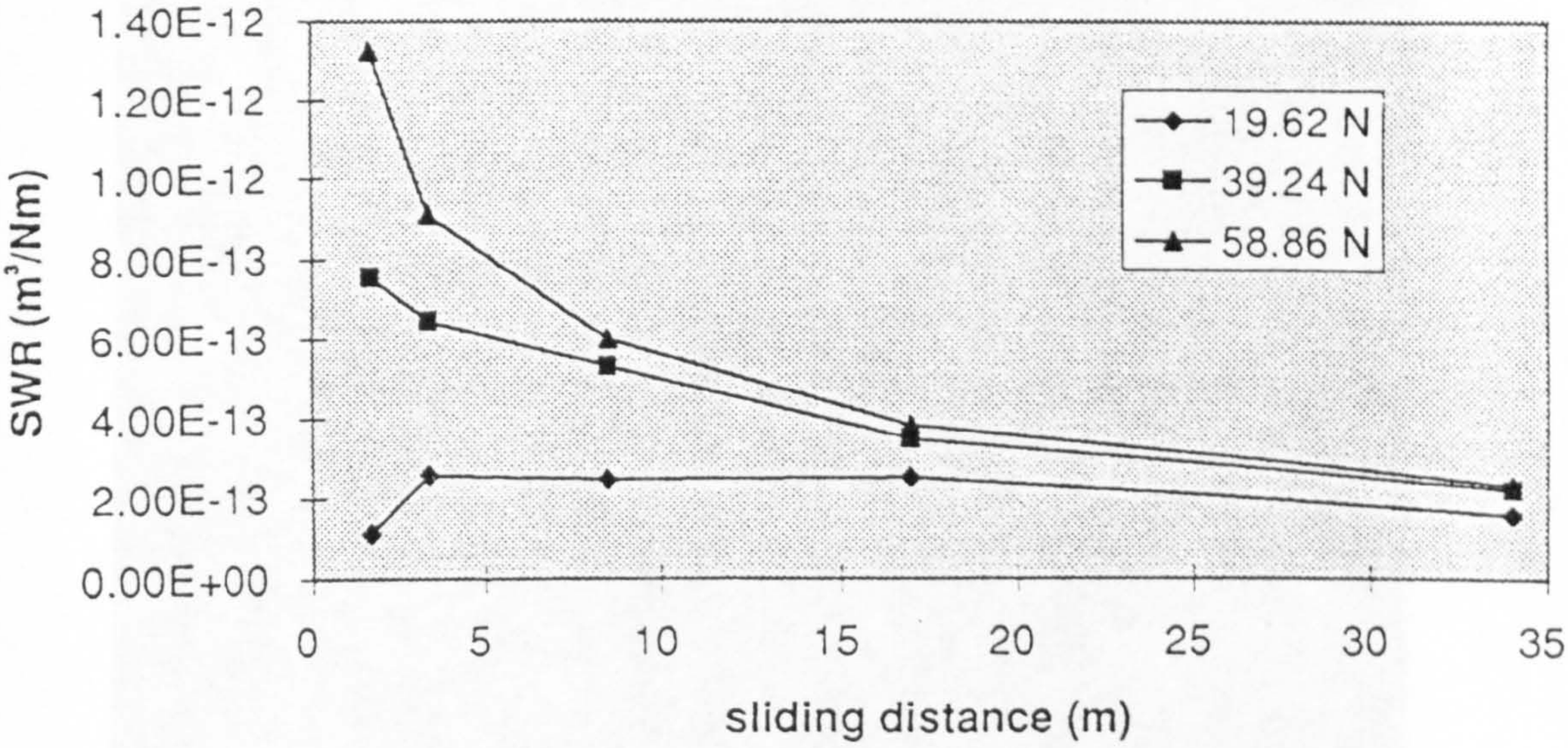

Figure 4.504 - Specific wear rate as a function of sliding distance for diamond-on-flat tests

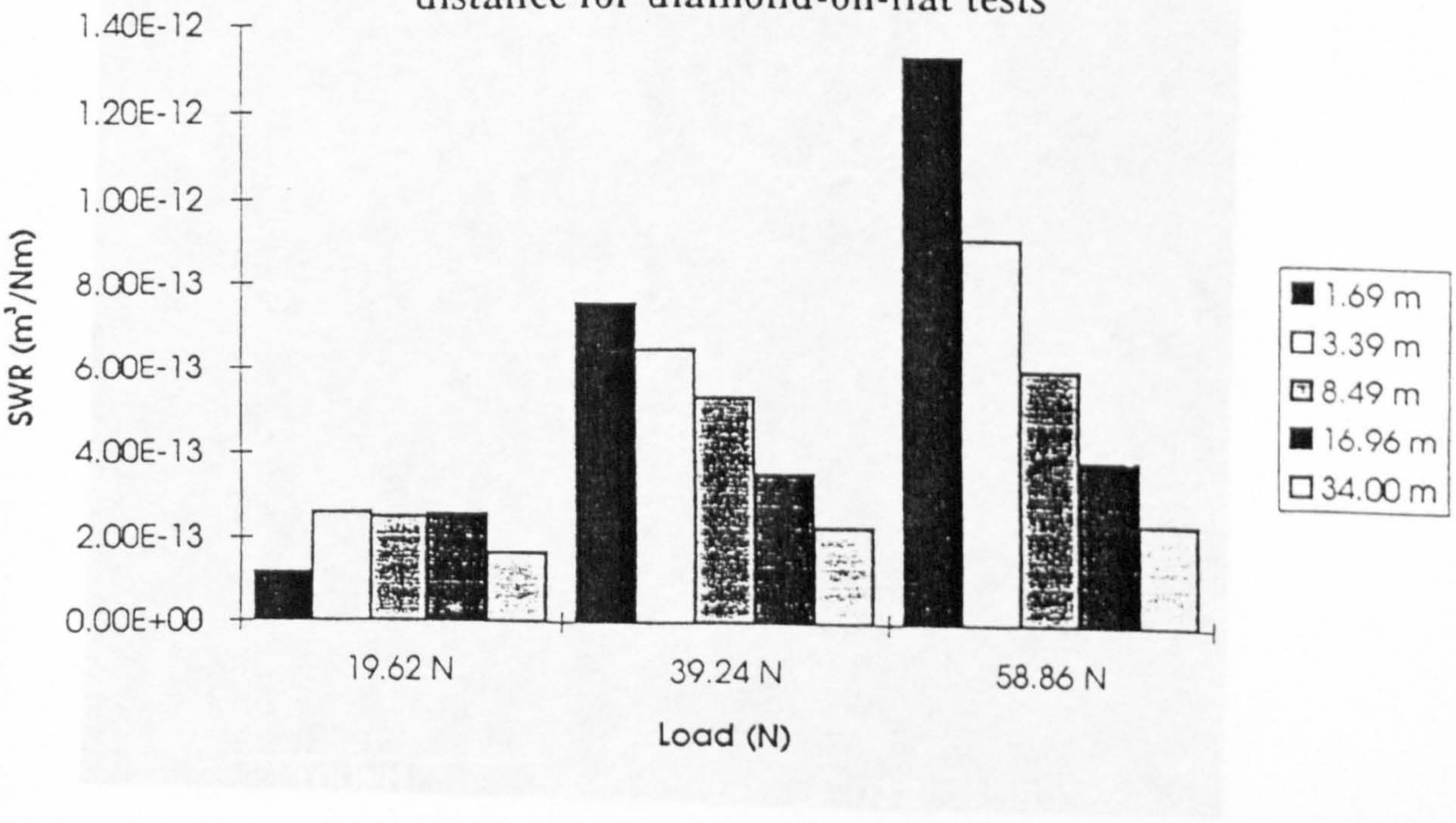

Fig. 4.511 - SEM micrographs of a taper section through LW45 following a diamond-on-flat test, *1 kg* load.

(a) After *1 min*

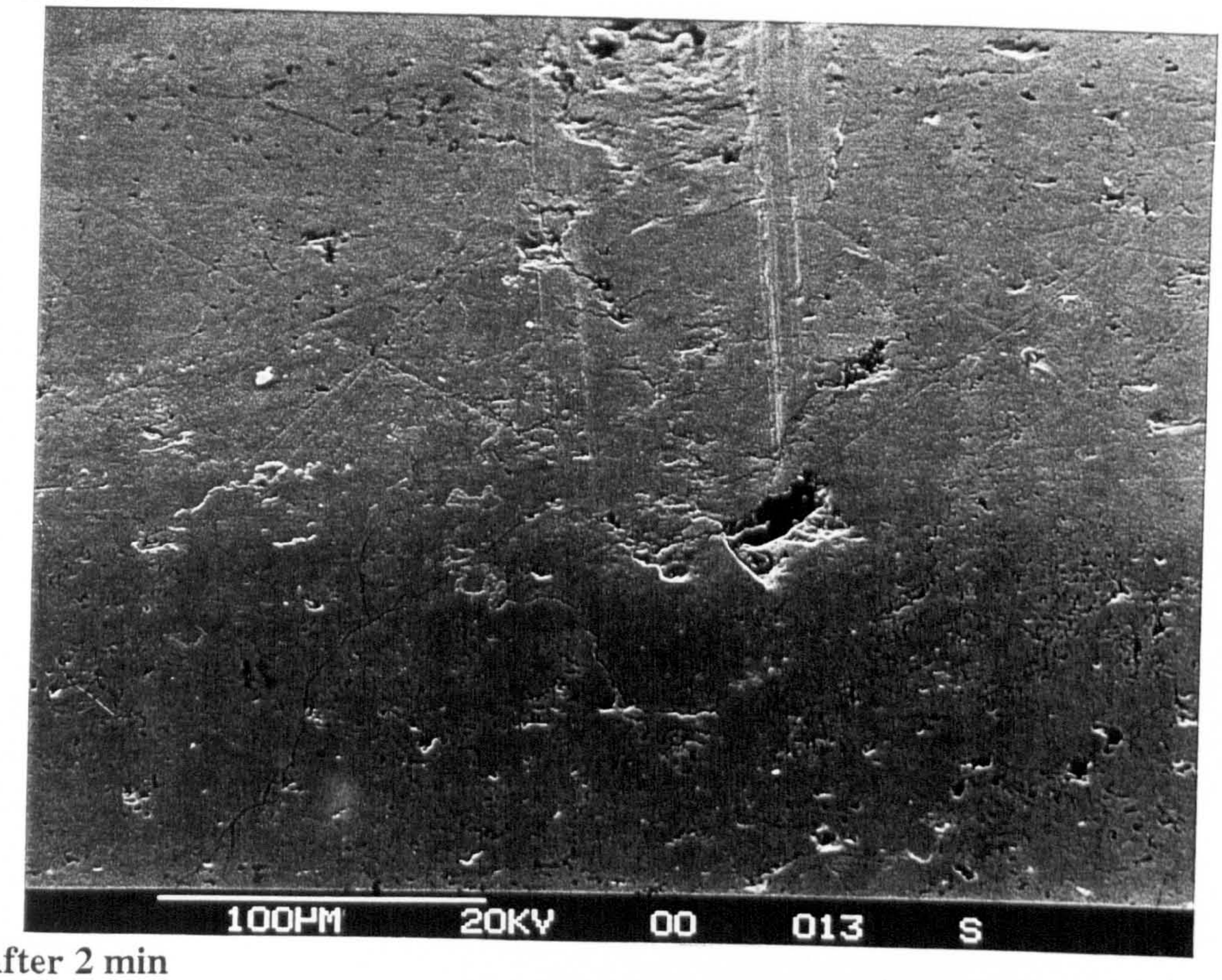

(b) After 2 min

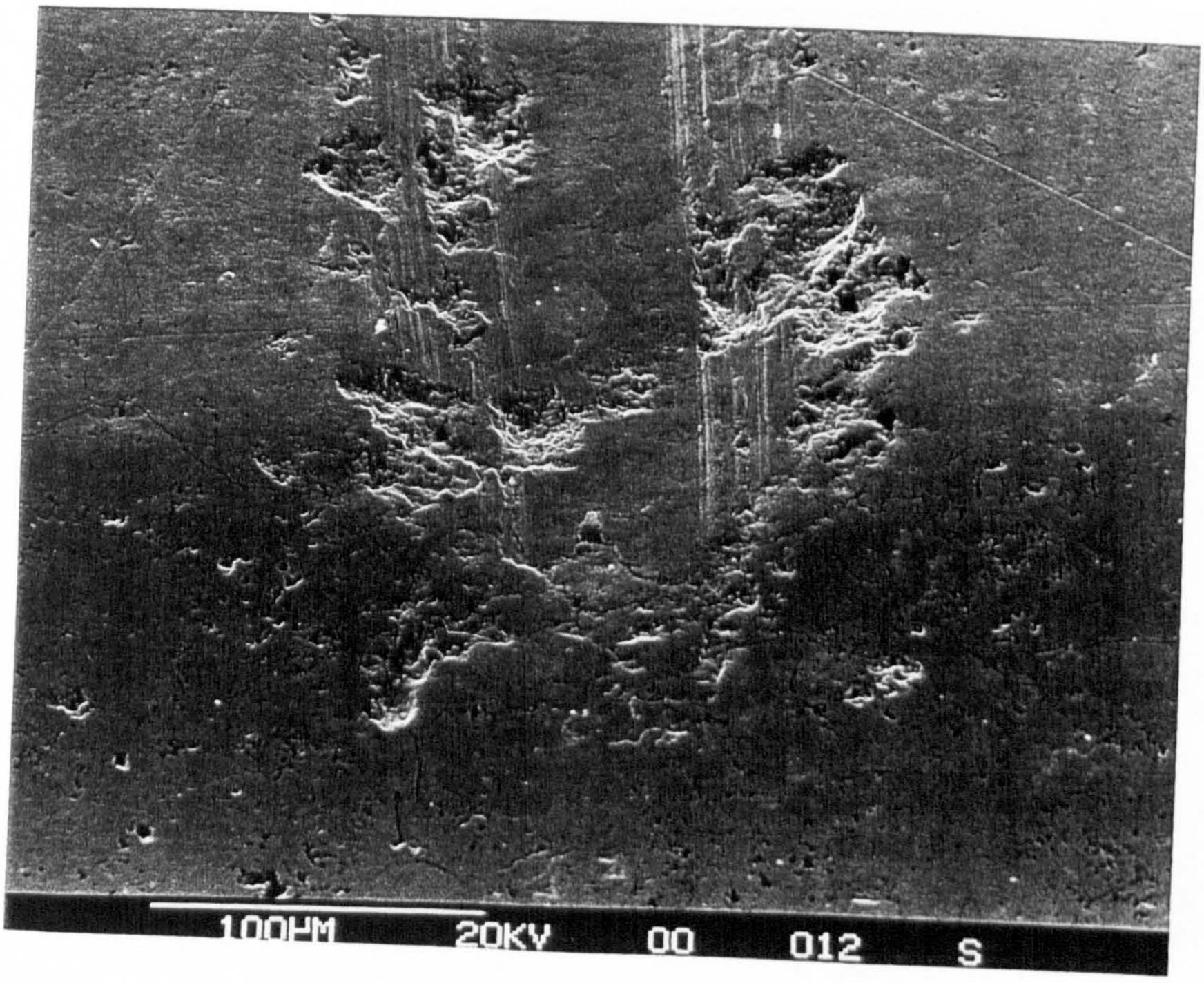

Fig. 4.512 - SEM micrographs of a taper section through LW45 following a diamond-on-flat test, *2 kg* load.

(a) After 1 min

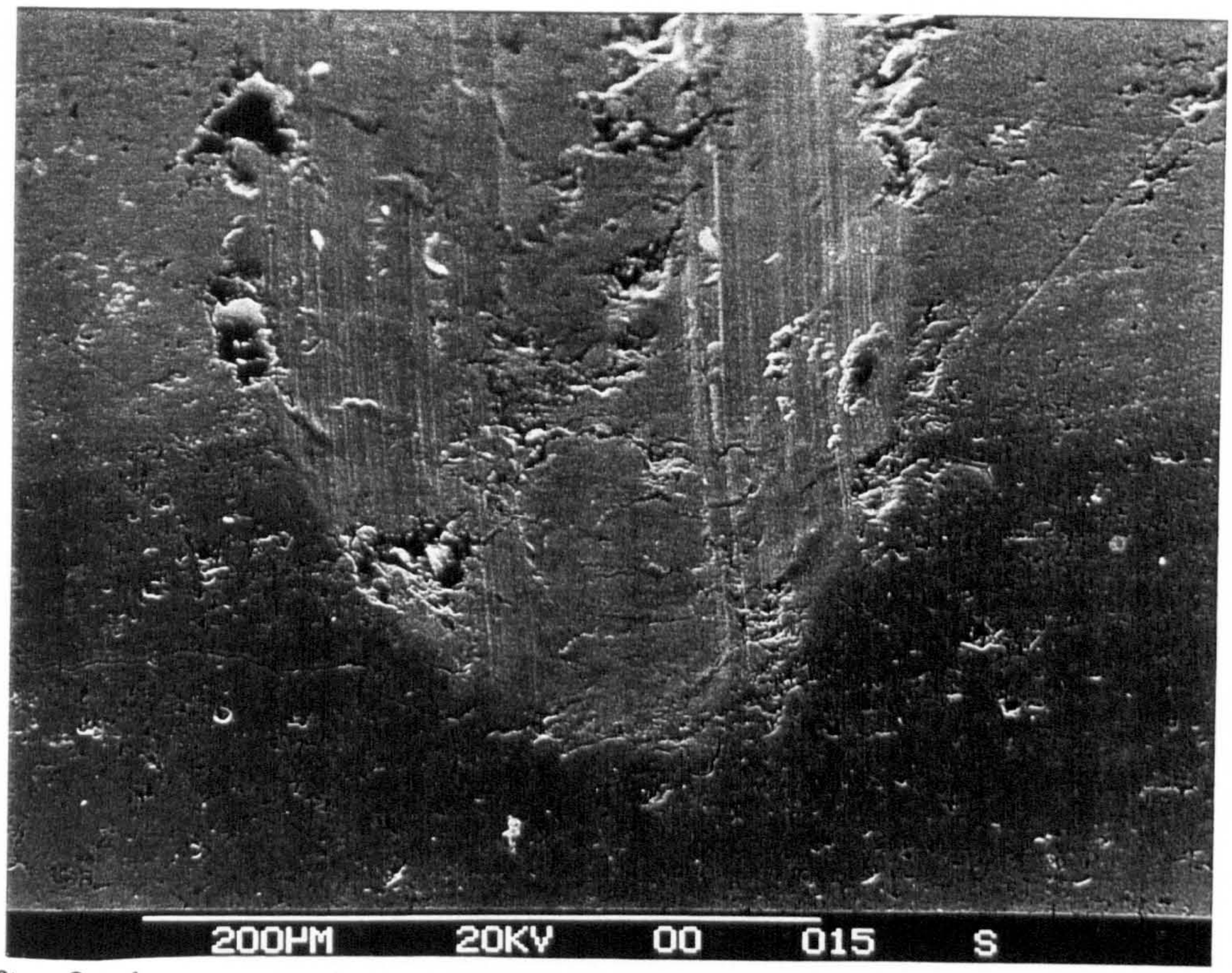

(b) After 2 min

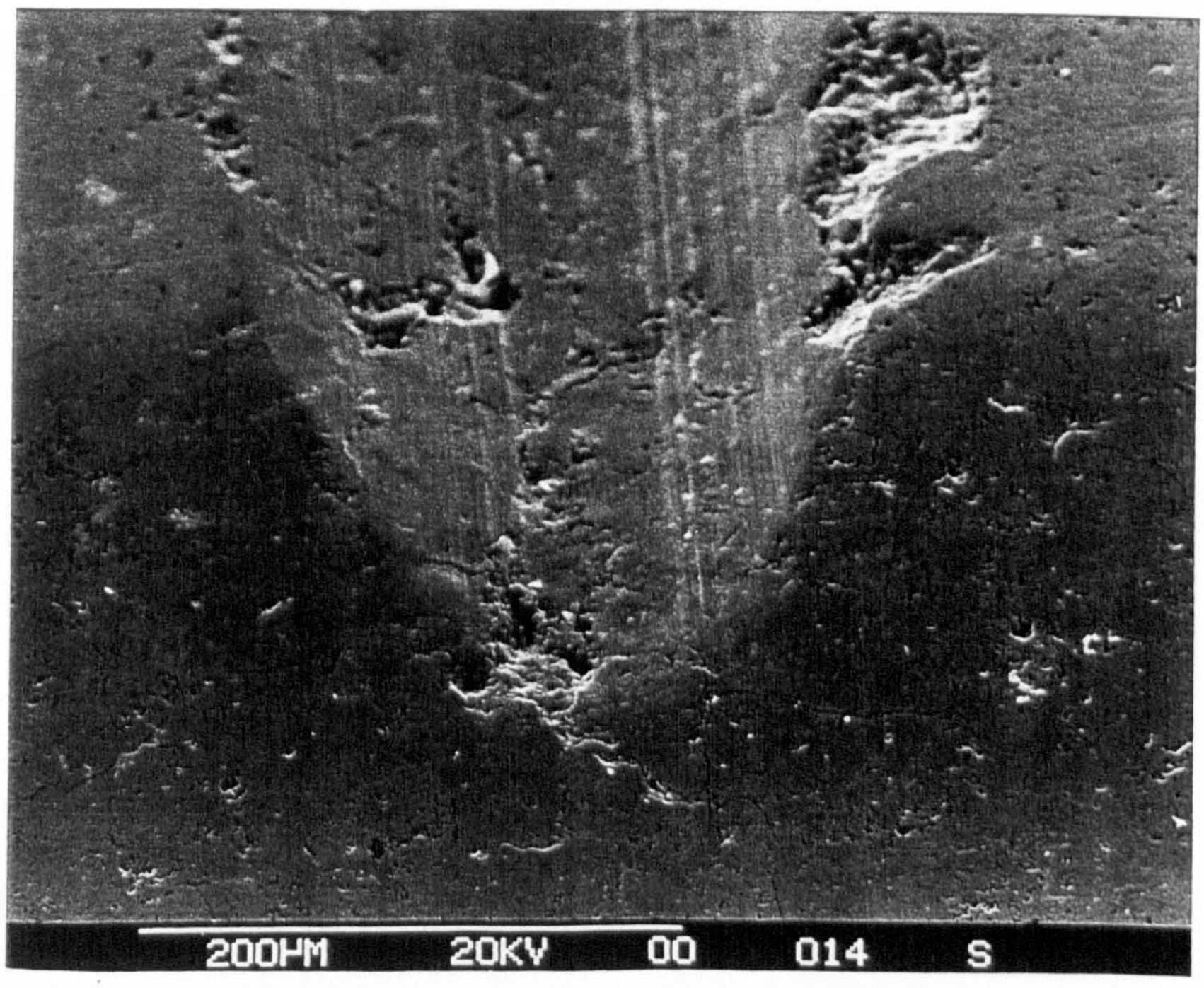

Fig. 4.513 - SEM micrographs of a taper section through LW45 following a diamond-on-flat test, *3 kg* load.

(a) After 1 min

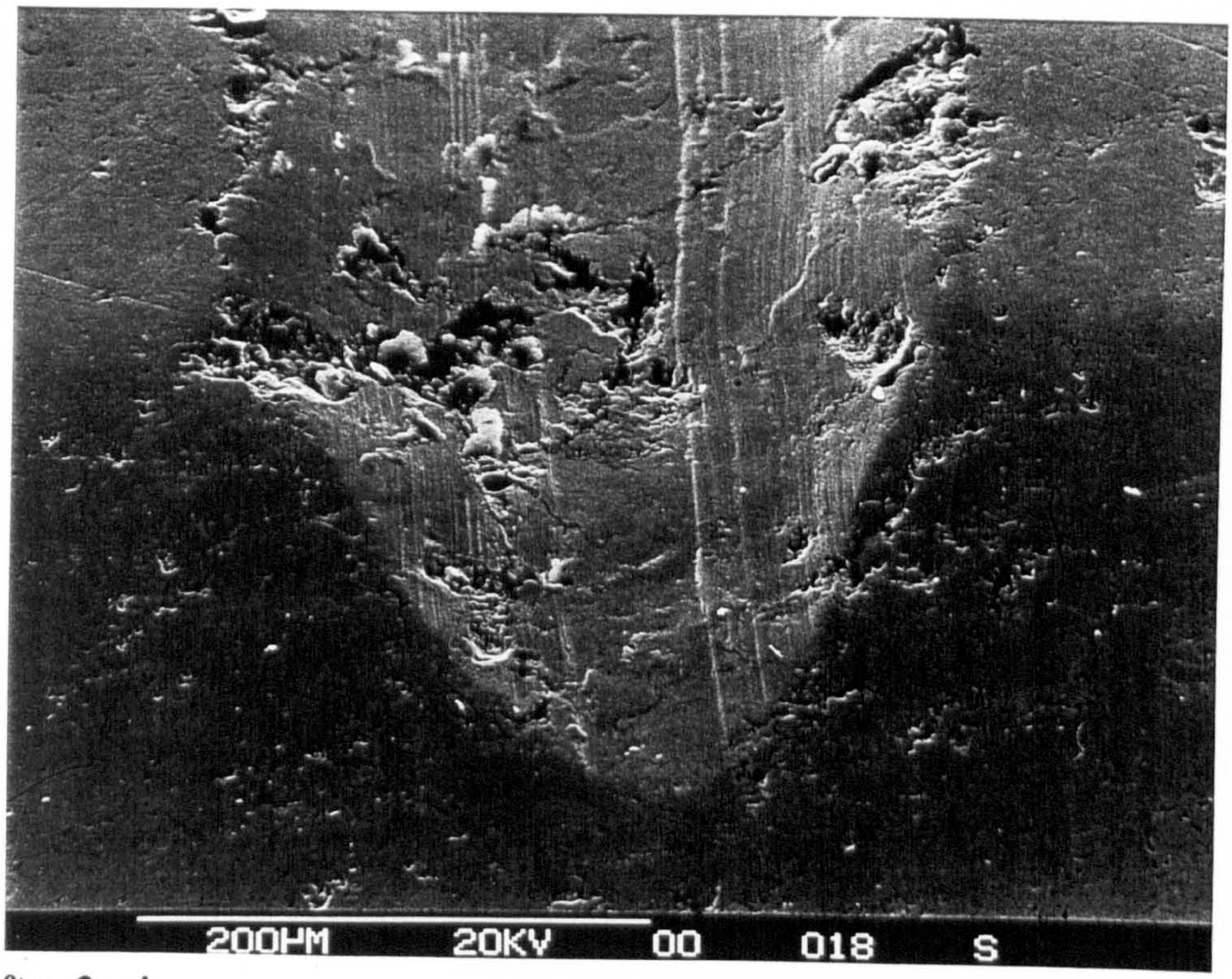

(b) After 2 min

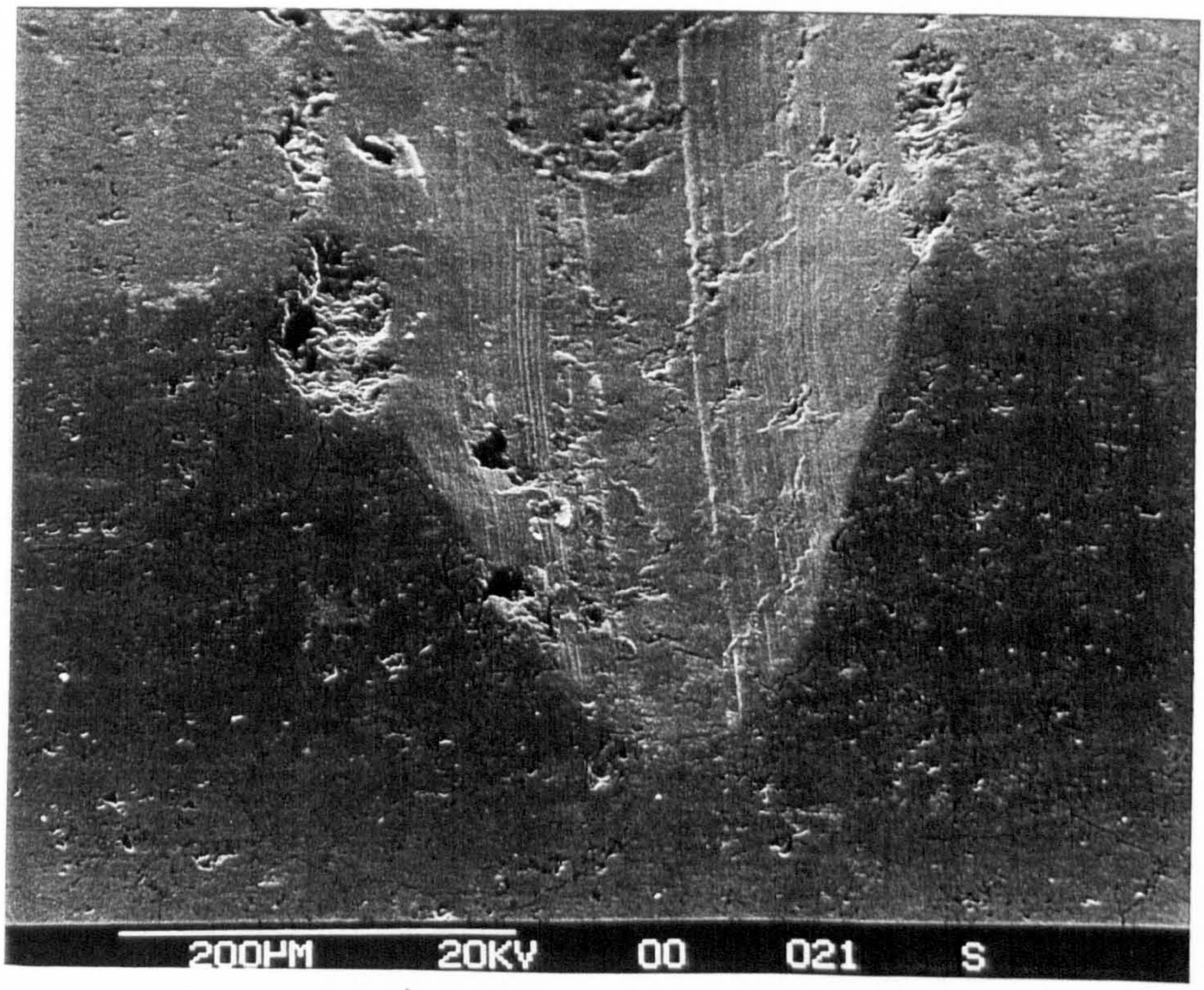

Fig. 4.513 (cont.) - SEM micrographs of a taper section through LW45 following a diamond-on-flat test, *3 kg* load.

(c) After 20 min

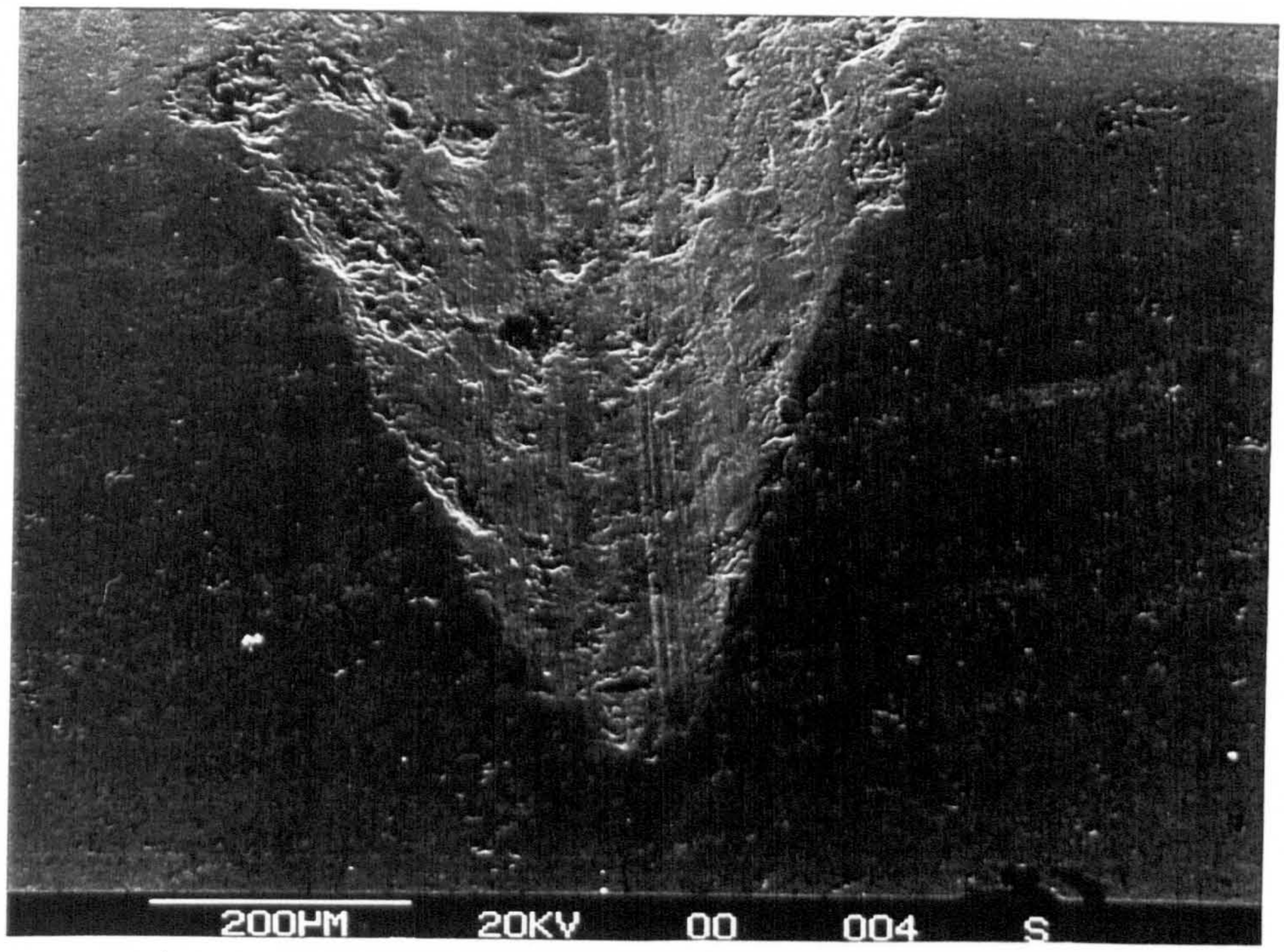

Fig. 4.514 - SEM images of the edge of a diamond-on-flat wear track for LW45 showing plastic deformation.

(a) X 430

(b) x 2200

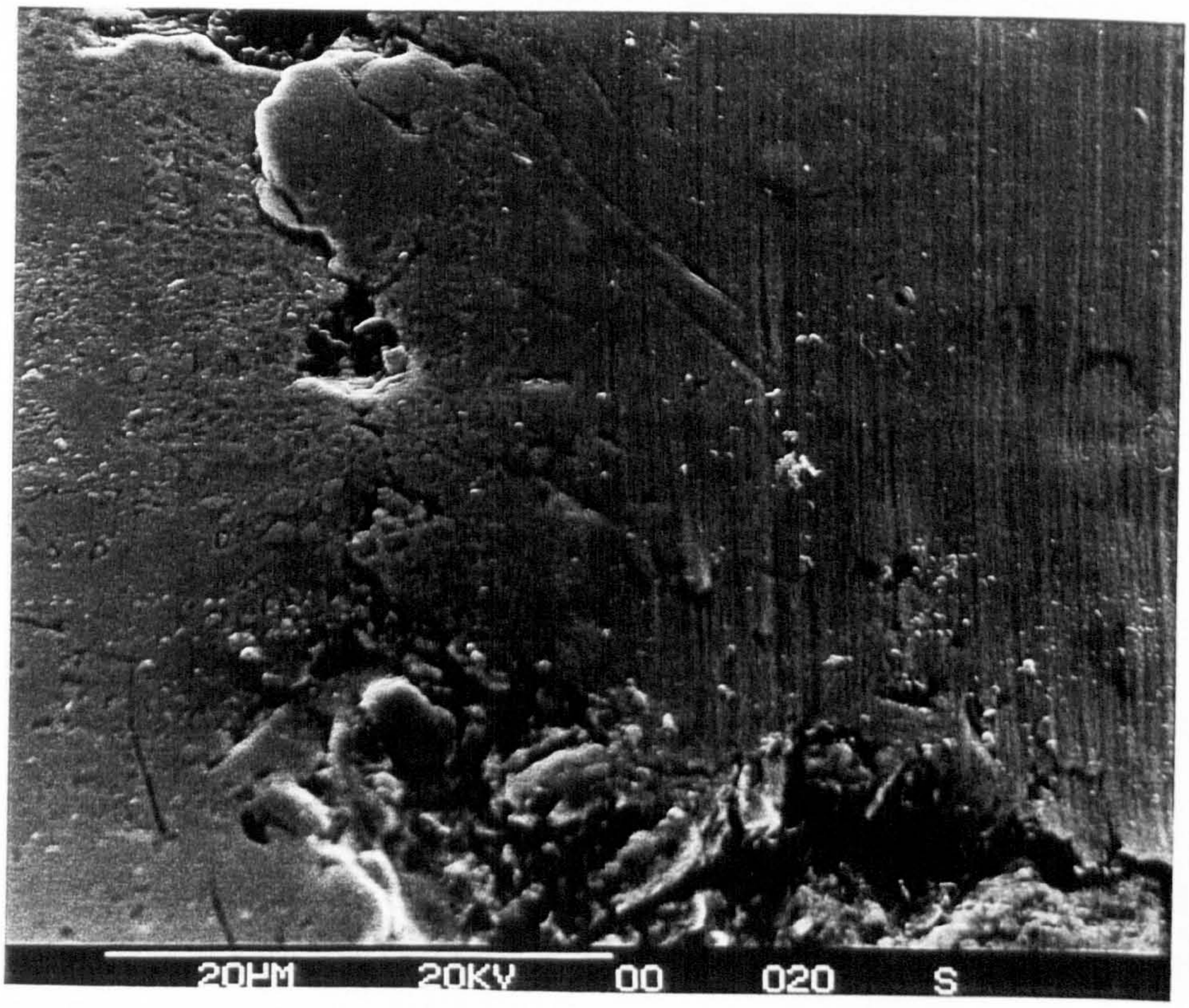

Fig. 4.515 - SEM images of a taper section through LW45 after a diamond-on-flat test, 3kg, 20 min. Centre of wear track.

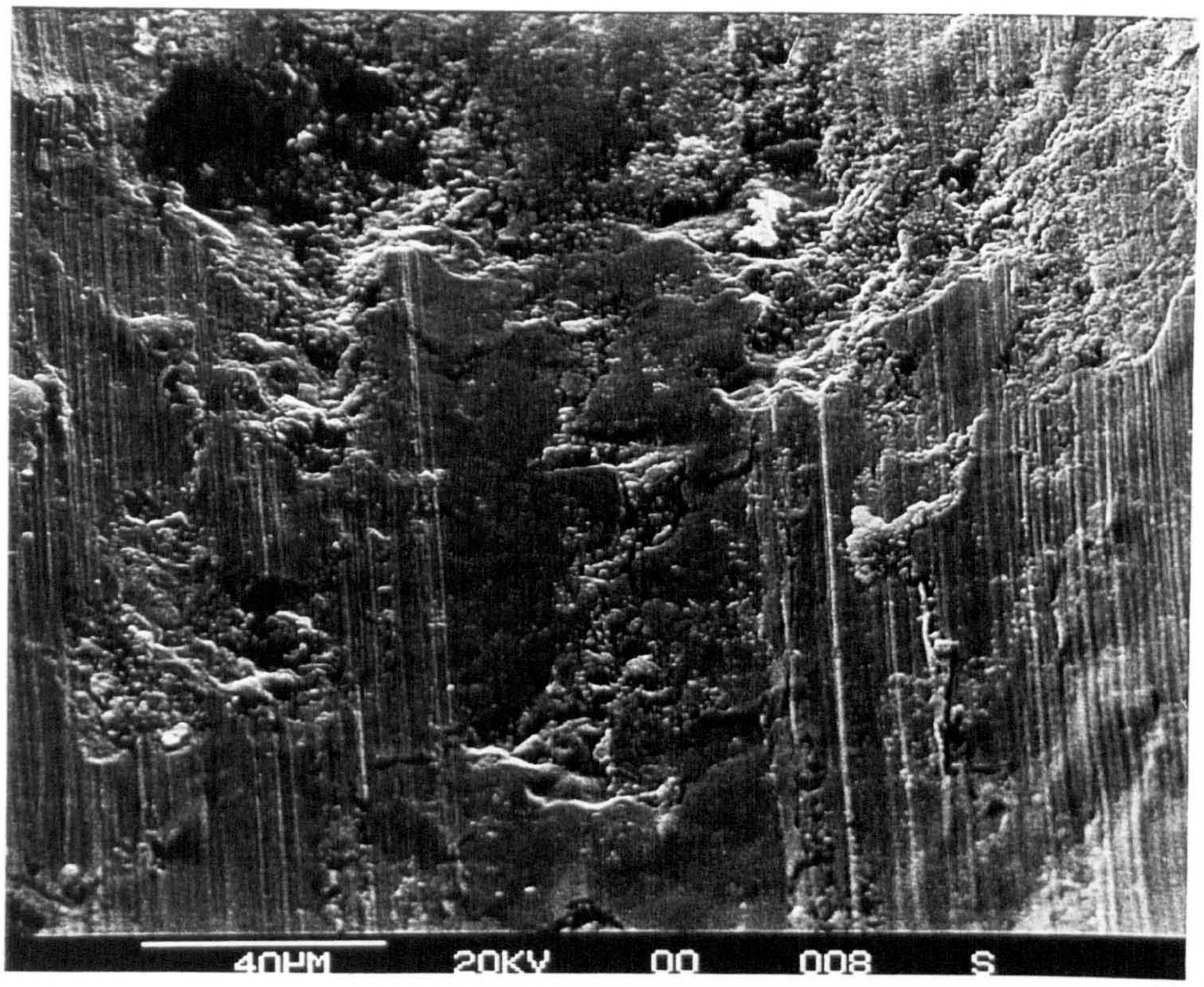

Fig. 4.516 - SEM image showing crack propogation adjacent to wear track, 3kg, 20 mins.

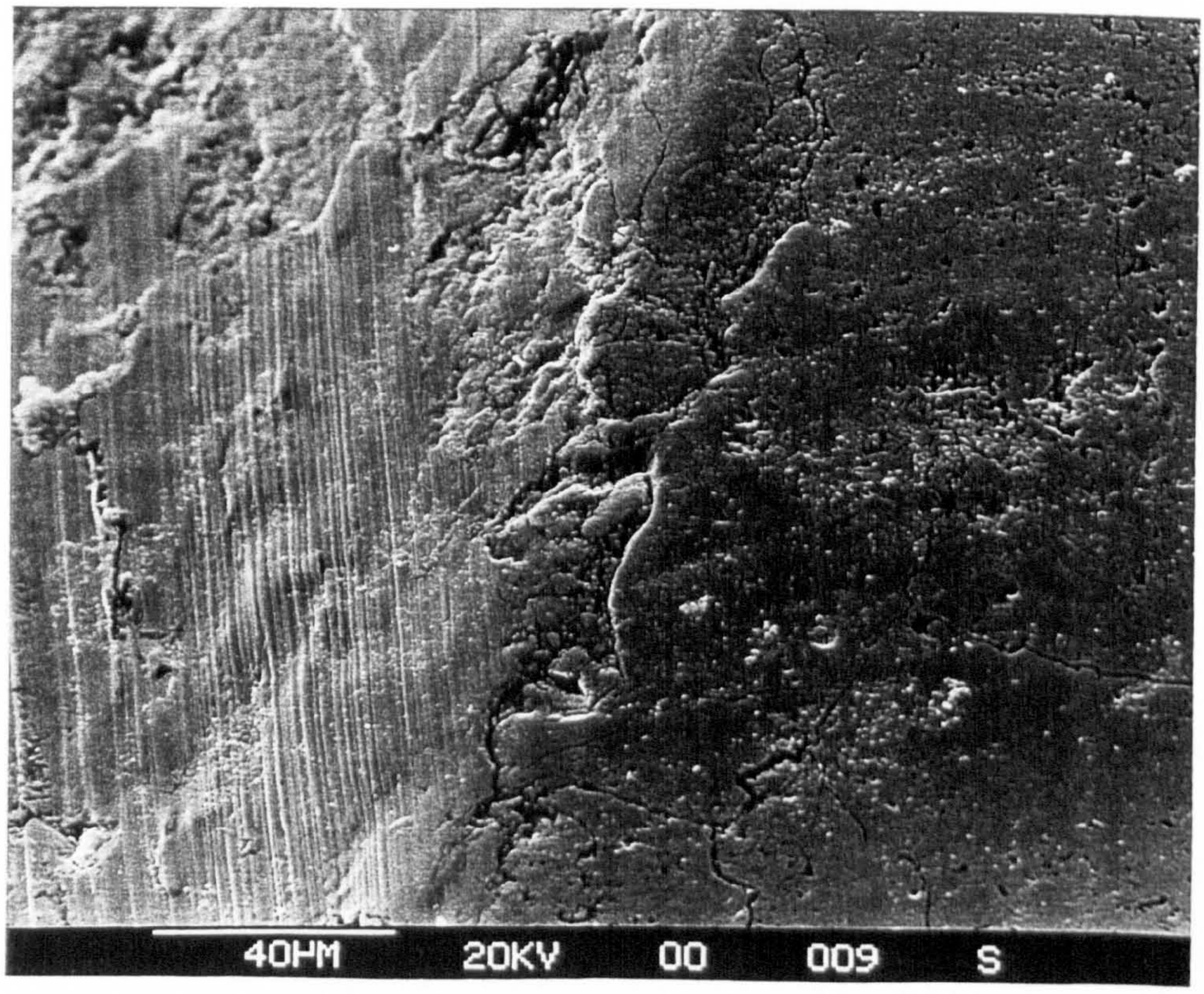

Fig. 4.521 Wear volumes for substrate material after Diamond-on-Flat Tests

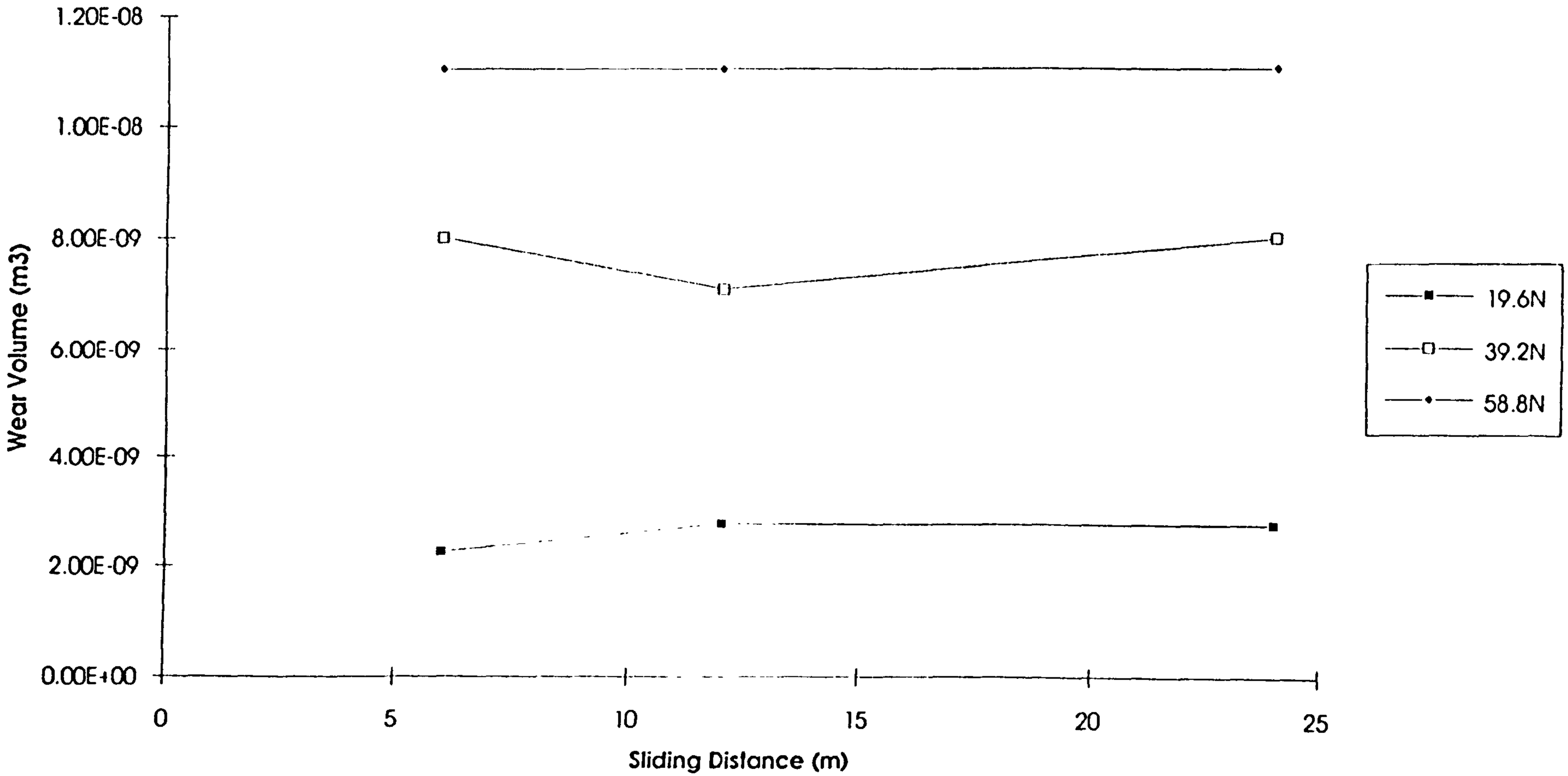

Fig. 4.522 Specific Wear Rates for substrate material following Diamond-on-Flat tests

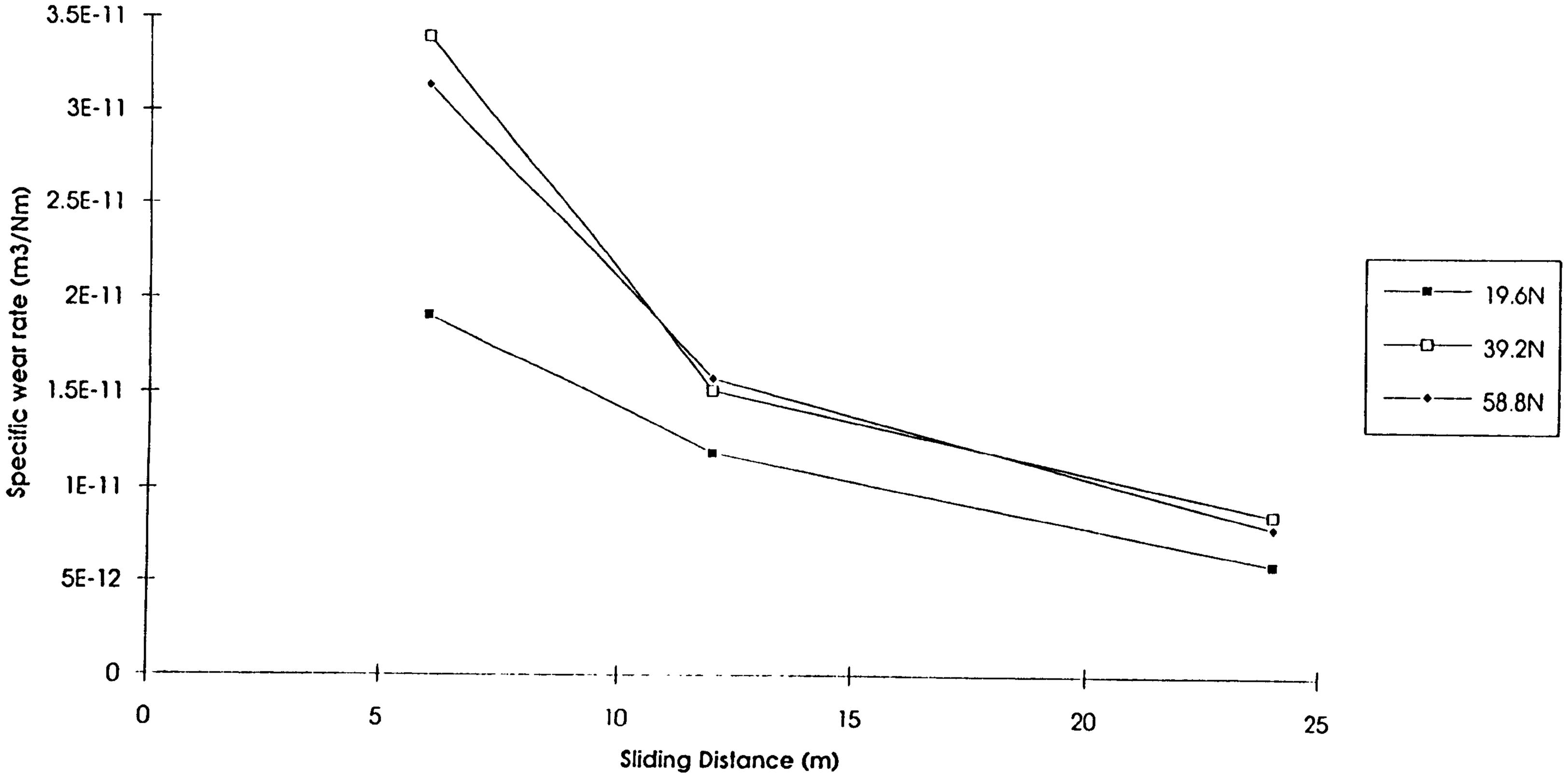

Fig. 4.523 Wear volume of substrate following Diamond-on-Flat test, 58.8N

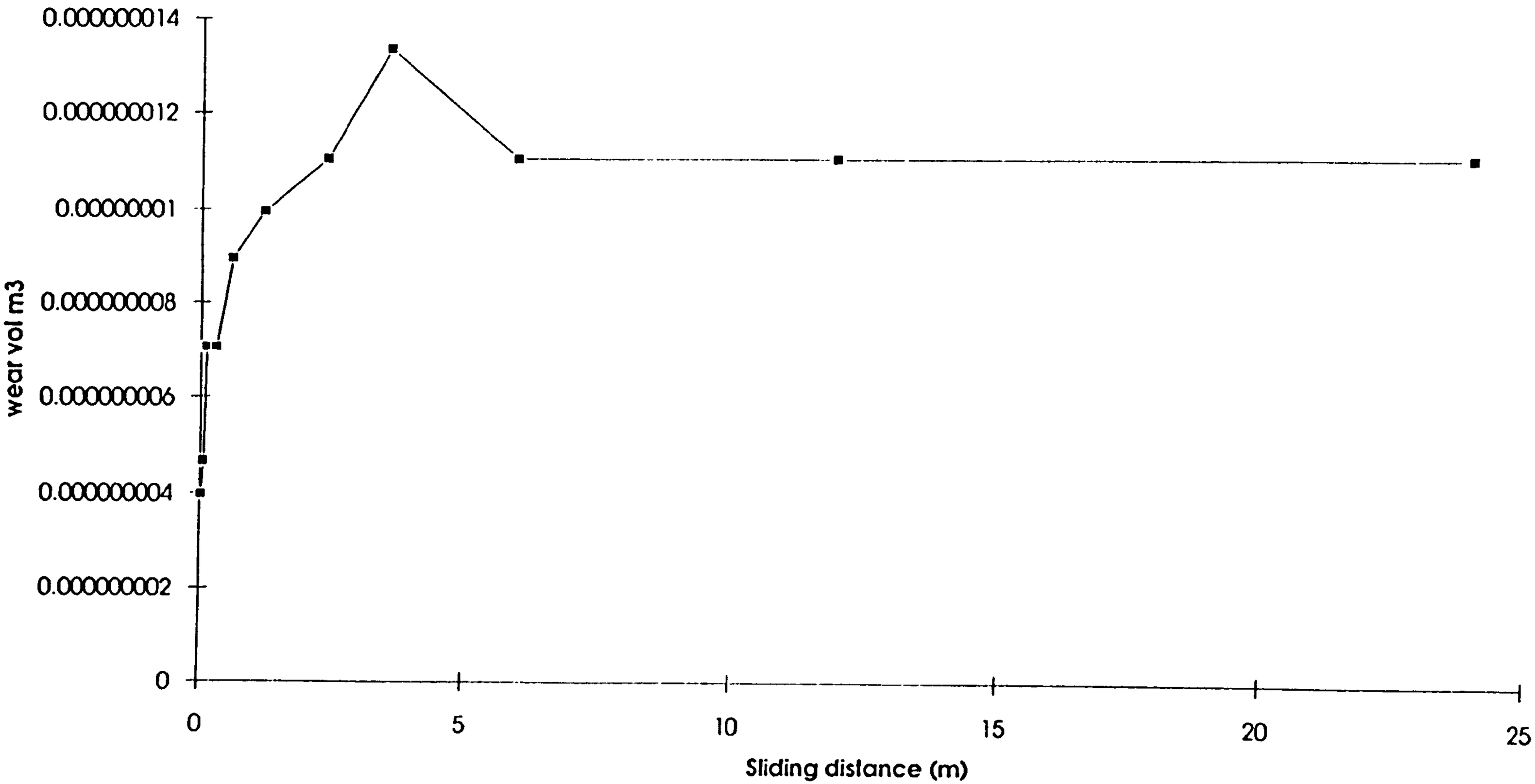

Fig. 4.524 - Specific Wear Rate of substrate following Diamond-on-Flat Test, 58.8N

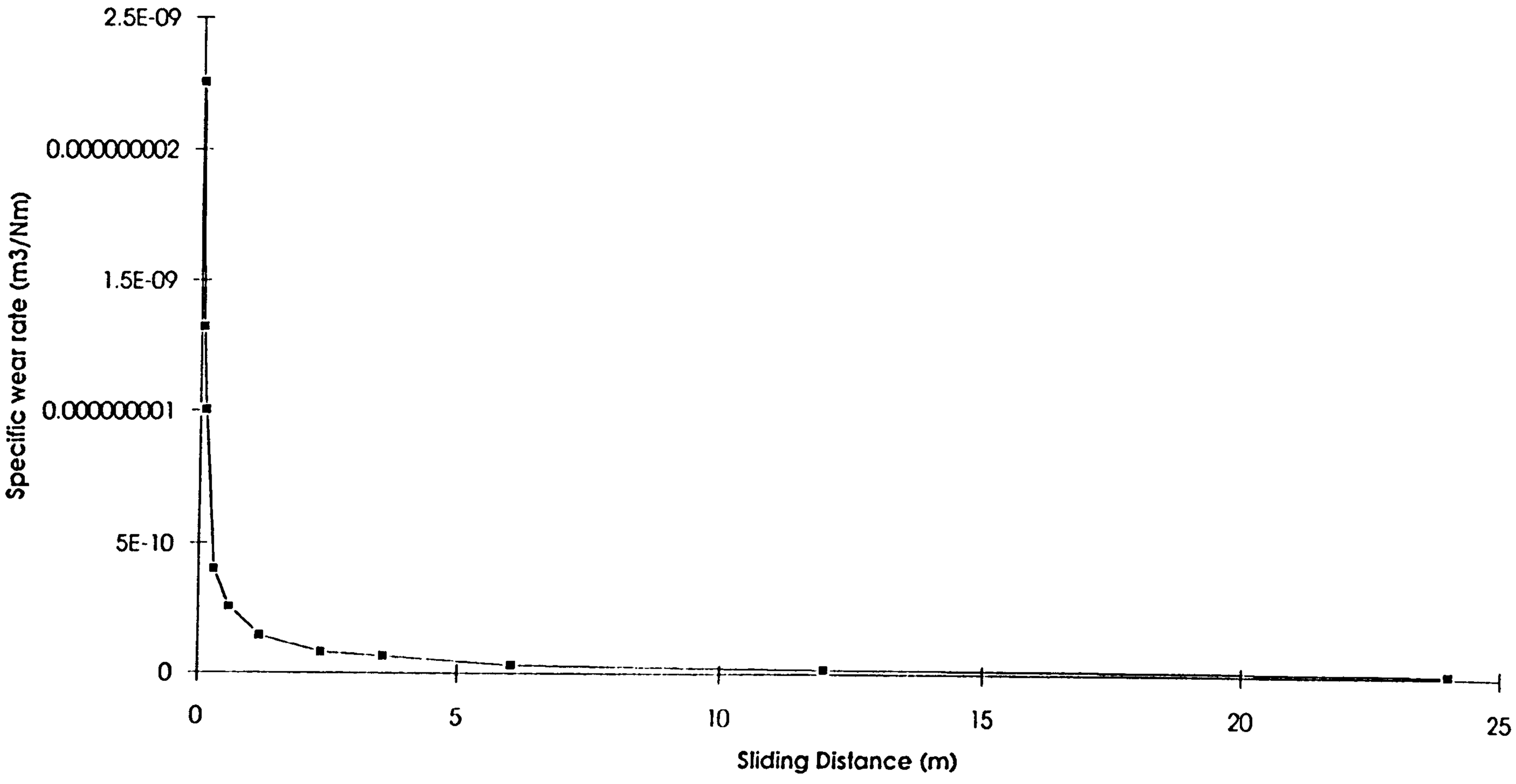

Fig. 4.621- Erosion of F255

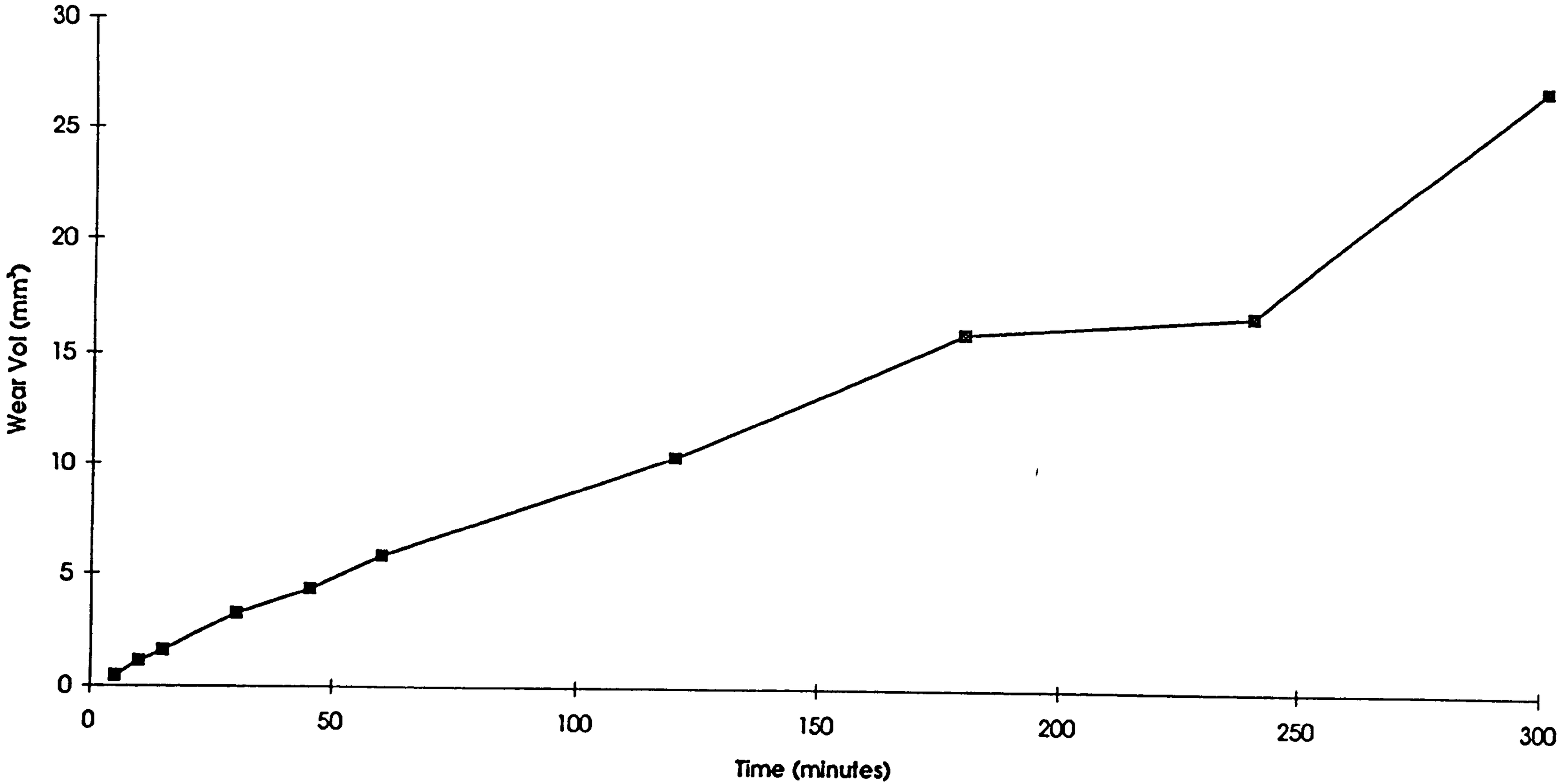

Fig.4.622 Erosion of F255

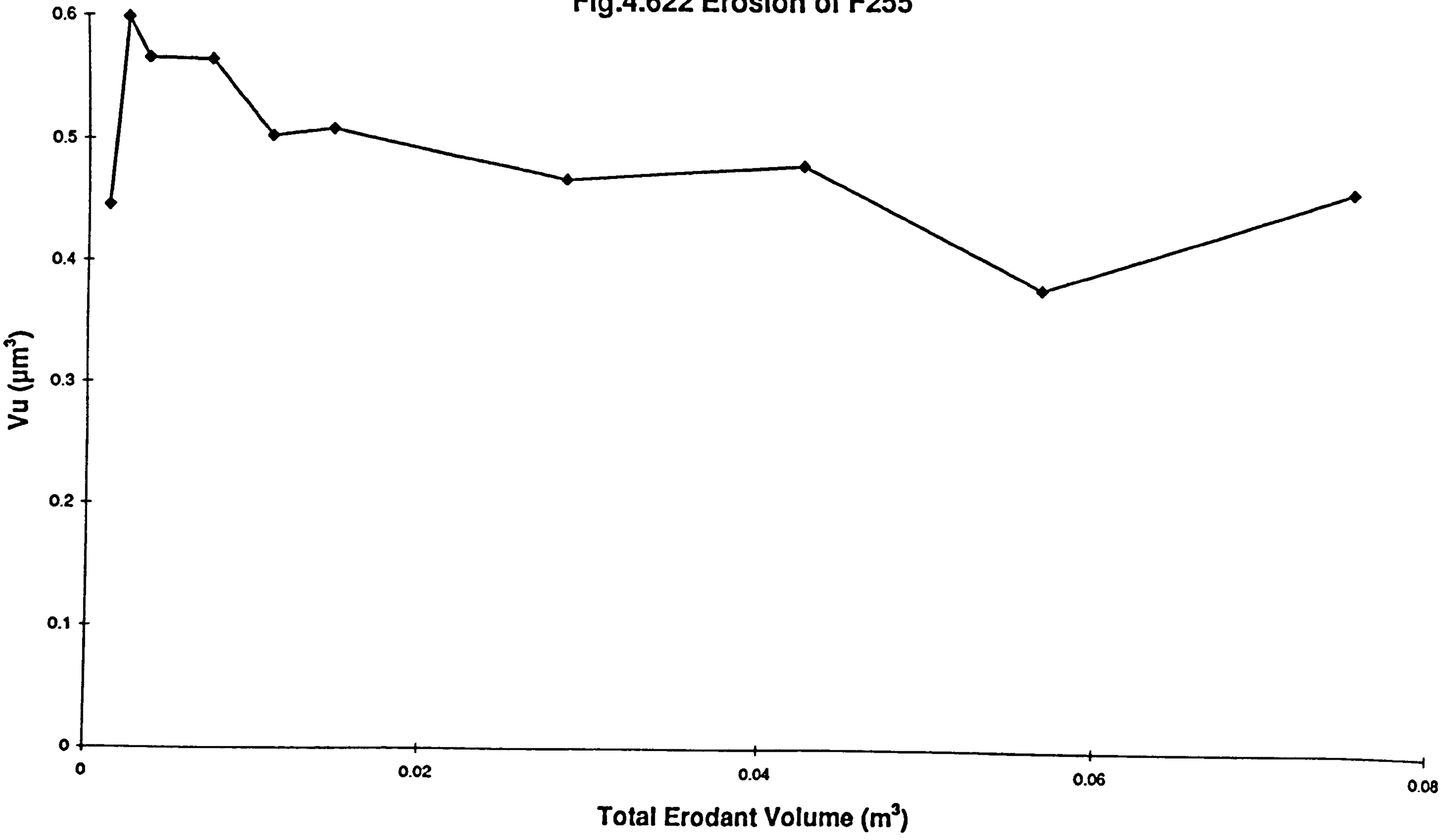

Fig. 4.631Erosion of LW45

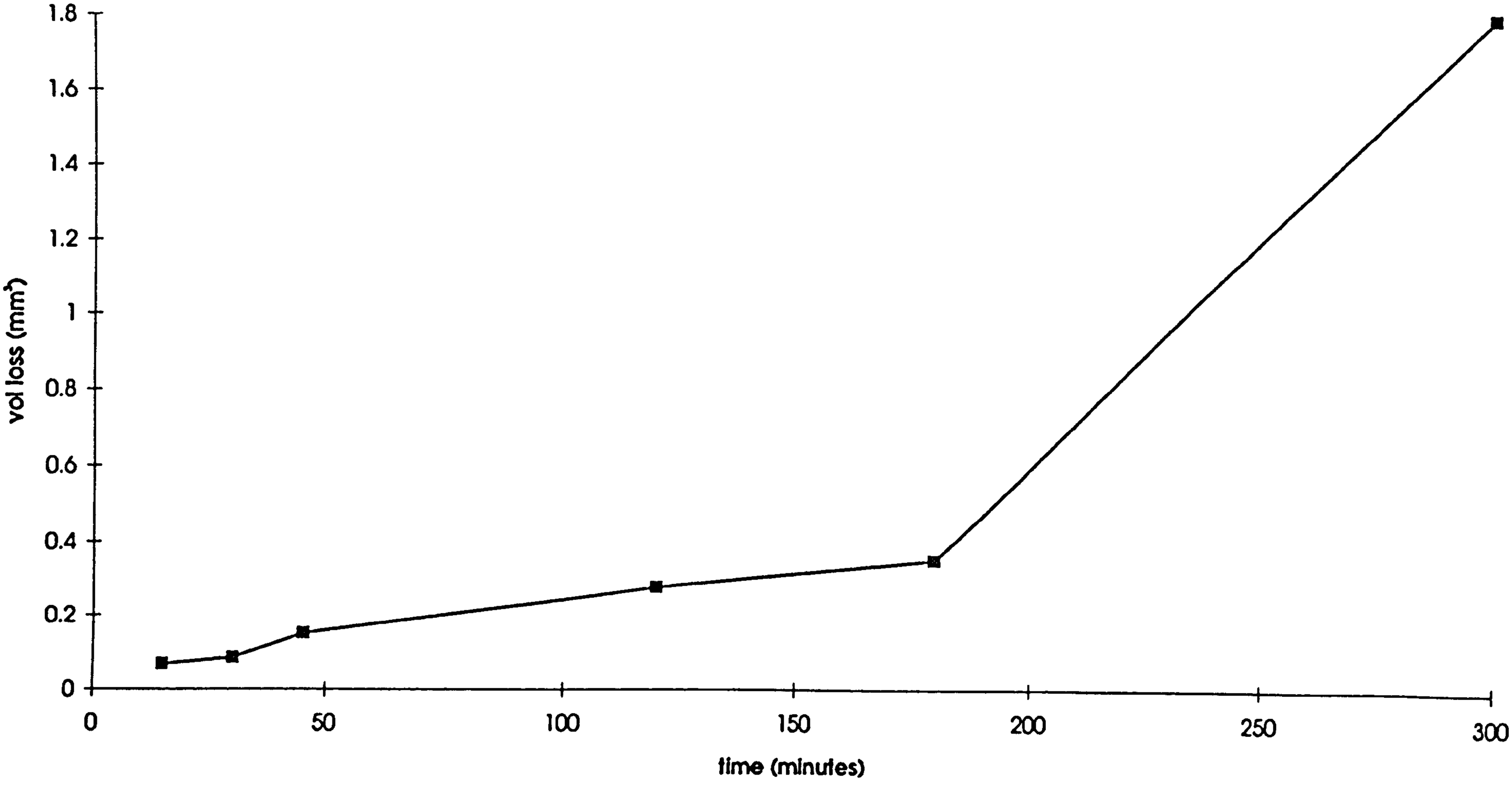

Fig. 4.632 Erosion of LW45

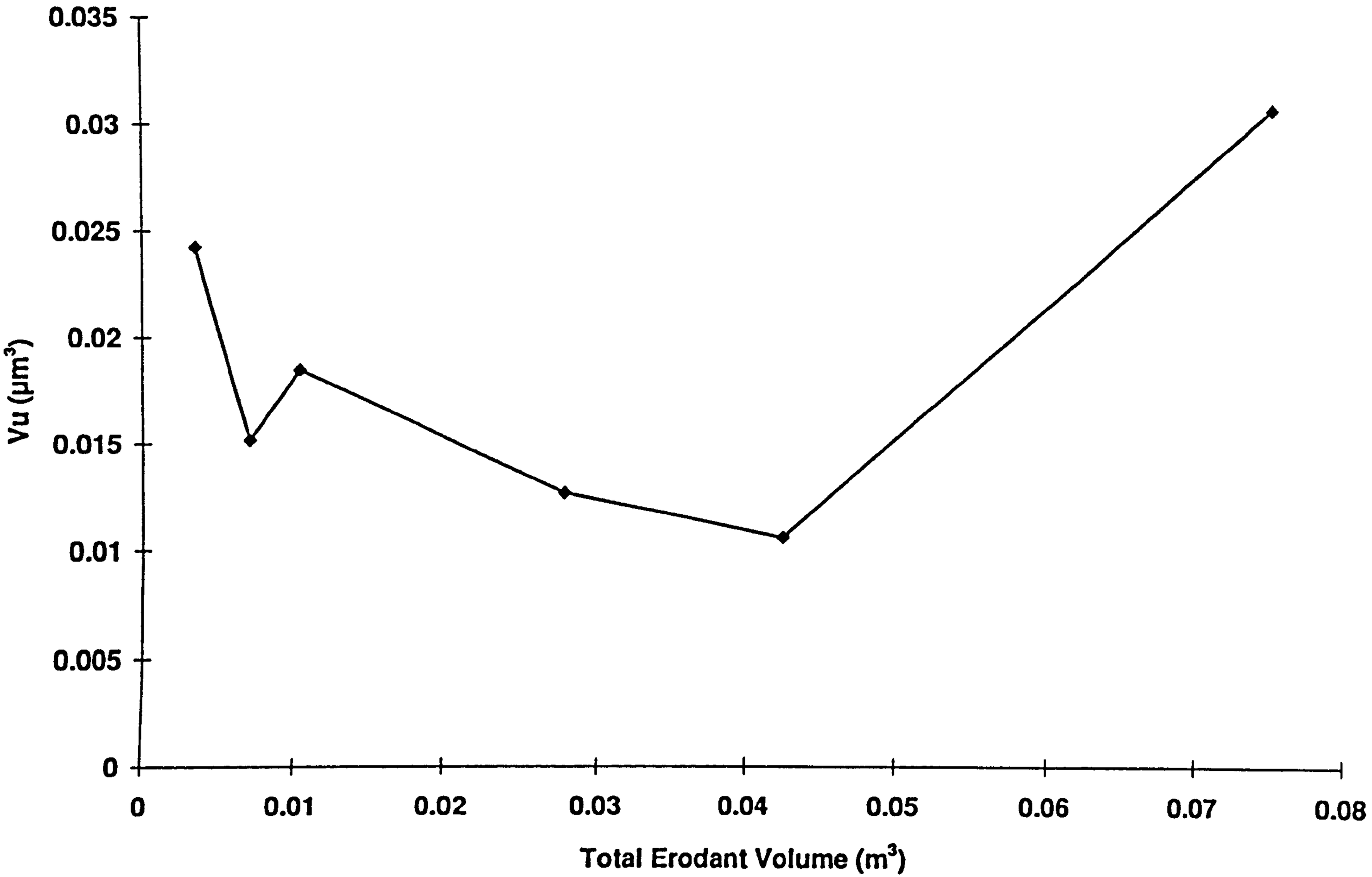

Fig. 4.633 Comparative Erosion of F255 and LW45

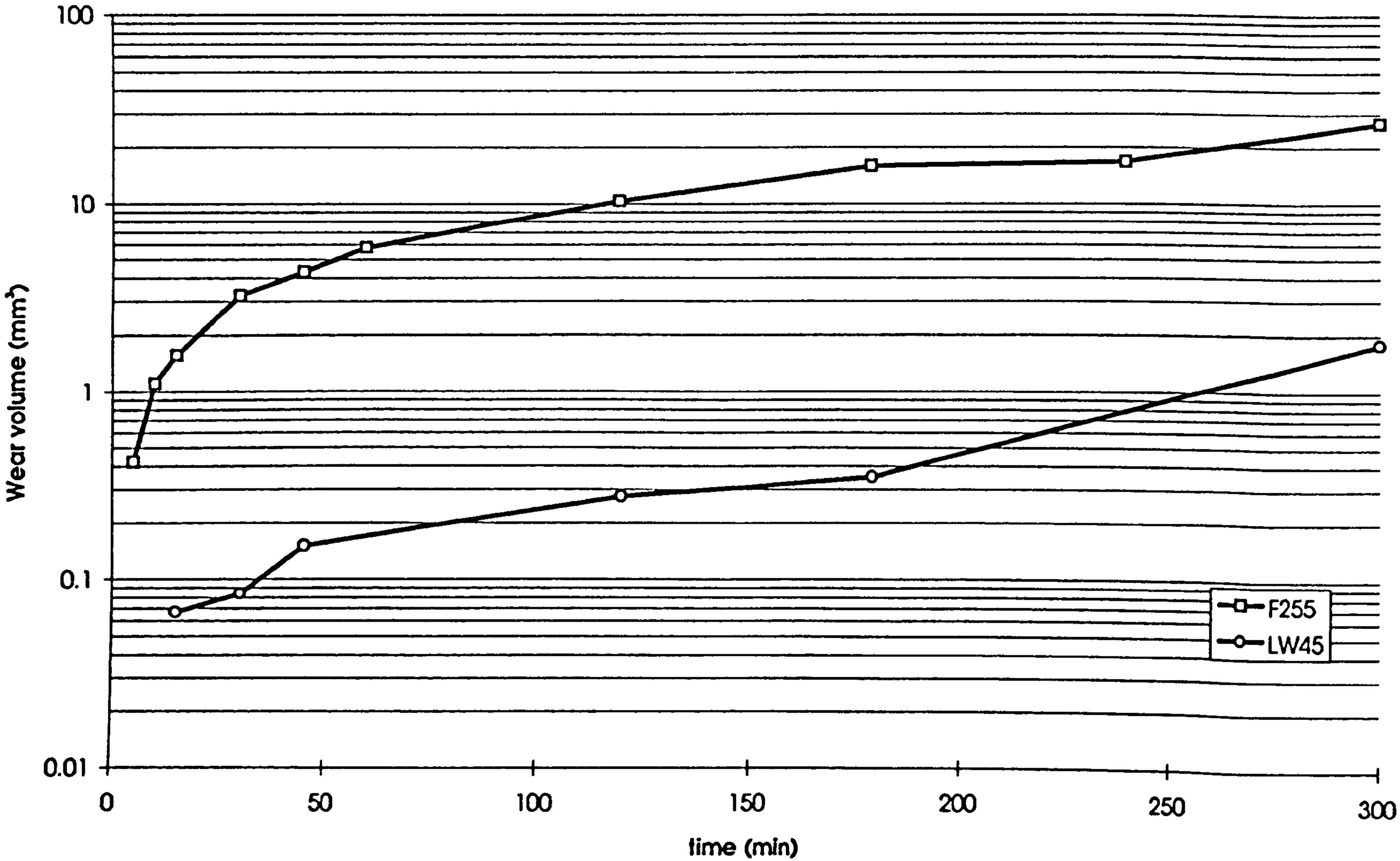

Fig. 4.634 Comparative Vu's of LW45 and F255

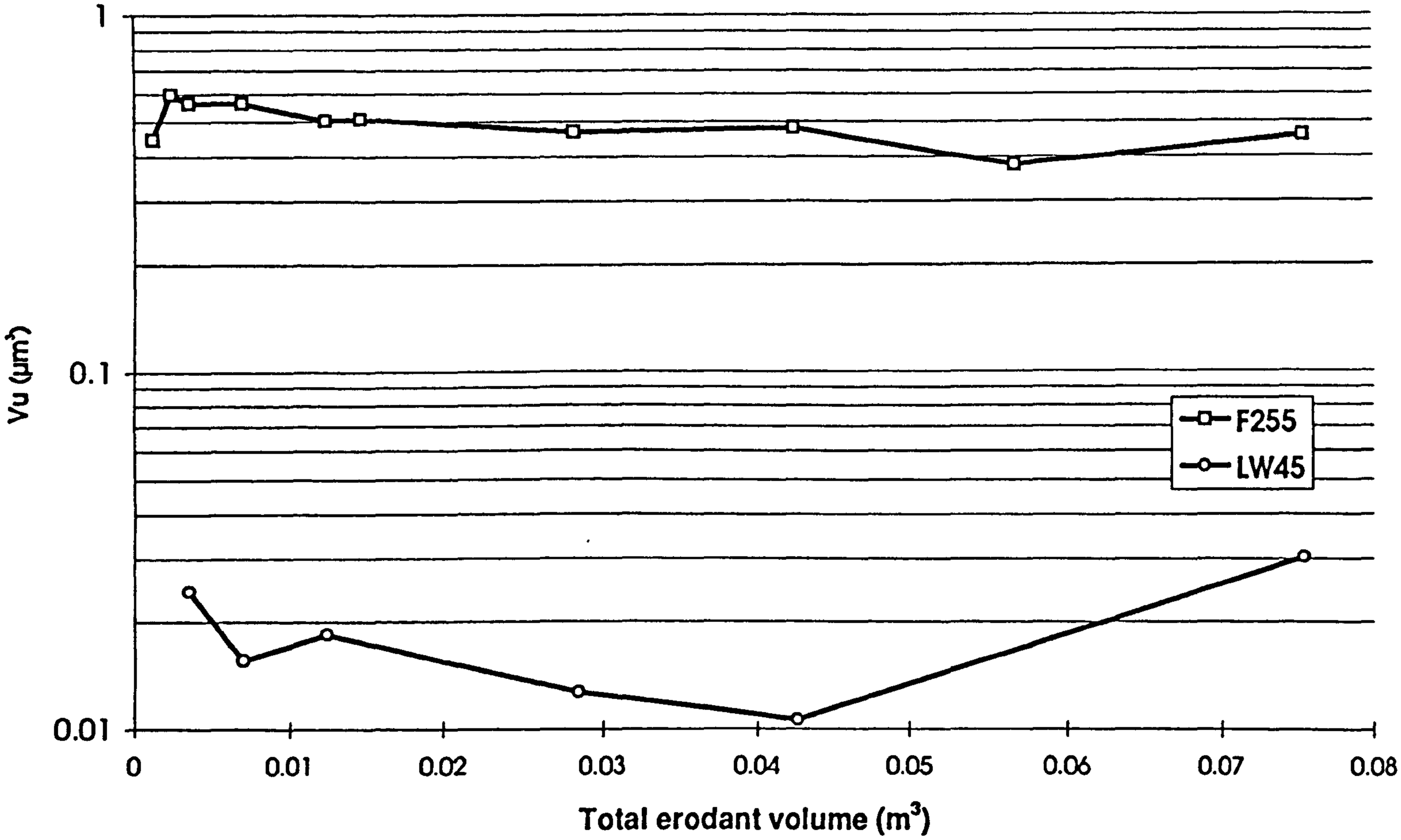

Fig. 4.641 - 3D profiles of erosion scars (300 minute test)

(a) LW45 (x5000)

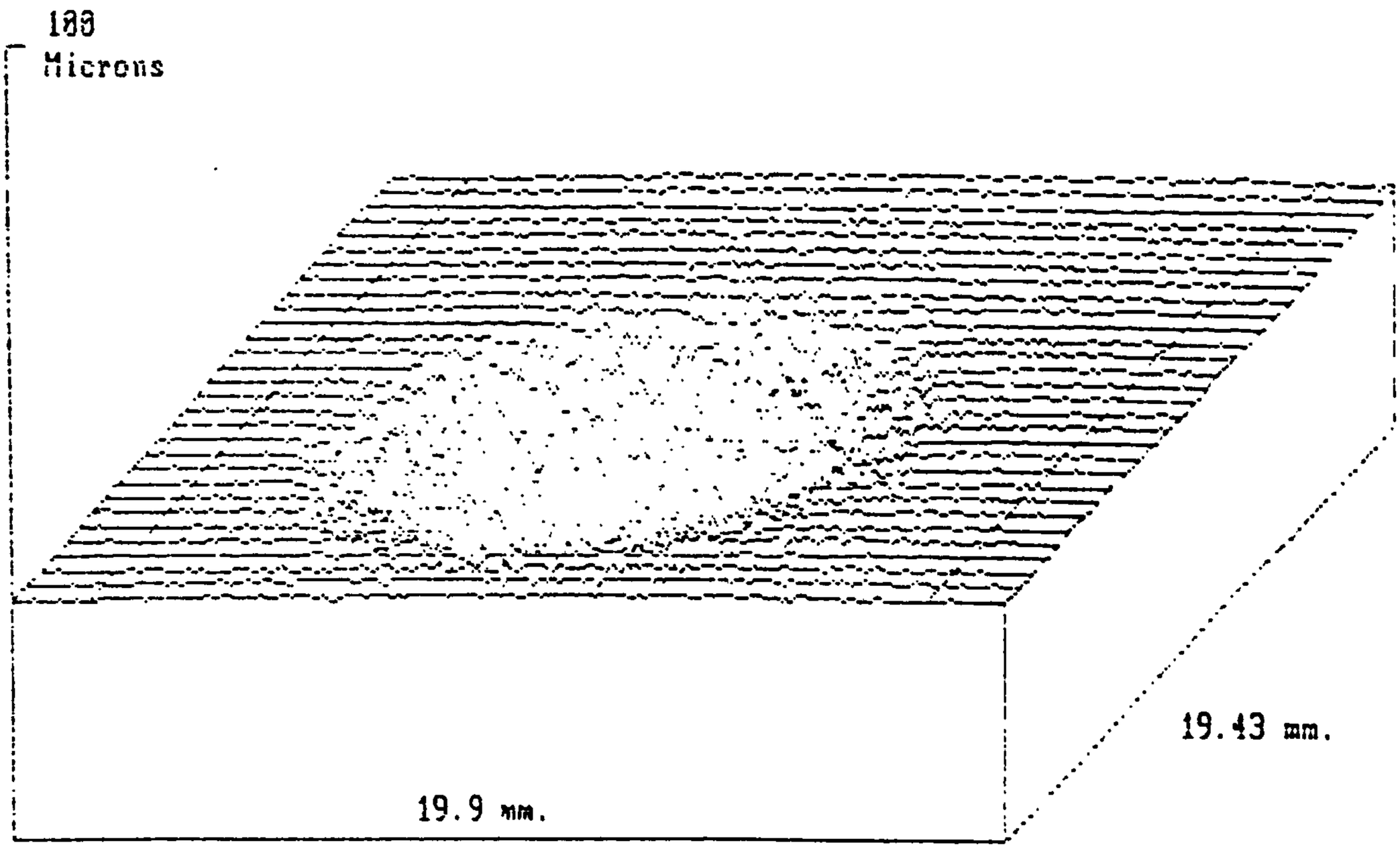

(b) F255 (x500)

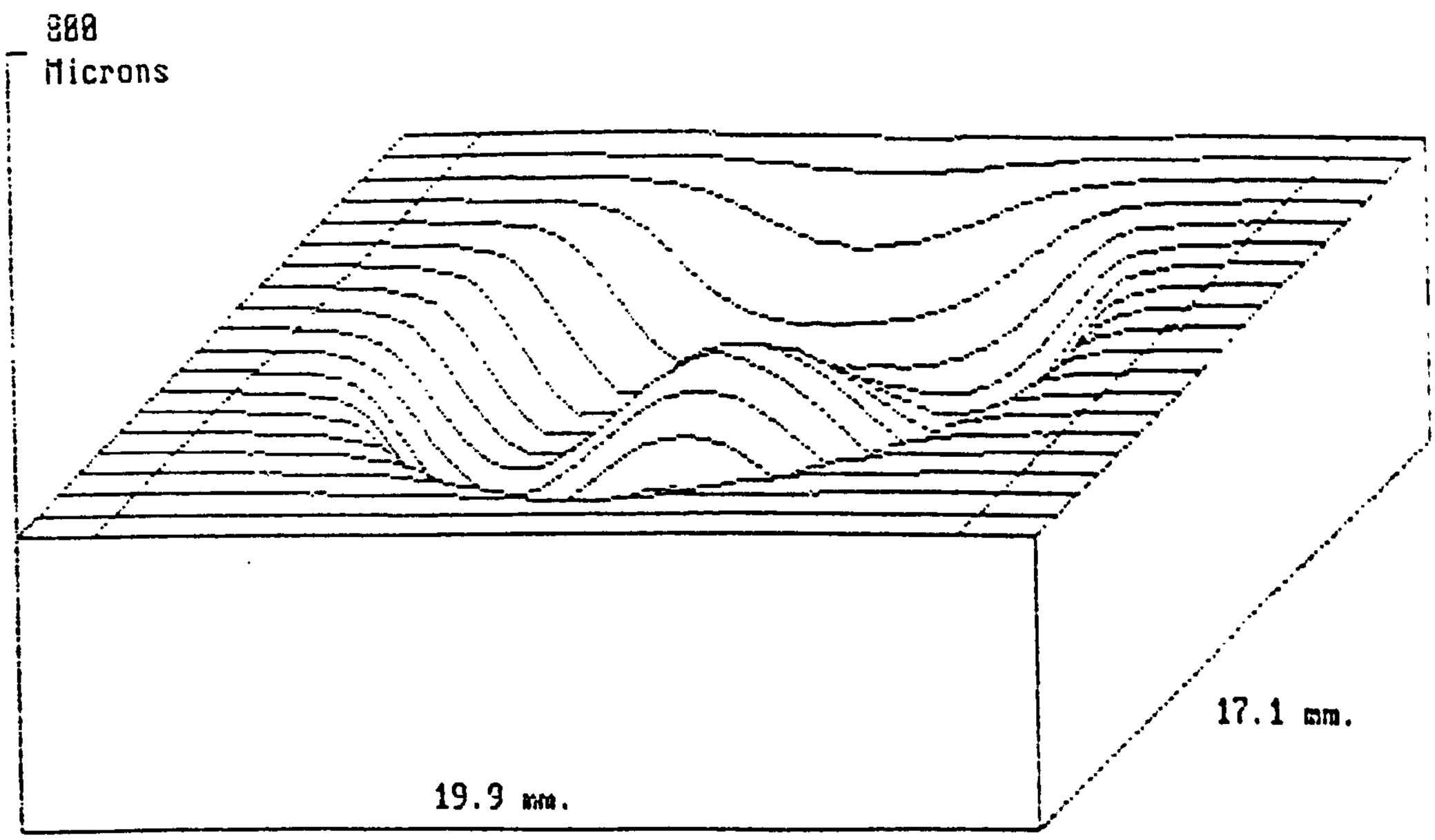

Fig. 4.642 - Single profile traces across centre of erosion scar
(a) LW45 ("U" shaped)

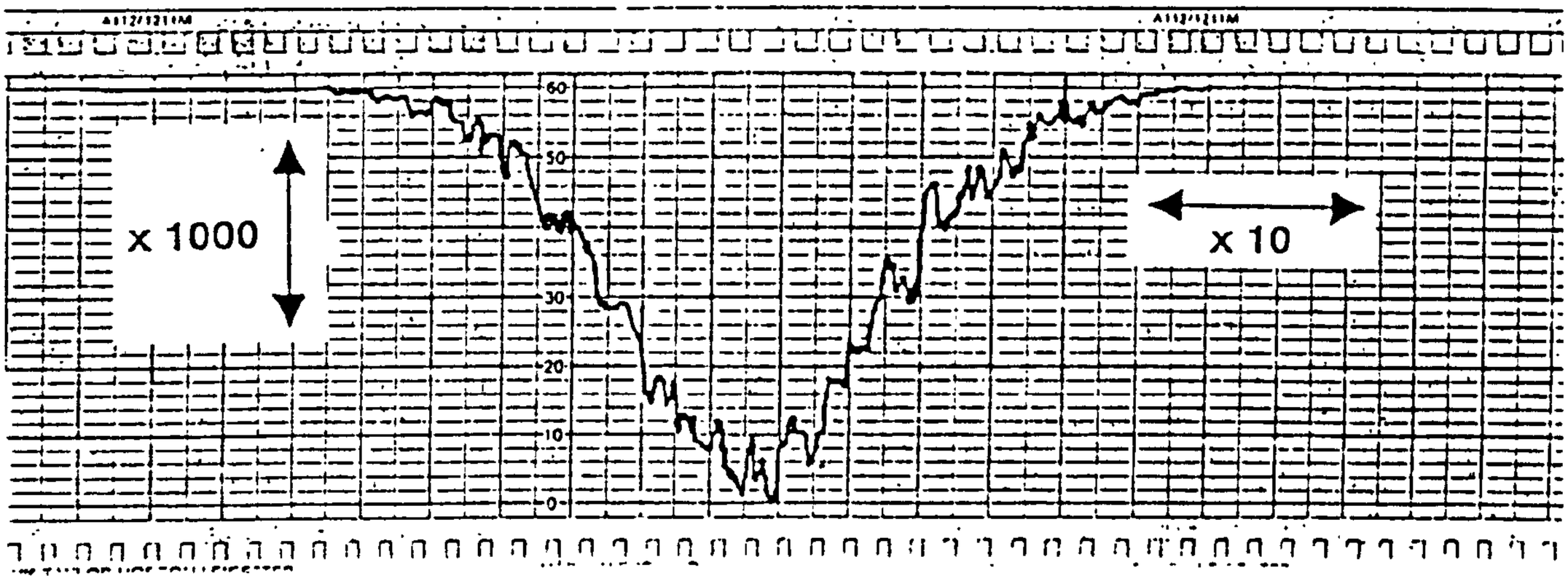

(b) F255 ("W" shaped)

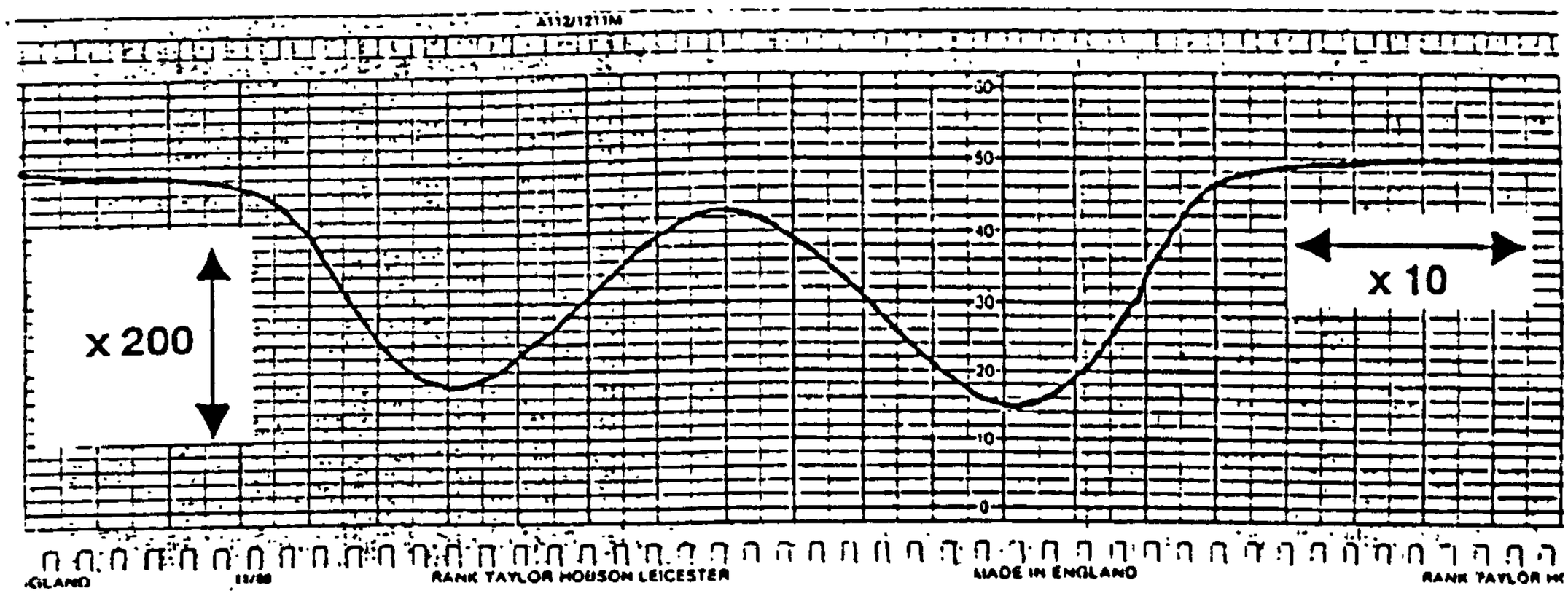

Fig. 4.643 - 3D profiles showing progressive erosion of F255

(a) after 15 mins

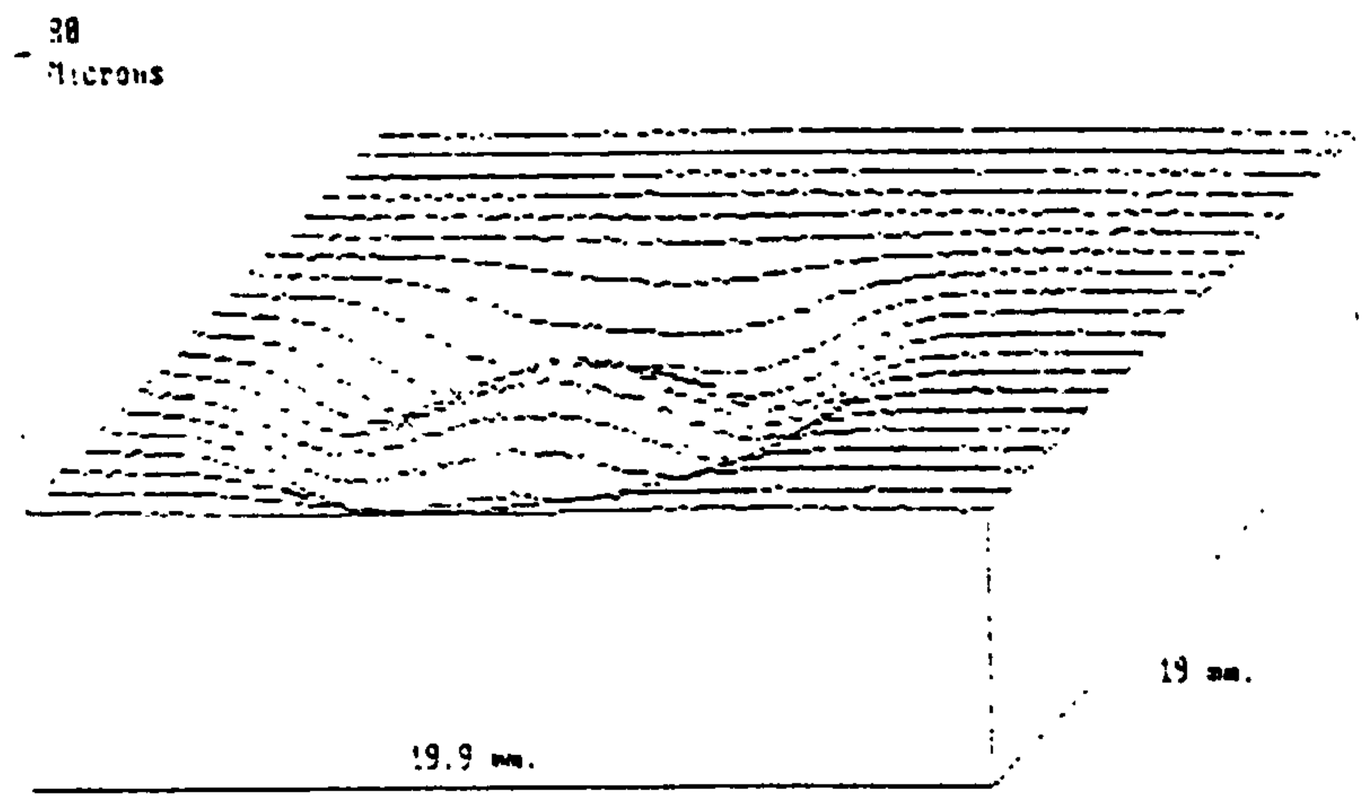

(b) after 30 mins

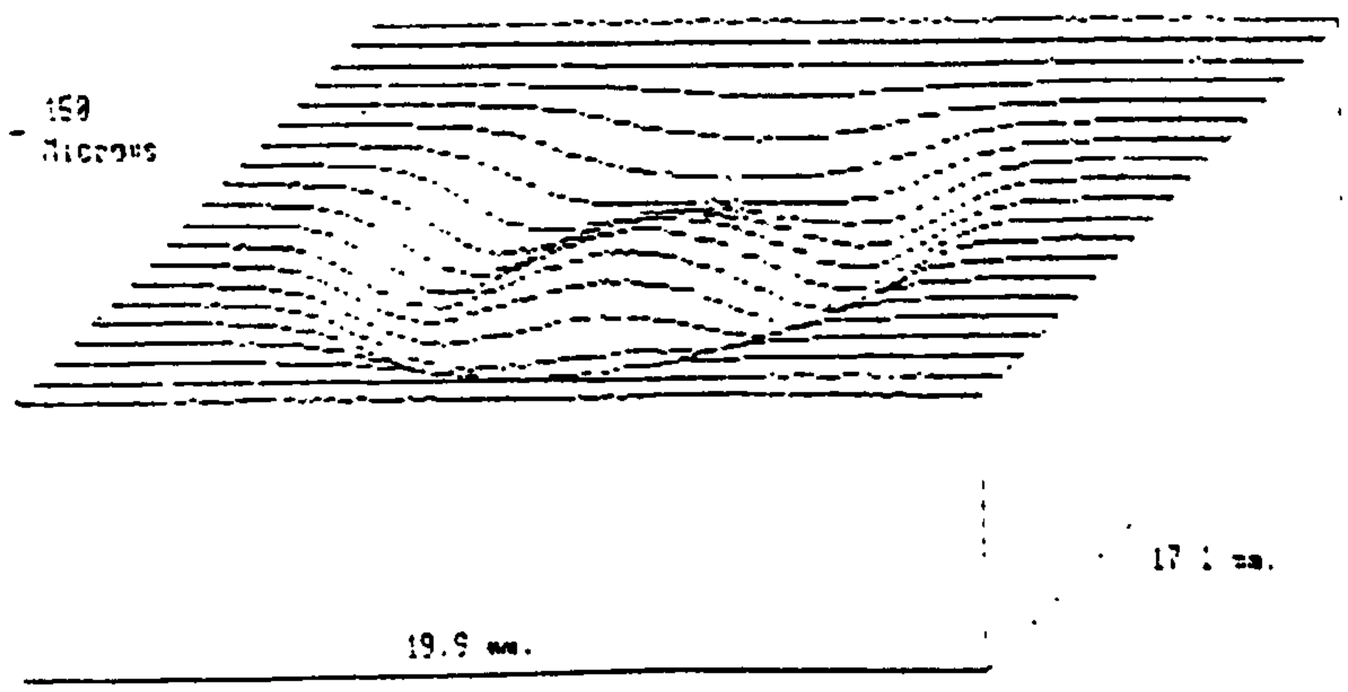

(c) after 60 mins

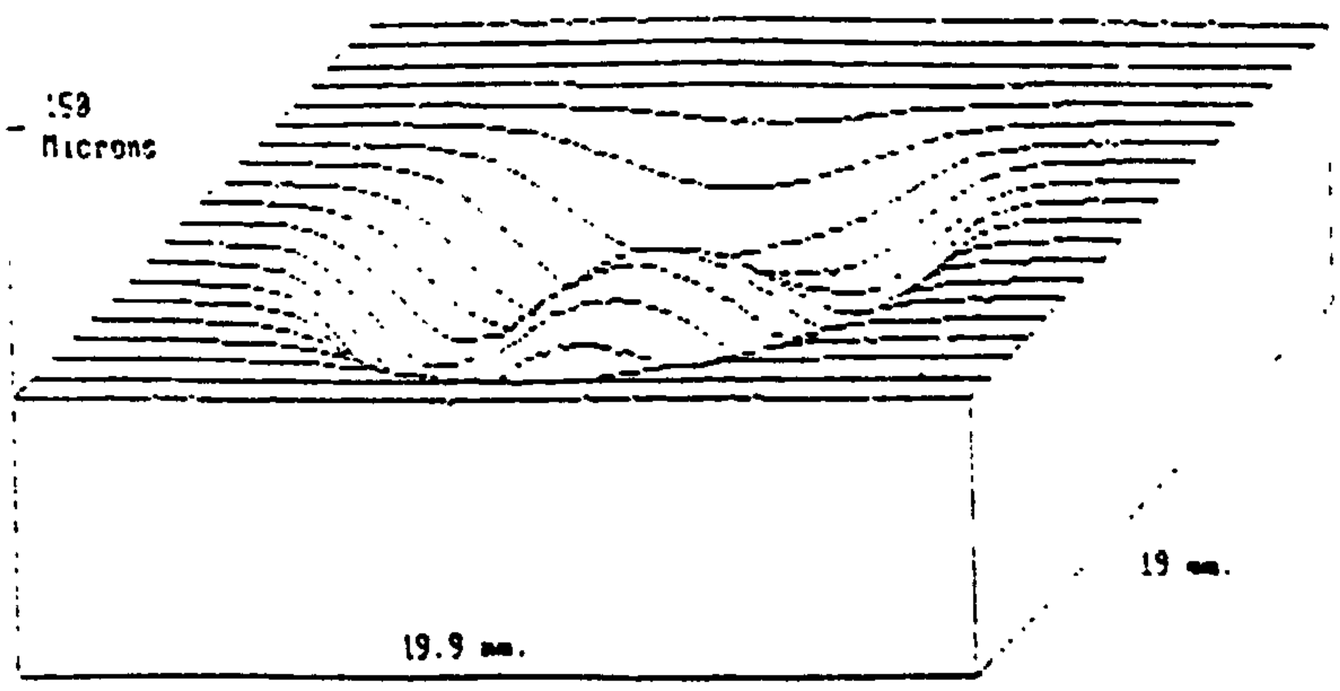

(d) after 120 mins

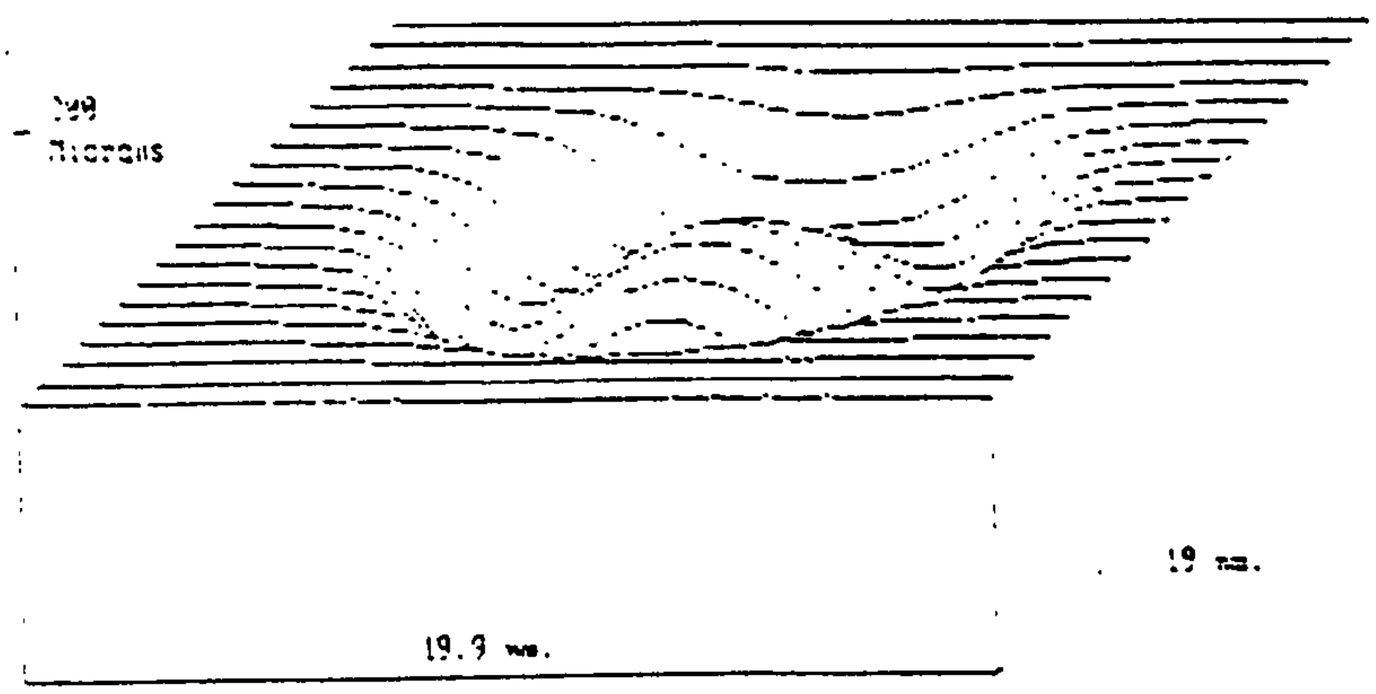

(e) after 300 mins

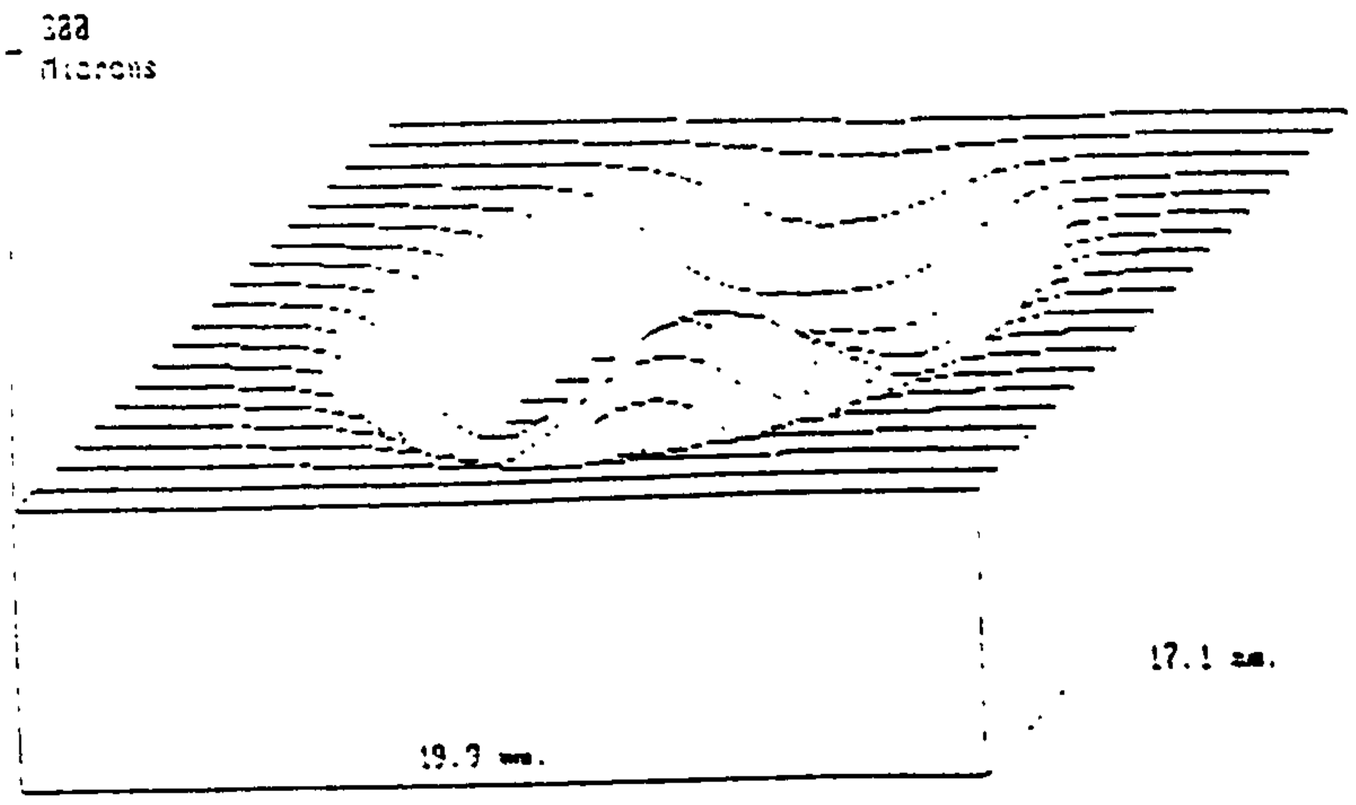

Fig. 4.644 - 3D profile of erosion scar for F255, 120 min test duration, 30° impingement angle

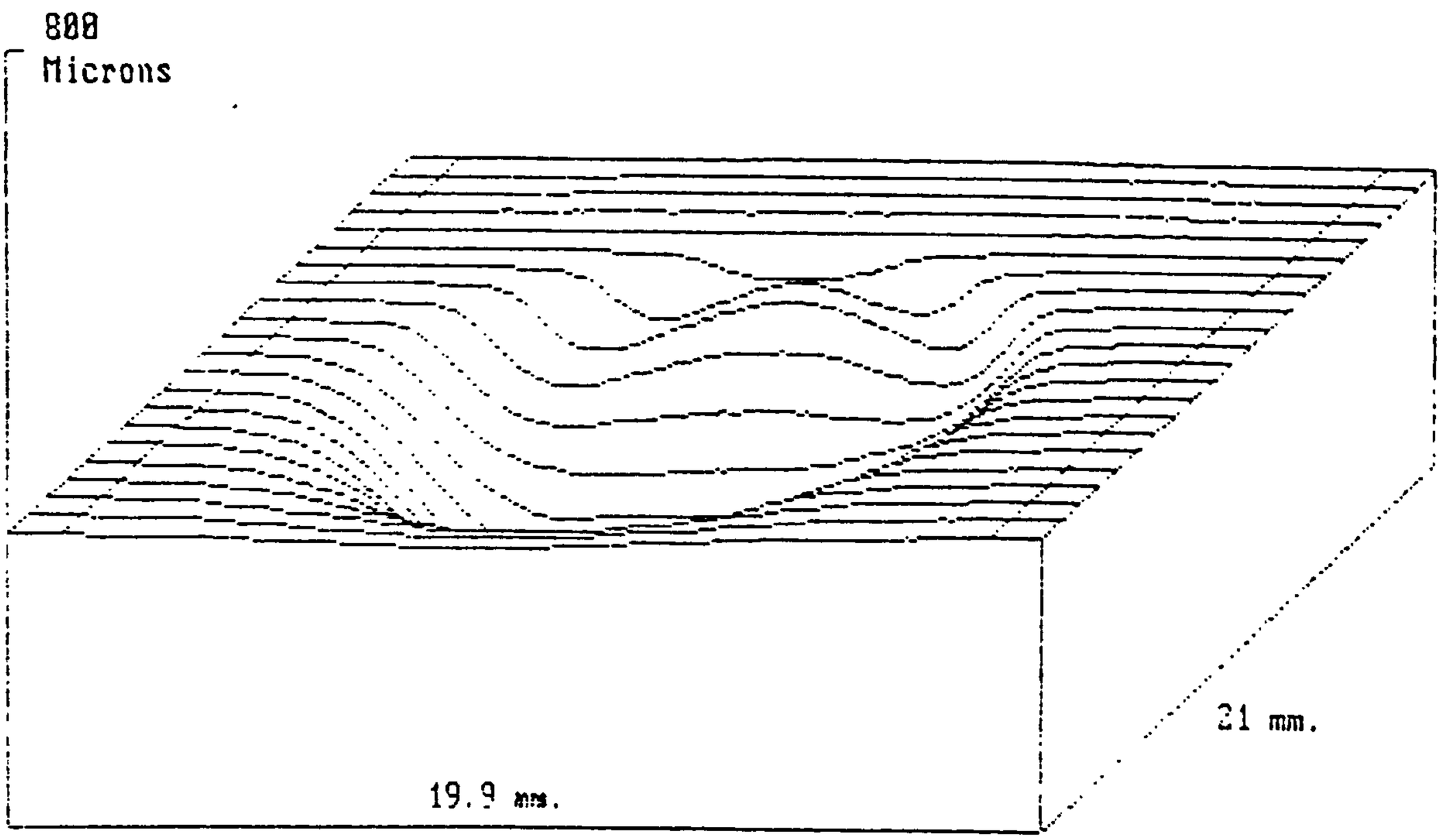

Fig. 4.645 - Single trace profiles through the centre of F255 erosion scar at 30° impingement angle.

(a) parallel to flow

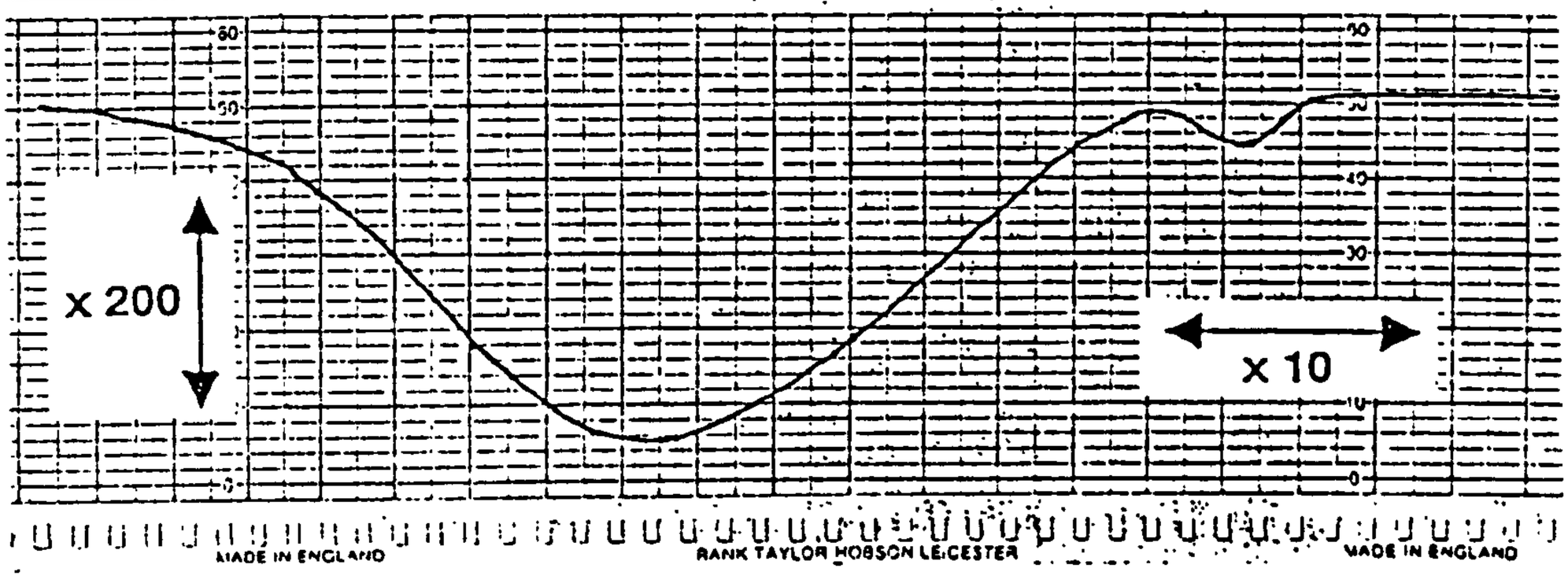

(b) perpendicular to flow

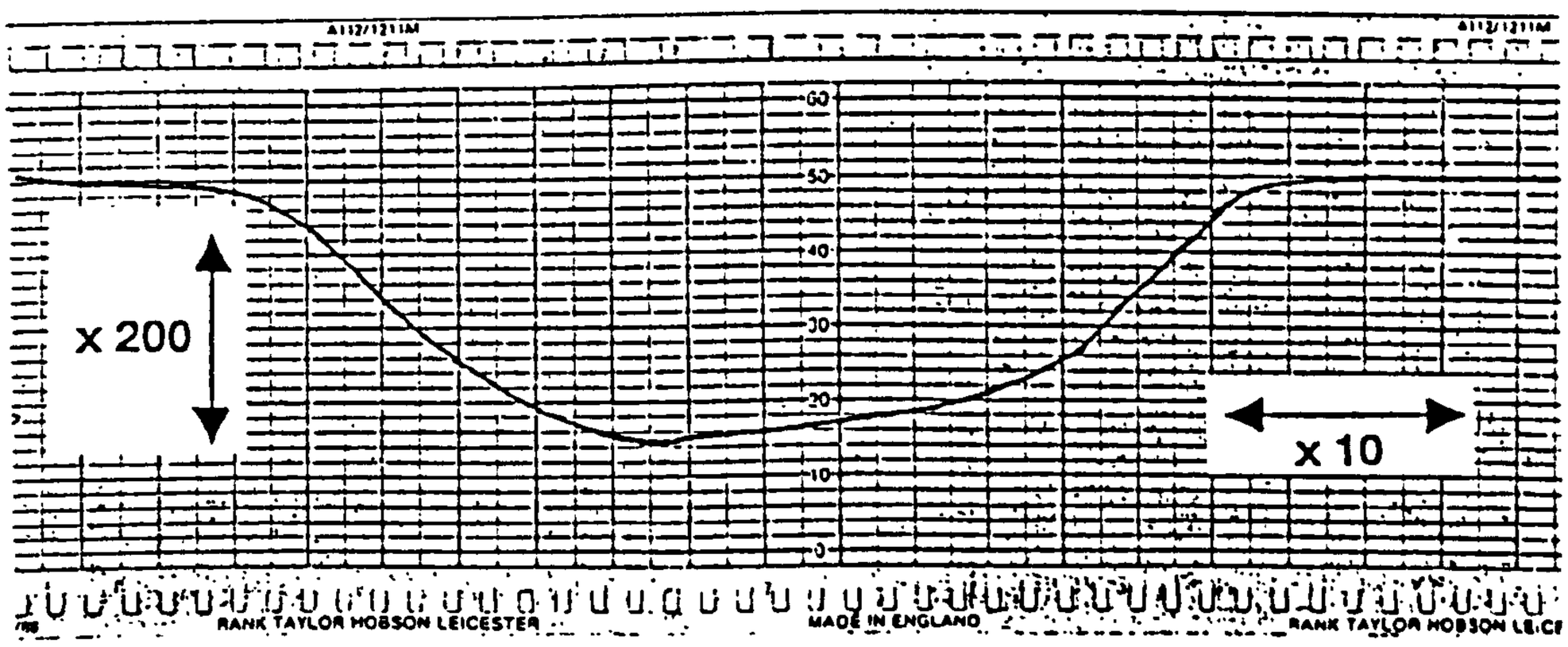

Fig. 4.651 - SEM images of LW45 after erosion

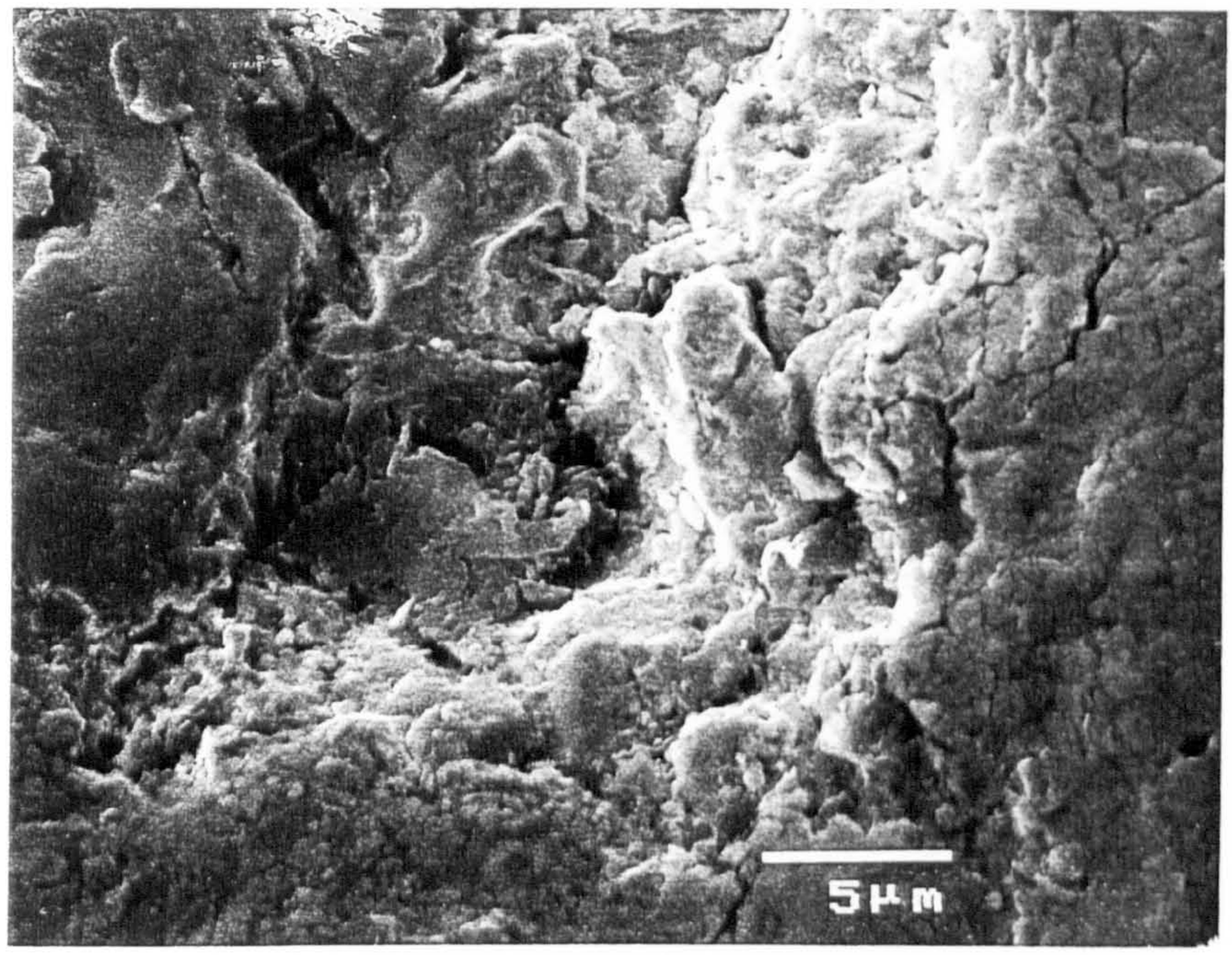

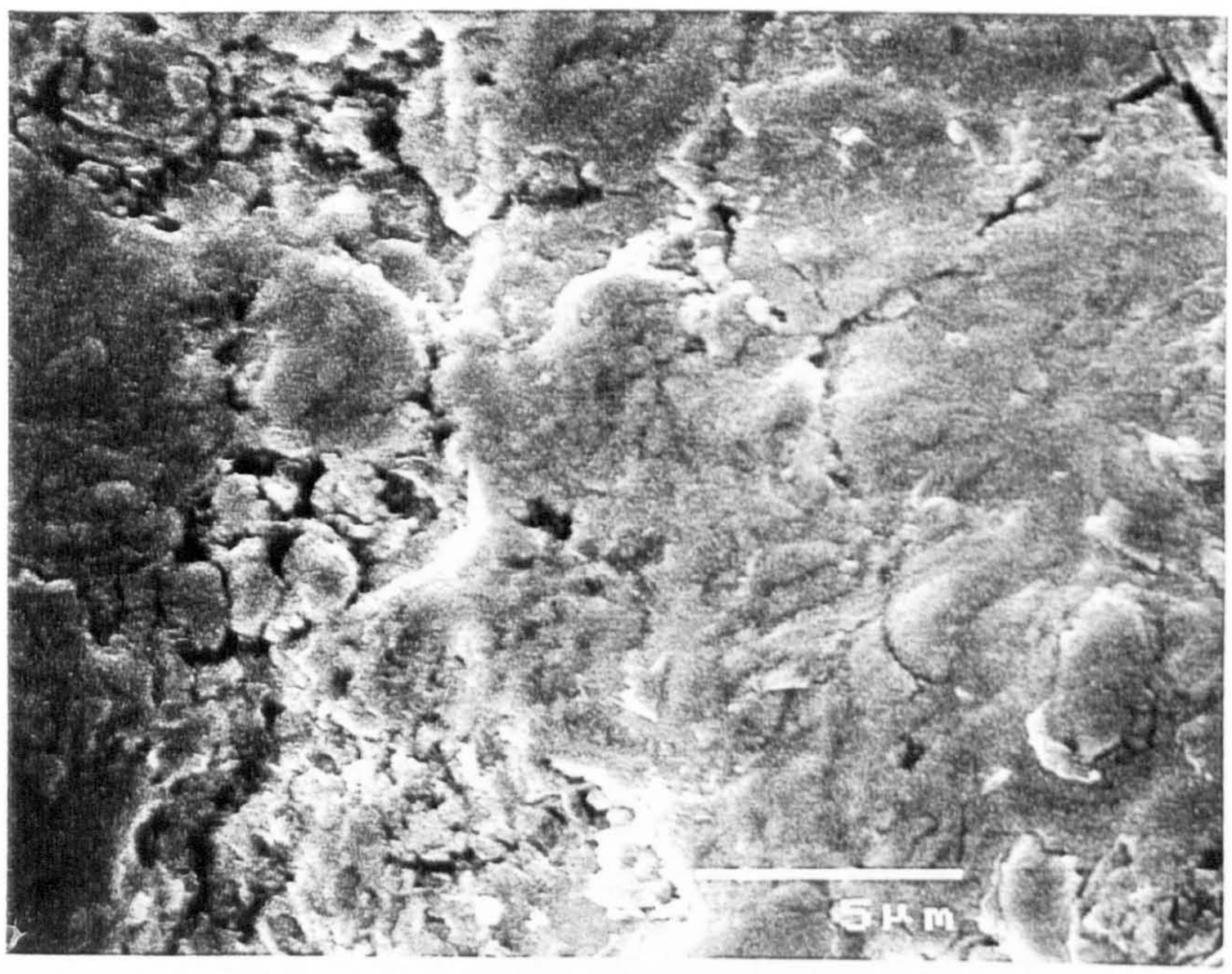

Fig. 4.651 cont.

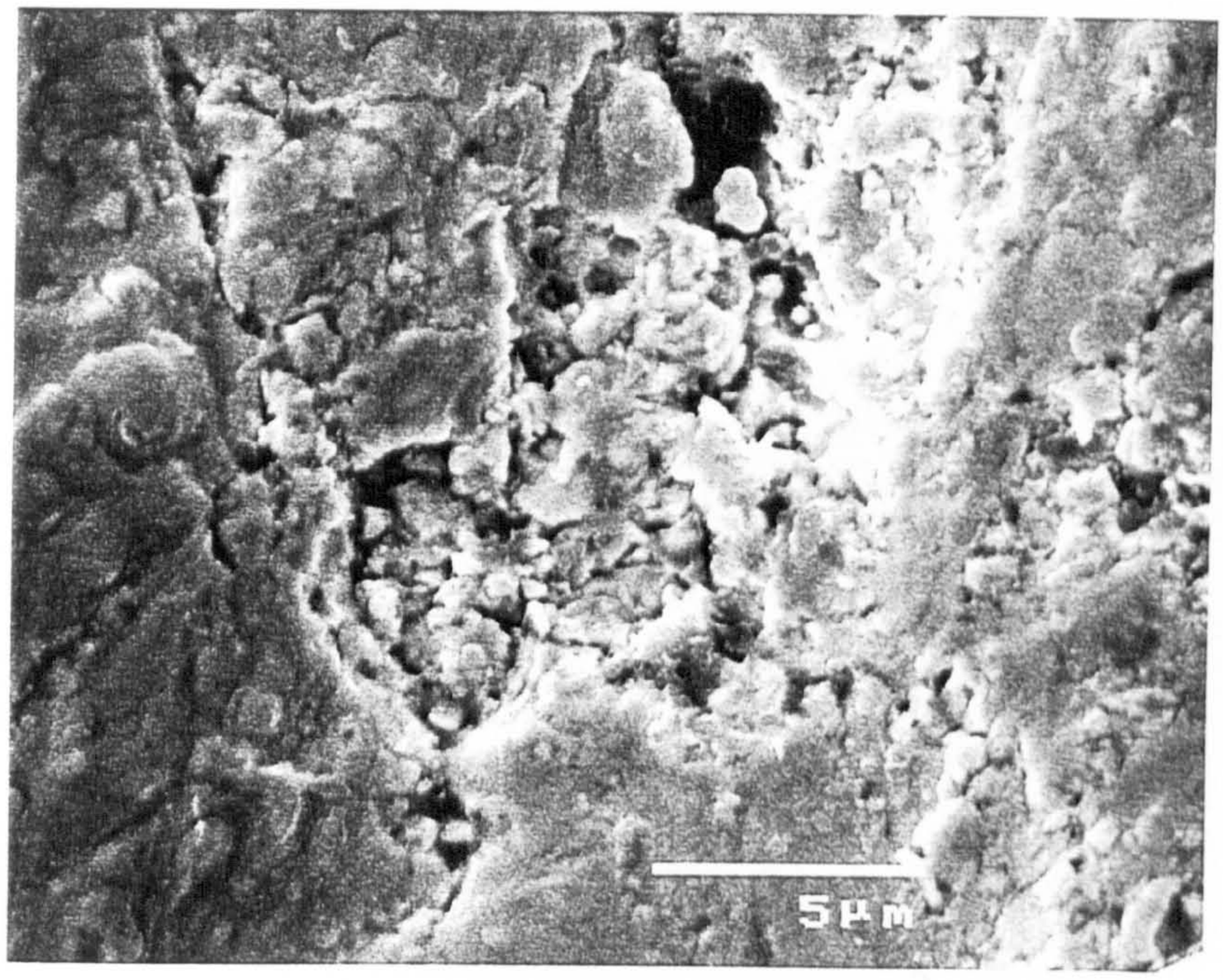

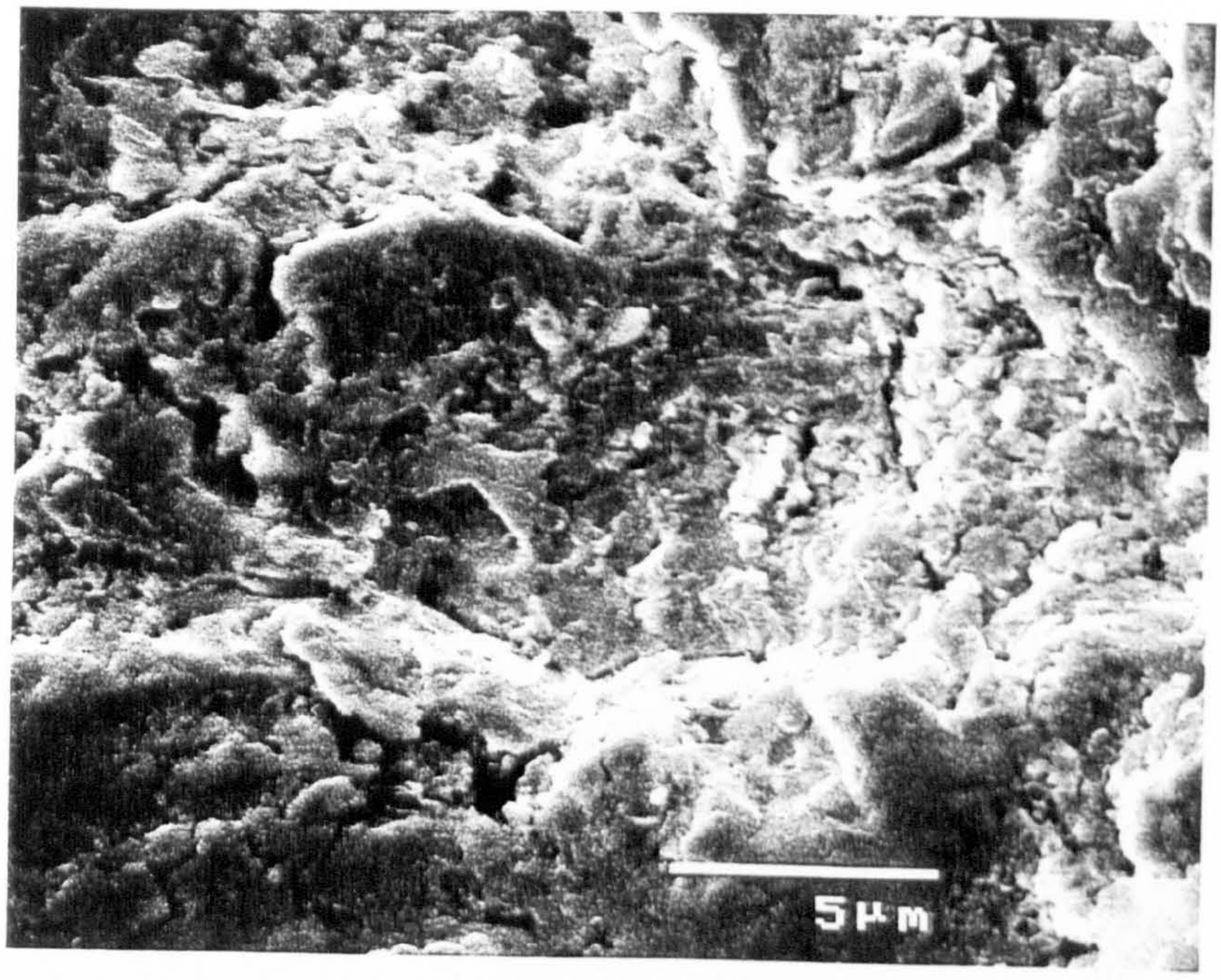

Figure 4.652 - SEM image of LW45 after erosion showing preferential binder removal, (a) normal contrast.

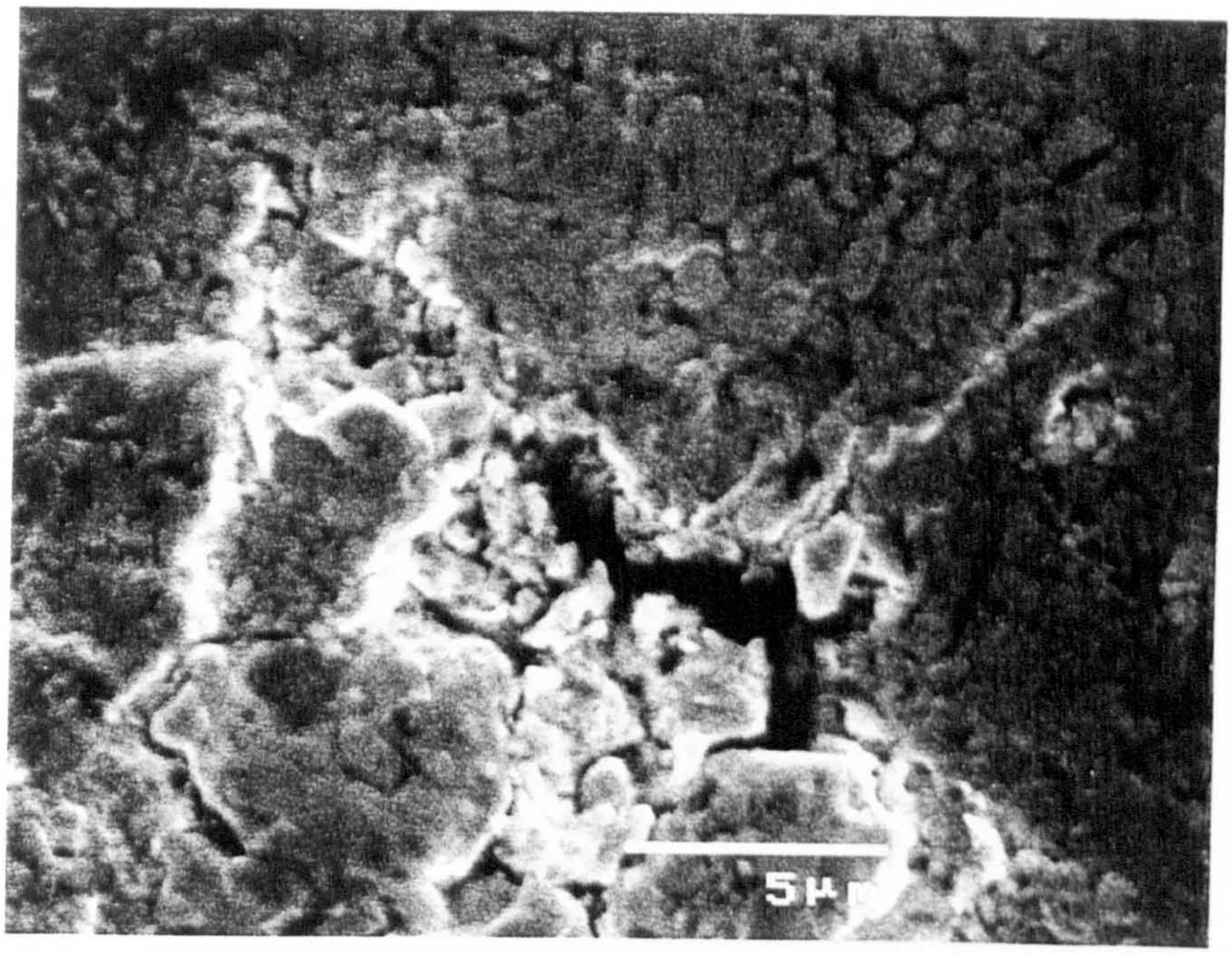

(b) Compositional contrast

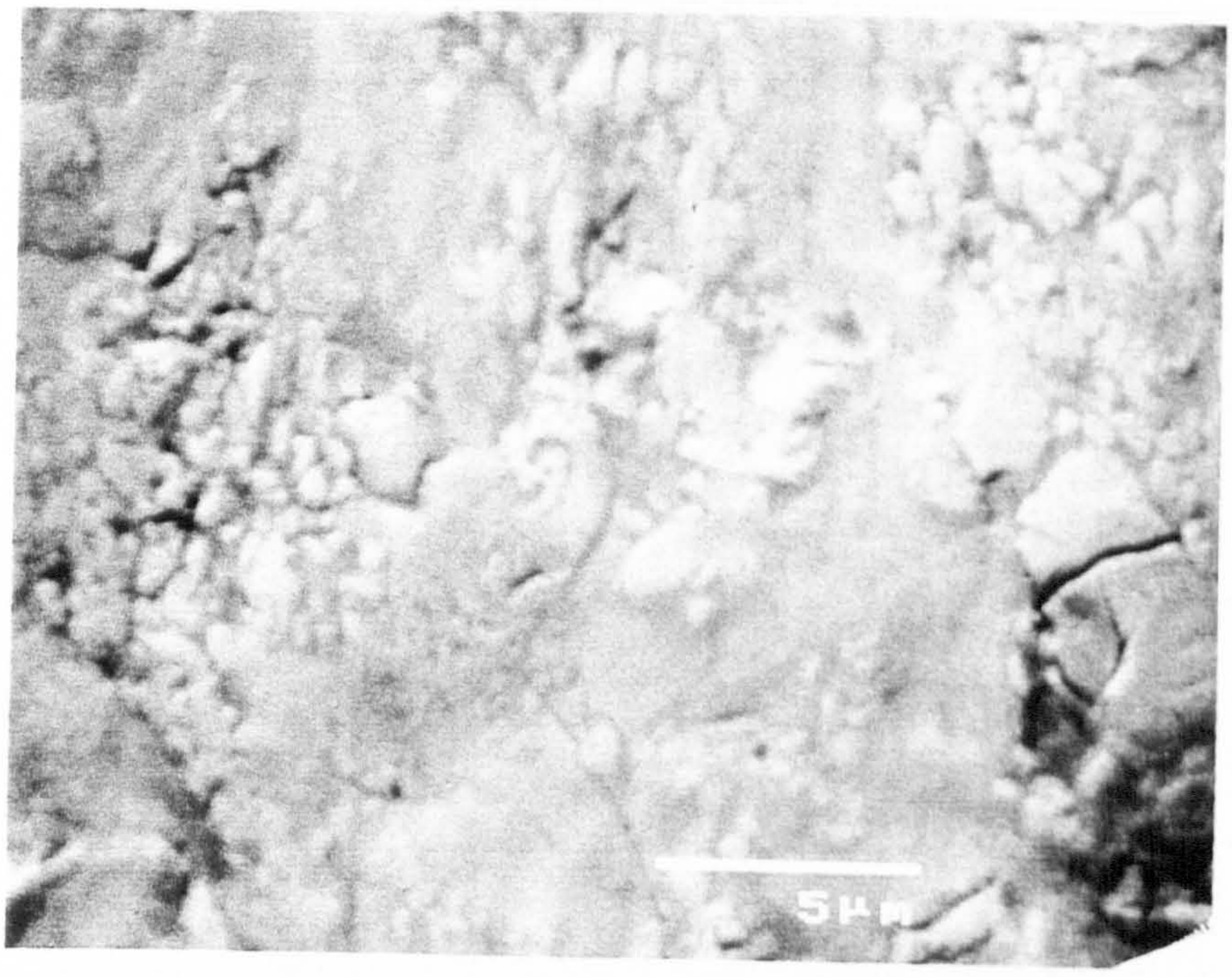

Fig. 4.653 - SEM image showing F255 after erosion

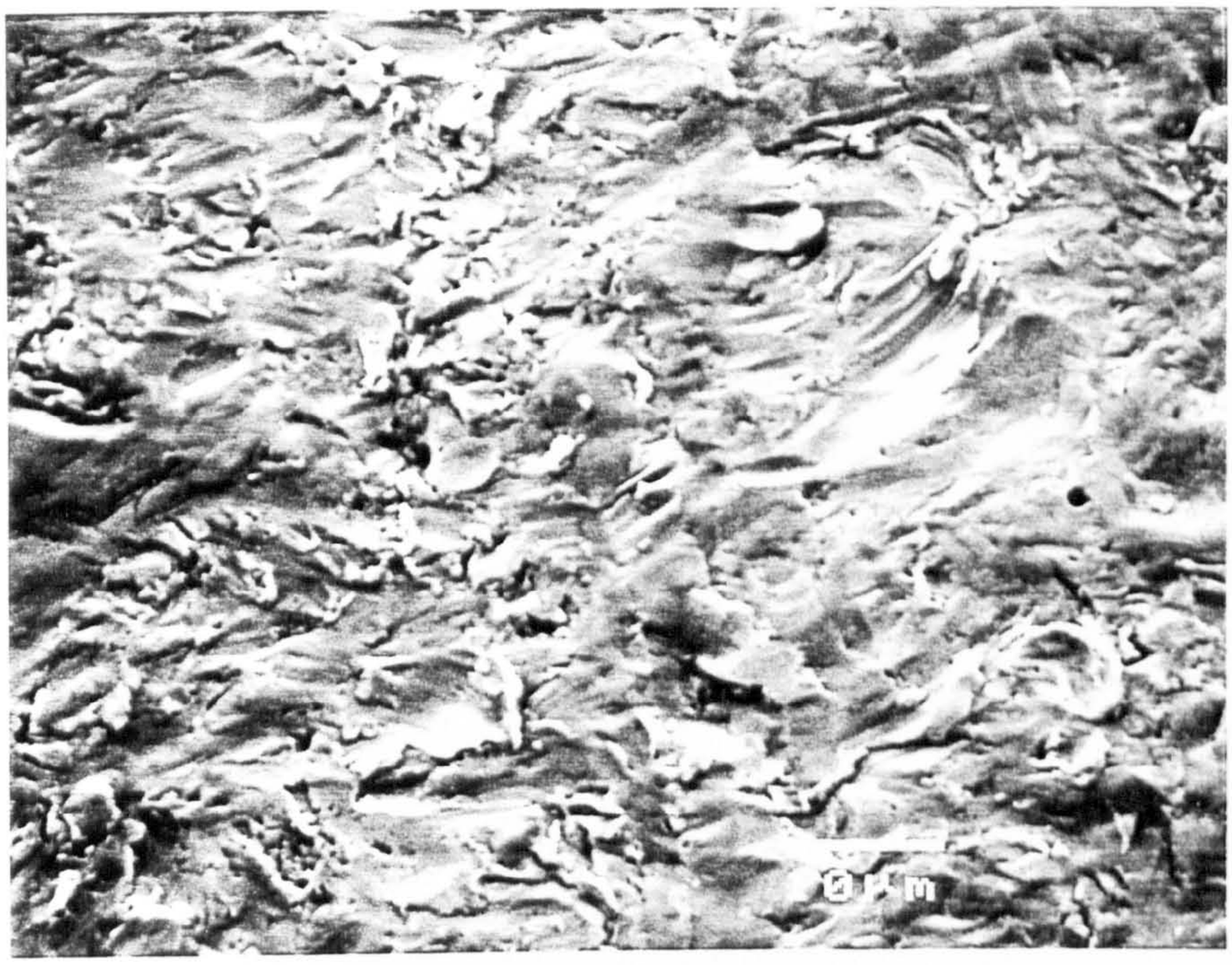

Fig. 4.661 - Taper section through eroded area of LW45

(a) optical micrograph

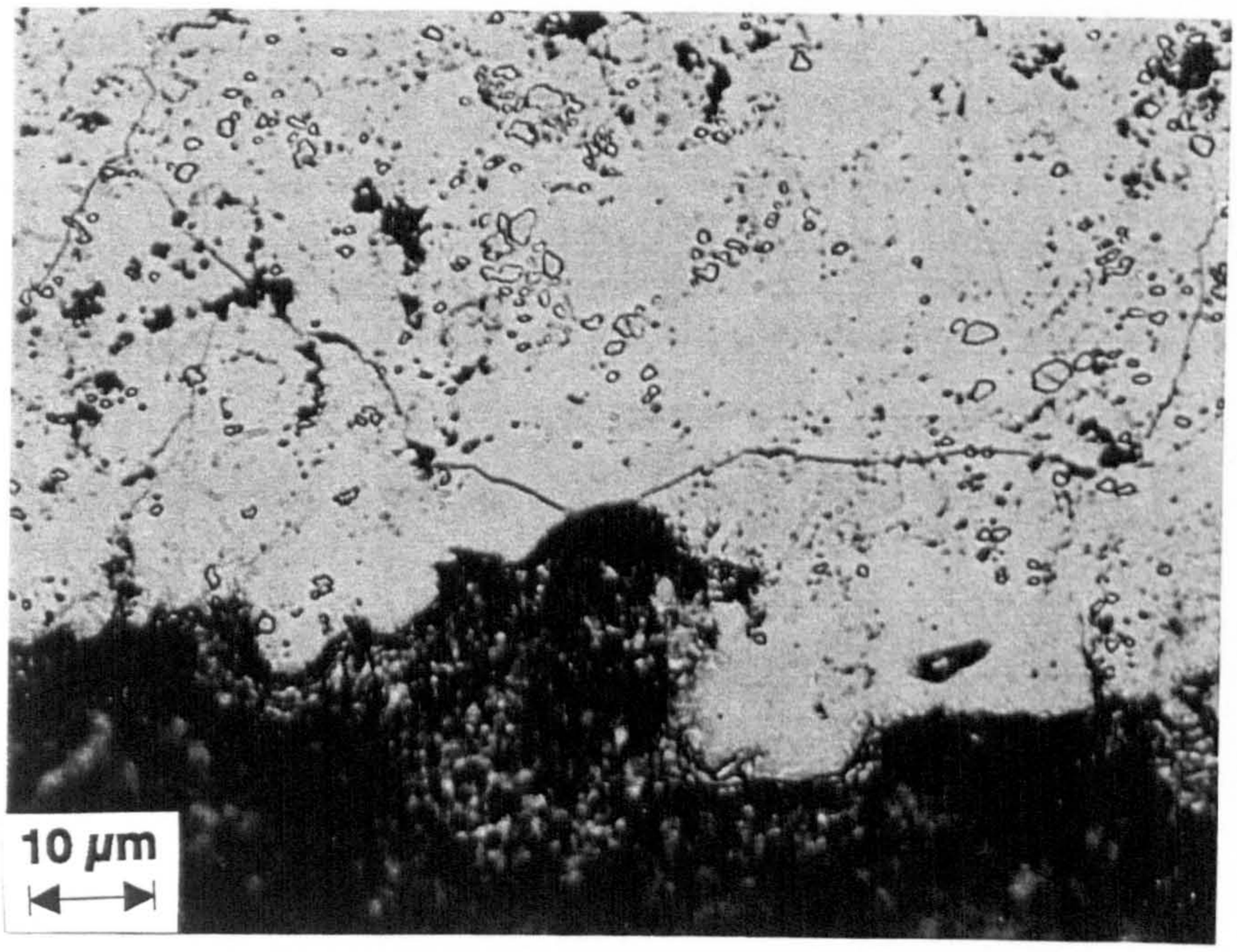

(b) SEM micrograph

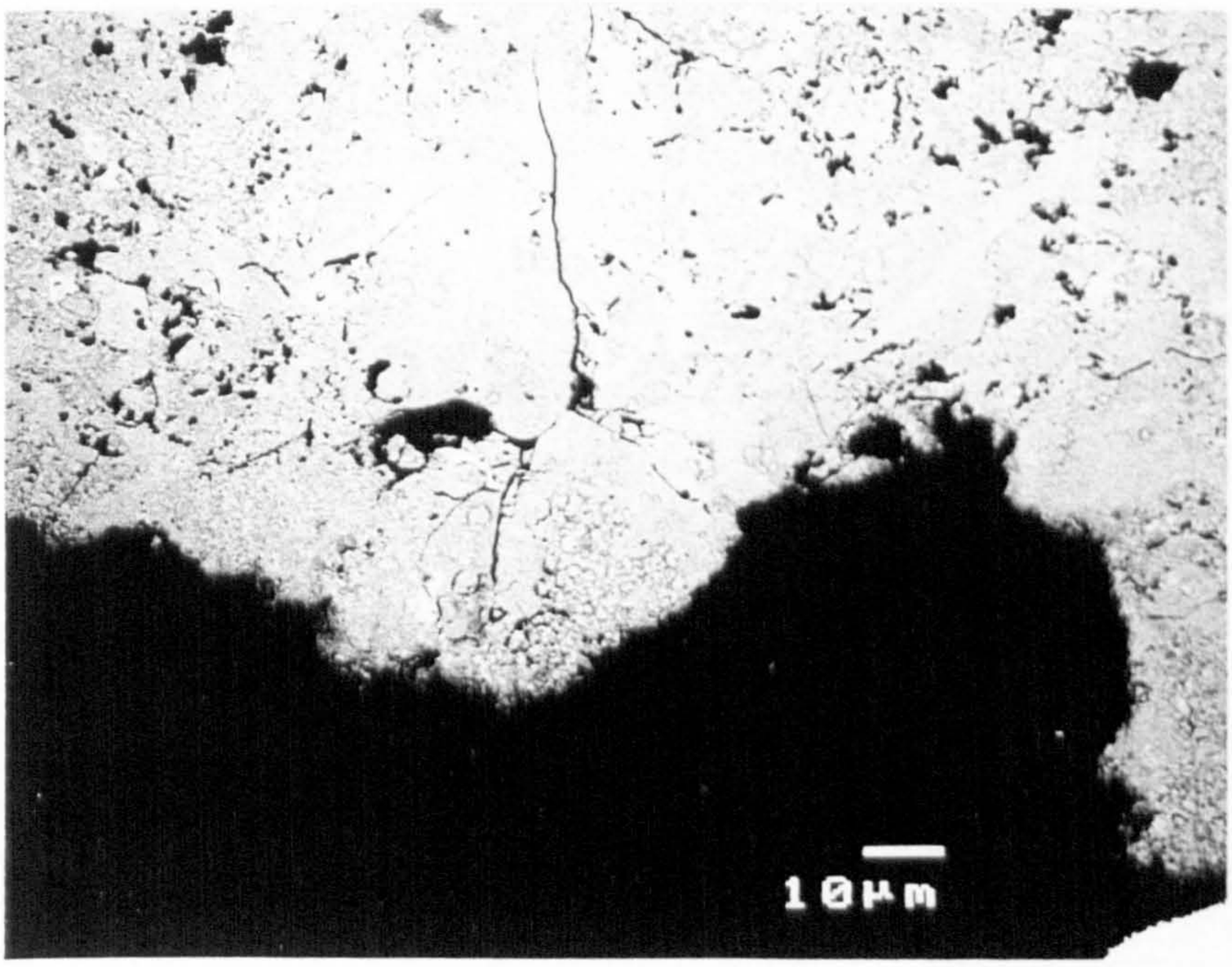

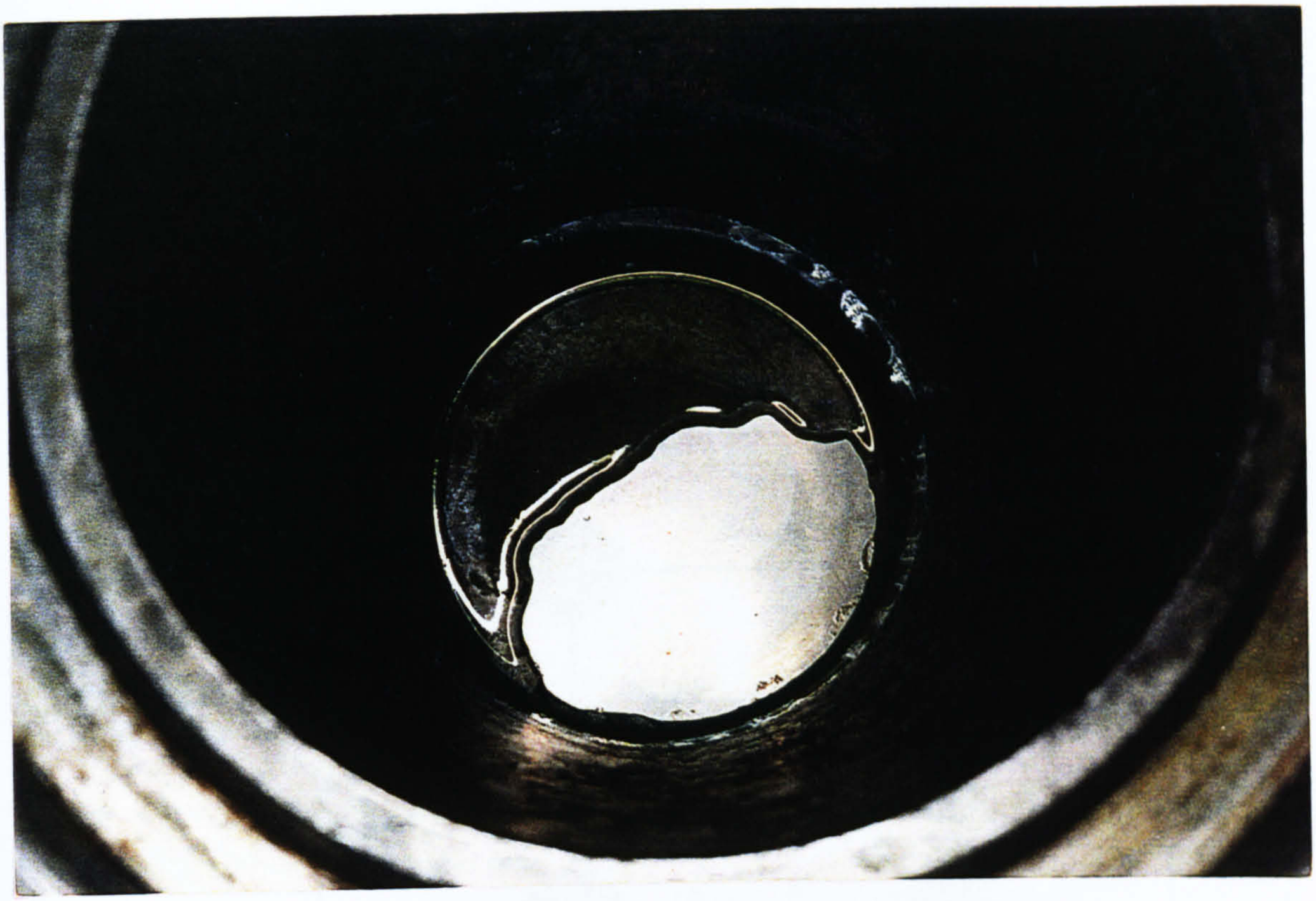

Figure 5.1 - Example of Valve Leakage under Water Pressure Test

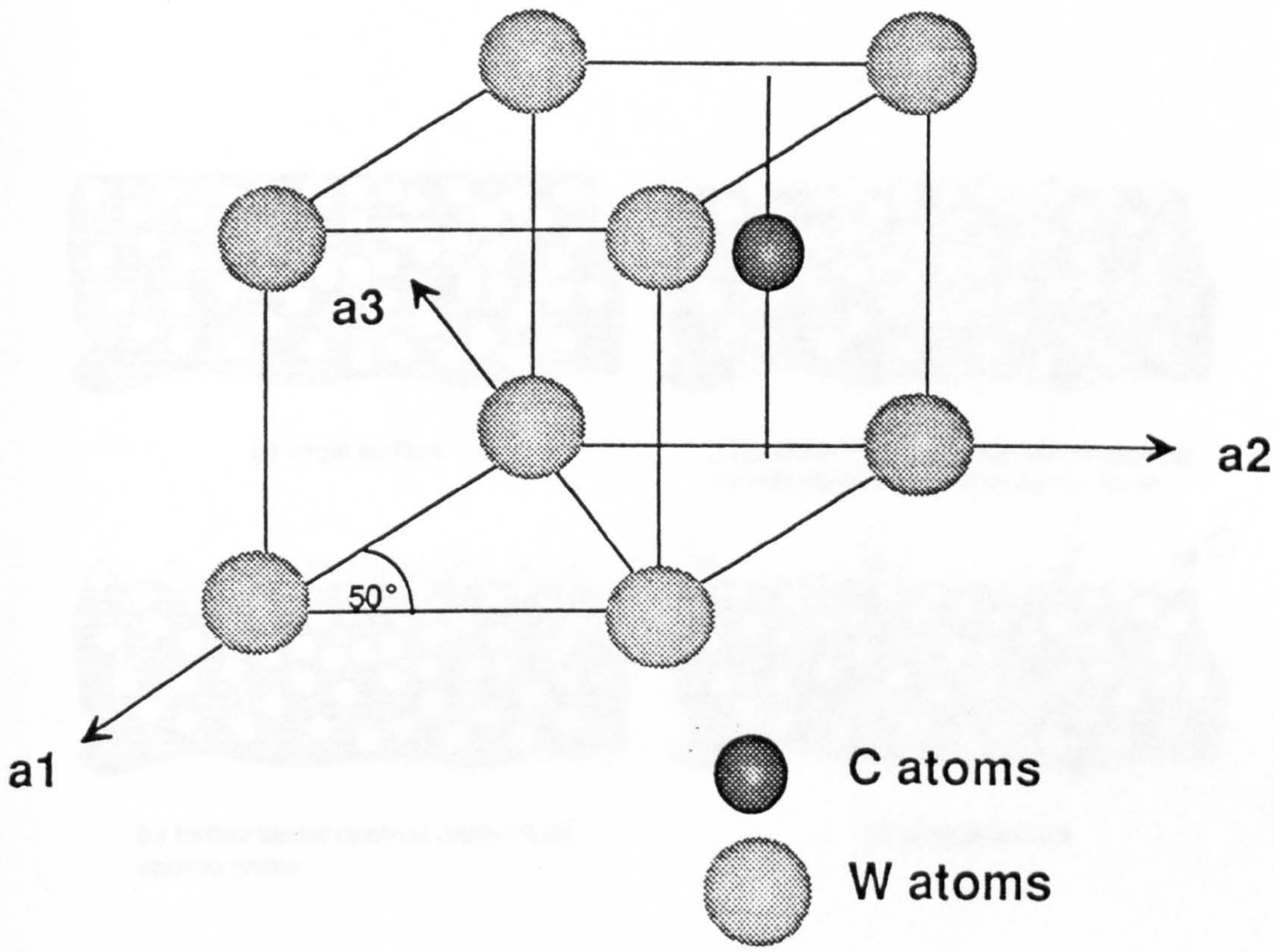

Figure 5.2 - The Structure of Tungsten Carbide

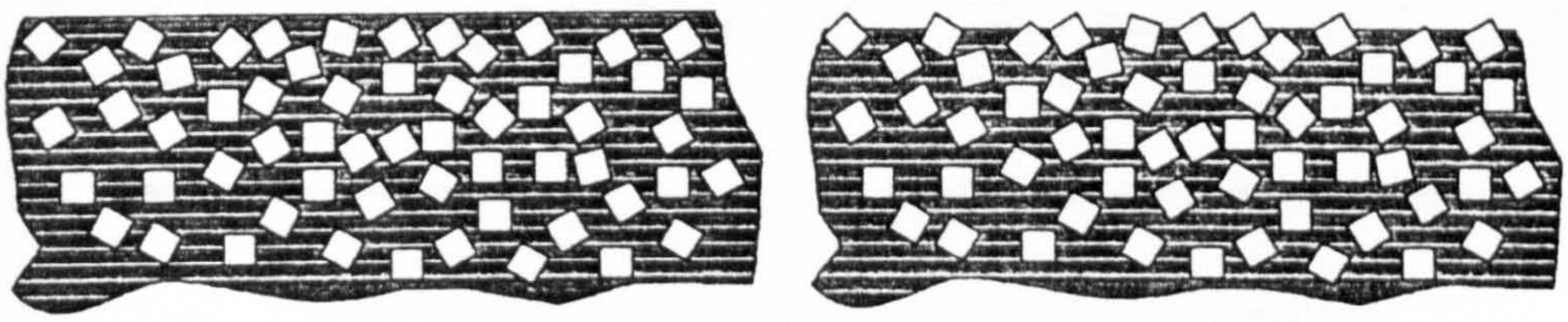

(a) virgin surface

(b) preferential binder removal (protruding carbide particles minimise further wear

(c) further binder removal undermines carbide grains

(d) carbide fall out

Figure 5.3 - Schematic Representation of the Mild Wear Regime

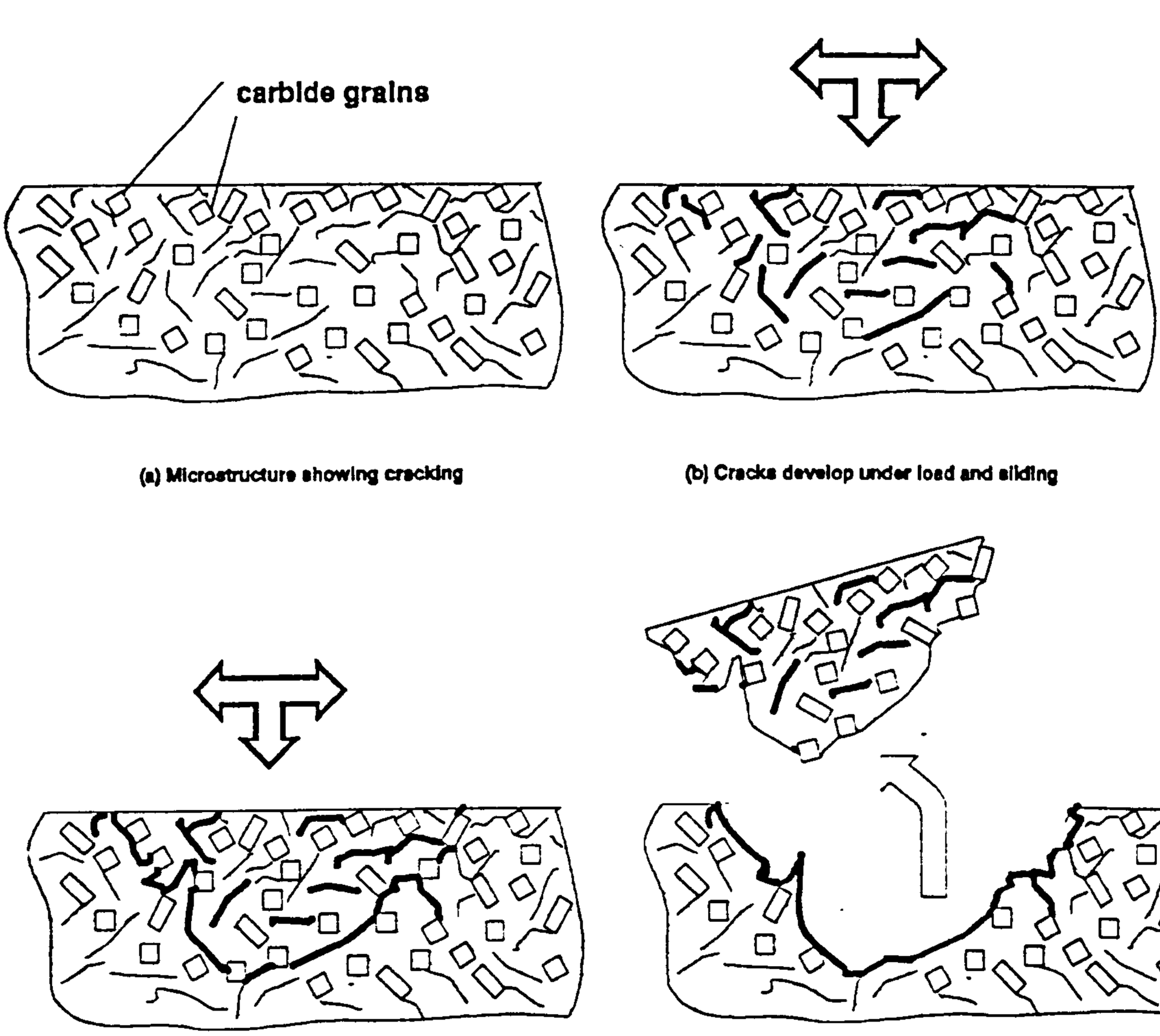

(a) Microstructure showing cracking

(b) Cracks develop under load and sliding

(c) cracks interlink

(d) large scale material removal

Figure 5.4 - Schematic Representation of the Severe Wear Regime

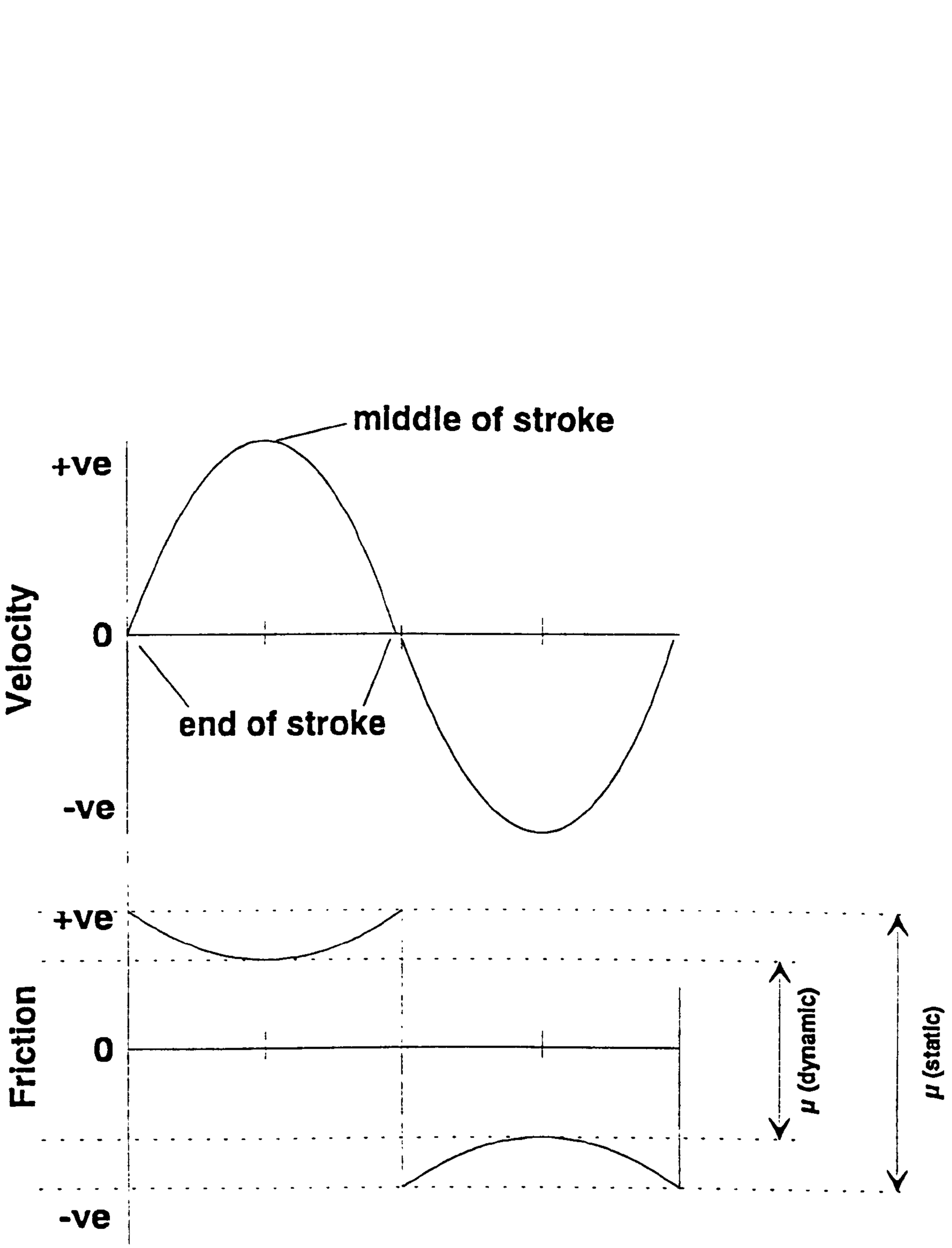

Figure 5.5 - Variation in Sliding Speed and Friction during the Reciprocationg Cycle

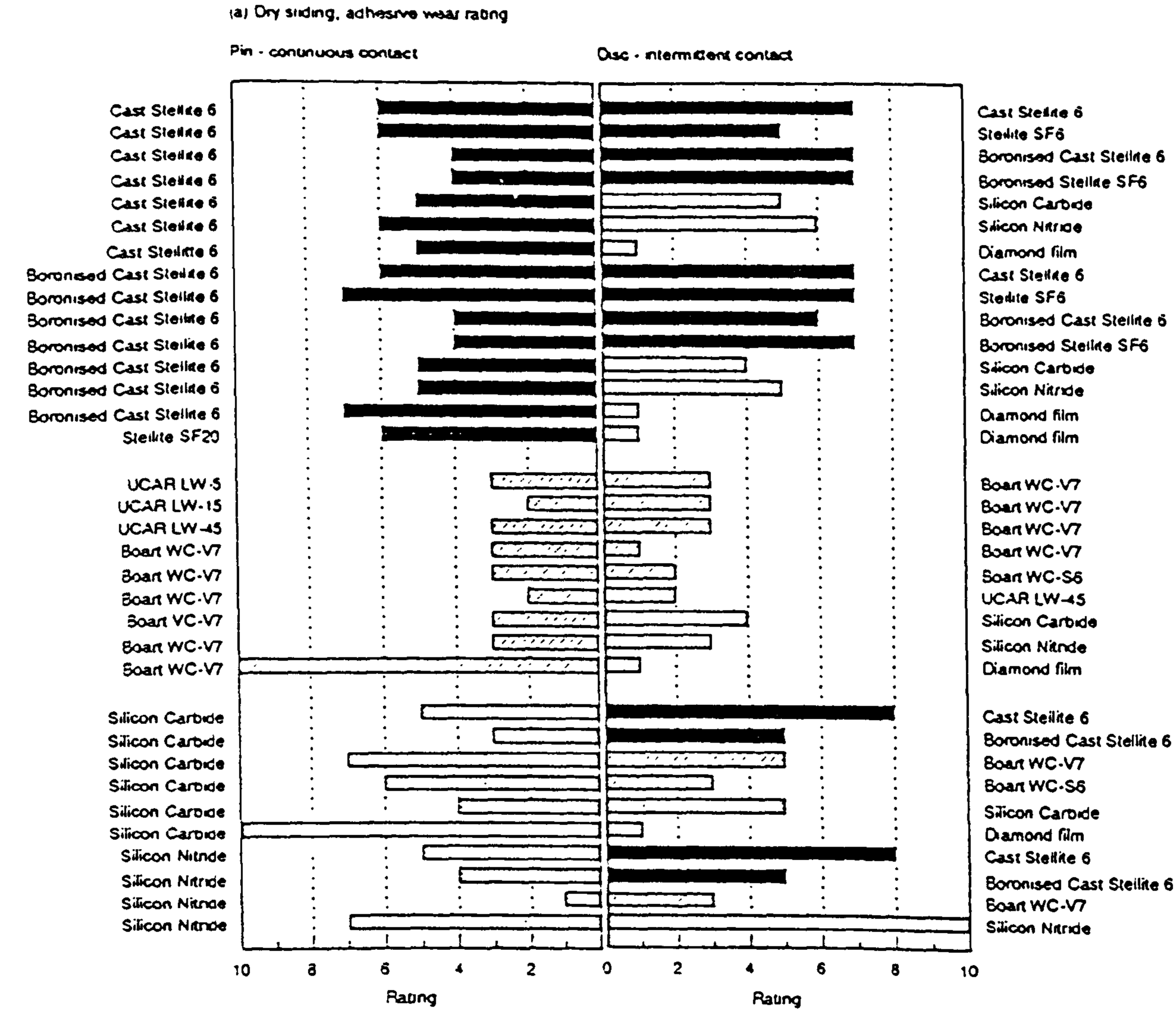

Figure 5.6 - Wear Performance of Candidate Oilfield Materials[73]

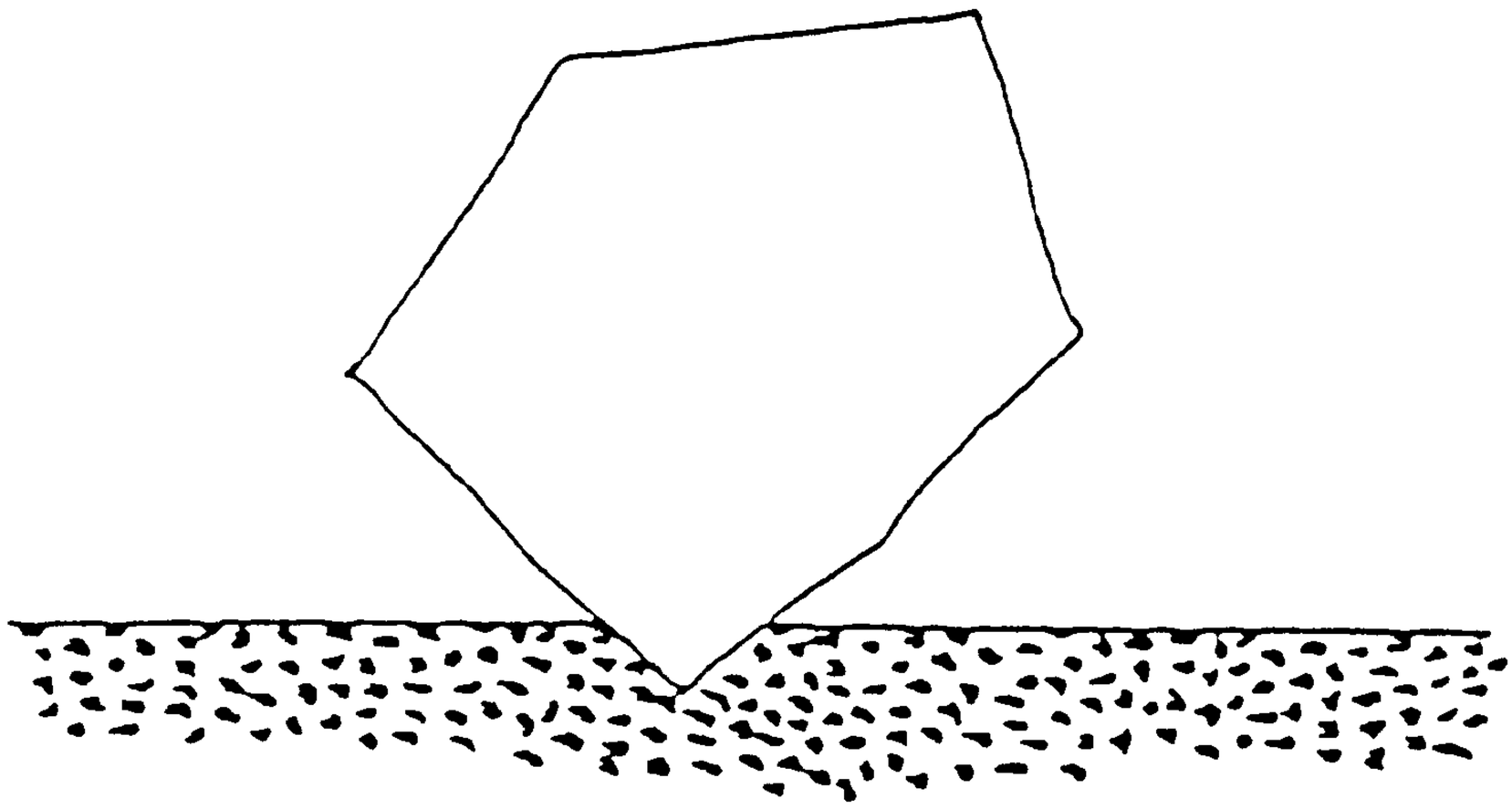

(a) Material behaves homogeneously

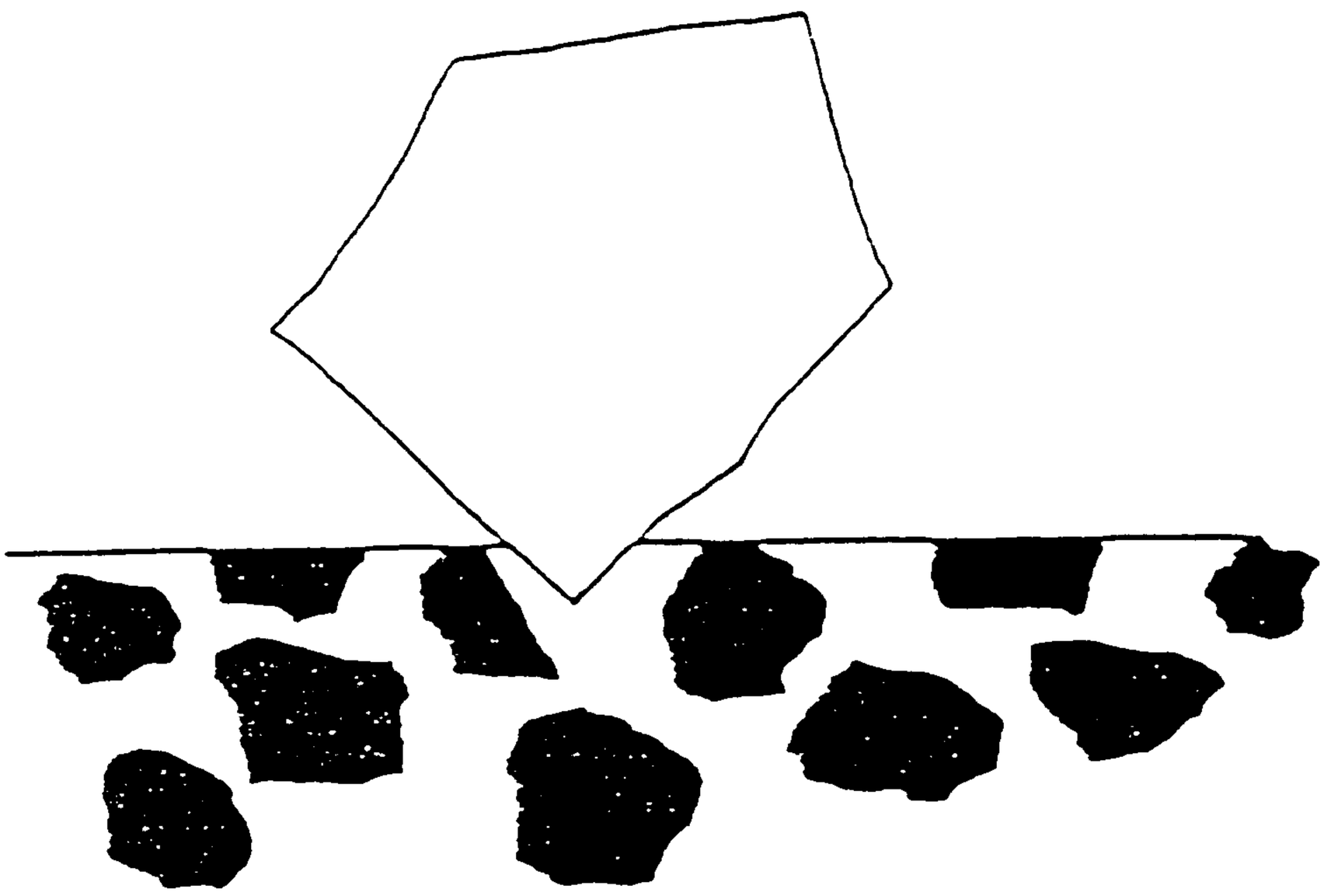

(b) Material behaves heterogeneously

Figure 5.7 - The importance of the relative sizes of the particle contact zone and the hard phase regions in the abrasive wear of a two phase (or composite) material[11].

Fig. 5.8 - Variable velocity through a typical gate valve dependent upon degree of opening

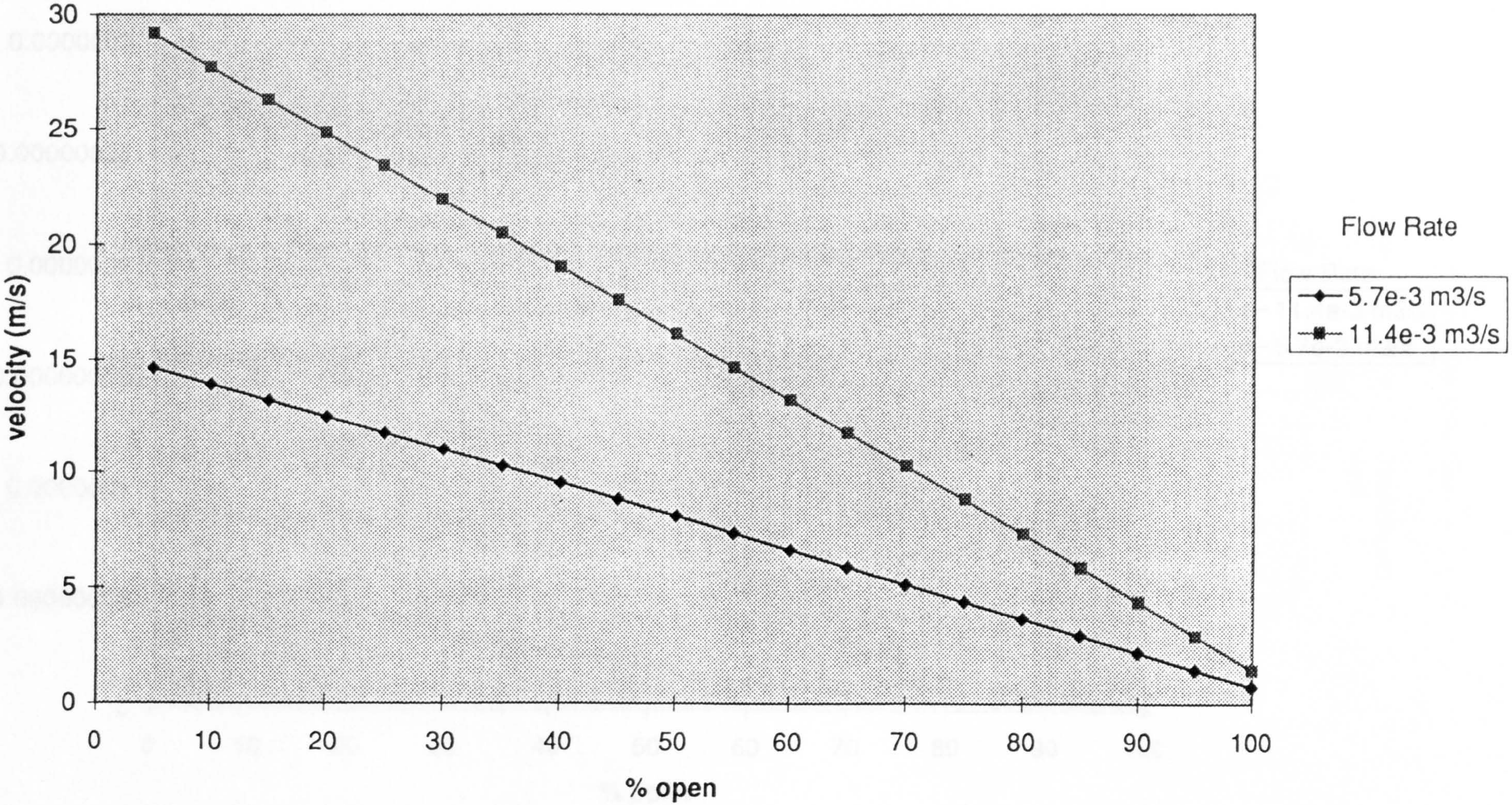

Figure 5.9 - Variation in kinetic energy as a function of valve opening

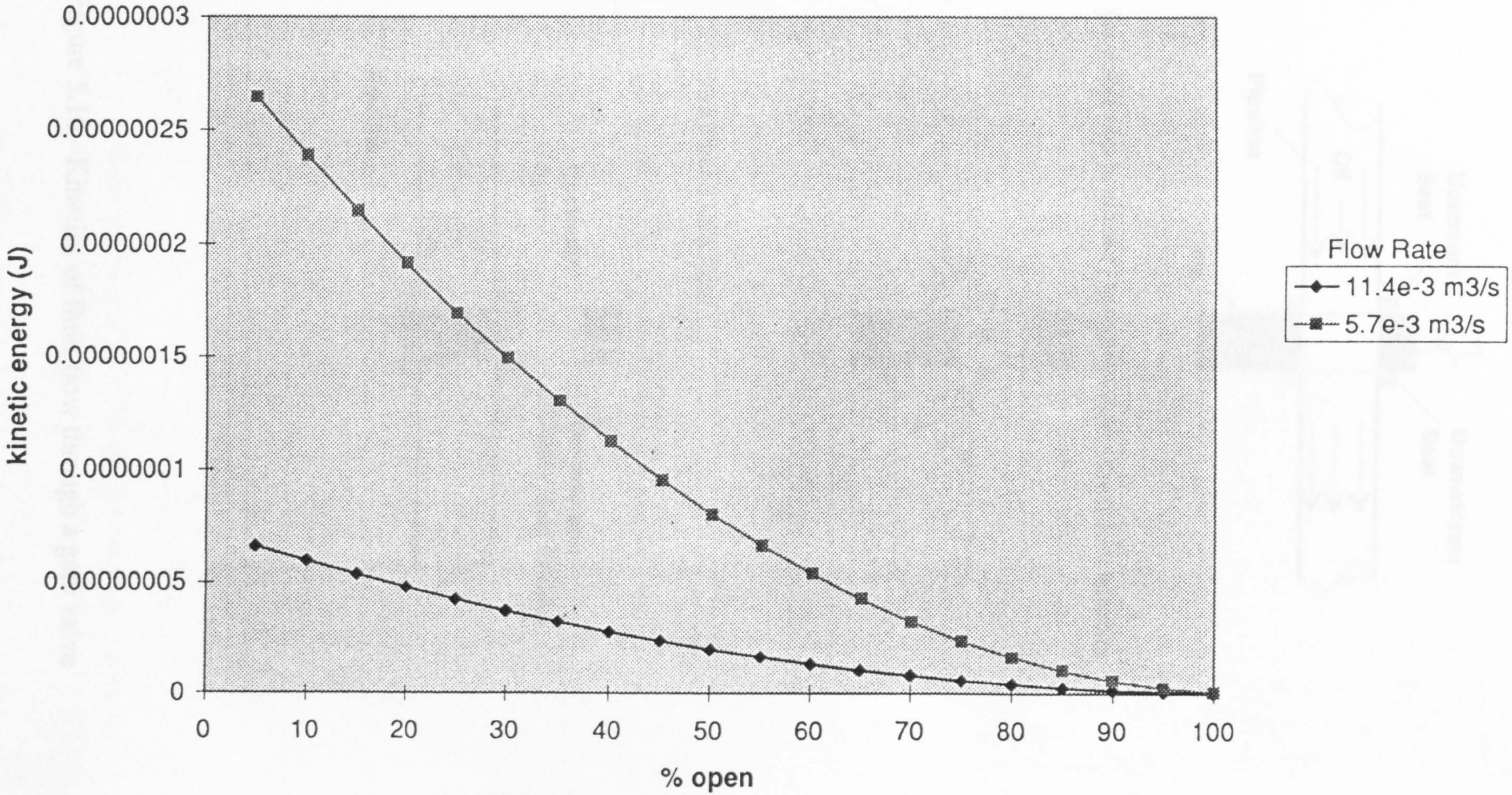

(a) Valve Open - non Interrupted fluid flow

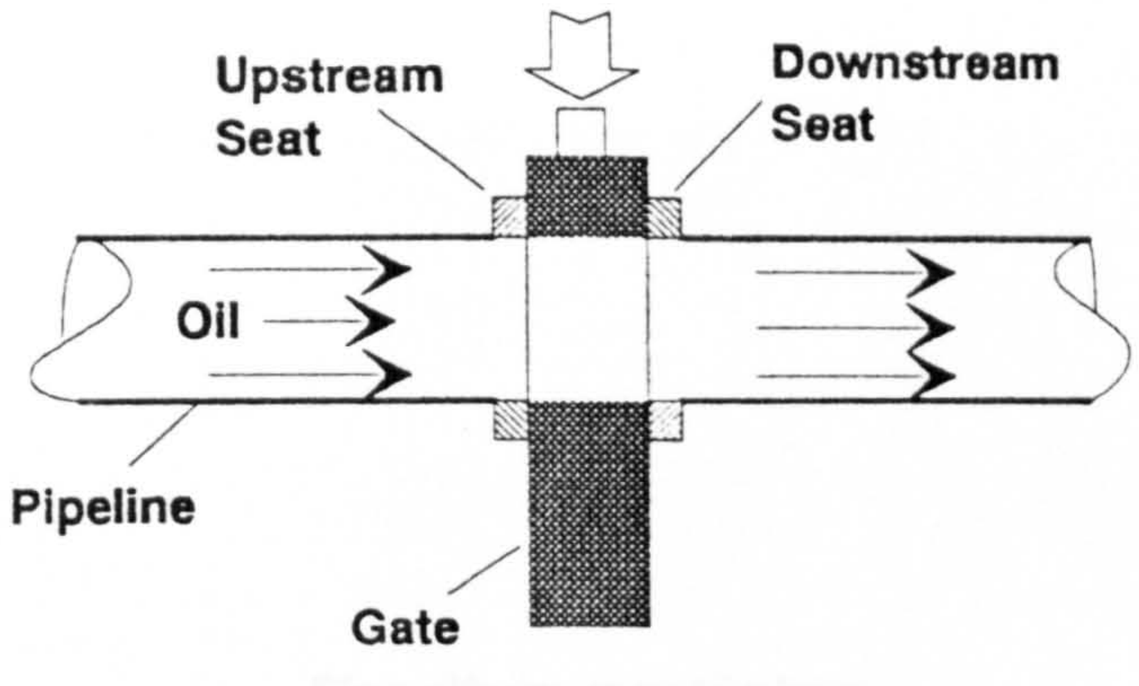

(b) Valve nearly closed - turbulent flow - maximum velocity

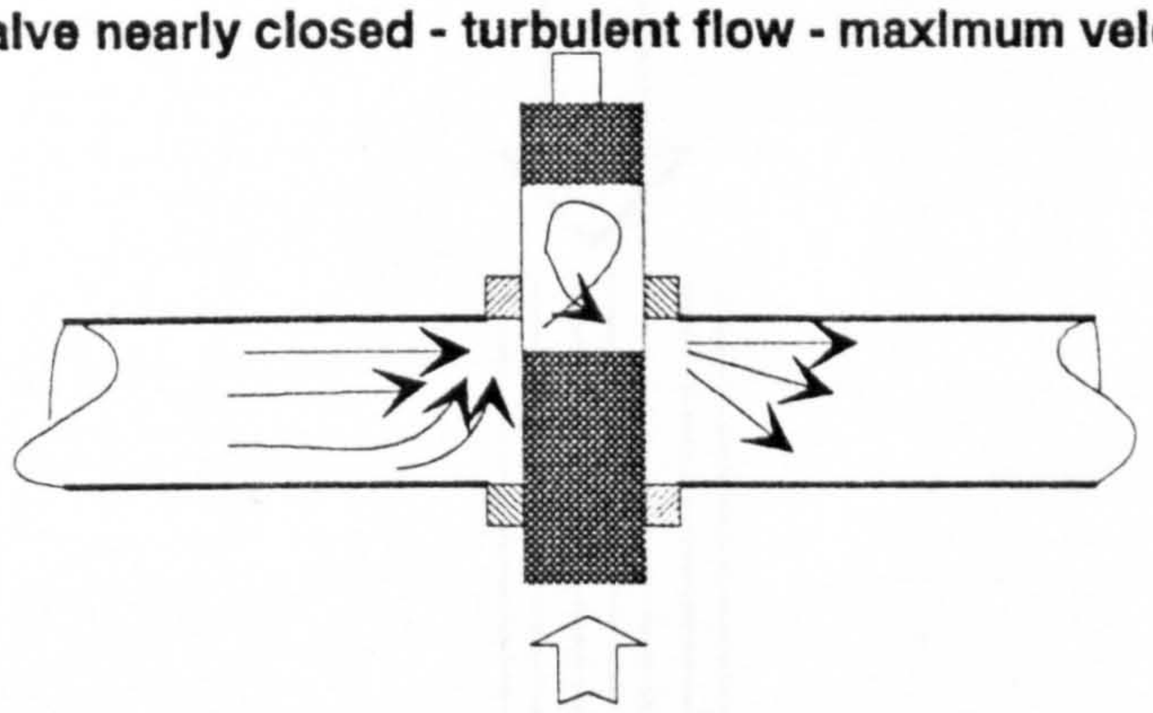

(c) Valve closed - No Flow

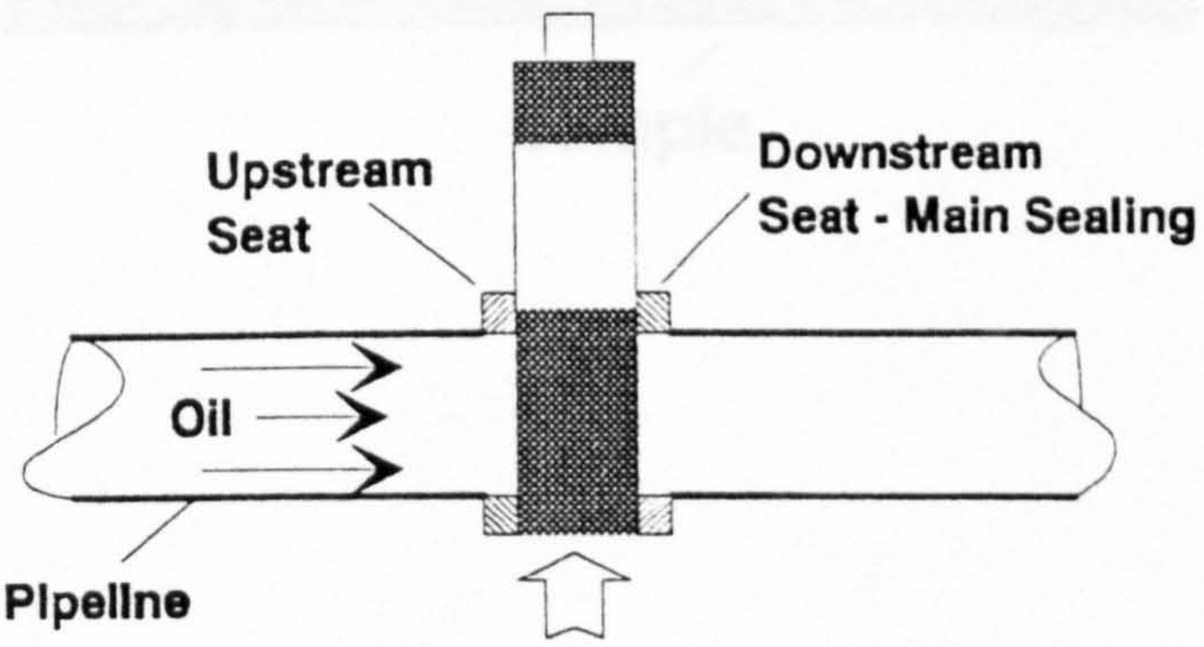

Figure 5.10 - Kinetics of fluid flow through a gate valve

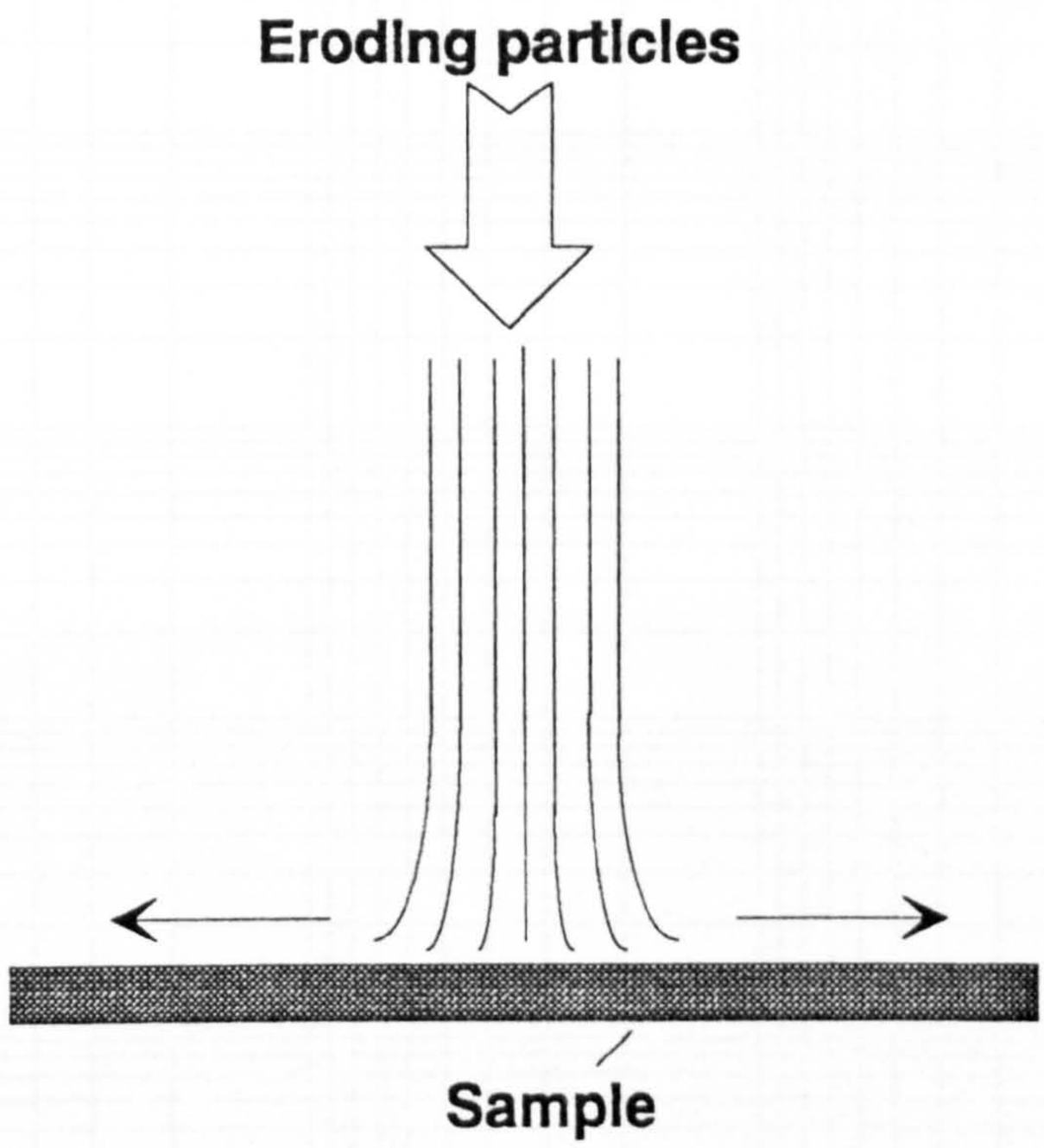

Figure 5.11 - Schematic diagram of the erosion stream showing differing impact angles

Figure 5.12 - The Effect of Particle Energy on the Erosion of LW45

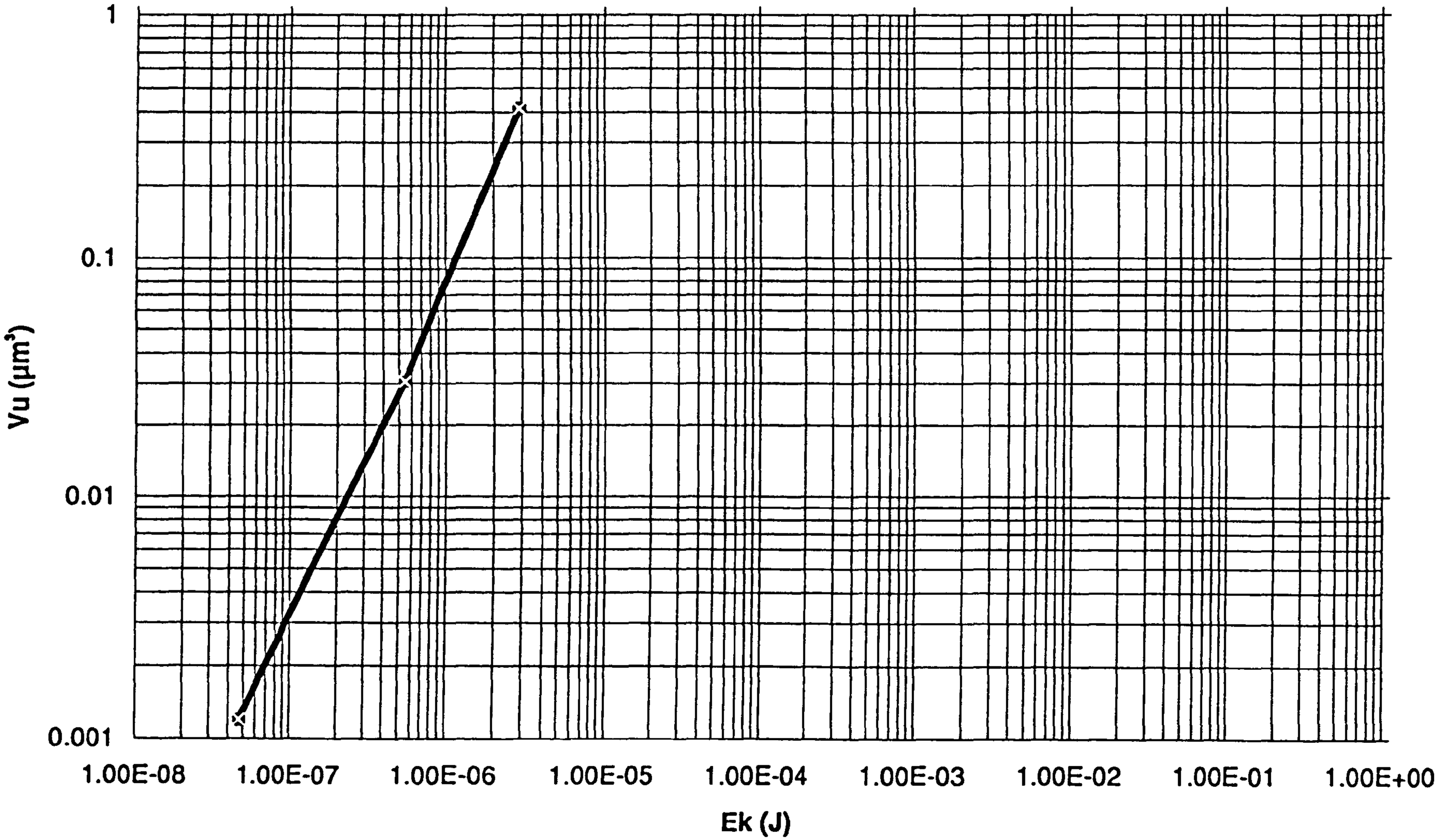

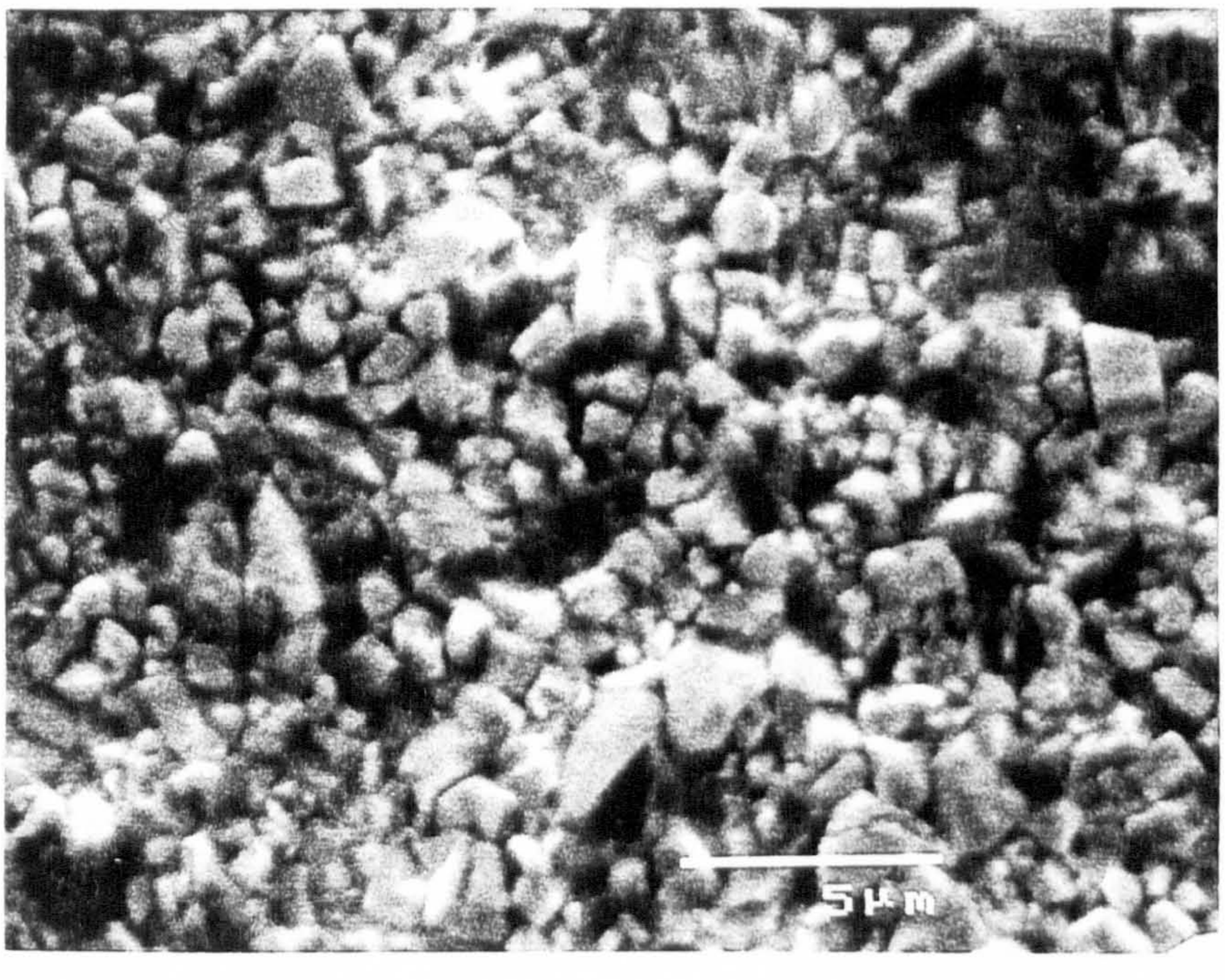

Figure 5.13 - Eroded Surface of Sintered Tungsten Carbide Boart V7

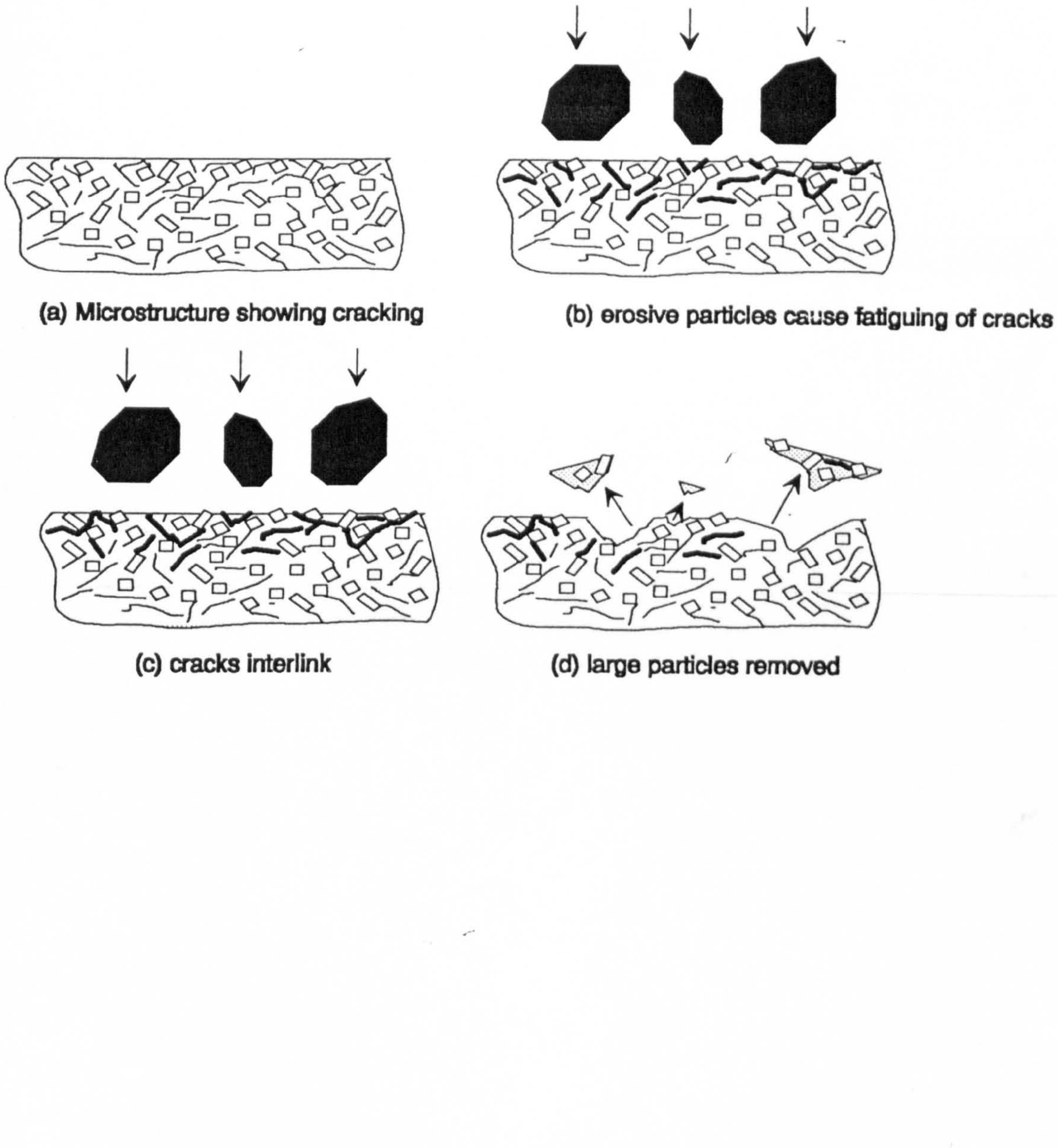

Figure 5.14 - Schematic diagram showing erosive wear mechanism for LW45